VOLCANIC STRATIGRAPHY AND LITHOGEOCHEMISTRY OF THE SENECA ZN-CU-PB PROSPECT, SOUTHWESTERN BRITISH COLUMBIA

by

SEAN D. MCKINLEY

B.Sc.(Hons.), Queen's University, 1992

A THESIS SUBMITTED IN PARTIAL FULFILLMENT OF
THE REQUIREMENTS FOR THE DEGREE OF
MASTER OF SCIENCE

in

THE FACULTY OF GRADUATE STUDIES
(Department of Geological Sciences)

We accept this thesis as conforming
to the required standard:

THE UNIVERSITY OF BRITISH COLUMBIA

March 1996

© Sean D. McKinley, 1996

In presenting this thesis in partial fulfilment of the requirements for an advanced degree at the University of British Columbia, I agree that the Library shall make it freely available for reference and study. I further agree that permission for extensive copying of this thesis for scholarly purposes may be granted by the head of my department or by his or her representatives. It is understood that copying or publication of this thesis for financial gain shall not be allowed without my written permission.

Department of GEOLOGICAL SCIENCES

The University of British Columbia
Vancouver, Canada

Date APRIL 15, 1996

ABSTRACT

The Seneca Prospect is a volcanic-hosted Zn-Cu-Pb deposit 120 km east of Vancouver in southwestern British Columbia. Volcanic strata at Seneca form part of the Weaver Lake Member of the Lower to Middle Jurassic Harrison Lake Formation of the Harrison Terrane.

The rocks at Seneca comprise four principal facies: 1) vent to vent-proximal facies consisting of basaltic to rhyolitic lavas and associated breccias; 2) vent-proximal to distal facies consisting of volcaniclastic debris flows and siltstones; 3) coeval intrusions consisting of basaltic andesitic to rhyolitic sills and dikes, and 4) distal marine facies consisting of a pumice-bearing argillaceous unit. The volcanic strata can be subdivided into three intervals from bottom to top as follows: 1) the Footwall Interval below the mineralized horizon which comprises subaqueously deposited basaltic lavas and felsic debris flows; 2) the Seneca Horizon which hosts the mineralized zones, and 3) the Hangingwall Interval which is consists largely of felsic flows, intrusions and volcaniclastic rocks. Volcaniclastic rocks in the Footwall Interval are dominated by coarse, poorly-sorted debris flows whereas the volcaniclastic rocks of the Hangingwall Interval are mostly massive to well-bedded ashes and volcanically-derived turbidites.

The Seneca volcanic sequence is a bimodal suite of rocks of calc-alkaline to transitional calc-alkaline-tholeiitic affinity (Zr/Y ratios >3.5, La_N/Yb_N ratios > 2.0). Pearce element ratio analysis of the mafic rocks shows that the chemical variation in a least-altered subset can be explained by the fractionation of plagioclase, olivine and clinopyroxene although variation within basaltic and basaltic andesitic subgroups can be explained by plagioclase fractionation alone. Major element variations in the least altered felsic rocks can be explained by fractionation involving the crystallization of feldspar, quartz ± pyroxene and/or hornblende. Trace element trends can be accounted for by 30 to 40 % fractional crystallization of the assemblage feldspar-hornblende-magnetite±apatite.

Mass change calculations revealed both a vertical zonation and spatial differences in the hydrothermally altered stockwork zones. In general, the stockworks can be subdivided into upper and lower alteration zones. The upper quartz-sericite zone has experienced net mass gain with mass gains of SiO_2 and K_2O and mass losses of Na_2O and CaO resulting from silicification and the destruction of feldspar. The lower sericite-chlorite zone has had small net mass gains or losses as a result of mass gains of K_2O and MgO and losses of Na_2O, CaO and in places SiO_2. The MgO gains throughout the Vent Zone are much smaller or absent in the Fleetwood Zone, perhaps indicating that the larger Vent Zone hydrothermal system was more capable of incorporating seawater magnesium than the Fleetwood Zone stockwork systems, which may have been sealed by overlying flows or volcaniclastic sediments.

Mineralization in the Pit Area consists of zones of disseminated to conformable massive sphalerite, pyrite, chalcopyrite, galena and barite hosted by the strongly altered ore zone conglomerate (OZC). Stratigraphic relationships indicate that these zones may have formed contemporaneously with the stockwork sphalerite-pyrite-chalcopyrite mineralization in the Fleetwood and Vent Zones. The stockwork zones possibly were vertical conduits for hydrothermal fluids which then migrated laterally through the permeable OZC where they interacted with seawater and formed the Pit Area sulphide mineralization.

The volcanic rocks which host the Seneca deposit have geological and geochemical similarities to younger rocks of the Lau Basin and Tofua Arc in the southwest Pacific and the Hokuroku Basin in Japan. These similarities suggest that the Seneca volcanic sequence and sulphide mineralization may be in rifted sub-basins within a calc-alkaline volcanic arc formed at a destructive plate margin involving two oceanic plates with little or no continental crustal influence.

TABLE OF CONTENTS

ABSTRACT ii
TABLE OF CONTENTS iv
LIST OF TABLES vii
LIST OF FIGURES vii
LIST OF PLATES x
ACKNOWLEDGMENTS xii
DEDICATION xiii
CHAPTER 1. INTRODUCTION 1
1.1 SCOPE OF STUDY 1
1.2 TERMINOLOGY 4
1.3 PROPERTY HISTORY 5
1.4 REGIONAL GEOLOGY 5
1.4.1 HARRISON TERRANE 5
1.4.2 HARRISON LAKE FORMATION 6
1.4.3 GEOCHRONOLOGY 7
1.4.4 STRUCTURE AND METAMORPHISM 8
CHAPTER 2. GEOLOGY OF THE SENECA DEPOSIT 9
2.1 INTRODUCTION 9
2.2 DISTRIBUTION OF VOLCANIC FACIES 17
2.2.1 FOOTWALL INTERVAL 17
2.2.2 SENECA HORIZON 19
2.2.3 HANGINGWALL INTERVAL 19
2.3 DESCRIPTION OF VOLCANIC FACIES 20
2.3.1 FACIES 1: LAVAS 20
2.3.1.1 MAFIC LAVAS 20
2.3.1.2 FELSIC LAVA FLOWS AND DOMES 22
2.3.2 FACIES 2: VOLCANICLASTIC ROCKS 24
2.3.2.1 FACIES 2.1: DEBRIS FLOWS, GRAIN FLOWS AND TURBIDITIC VOLCANICLASTICS 25
2.3.2.2 FACIES 2.2: VOLCANICLASTIC SILTSTONE 29
2.3.2.3 FACIES 2.3: DACITIC AND RHYOLITIC PUMICE BEDS 29
2.3.2.4 FACIES 2.4: ORE ZONE CONGLOMERATE 31
2.3.3 FACIES 3: SYNVOLCANIC INTRUSIONS 31
2.3.3.1 FELDSPAR-PHYRIC INTRUSIONS (FP) 34
2.3.3.2 MAFIC INTRUSIONS 34
2.3.3.3 QUARTZ-FELDSPAR-PHYRIC INTRUSIONS (QFP) 35
2.3.4 FACIES 4: ARGILLACEOUS BEDS 35
2.4 DISCUSSION 36

CHAPTER 3. PETROLOGY OF VOLCANIC SEQUENCE AT SENECA 40
3.1 INTRODUCTION 40
3.2 PETROGRAPHY OF THE VOLCANIC ROCKS AT SENECA 40
3.2.1 FACIES 1: LAVA FLOWS AND BRECCIAS 40
3.2.1.1: MAFIC LAVAS 40
3.2.1.2: FELSIC LAVAS 42
3.2.2 FACIES 2: VOLCANICLASTIC ROCKS 44
3.2.2.1 FACIES 2.1: VOLCANICLASTIC DEBRIS FLOWS 44
3.2.2.2 FACIES 2.2: VOLCANICLASTIC SILTSTONES 44
3.2.3 FACIES 3: SYNVOLCANIC INTRUSIONS 49
3.2.3.1 MAFIC INTRUSIONS 49
3.2.3.2 FELSIC INTRUSIONS 49
3.3 IGNEOUS LITHOGEOCHEMISTRY 56
3.3.1 METHODOLOGY 56
3.3.2 TECTONIC AFFINITY 60
3.3.3 GEOCHEMICAL CLASSIFICATION OF UNITS 66
3.3.3.1 MAFIC ROCKS 67
3.3.3.2 FELSIC ROCKS 67
3.3.4 IGNEOUS ROCK-FORMING PROCESSES 73
3.3.4.1 MAFIC ROCKS 75
3.3.4.2 FELSIC ROCKS 77
3.4 DISCUSSION 85
CHAPTER 4. ALTERATION 88
4.1 INTRODUCTION 88
4.2 DISTRIBUTION OF ALTERATION 88
4.3 CHARACTERIZATION OF HYDROTHERMAL ALTERATION 89
4.4 QUANTIFICATION OF ALTERATION PROCESSES 93
4.4.1 IZAWA ALTERATION DISCRIMINATION DIAGRAM 93
4.4.2 PER ANALYSIS 96
4.4.3 MASS CHANGE CALCULATIONS 99
4.4.3.1 METHODOLOGY 99
4.4.3.2 MASS CHANGE CALCULATIONS FOR FELSIC ROCKS 102
4.4 SUMMARY 115
CHAPTER 5. MINERALIZATION 117
5.1 INTRODUCTION 117
5.2 MINERALIZATION OF THE PIT AREA 117
5.3 MINERALIZATION OF THE VENT ZONE 122
5.4 MINERALIZATION OF THE FLEETWOOD ZONE 124
5.5 DISCUSSION 129

CHAPTER 6. DISCUSSION AND CONCLUSIONS 131
6.1 INTRODUCTION 131
6.2 STRATIGRAPHY AND GEOCHEMISTRY 131
6.2.1 STRATIGRAPHIC SUBDIVISIONS 131
6.2.2 FACIES INTERPRETATIONS 132
6.2.3 GEOCHEMISTRY OF THE VOLCANIC SEQUENCE AT SENECA 133
6.2.4 COMPARISONS OF THE SENECA VOLCANIC SEQUENCE WITH MODERN SETTINGS 134
Lau Basin, southwest Pacific 134
Puertocitios Volcanic Province, northeastern Baja California 139
Medicine Lake Volcanic Center, northern California 140
Hokuroku Basin, northern Honshu, Japan 143
6.2.5 SUMMARY 145
6.3 ALTERATION AND MINERALIZATION 146
6.4 CONCLUSIONS 151
Volcanic Stratigraphy and Facies Distribution 151
Geochemistry 153
Alteration 153
Mineralization 154
6.5 CLOSING REMARKS 155
REFERENCES 157
APPENDIX A - LITHOGEOCHEMICAL DATA 163
APPENDIX B - MASS CHANGE CALCULATIONS 179
APPENDIX C - ESTIMATES OF PRECISION AND ACCURACY 185

LIST OF TABLES

Table 2.1. Summary of the major volcanic facies at the Seneca property 38

Table 3.1. Geochemical composition of least altered samples 58

Table 3.2. Mineral/melt partition coefficients for Zr, Y and Ti for andesitic to rhyolitic melts 80

Table 3.3. Summary of results of fractional crystallization modelling 84

Table 4.1. Summary of sericitization index calculations 97

Table 4.2. Mass change calculations for strongly altered felsic rocks 103

Table 5.1. Summary of typical assay values for selected mineralized intervals in the Pit Area 120

Table 5.2. Summary of selected assay data from the main Fleetwood Zone stockwork 124

Appendix A.1. Chemical composition of felsic volcanic rocks at Seneca 165

Appendix A.2. Chemical composition of mafic volcanic rocks at Seneca 172

Appendix A.3. Chemical composition of volcaniclastic rocks at Seneca 174

Appendix B. Mass change calculations for major elements 181

Appendix C.1. Analyses of in-house standards 188

Appendix C.2. Analyses of duplicate samples 193

LIST OF FIGURES

Figure 1.1. Location map of the Seneca deposit 2
Figure 1.2. Map of the Seneca property 3
Figure 2.1. Geological cross-sections through the Seneca property 10
Figure 2.2. Simplified stratigraphic cross-section through the Fleetwood Zone 11
Figure 2.3. Simplified stratigraphic cross-section through the Vent Zone 12
Figure 2.4. Simplified stratigraphic cross-section through the Pit Area 13
Figure 3.1. AFM plot of least altered volcanic rocks at Seneca 61
Figure 3.2. Zr-Ti-Y and Zr-Ti discrimination plots for basalts and basaltic andesites 62
Figure 3.3. TiO_2-(Mn*10)-(P_2O_5*10) geochemical discrimination plot 63
Figure 3.4. Chondrite normalized rare earth element plots for felsic and mafic rocks 64
Figure 3.5. Zr/TiO_2 vs. SiO_2 geochemical discrimination plot 68
Figure 3.6. Harker-type variation diagrams for major elements vs. SiO_2 69
Figure 3.7. Harker-type variation diagrams for selected trace elements vs. SiO_2 70
Figure 3.8. Binary geochemical plots of Al_2O_3 vs. TiO_2 and SiO_2 vs. TiO_2 71
Figure 3.9. TiO_2 vs. Zr and Y vs. Zr plots for least altered felsic data 72
Figure 3.10. Pearce element ratio plots for mafic samples 76
Figure 3.11. Pearce element ratio plots for least altered felsic samples 78
Figure 4.1. Izawa alteration discrimination diagram for felsic rocks 94
Figure 4.2. (2Ca+Na+K)/Zr PER vs. Al/Zr PER plot of felsic data 95
Figure 4.3. Al_2O_3 vs. TiO_2 immobile element binary of for felsic data 100
Figure 4.4. Mobile-immobile element plots of least altered felsic data 106
Figure 4.5. Mass change diagrams for all felsic data 107
Figure 4.6. Summary of mass changes for most strongly altered stockwork samples 109
Figure 4.7. Downhole mass changes for drillholes 91-18 and 91-18 110
Figure 4.8. Downhole mass changes for drillholes 91-10 and 86-13 111
Figure 5.1. Mineral paragenesis diagram for the massive sulphides in the Pit Area 122
Figure 5.2. Graphic geological log of drillhole 91-16 highlighting the stockwork zone 125
Figure 6.1. Variations of silica content time for volcanic glasses, Tonga Platform, SW Pacific 136
Figure 6.2. REE patterns of rocks from Seneca and Miocene volcanic suites (Lau Basin & Baja) 138
Figure 6.3. REE patterns of volcanic rocks from Seneca and Medicine Lake, California 141
Figure 6.4. REE patterns of volcanic rocks from Seneca and Hokuroku Basin, Japan 144
Figure 6.5a. Schematic illustration of the early stages in the formation of the Seneca sequence 147
Figure 6.5b. Schematic illustration of the later stages in the formation of the Seneca sequence 148
Figure 6.6. Schematic model for the formation of hydrothermally altered stockwork zones 149
Figure A.1. Location map of sampled drillholes 165
Figure C.1. Measured vs. accepted element concentrations for MDRUstandard ALB-1 190
Figure C.2. Measured vs. accepted element concentrations for MDRUstandard P-1 191
Figure C.3. Measured vs. accepted element concentrations for MDRUstandard QGRM-100 192

Figure C.4. Plots of major element concentrations for duplicate samples 194
Figure C.5. Plots of selected trace element concentrations for duplicate samples 195

LIST OF PLATES

Plate 2.1a: Footwall Interval - basaltic lava erupted subaqueously by lava fountaining 14
Plate 2.1b: Seneca Horizon - coarse grained, debris flows 14
Plate 2.2a: Seneca Horizon - Ore zone conglomerate (OZC) 15
Plate 2.2b: Seneca Horizon - basaltic andesite intrusion 15
Plate 2.3a: Hangingwall Interval - Rhyodacite flows 16
Plate 2.3b: Hangingwall Interval - Volcaniclastic siltstone and sandstone 16
Plate 2.4a: Basaltic lava - 'fire fountain debris' 21
Plate 2.4b: Volcaniclastic turbidites 21
Plate 2.5a: Block lapilli tuff unit ('BLT') 26
Plate 2.5b: Coarse felsic fragmental units 26
Plate 2.6a: Pumiceous beds 30
Plate 2.6b: Peperites - sill-sediment contact interactions 30
Plate 2.7: Drillcore samples of synvolcanic intrusions 32
Plate 2.8a: Feldspar-porphyritic (FP) intrusions 33
Plate 2.8b: Quartz-feldspar-porphyritic (QFP) intrusions 33
Plate 3.1a: Photomicrograph of basaltic lava 41
Plate 3.1b: Photomicrograph of vesicular glassy rhyolitic lava 41
Plate 3.2a: Photomicrograph of classic perlite in rhyodacitic glass 43
Plate 3.2b: Photomicrograph of banded perlite in rhyodacitic flow 43
Plate 3.3a: Photomicrograph of crystal-rich volcaniclastic sandstone 45
Plate 3.3b: Photomicrograph of fiamme in coarse grained debris flow 45
Plate 3.4a: Photomicrograph of heterolithic breccia 46
Plate 3.4b: Photomicrograph of bedding contact between reworked basaltic hyaloclastite 46
Plate 3.5: Photomicrographs illustrating the typical glassy fragmental textures of ashes 47
Plate 3.6a: Photomicrograph of volcaniclastic siltstone/ash 48
Plate 3.6b: Photomicrograph of pyritic lamination in volcaniclastic ash 48
Plate 3.7a: Photomicrograph of basaltic andesite 50
Plate 3.7b: Photomicrograph of peperitic basaltic andesite sill 50
Plate 3.8a: Photomicrograph of typical FP dacite intrusion 51
Plate 3.8b: Photomicrograph of rhyodacite FP intrusion 51
Plate 3.9a: Photomicrograph of spherulitic groundmass of a QFP intrusion 53
Plate 3.9b: Photomicrograph of QFP rhyolite intrusion 53
Plate 3.10: Photomicrograph of group A felsic unit 54
Plate 3.11a: Photomicrograph of group C felsic unit 55
Plate 3.11b: Photomicrograph of group D felsic unit 55
Plate 4.1a: Drillcore sample of intensely silicified and sericitized rhyodacite breccia 90
Plate 4.1b: Altered and mineralized basaltic fire fountain debris 90
Plate 4.2a: Photomicrograph of a moderately altered FP rhyodacite 91

Plate 4.2b: Photomicrograph of an intensely hydrothermally altered FP rhyodacite 91
Plate 4.3a: Photomicrograph of a strongly quartz-sericite altered felsic rock 112
Plate 4.3b: Photomicrograph of a strongly quartz-sericite altered felsic rock 112
Plate 4.4a: Photomicrograph of a strongly sericite-chlorite-quartz altered felsic rock 113
Plate 4.4b: Photomicrograph of a strongly sericite chlorite altered felsic rock 113
Plate 5.1a: Representative samples of the mineralized ore zone conglomerate (OZC) 118
Plate 5.1b: Photomicrograph of massive sulphides and barite in the upper part of the OZC 118
Plate 5.2a: Photomicrograph of massive sulphides and barite from OZC 119
Plate 5.2b: Photomicrograph of Sample 85-03-104 massive sulphides and barite 119
Plate 5.3a: Grab sample from the Vent Zone stockwork outcrop 123
Plate 5.3b: Drillcore samples from DDH 86-28 in the Vent Zone 123
Plate 5.4: Representative drillcore samples from the Fleetwood Zone stockwork 126
Plate 5.5a: Mineralized flow breccia from a Fleetwood Zone stockwork (DDH 91-18) 127
Plate 5.5b: 33-Zone massive sulphides 127

ACKNOWLEDGMENTS

I would like to thank a number of people who have contributed their time and personal expertise to the completion of this study. Dr. John Thompson provided excellent supervision and guidance over the course of the project and was extremely helpful in keeping the project focussed without causing me any undue stress. (John's assistance on the soccer field was also greatly appreciated.) I cannot thank Tim Barrett enough for his help during this study. His expert insights, friendly attitude and willingness to discuss at whatever length required virtually any subject from volcanology and lithogeochemistry to baseball, hockey (Go Habs Go !) and Phylum Cephalopoda, interspersed with the occasional attempt to play snooker made this a much more pleasurable project to complete. I also wish to thank Dr. Kelly Russell and Dr. Alastair Sinclair for their guidance. Dr. Russell's edits greatly improved the validity and flow of the text. Rod Allen provided excellent input on volcanic textures and facies interpretations. Julia Matsubara provided assistance in the field. I would also like to thank other people at MDRU and UBC - Ross Sherlock, Rob Macdonald, Chris Sebert, Sonya Tietjen, Arne Toma, Fiona Childe and Brian Mahoney - for helpful discussions, input, and general assistance during the last couple of years.

Inmet Mining Corp. (formerly, Metall Mining), and in particular Colin Burge and Gary Wells, supplied maps, sections and access to drillcore at the Seneca property which provided the groundwork for the project. Funding for this study was provided by the Mineral Deposit Research Unit (MDRU) as part of the *Volcanogenic Massive Sulphide Deposits of the Cordillera* project. Financial support was given to MDRU by eleven member companies, the Science Council of British Columbia and by a Natural Science and Engineering Research Council (NSERC) grant.

I would also like to thank a number of people who provided moral support and kept me relatively sane during the course of this project. I thank my family members - Mom, Dad, Kelly and Conor - for providing constant support and encouragement. Thanks also to all my friends - Rob, Theresa, Leslie, Gwyn, Shannon, Hamish and Bill to name a few - for their support, sympathetic ears and general entertainment.

DEDICATION

This thesis is dedicated to the memory of Johanna Marie Goldthorpe, my best friend and confidante and fellow geologist, who tragically passed away in September, 1992. Johanna's support and confidence in me provided me with the incentive to pursue my Master's degree and without which I may not have undertaken this project. Memories of Johanna's love of life and cheerful outlook have been a constant source of inspiration. I will remember you always.

CHAPTER 1
INTRODUCTION

The Seneca property in southwestern British Columbia is located approximately 120 kilometres east of Vancouver (Figure 1.1). The property is accessible from the Lougheed Highway at Harrison Mills by the Morris Valley Road and the Chehalis-Fleetwood logging road.

The property has been described as a zinc-copper-lead-barite volcanogenic massive sulphide environment similar to the Kuroko-type deposits (Urabe et al., 1983). Current geological reserves are estimated at 1.5 million tonnes grading 3.57% zinc, 0.63% copper and 0.15% lead (Hoy, 1991). Mineralization occurs as massive and matrix-filling sulphides associated with volcaniclastic sediments and as stockwork-style stringer and massive sulphides hosted in a sequence of felsic to intermediate volcanic rocks of the Harrison Lake Formation (McKinley et al., 1995).

1.1 SCOPE OF STUDY

This study constrains the spatial, temporal and geochemical relationships of the lithological units in the study area, the mineralization and the accompanying alteration within the volcanic sequence that hosts the Seneca deposit. Surface exposure on the property is poor and diamond drillcores were used almost entirely to infer relationships and the distributions of the various volcanic facies. The distribution of drillholes on the property is sufficient to allow adequate observation of vertical and lateral facies changes. However, the use of drillcores allows only limited interpretation of structural elements, namely the strikes of faults, dikes and bedded volcaniclastic units. The varying depths of the drillholes in different parts of the property also restricted the study to a 200 to 450 m thick portion of the volcanic sequence. Forty drillholes were logged in detail, and on the basis of igneous textures and contact relationships, extrusive lavas and synvolcanic intrusions were differentiated; clast size and

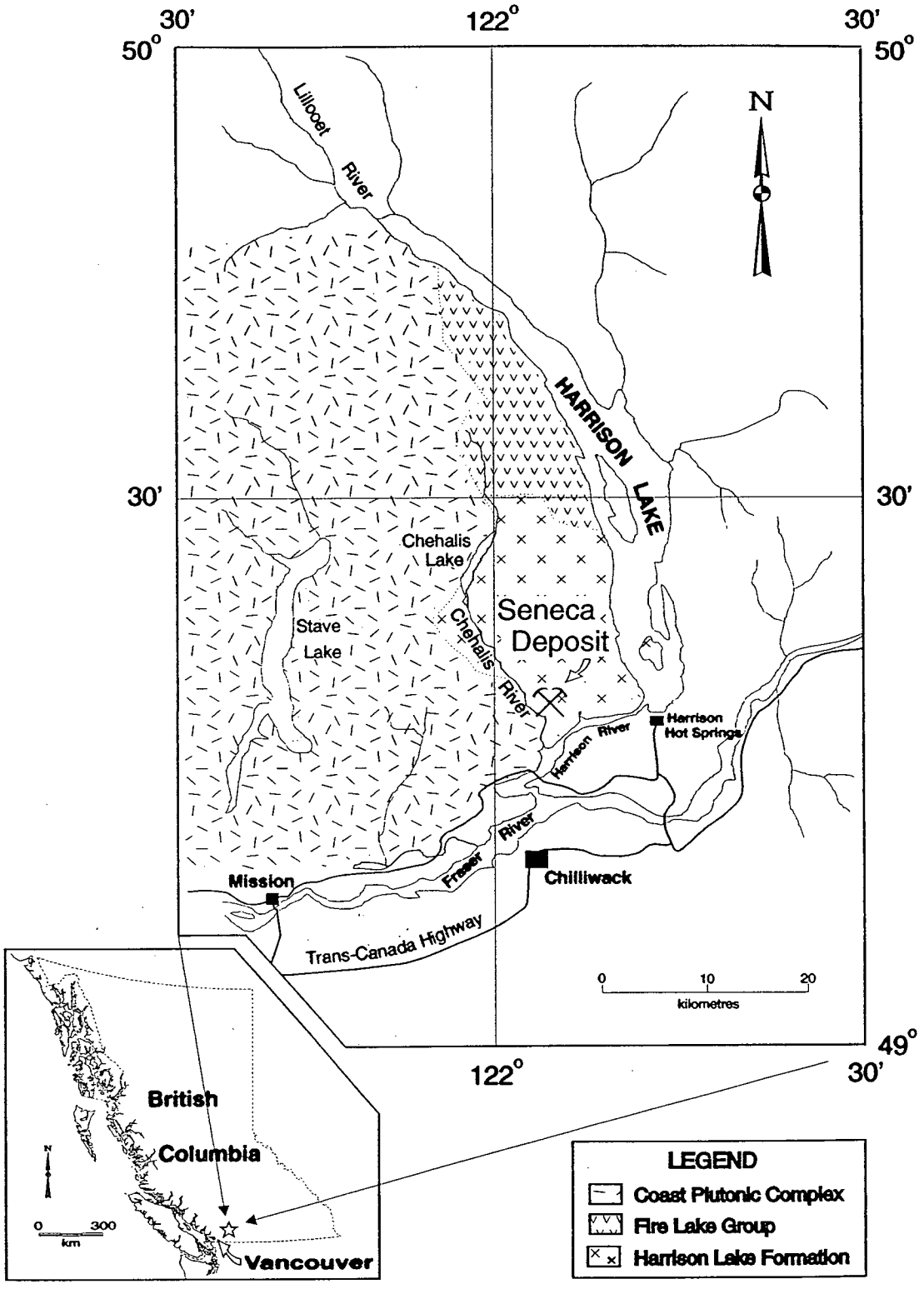

Figure 1.1. Location map of the Seneca deposit showing a simplified geology of the area west of Harrison Lake (modified after Thompson, 1972; geology modified after Journeay and Csontos, 1989).

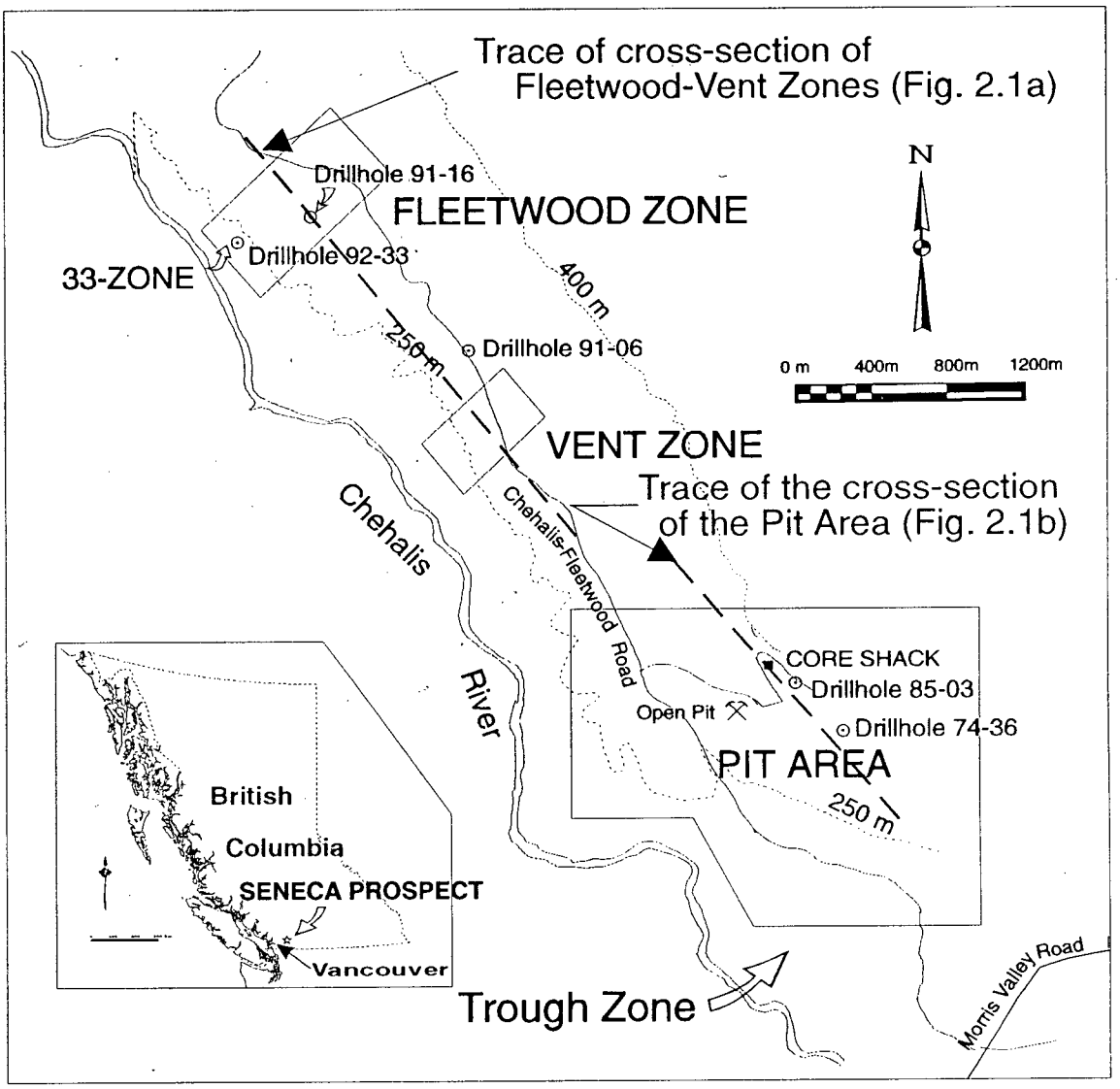

Figure 1.2. Map of the Seneca property showing the locations of the different zones described in the study and the surface traces of the geological cross-sections shown in Figure 2.1.

compositional variations among the volcaniclastic units were used to track volcano-sedimentary facies changes.

Major, trace and rare earth element geochemical data are used in this study to infer the tectonic affinity, possible genetic relationships and the effects of hydrothermal alteration among the volcanic rocks in the study area.

1.2 TERMINOLOGY

The volcanic stratigraphy at the Seneca property, like other volcanic belts, is quite complex and varied. Since there is such a wide variety of different lithologies present, naming the units by simple conventional classification schemes, such as that of Fisher (1966), does not do justice to the many compositional and textural variations observed. This is especially true for the volcaniclastic rocks which show extreme variation. As such the volcanic rocks in this study are described using non-genetic, yet descriptive, terminology and are interpreted using the volcanic 'facies architecture' approach as outlined by Allen (1993) and by McPhie and Allen (1992).

The term 'vent' is used in this study to refer to a volcanic centre or feeder. However, the same term can also be used to describe a centre for hydrothermal activity; this is the case for origin of the name of the Vent Zone at Seneca. When describing facies relationships, however, terms such as vent-proximal are in reference to a volcanic vent.

The Seneca property is subdivided into four different areas. From northwest to southeast, these different zones have been named the Fleetwood Zone, the Vent Zone, the Pit Area and the Trough Zone (Figure 1.2) each of which comprise different combinations of lithologies and volcanic facies and styles of mineralization and alteration.

1.3 PROPERTY HISTORY

The Seneca Prospect, formerly known as the Lucky Jim property, was discovered in 1951 as an indirect result of logging operations and was optioned by Noranda Exploration Company at that time (Thompson, 1972). The sulphide mineralization was believed to be part of a steeply dipping vein or shear system. In 1961 stripping, trenching, and some underground work were carried out, but the results were not encouraging. The property was held by Noland Mines, Ltd. from 1964 to 1965 and was bought by Zenith Mining Corporation, Ltd. in 1969. Cominco Ltd. optioned the property in 1971 and carried out further exploration based on the concept that the zone represented Kuroko-style conformable mineralization. The property was acquired by Chevron Standard Ltd. in 1977 and further diamond drilling was completed over the next ten years in joint ventures with International Curator Resources Ltd. and B.P. Canada Inc. Further logging in the area indirectly led to the discovery in 1986 of the Vent zone stockwork mineralization 1.75 kilometres to the west of the original discovery. In 1991 drilling by Minnova, Inc. (subsequently Metall Mining Corp., and now Inmet Mining Corp.), 1 kilometre to the west of the Vent zone, led to the discovery of the Fleetwood zone. In 1992, further drilling in that area intersected the 33-zone massive sulphides. The property is currently held by International Curator Resources Ltd. of Vancouver, British Columbia.

1.4 REGIONAL GEOLOGY

1.4.1 HARRISON TERRANE

The Harrison Terrane on the west side of Harrison Lake is a sequence of Triassic to Cretaceous volcanic and sedimentary rocks adjacent to Upper Jurassic quartz diorite batholiths situated to the west of the property. The terrane is bounded to the east by the Harrison Fault, a major structural feature juxtaposing the highly deformed and metamorphosed rocks east of the fault with the relatively

undeformed rocks west of Harrison Lake (Arthur, 1986). Arthur et al. (1993) suggest that the Middle Jurassic volcanic rocks of this belt are correlative with the Wells Creek volcanics of Washington and perhaps the Bowen Island Group to the west near Vancouver.

1.4.2 HARRISON LAKE FORMATION

The Harrison Formation is a Lower to Middle Jurassic succession that strikes north-northwest, with gentle to moderate easterly dips and which may be up to 2500 metres thick (Monger, 1970; Mahoney, 1994). From oldest to youngest, the Harrison Lake Formation is composed of the Celia Cove Member, the Francis Lake Member, the Weaver Lake Member and the Echo Island Member (Arthur, 1986; Mahoney, 1994). This sequence is overlain by Upper Jurassic to Lower Cretaceous conglomerates of the Fire Lake section (Figure 1.1; Journeay and Csontos, 1989). Mahoney et al. (1995) describe the Harrison Lake Formation as a volcanic arc having a medium to high-K, calc-alkaline affinity and having Nd and Sr isotope values which suggest a relatively juvenile magmatic system derived from a slightly enriched mantle wedge.

The Celia Cove Member comprises mostly deep water sedimentary rocks unconformably overlying the Middle Triassic age argillites, sandstones, tuffs and volcanic flows of the Camp Cove Formation. Arthur at al. (1993) propose that these rocks formed part of the western margin of a Triassic ocean basin represented by the Bridge River-Hozameen assemblage to the east. Early and Late Toarcian ammonites have been collected from a calcareous argillite above and below a volcanic flow within the Francis Lake Member (Arthur, 1986). This flow may represent the onset of the volcanism that characterizes the Harrison Lake Formation.

Regionally the Weaver Lake Member is dominated by intermediate to felsic volcanic rocks and related intrusions (Mahoney, 1994). This voluminous unit covers an area of approximately 10 km from east to west (from Harrison Lake in the east to the Chehalis River valley in the west) and 15 km

north to south (from Mount McRae in the north to the Harrison River in the south). The composition of the flows and related breccias and tuffs vary from basalt and basaltic andesite to rhyodacite. Volcaniclastic rocks are plentiful and vary from fine ashes to volcanic breccias. Mahoney (1994) observed an overall change upwards from mafic-dominated volcanic rocks lower in the sequence to felsic-dominated volcanic rocks in the upper parts of the sequence. Although not fully constrained, the predominance of felsic rocks at Seneca property suggests that it is situated within the upper part of the Weaver Lake Member.

The Echo Island Member, which outcrops to the north and south of the Weaver Lake Member and on Echo Island in Harrison Lake, comprises mostly finely-banded volcaniclastic sediments and argillites with minor plagioclase-porphyritic flows (Arthur, 1986; Mahoney, 1994). Callovian ammonites in the overlying Mysterious Creek Formation suggest that the Echo Island Member may be Bajocian or Bathonian (Arthur, 1986).

1.4.3 GEOCHRONOLOGY

A sample of a rhyolite dome complex from the upper part of the Weaver Lake Member on Echo Island was analysed using U-Pb zircon dating and has an estimated age of 166 ± 0.4 Ma (Mahoney et al., 1995). A sample of a quartz feldspar porphyry stock was dated by U-Pb at 165.9 +6.4/-0.3 Ma (Monger, 1987, as cited by Mahoney et al., 1995). The Harrison Lake Formation is intruded by the Mt. Jasper pluton, a tonalite/granodiorite intrusion which yields a 167 ± 4 Ma U-Pb zircon age (Friedman and Armstrong, 1994). Mahoney et al. (1995) report that the rhyolite dome complex from Echo Island and the quartz feldspar stock have similar Nd and Sr isotopic values which, while also considering their similar ages, suggests that they may be comagmatic and that the granitoid rocks are subvolcanic roots to the Middle Jurassic volcanic rocks of the Harrison Lake Formation.

1.4.4 STRUCTURE AND METAMORPHISM

Structural interpretations are limited by poor outcrop in the study area. The Harrison Lake Formation is deformed, forming a broad, west-northwest trending, shallowly plunging anticline (Pearson, 1973; Arthur, 1987; Mahoney et al., 1995). The structure in the area around the south slope of Mount Keenan, which includes the study area, is described as a southwestward-dipping homocline (Thompson, 1977). The contrasting structural styles between the Harrison Lake Formation and the overlying Mysterious Creek Formation suggests a compressional event in the region in Early Bathonian to Early Callovian time (ca. 165 to 160 Ma; Mahoney et al., 1995). Penetrative fabrics are absent in the study area and throughout the entire Harrison Lake Formation except for a narrow zone adjacent to the Harrison Fault (Thompson, 1972; Journeay and Csontos, 1989).

There is little evidence of metamorphism of the rocks in the study area. Zeolites are present in some of the flows at Seneca, but it is unclear if they are simply amygdules or the result of low grade metamorphic recrystallization. Journeay and Csontos (1989) describe the metamorphism of the entire Harrison Lake Formation as sub-greenschist facies.

CHAPTER 2
GEOLOGY OF THE SENECA DEPOSIT

2.1 INTRODUCTION

The major lithologic units at Seneca are subdivided on the basis of their proximity to their primary source, which is in this case a volcanic centre or vent(s). The four principal volcanic facies are described as follows:

- *Facies 1* - Vent to vent-proximal facies: Lavas consisting of basaltic to rhyolitic composition flows, domes and associated in situ hyaloclastites and autoclastic breccias;
- *Facies 2* - Vent-proximal to distal facies: Volcaniclastic rocks consist of juvenile to reworked coarse volcanic breccias and tuffs to fine grained siltstones and ashes; and
- *Facies 3* - Coeval Intrusions: Intrusions consist of basaltic to rhyolitic composition sills and dykes that have intruded lavas and wet volcaniclastic sediments.
- *Facies 4* - Distal Marine: Rocks of volcano-sedimentary origin consisting of an argillite that often contains flattened feldspar (± quartz)-phyric pumice clasts (fiamme).

Facies 1 to 3 are generally observed in all drillholes, but their relative abundances vary greatly from hole to hole, often over small distances, thus making correlation on the basis of facies difficult. The fourth facies is often in close proximity to mineralization and is spatially restricted to the Pit Area and the Trough zone and does not correlate to other parts of the property. Observations in drillcore suggest that strata on the property strike approximately to the northwest and are essentially flat lying or moderately dipping in an easterly direction.

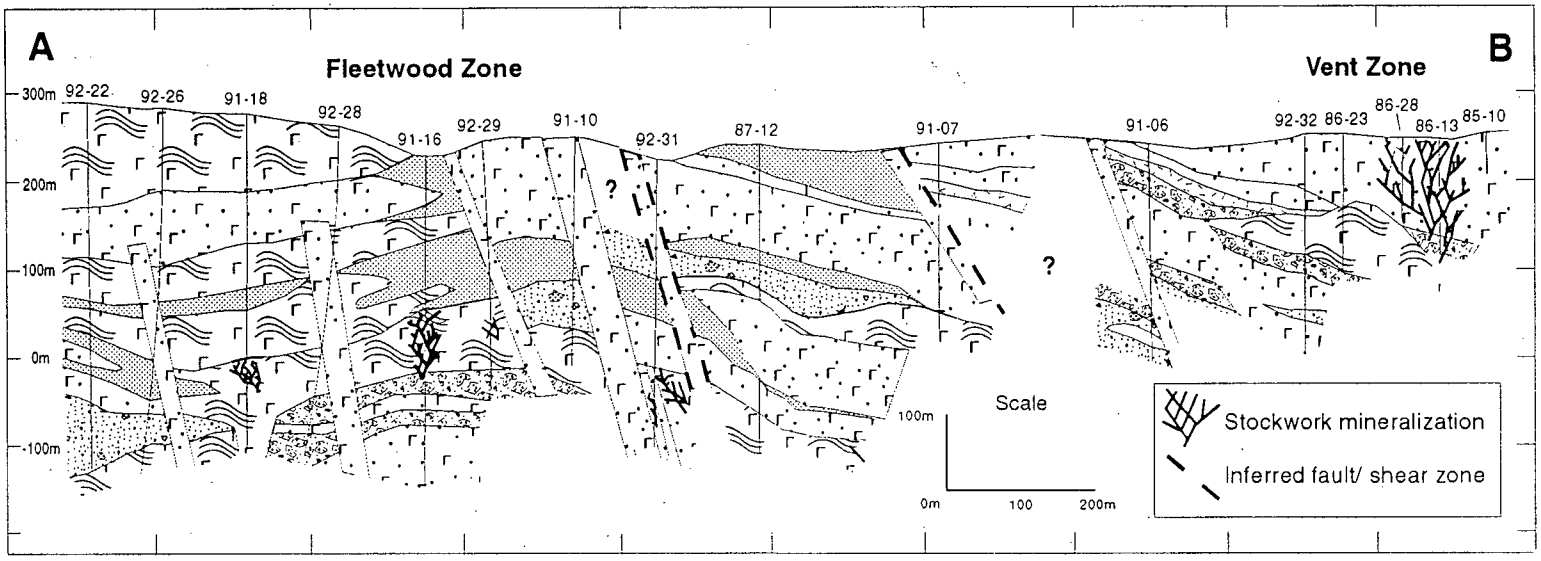

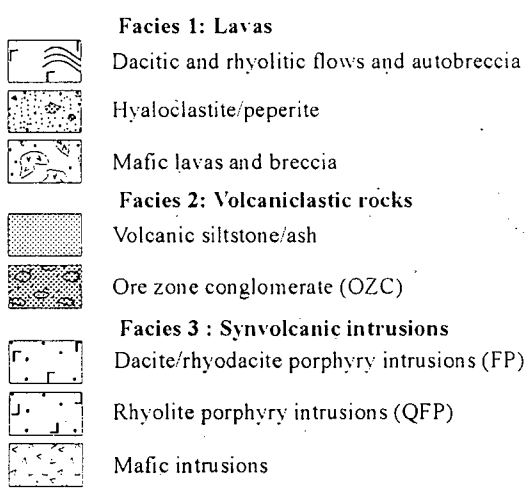

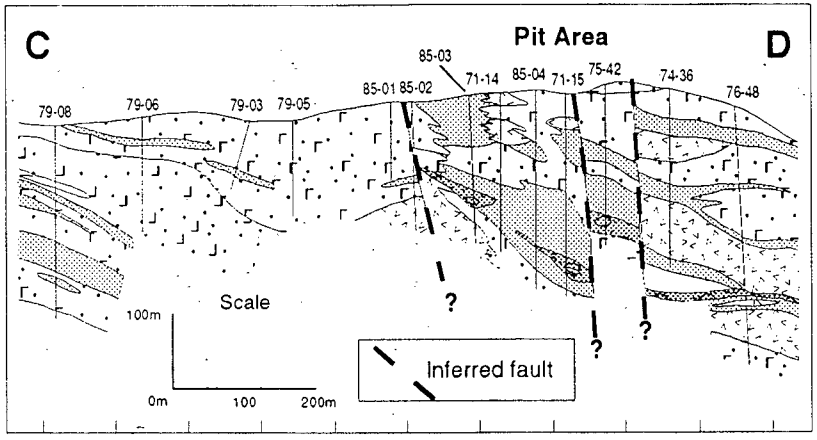

Figure 3. Geological cross-sections through the Seneca property illustrating the geology and volcanic facies distribution of the Fleetwood-Vent Zone and the Pit Area. Locations of these sections are shown in Figure 2.

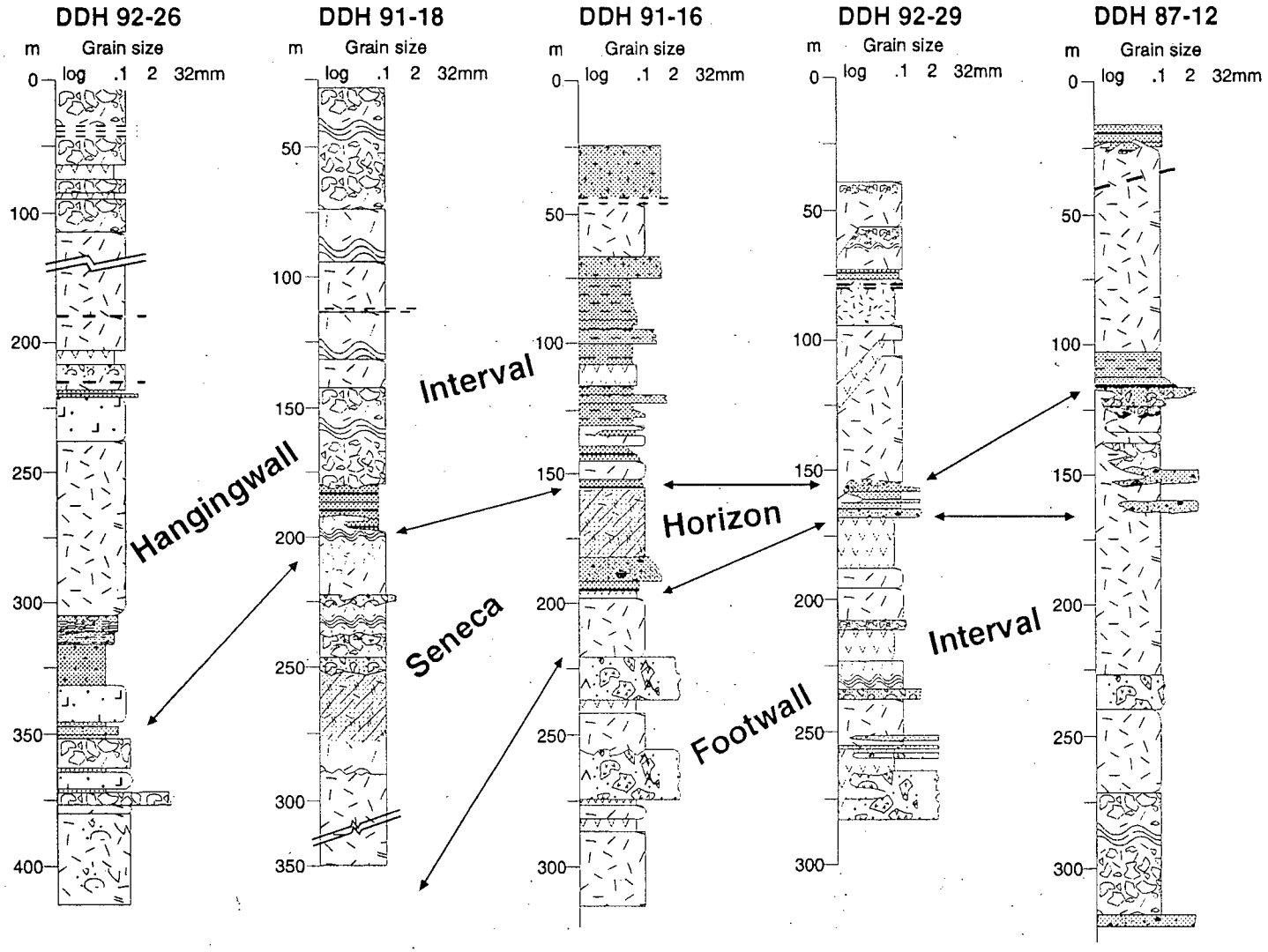

Figure 4. Simplified stratigraphic cross-section through the Fleetwood Zone showing detailed pictorial logs of selected drillholes. Volcanic facies distributions and correlations of the three stratigraphic intervals are illustrated. Actual drillhole locations are shown on Figure 3. Legend is the same as in Figure 3.

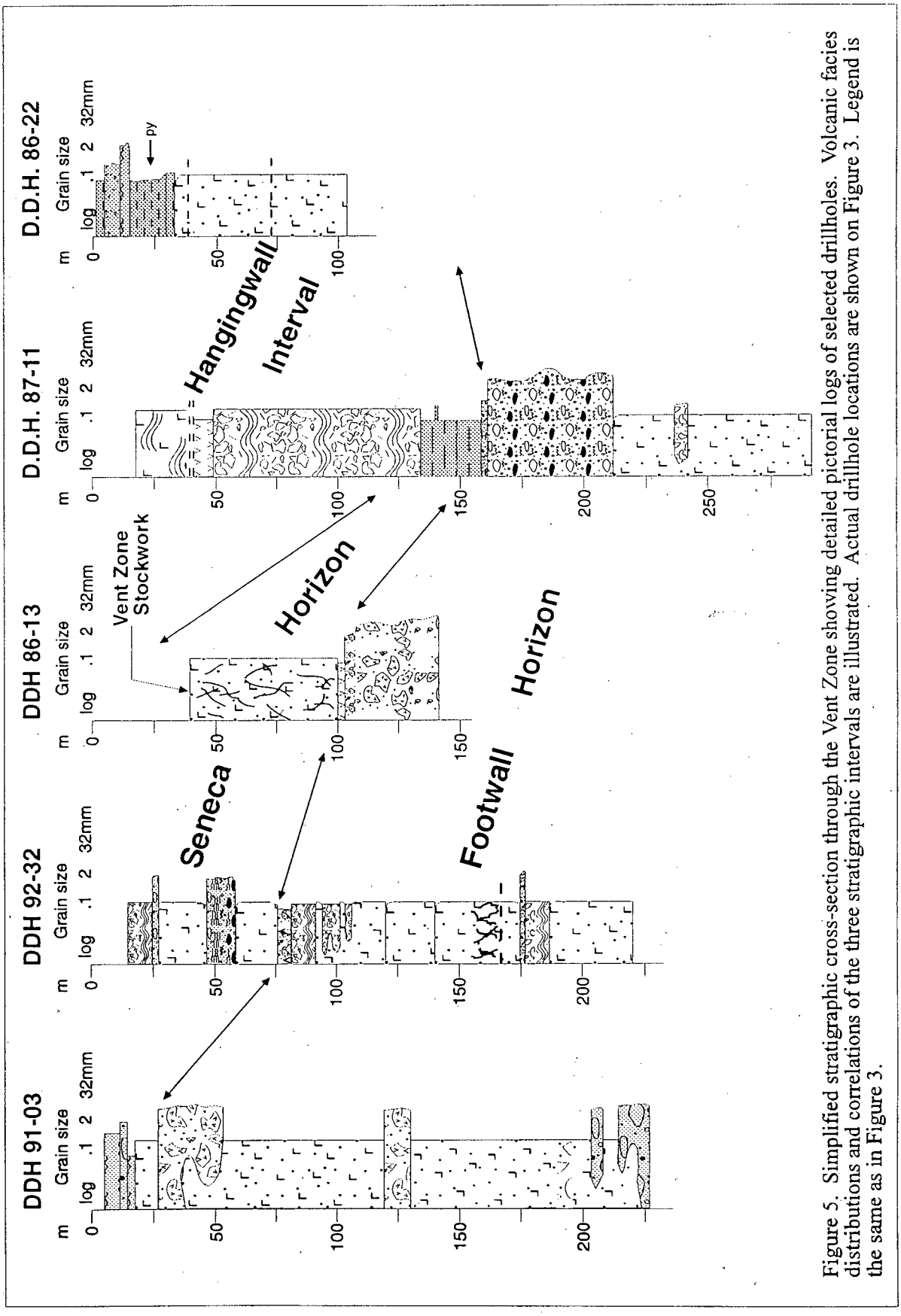

Figure 5. Simplified stratigraphic cross-section through the Vent Zone showing detailed pictorial logs of selected drillholes. Volcanic facies distributions and correlations of the three stratigraphic intervals are illustrated. Actual drillhole locations are shown on Figure 3. Legend is the same as in Figure 3.

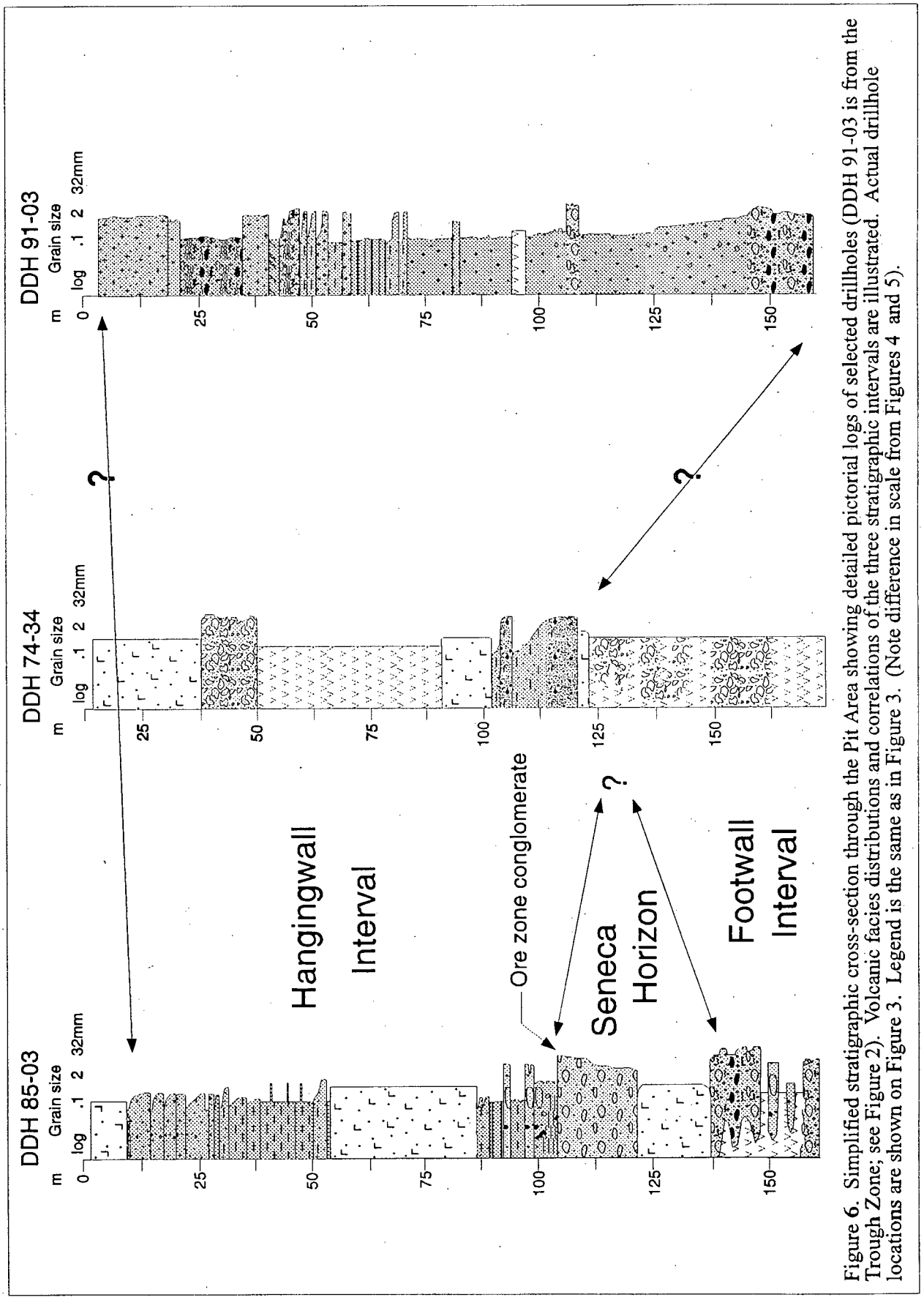

Figure 6. Simplified stratigraphic cross-section through the Pit Area showing detailed pictorial logs of selected drillholes (DDH 91-03 is from the Trough Zone; see Figure 2). Volcanic facies distributions and correlations of the three stratigraphic intervals are illustrated. Actual drillhole locations are shown on Figure 3. Legend is the same as in Figure 3. (Note difference in scale from Figures 4 and 5).

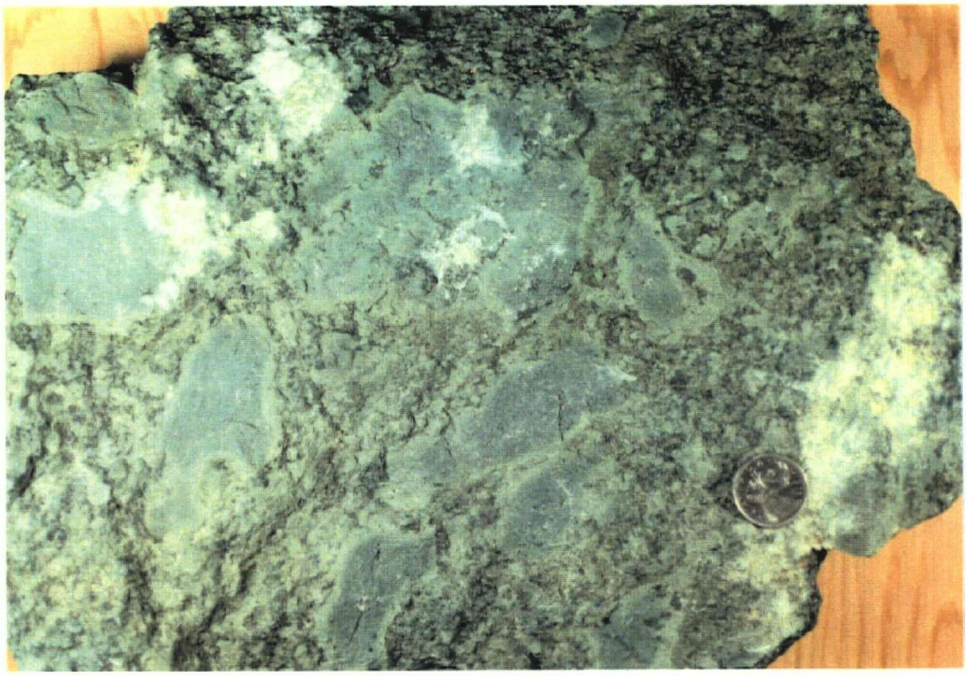

Plate 2.1a: Footwall Interval - basaltic lava erupted subaqueously by lava fountaining (Sample 94-FF-01). This rock consists of amoeboid lava clasts with lighter green (chloritized) chilled margins in a matrix of chloritized hyaloclastite which has spalled off the clasts by quench fragmentation. Sample was collected at Morris Creek to the southeast of the Seneca property.

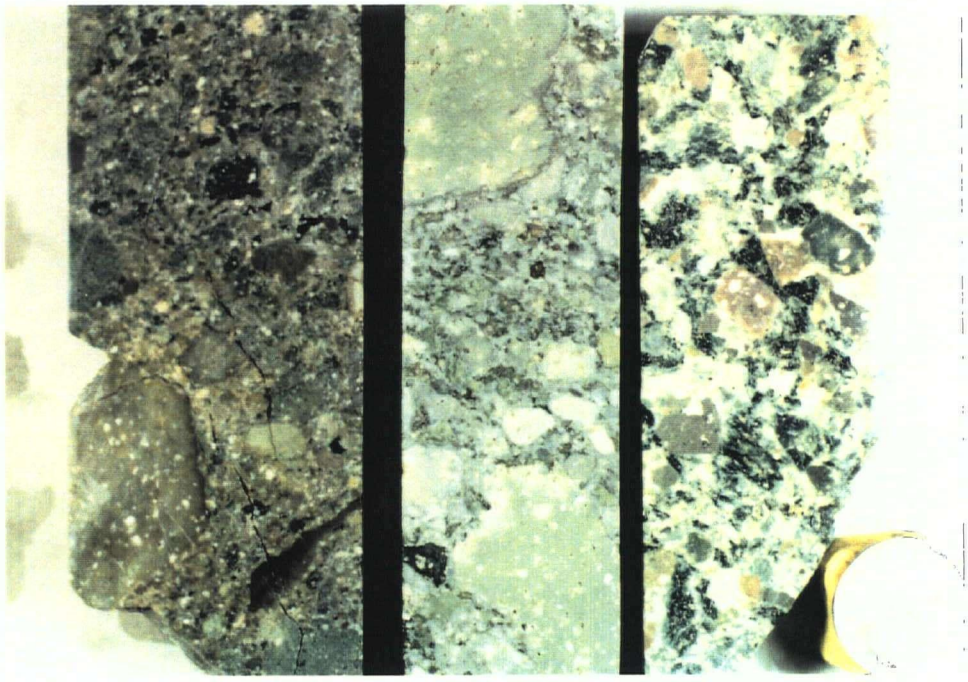

Plate 2.1b: Seneca Horizon - coarse grained, debris flows. These rocks are associated with mineralized zones and are dominated by poorly sorted dacitic and rhyolitic lava clasts (often variably altered), vitric clasts (dark green) and sandy material. Mafic clasts are sometimes present.

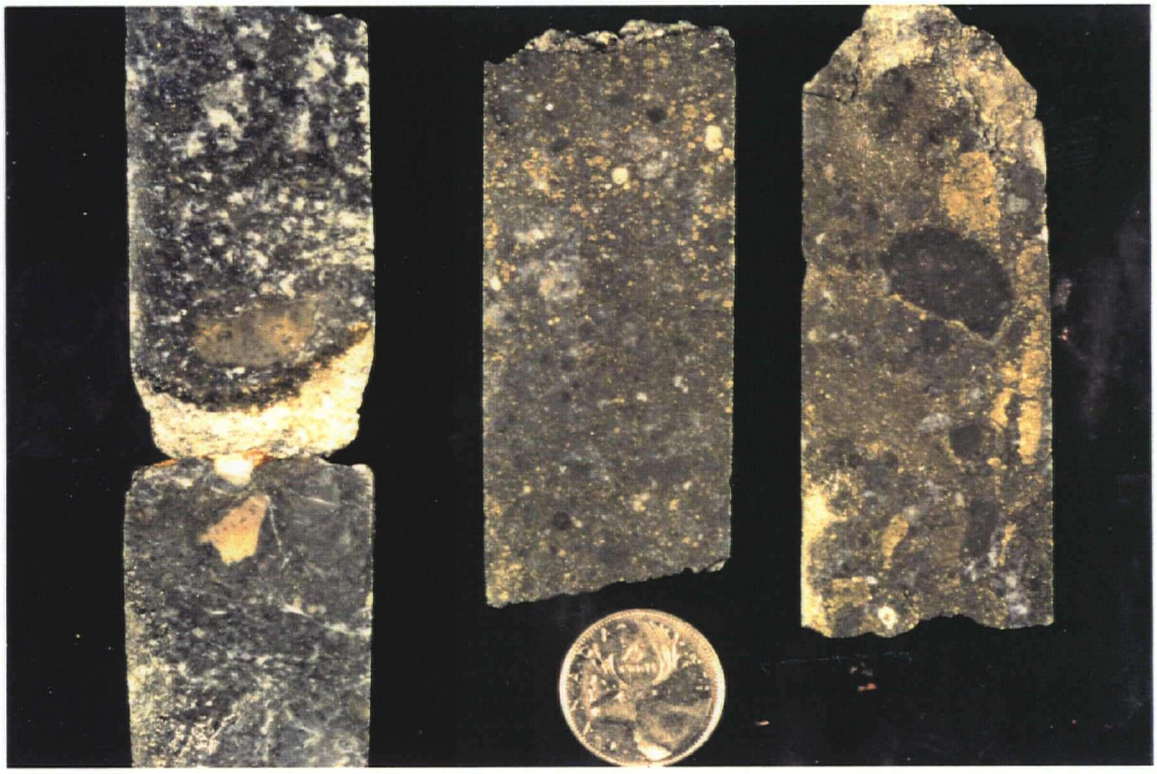

Plate 2.2a: Seneca Horizon - Ore zone conglomerate (OZC). This unit consists of subangular to subrounded felsic clasts of sand to pebble size that have been strongly sericitized and silicified. This unit hosts disseminated matrix-filling sulphides to massive mineralization (pyrite-sphalerite-chalcopyrite-galena).

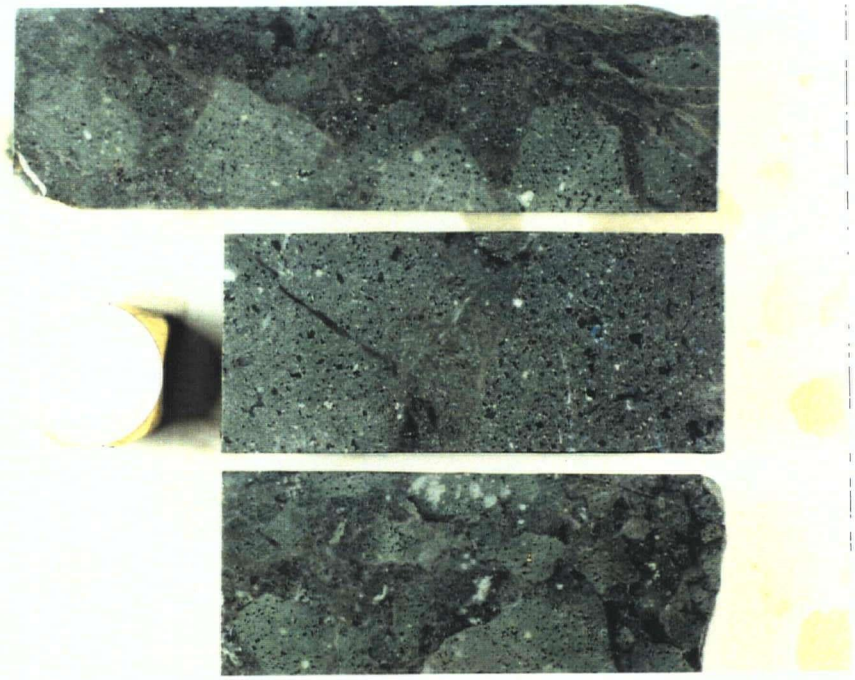

Plate 2.2b: Seneca Horizon - basaltic andesite intrusion. These rocks are often associated with the OZC in the Pit Area. They are intruded as narrow sills that often display peperitic textures as shown in these photos, and incorporate clasts of the units they intrude.

Plate 2.3a: Hangingwall Interval - Rhyodacite flows. This unit is common in the Fleetwood and Vent Zones. The rocks consist of massive to autobrecciated feldspar±quartz-phyric lavas often forming thick flow-flow breccia and flow-dome sequences up to 100 metres thick. Flow banding is accentuated by variable silicification and chloritization. Samples are from DDH 87-11 east of the Vent Zone

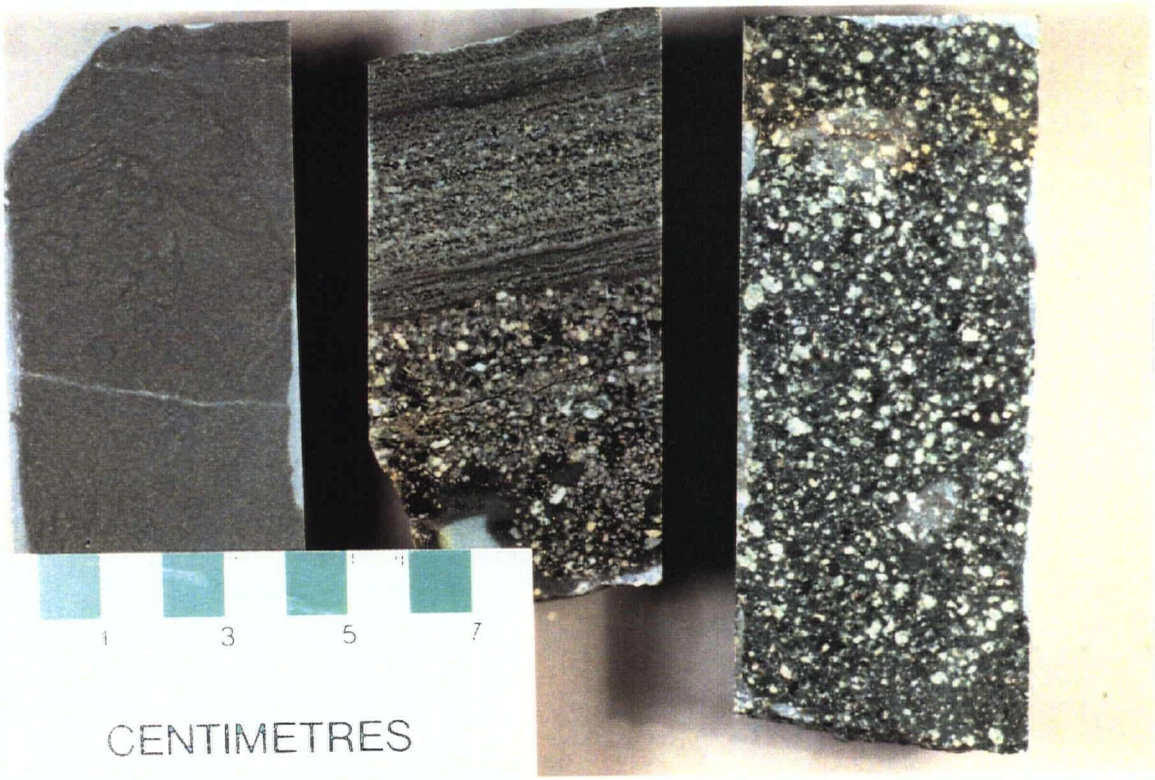

Plate 2.3b: Hangingwall Interval - Volcaniclastic siltstone and sandstone (DDH 85-03). The sample to the left consists of massive volcanic ash; the centre sample is well-bedded crystal-rich volcanic sandstone; the sample to the right is a massive bed of vesicular dacite lava clasts and hyaloclastite. These units were deposited by gravity settling and as turbidites derived from the flanks of a volcanic edifice or from pyroclastic eruptions.

2.2 DISTRIBUTION OF VOLCANIC FACIES

Figure 2.1 illustrates the distribution of the three principal facies along two northwest to southeast trending longitudinal sections across the property. The sections are continuous except for a 500 m separation where there is no drillhole coverage. Distinct marker units are not evident, but at least three packages of distinct lithologies and facies are identified at specific stratigraphic and are correlatable across the Seneca property (Figures 2.2 to 2.4). Each of these horizons comprises varying proportions of all three volcanic facies, but each horizon has a particular unit, or sub-facies, or a facies association making it unique. The three horizons are named on the basis of their positions relative to the mineralized zones and are, from stratigraphically lowest to highest: the Footwall Interval, the Seneca Horizon and the Hangingwall Interval.

2.2.1 FOOTWALL INTERVAL

The Footwall Interval is characterized by the presence of mafic lavas and breccias (Plate 2.1a), or by the presence of coarse volcaniclastic units having a mafic component that has been derived from these mafic lavas. Synvolcanic sills and dikes (Facies 3) of dacitic to rhyolitic composition are common. Felsic flows and volcaniclastic units are also present, but are much less common than the other units. Due to its position stratigraphically below the main mineralized zones, the Footwall Interval hosts some minor mineralization in the form of disseminated and stringer sulphides. Localized areas of strong hydrothermal alteration are present, but overall the horizon is only weakly to moderately altered.

The Footwall Interval is best exposed in drillcores from the Fleetwood and Vent Zones which generally penetrate deeper into the sequence than drillcores from the Pit Area. True extrusive mafic lavas, or 'fire fountain debris', distinguished by their hydroclastic fragmental textures, were observed in the lowermost portions of drillcores in the Fleetwood and Vent Zones, but were not observed in the

Pit Area. An outcrop of the texturally distinct fire fountain debris exists several kilometres to the southeast of the Seneca property at a stratigraphically similar position suggesting that the mafic lavas may be a regionally extensive unit. The last, or uppermost, occurrence of this mafic unit marks the upper boundary of the Footwall Interval.

2.2.2 SENECA HORIZON

The Seneca Horizon hosts all major sulphide mineralized zones on the property. It is thinner and more discontinuous than the two other horizons and is comprised of felsic flows and flow breccias, poorly-bedded, coarse grained, felsic-dominated volcaniclastic units as well as felsic, and lesser mafic, synvolcanic intrusions. The base of the horizon is commonly marked by a moderately to poorly sorted volcanic breccia or debris flow unit dominated by angular to subround feldspar-phyric clasts and lesser mafic clasts (Plate 2.1b). Mafic lavas are uncommon in this horizon and coarse-grained volcaniclastic debris flows are more prevalent than well-bedded volcaniclastic siltstones and turbidites. The Seneca Horizon includes the sequence of rocks overlying the uppermost occurrence of mafic lavas and which underlies the lowermost occurrence of dominantly fine-grained volcaniclastic units. Alternatively, the Seneca Horizon is marked by the presence of stockwork and semi-massive sulphides (pyrite-sphalerite-chalcopyrite±galena) and associated zones of strong silica and sericite alteration. The former criteria are used when mineralization or strong alteration are absent.

In the Pit Area the Seneca Horizon is characterized by a coarse volcaniclastic unit, termed the ore zone conglomerate (OZC). This unit is texturally distinct from other units. It contains rounded and subrounded felsic clasts, is generally moderately to strongly hydrothermally altered and hosts disseminated to semi-massive sulphides (Plate 2.2a). The OZC is interpreted to be a mass flow unit having a discontinuous sheet-like, or possibly channelized morphology (R. Allen, personal communication). This unit is not present in the Fleetwood and Vent Zones to the northwest, but is

considered part of the Seneca Horizon because of its similar stratigraphic position to the other mineralized zones and its similar relationship with bounding lithologies; the OZC is underlain by felsic volcanic breccias and is overlain by the first, or lowermost, occurrence of well-bedded, finer-grained volcaniclastic siltstones and turbidites. Basaltic andesite commonly intrudes the Seneca Horizon/OZC in the Pit Area. These mafic units are interpreted to be synvolcanic sills based on their massive nature, their common peperitic margins and their lateral continuity (McPhie et al., 1993) (Plate 2.2b). Also commonly associated with the OZC is a thin dark brown to black argillite unit which often contains suspended clasts of rhyolitic pumice.

2.2.3 HANGINGWALL INTERVAL

The Hangingwall Interval comprises essentially all units stratigraphically overlying the mineralized zones of the Seneca Horizon. It is composed almost entirely of dacitic to rhyolitic rocks. Vent to vent-proximal flows and breccias are common in the Fleetwood and Vent Zones (Plate 2.3a); portions of the stockwork zones in these areas are hosted by distinctly banded and brecciated felsic flows. Synvolcanic sills are more prevalent than flows in the Pit Area. The distinctive lithologies common to all areas, however, are well-bedded volcaniclastic turbidites and massive to bedded and laminated gravity-settled volcaniclastic sandstones to siltstones (Plate 2.3b). These units are intercalated with the felsic flows in the Fleetwood-Vent Zones and are intruded by the synvolcanic sills in the Pit Area. Coarser-grained fragmental units are present in the Hangingwall Interval, but they tend to be subordinate to the fine-grained material. This horizon is essentially unaltered and unmineralized, in sharp contrast to the underlying Seneca Horizon.

Trough Zone

Drillhole 91-03 (Figure 2.3) located 1.5 km south of the Pit Area intersects a 150 m thick sequence of uninterrupted Facies 2 volcaniclastic beds - the most continuous section of distal facies

rocks observed at Seneca (Plate 2.4b). The lowermost 75 to 80 m of the drillcore consists of massive, unbedded, but internally normally-graded volcaniclastic sandstone. Bedding was not observed within this interval. Overlying this is a sequence of well-bedded and laminated volcaniclastic turbidites. Some of the fine grained ash/siltstone beds contain suspended 'rafts' of quartz-feldspar-phyric pumice up to 10 cm in diameter, and are intercalated with quartz-feldspar crystal-rich beds. This sequence also contains several thin argillaceous beds. Unlike all other drillcores examined, DDH 91-03 is unique in that no flows or synvolcanic intrusions were intersected. Despite its distance from drillholes in the Pit Area, DDH 91-03 has some notable similarities to parts of the Pit Area stratigraphy. The volcaniclastic units in both areas display an upward transition from poorly-bedded to well-bedded material and show an overall fining-upward trend. Pumiceous clasts and argillaceous beds are also more common in the upper sections of each area. Although no mineralization or hydrothermal alteration was observed in the Trough Zone, it appears to be roughly correlatable with Seneca-Hangingwall Interval observed in the Pit Area drillcores.

2.3 DESCRIPTION OF VOLCANIC FACIES

2.3.1 LAVAS

Lava flows are defined by their contact relationships and the occurrence of flow textures and autobrecciation at their margins.

2.3.1.1 MAFIC LAVAS

Unbrecciated basaltic andesites at Seneca tend to be featureless and without pillow forms; the occurrence of extrusive mafic flows has not been confirmed. However, massive coherent mafic flows are inferred by the presence of stretched amygdules and their association with accompanying autoclastic breccia. A unit that consists of subrounded to amoeboid fragments of vesicular basalt

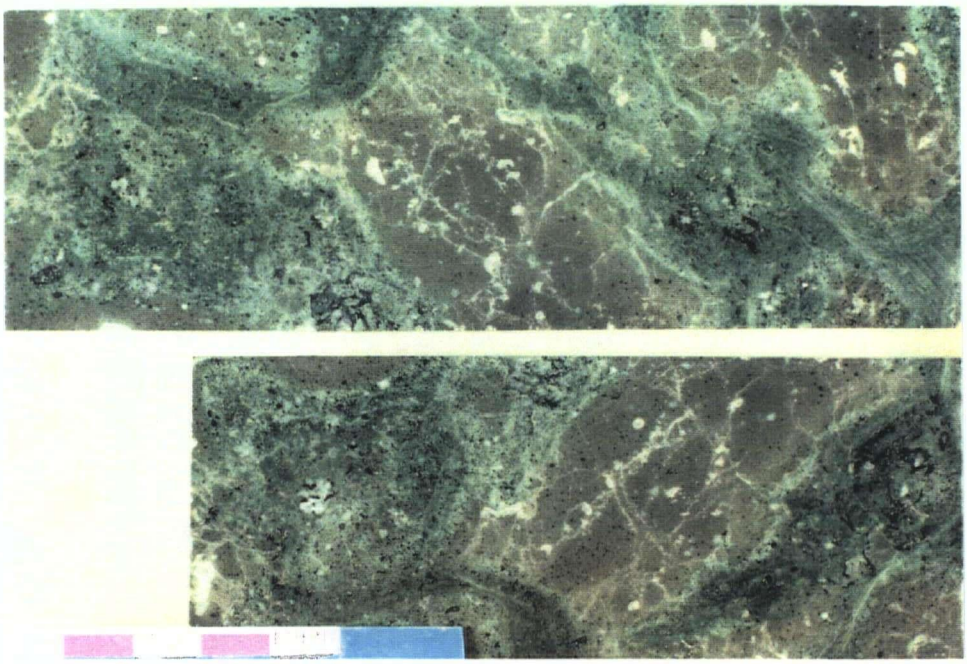

Plate 2.4a: Basaltic lava - 'fire fountain debris'. This unit formed as lava 'fountained' into the water column. This is inferred by the amoeboid-shaped fragments, chilled margins on the clasts and the abundance of quench-derived hyaloclastite in the matrix (dark green). (Large divisions on scale are 1 cm).

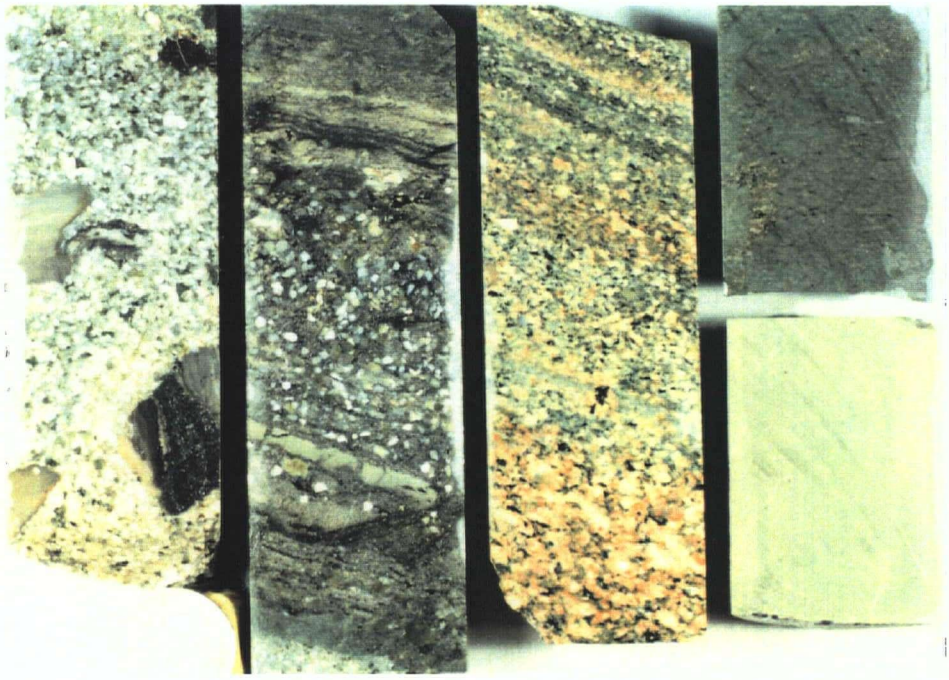

Plate 2.4b: Volcaniclastic turbidites. These samples from left to right represent a top to bottom sequence from DDH 91-03 in the Trough Zone (distal facies). The sample on the right is part of a thick massive, unbedded interval of volcanic sand and ash likely representing a single continuous eruptive event. The three samples to the left are from normal graded beds and are feldspar and quartz crystal-rich. These upper units likely represent the reworking of volcanic debris as turbidites during the waning and post-eruption stages of volcanic activity at that time. The left sample contains silty rip-ups from the underlying bed.

surrounded by angular lava clasts and hyaloclastite (*cf.* Dimroth et al., 1978) occurs in the western part of the property (Plate 2.4a). These fragments are typically 1 to 10 cm in size, are light green or purplish grey in colour and consist of a core of massive basaltic andesite lava with chilled or brecciated rims.

The textures of the fragments together with their amoeboid shape and tail-like ends, suggests that they were ejected in a subaqueous environment (Carlisle, 1963; R. Allen, personal communication). However, the basaltic lava clasts often have irregular shapes and lack the tapered or teardrop-shaped morphologies of molten subaerial ejecta. This unit must be proximal to a vent, as the surrounding angular hyaloclastite has not been greatly reworked. This facies is termed 'fire fountain debris' and is only seen in lower parts of the drillholes in the Fleetwood and Vent Zones. It also outcrops several kilometres southeast of the property beside Morris Lake (sample 94-FF-01) and as large boulders in Sakwi Creek along the Hemlock Valley Road. The drillcores examined in this study generally do not penetrate below this mafic unit and as such the true thickness of the unit has not been determined; observed intersections of the unit indicate a thickness of at least 50 m. Infrequently the upper parts of the unit contain scattered felsic lava clasts indicating that at least a small amount of mixing has occurred between the mafic breccias and adjacent or overlying felsic fragmental units.

2.3.1.2 FELSIC LAVA FLOWS AND DOMES

Dacitic to rhyolitic composition flows and flow domes are more widespread than mafic flows at the Seneca property.

The domes and flows are intruded into and extruded through other lavas, fine-grained volcaniclastic sediments and coarse lava clast breccias (Figure 2.1). Individual felsic flows range from one to several tens of metres thick, and have flow brecciated upper contacts and chilled and/or slightly brecciated lower contacts. The flows and breccias have generally been weakly to moderately silicified,

probably by syndepositional seawater interaction. The silicification often enhances the flow banding by creating alternating lighter and darker bands (Plate 2.3a). The cores of the thicker flows are typically massive or weakly to strongly flow-banded, and are light greyish green in colour. They are often accompanied by a lateral transition from autobreccia to reworked hyaloclastite and volcaniclastic sediments at the margins. Such transitions and associations of coherent lava and hyaloclastite have been documented in Canadian Archean rhyolites (de Rosen-Spence et al., 1980) and in Miocene lavas of the Ushikiri Formation, Japan (Kano et al., 1991). The flows have often incorporated clasts of autobreccia where they have apparently flowed over older flow breccias. It appears that fragments of the autobrecciated flow carapace may have foundered into the less dense molten portion of the flow interior. In such cases the breccias appear to have a 'matrix' of lava having apparently the same composition as the clasts. The autobrecciated lava clasts themselves are often flow banded and are rotated possibly during the advancement of the flow . The uppermost portions of the flow breccias often contain angular felsic hyaloclastic fragments interstitial to the large flow-banded lava clasts. The angular nature of these clasts is indicative of quench-induced fragmentation due to the interaction of lava with cold seawater (Hanson, 1991). Where the flow tops were observed, there is some reworking of the autobreccia and hyaloclastite which created a weak normal grading and diffuse lamination of the finer-grained sand-size lava debris.

In some instances several coherent flow-flow breccia sequences occur in a vertical succession up to 100 m thick, but less than 200 m in lateral extent, forming a dome-like morphology (*cf.* Allen, 1992). There can be considerable variability in the thicknesses of flow-flow breccia sequences between adjacent drillholes again suggesting a non-tabular morphology. However, discrete flows exist that are enclosed within volcaniclastic rocks. Such flows tend to be less than 10m thick, have sharp lower contacts and brecciated upper contacts and appear to be more tabular in nature. The volcaniclastic sediments immediately below the flows are often silicified, probably due to interaction between the wet

sediments and the hot lava (Kokelaar, 1982). Intersections in which autobrecciated layers are thicker than coherent, massive or banded layers likely represent the margins of flow dome or flow-fronts, whereas intersections in which coherent lavas predominate over autobreccias likely represent the cores of the flows and domes (McPhie et al., 1993). Such relationships between lateral and vertical dimensions and lava textures suggest that the felsic flows have both tabular and dome-like morphologies similar to those described by McPhie and Allen (1992) for the Mount Read Volcanics in western Tasmania.

2.3.2 VOLCANICLASTIC ROCKS

There is a wide variety of volcanically-derived sediments and breccias on the Seneca property with clasts ranging from silt size to block size (<15 cm). These rocks show tremendous variation in textural maturity and composition. Such characteristics are important indicators of the processes of transportation and deposition which operated in the area, and of the proximity of a unit to its source. These fragmental units represent the deposition and reworking of volcanic debris derived from lava flows, domes and pyroclastic eruptions, with the probable addition of fine sediments of a more distal origin. They are subdivided into four facies:

- *Facies 2.1.* Monolithic to heterolithic, massive to well bedded/laminated and normal density graded, moderately to poorly sorted lava clast breccias, pebble conglomerates, vitric-crystal tuffs and volcanic sandstones, interpreted to have been deposited as debris flow deposits, subaqueous pyroclastic flows and turbidites (Plates 2.4b and 2.5).
- *Facies 2.2.* Massive to well laminated volcanic siltstone/fine ash deposited subaqueously by gravity settling.

- *Facies 2.3.* Dacitic to rhyolitic pumiceous beds often associated with argillaceous beds (Plate 2.6a).
- *Facies 2.4.* Reworked dacitic debris flow/conglomerate interpreted to have been deposited in a fluvial or deltaic environment.
- *Facies 2.5.* Argillaceous beds consisting of thin layers of dark brown to black fine sand to silty tuffaceous sediments which possibly correspond to more normal, non-volcanic dominated period of sedimentation.

2.3.2.1 FACIES 2.1: DEBRIS FLOWS, GRAIN FLOWS AND TURBIDITIC VOLCANICLASTICS

Fragmental rocks composed of sand to block-sized volcanic clasts form a large portion of the volcaniclastic facies at Seneca. The coarsest and most poorly sorted unit is termed the 'block-lapilli tuff' (BLT) (Plate 2.5a). This unit consists of large 2-15 cm clasts of felsic lava (FP and lesser QFP) with a matrix of sand-sized clasts of mostly felsic composition with lesser vesicular mafic lava clasts, fine grained volcaniclastic rip-ups and crystal fragments. The large clasts often have angular or cuspate edges similar to the hydroclastic breccias (Hanson, 1991), but can also be rounded; they are generally massive and unvesiculated, but can be flow-banded. Colour variations imposed by different degrees of silicification or chloritization of the clasts give the rock a more polymictic appearance although the unit usually has less than 10 % mafic clasts. These coarse grained beds are up to 10 m thick and are generally in sharp contact with overlying fine grained volcaniclastics or felsic flows and autobreccias. The coarse nature and delicate hydroclastic shapes of the felsic clasts suggests that the BLT unit is essentially locally-derived and has not undergone much transportation, however, the incorporation of clasts of varying compositions implies a certain degree of reworking. The lack of grading or well developed stratification of the unit suggests transportation of the volcanic detritus by a debris flow or subaqueous pyroclastic flow (Lowe, 1982;Fisher and Schminke, 1984; Busby-Spera,

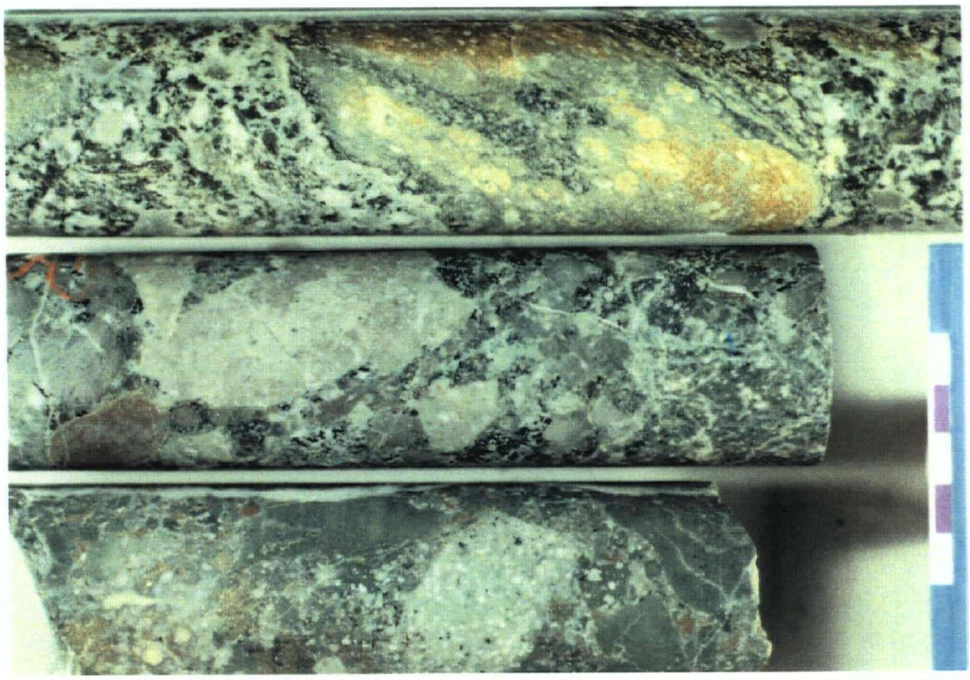

Plate 2.5a: Block lapilli tuff unit ('BLT'). These poorly sorted fragmental rocks were deposited as debris flows and often overlie the basaltic lavas in the lower parts of the stratigraphy. The upper sample contains flow-derived clasts and hyaloclastite. The lower samples are mostly variably altered rhyodacitic clasts, but some mafic material is present. These two rocks may have formed from slumps associated with formation of basin-bounding scarp faults. (Scale divisions = 1 cm).

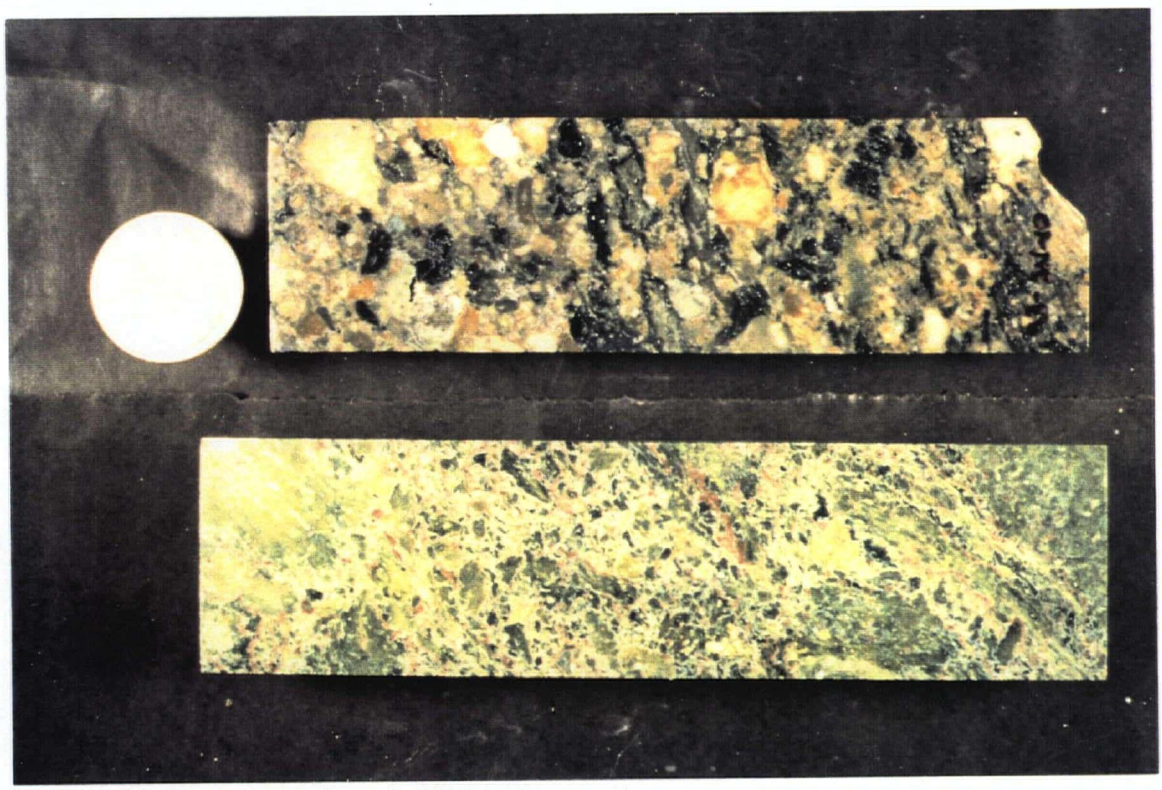

Plate 2.5b: Coarse felsic fragmental units. The upper sample consists of rhyodacitic lava clasts and vitric clasts perhaps derived from a subaqueous pyroclastic eruption. This unit is common in the lower portions of the Pit Area stratigraphy. The lower sample consists of in-situ hyaloclastite and is interpreted as a proximal facies (i.e. has not been reworked) to a felsic flow.

1988; McPhie et al., 1993). Such debris flows were likely localized phenomena, and may have been channelized or topographically-controlled, since there is little lateral continuity to the unit. The essentially monolithologic nature of the BLT and textural similarities between the large clasts in the BLT and those of the hydroclastic and flow breccias suggest that the felsic detritus was derived from the brecciated margins of flows or emerging cryptodomes which may have slumped due to oversteepening or perhaps seismic events (Dimroth et al., 1978; Cas et al., 1990; McPhie et al., 1993). The large felsic clasts may be blocks and bombs derived from a more distal, subaerial eruption, but the proximity of the BLT unit to observed felsic flows favours a more local source.

Better sorted, coarse volcaniclastic units are much more common. Although such units themselves are relatively poorly sorted, they do not show the extreme range of clast sizes observed in the BLT. Dense, mostly non-vesicular, feldspar-phyric clasts are the dominant fragment type in these felsic lava clast breccias (Plate 2.5b). Altered dark green vitric clasts are also common. These clasts contain similar amounts and types of phenocrysts as the lighter coloured felsic lava clasts, and thus are inferred to be quenched, glassy equivalents of the lavas. Vitric clasts are altered to chlorite (± sericite), and they often have an internal foliation parallel to the length of the clast which may result from the flattening of an originally vesicular and/or semi-molten pumiceous bomb. Clast sizes range from less than 1 mm to 5 cm, in general, and the beds tend to lack internal stratification or grading. Bed thicknesses vary from one to ten metres. Contacts of the beds can be either sharp or show a rapid change in grain-size to the overlying finer grained beds. The monomict nature and lack of internal stratification or grading of these coarse beds suggests that transportation of the volcanic debris was by turbulent debris flows (Walker, 1984), as opposed to gravity settling of volcanic clasts from a subaerial eruption which likely would have resulted in at least some density grading in the beds.

A dacite lava breccia (Facies 2.1; Plate 2.1b) occurs stratigraphically below the OZC in the Pit Area, and generally above the major andesitic units in the Fleetwood and Vent zones. Typically the

unit is clast supported (up to 90% clasts up to 10 cm in diameter) and consists dominantly of subangular dense fragments of feldspar-phyric dacite lava and lesser amounts of dark green vitric or pumiceous clasts, andesitic fragments and occasional silty rip-up clasts. The dacite clasts vary in colour from light grey to reddish tan, possibly representing subaerial deposition and later reworking. The unit is moderately to poorly sorted, suggesting deposition by debris flows.

The true thickness of the unit is difficult to determine due to synvolcanic intrusions, but individual intersections are in the some 5 to 10 metres thick. Andesite lava breccias are less common at higher stratigraphic levels, and where they do occur, contain smaller clasts that are more rounded.

Fine-grained volcaniclastic sediments (Facies 2.1 and 2.2) are common throughout the property, particularly in the upper parts of the examined stratigraphy and are volumetrically more significant than the BLT and coarse-grained, non-stratified lava clast breccias at Seneca. These units are composed mostly of three clast types: dense lava clasts, crystal fragments and pumiceous or glassy debris. Siltstone intraclasts derived from underlying beds have also been observed in the sandy beds, but are relatively rare. The relative amounts of these clast types can vary greatly between individual beds. Where discernible, non-vesicular feldspar (± quartz)-phyric lava clasts and feldspar crystals are the dominant fragment types. Crystal fragments are apparently entirely plagioclase and quartz

The volcaniclastic sediments form light to dark grey beds of silt to sand-sized material. Individual beds of sand-sized detritus range from 2 cm to 5 m thick, and vary from massive to well laminated and graded. The basal contacts of normal graded beds are often sharp and are characterized by coarse sand to gravel-sized material, often with a component of dacite pumice fragments. These beds grade upward through massive or weakly laminated sands to well-laminated and occasionally cross-bedded fine sand, silt and mud. Graded beds become more common higher in the stratigraphy. Loading structures have been observed where coarser grained beds have sunk into finer silty beds.

Although they were observed in the upper portion of the Pit Area stratigraphy, cross-beds on the whole are rare. The well-bedded and laminated, often graded, and rhythmic nature of these volcaniclastic sand-dominated beds suggests they were deposited as discrete turbidites or grain flows (Walker, 1984; Fisher, 1984; Busby-Spera, 1988) that were generated by subaqueous eruptions and slumping due to slope oversteepening.

2.3.2.2 FACIES 2.2: VOLCANICLASTIC SILTSTONE

Massive to well-laminated volcaniclastic siltstone beds are quite common at Seneca. They are distinguished by their lack of discernible macroscopic grains, and are light to dark grey in colour. These units contain glassy shards and crystal fragments that are the only features distinguishable from the massive, fine-grained matrix. Individual beds can be distinguished where there are subtle grain size or colour differences. Beds of volcanic siltstone vary from less than one to several metres in thickness, and vertically continuous series of fine grained beds reach up to 10 m thick. The massive nature of these beds suggests that they may have been deposited by gravity settling from suspension (Ledbetter and Sparks, 1979; Branney, 1991). This material likely rained down through the water column during the waning stages of eruptions. It is not clear whether the fine ash was erupted subaerially or subaqueously, but its close spatial association with the coarser volcaniclastics suggests that it may be a fine grained equivalent of the coarse detritus that was density sorted within the eruption column.

2.3.2.3 FACIES 2.3: DACITIC AND RHYOLITIC PUMICE BEDS

Pumice beds are common in the volcaniclastic sequence. The pumice clasts are feldspar (± quartz)-phyric and have an altered glassy groundmass. They occur either as bombs in fine-grained detritus or as discrete beds usually less than 1 m in thickness (Plate 2.6a). The pumice is often flattened giving the beds a flow-like texture. Although the individual beds are quite thin, they

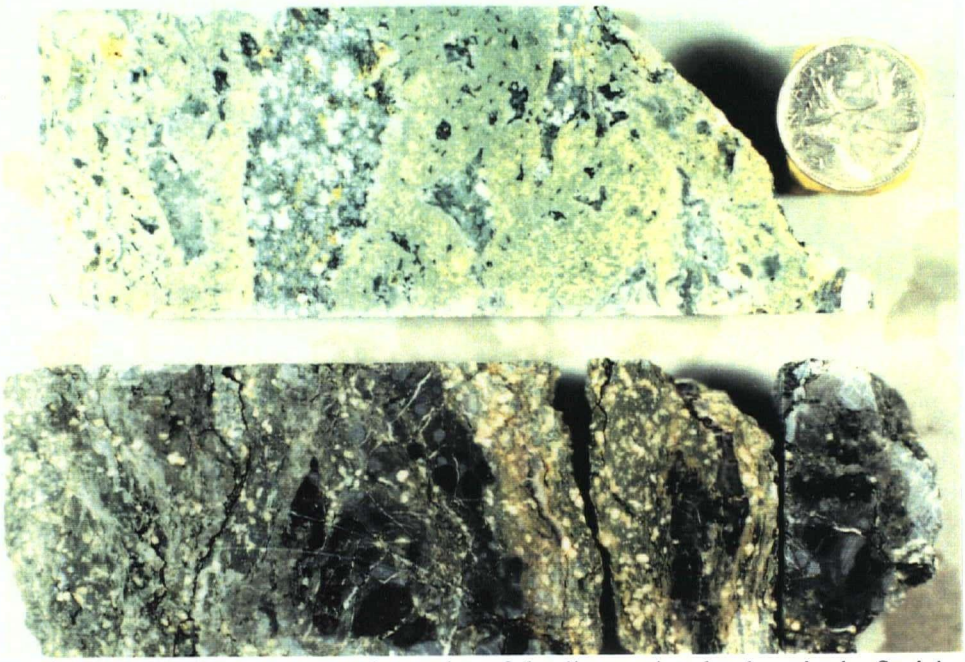

Plate 2.6a: Pumiceous beds. The upper sample consists of rhyolite pumice shards and ash. Such beds are common in the volcaniclastic sequence and likely represent single, explosive eruptive events some distance from the depositional site. The lower sample consists of flattened pumiceous material within a dark brown to black argillaceous bed. This unit is often associated with the OZC in the Pit Area.

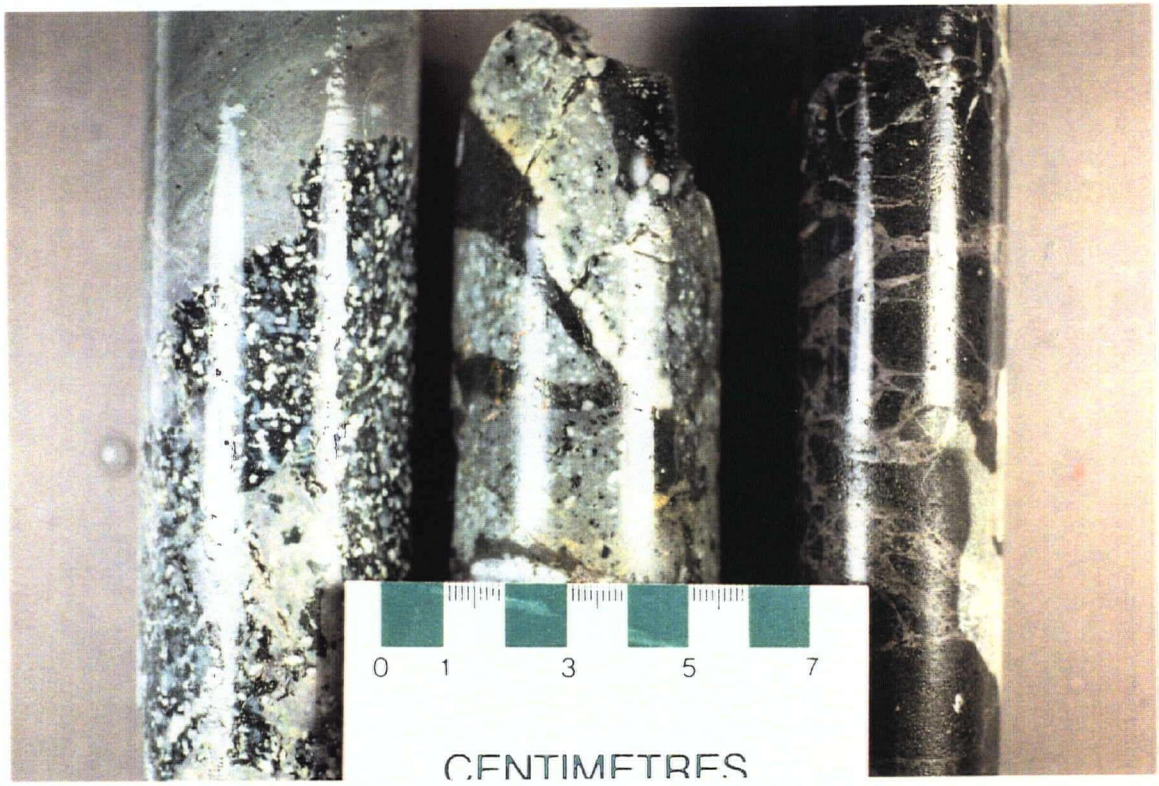

Plate 2.6b: Peperites - sill-sediment contact interactions. From left to right are rhyolitic, rhyodacitic and andesitic peperite zones which form when synvolcanic sills intrude wet, unconsolidated volcaniclastic beds. The sill margins become chilled and quench brecciated while the fine sediments are fluidized and silicified.

punctuate virtually all parts of the upper volcaniclastic sequence in all areas. As such the pumiceous beds are useful as a basis for stratigraphic correlation in that each bed likely represents an individual eruptive event, either subaqueous or subaerial, that would distribute volcanic debris over a wide area.

2.3.2.4 FACIES 2.4: ORE ZONE CONGLOMERATE

The 'ore zone conglomerate' (OZC), located entirely in the Pit Area, hosts disseminated to massive sulphide mineralization, and varies from 1 to 15 metres in thickness. The OZC consists of moderately silicified, mostly subrounded dacite lava clasts ranging from sand size up to 3 cm in diameter in a sandy or silty matrix (Plate 2.2a). The unit can be matrix or clast supported, and also contains clasts and matrix that have been replaced and/or infilled by sulphides. The term ore zone conglomerate refers to the entire unit which hosts sulphide mineralization and that much of the unit contains only sparsely disseminated sulphides, but is texturally distinct from other volcaniclastic units.

2.3.3 FACIES 3: SYNVOLCANIC INTRUSIONS

Synvolcanic intrusions are distinguished from flows by their contact relationships and textural features such as peperite (Plate 2.6b). Commonly, the contacts are bedding parallel and the units lack flow banding and autobreccia. Chilled margins and contacts at high angles to stratigraphy provide simple criteria for the recognition of dikes. The felsic intrusions comprise a volumetrically large portion of the volcanic sequence at Seneca and complicate stratigraphic interpretations by splitting up and displacing units and by 'inflating' the stratigraphy. Many drillcore intersections of massive felsic intrusions may in fact be relatively thin dikes that have steep dips which increases the apparent thicknesses in drillcore.

Plate 2.7. Synvolcanic intrusions. Photo illustrates the range in compositions of the synvolcanic sills and dikes that occur at Seneca. These range from QFP rhyolite (left) to FP dacite/rhyodacite (middle) to basaltic andesite (right).

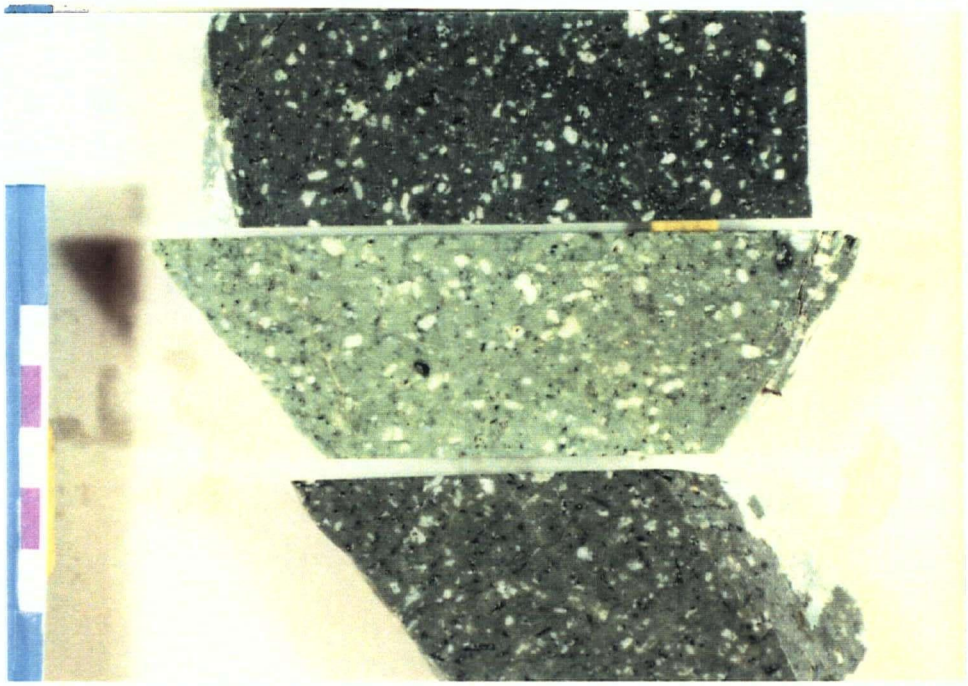

Plate 2.8a: Feldspar-porphyritic (FP) intrusions. These units are dacitic to rhyodacitic in composition and occur as both synvolcanic sills and dikes. They contain plagioclase and hornblende/pyroxene phenocrysts with occasional quartz and are generally massive with sharply defined chilled margins. (Large scale divisions = 1 cm).

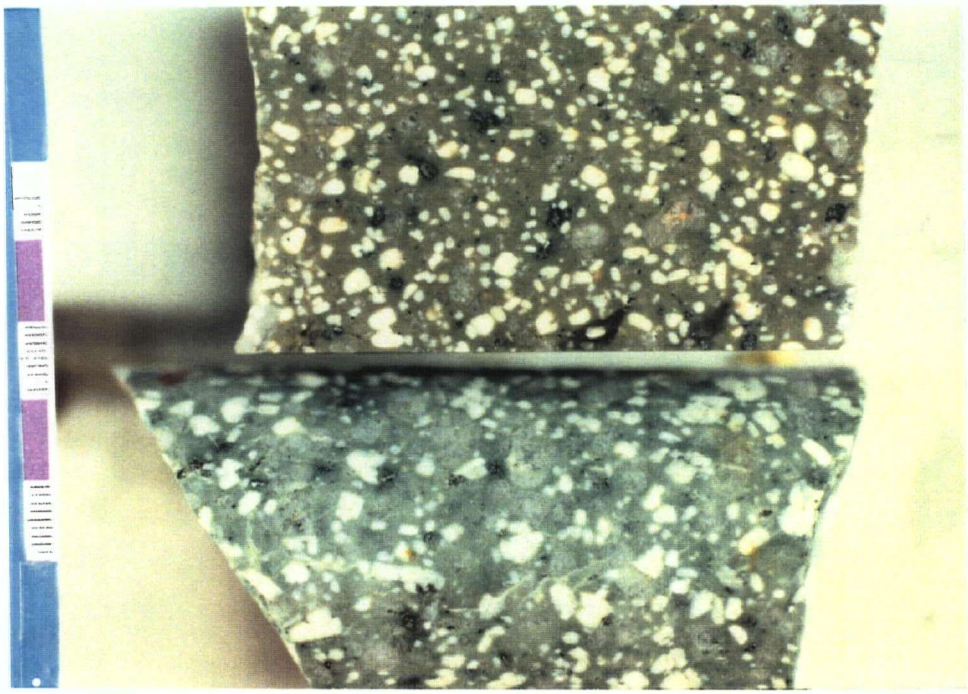

Plate 2.8b: Quartz-feldspar-porphyritic (QFP) intrusions. These units are rhyolitic in composition and form synvolcanic sills, intrusive domes and dikes. They contain plagioclase phenocrysts and up to 10 % quartz phenocrysts. They are generally more coarsely porpyritic than the FP intrusions shown above. (Large scale divisions = 1 cm).

2.3.3.1 FELDSPAR-PHYRIC INTRUSIONS (FP)

The most common intrusions are feldspar-phyric dacite to rhyodacite porphyry sills (FP) (Plate 2.7a). The sills range from one to several tens of metres thick, and are often columnar jointed when exposed in some outcrops. Mineralogically, and often texturally, these rocks are identical to the dacite flows described earlier and are only distinguishable by their contact relationships. Dacite sills, where they cut other intrusions or flows, commonly have chilled contacts over widths of 10 cm to more than 1 m, and are only slightly brecciated. Where the sills intrude the volcaniclastic sediments and breccias, the contacts commonly have peperitic textures. In peperitic zones the contacts tend to be quenched and brecciated with angular to cuspate hyaloclastic fragments less than 1 cm to 20 cm in size with a matrix of the finer sediment (Plate 2.6b). Kokelaar (1982) documents similar textures and suggests that the unconsolidated sediments are fluidized due to the heat from the sills and can thus flow more easily into the matrix of the brecciated margins of the intrusion. The hyaloclastite fragments and surrounding sediments are often silicified. These peperites reach thicknesses of several metres and usually occur at the top of the sills. Quench-induced fractures extend from the brecciated zone into the massive sill. These fractures have a silicified envelope which destroy the porphyritic texture of these rocks and replace it with a 'pseudobrecciated' texture. The textures indicate that the sills have intruded into wet, unconsolidated sediments (McPhie and Allen, 1992; McPhie et al., 1993).

2.3.3.2 MAFIC INTRUSIONS

Mafic intrusions are less common than felsic and tend to occur in the lower part of the stratigraphy. Similar to the dacite porphyries, they have both crosscutting and bedding-parallel contacts with chilled margins. The andesites are generally massive and dark green with chlorite-filled amygdules 0.5 to 1 mm in diameter. Where the andesites intrude sediments, they exhibit quenching, brecciation (Plate 2.2b), and mixing similar to the felsic intrusions, except that brecciated zones tend to

be more extensive (in the range of several metres). These hydroclastic breccias consist of angular or cuspate-shaped fragments with a 'slurry' matrix of fine grained volcaniclastic sediments. In many of the drillholes in the Pit Area, these mafic sills intrude the OZC and units immediately above and below it.

2.3.3.3 QUARTZ-FELDSPAR-PHYRIC INTRUSIONS (QFP)

The third type of intrusion is quartz-feldspar-phyric rhyolite porphyry (QFP) (Plate 2.7b). These are less common than the other two types and their mode of emplacement is uncertain. They occur at higher levels in the stratigraphy and as a result their upper contacts are not always seen. Their size and massive nature suggest that they may be synvolcanic sills, but they may also represent emergent domes. Thick intersections of coarsely porphyritic QFP occur in the Fleetwood zone. These units do not correlate with adjacent drillholes and are thus interpreted as moderately or steeply dipping dikes. The rhyolite porphyries are easily distinguishable from the dacite porphyries by their greyish brown groundmass and by the presence of up to 10% subrounded quartz phenocrysts 2 to 7 mm in diameter. The rhyolite porphyry bodies range from a few to more than 30 metres thick. They have not been observed to exhibit the same sediment interaction textures as the dacites and andesites.

2.3.4 FACIES 4: ARGILLACEOUS BEDS

Thin dark brown to black beds of fine grained sediments less than 1 metre thick were observed in the lower parts of the Hangingwall Interval in the Pit Area and in the Trough Zone (Plate 2.6a, bottom). These beds are also associated with the OZC in the Seneca Horizon. This unit was not observed in the Fleetwood Zone and, therefore, may represent a more distal basinal facies formed by normal sedimentary processes without a large volcanic input, perhaps during a period of volcanic quiescence. Flattened felsic clasts are often observed within the argillaceous beds.

2.4 DISCUSSION

The distribution of the different volcanic facies across the Seneca property and at different stratigraphic intervals is summarized in Table 2.1. The prevalence of both mafic and felsic lavas, flow breccias and coarse hydroclastic breccias in the Fleetwood and Vent Zones suggests a vent to vent-proximal facies. Mafic lavas in the Footwall Interval appear to be continuous between these two zones. However, the felsic lavas that dominate the Hangingwall Interval form two, or possibly more, separate flow-dome complexes centred roughly around drillholes 91-18 and 86-22. The brecciated margins of these flows were eroded and redeposited to form the coarse hydroclastic beds at the base of the Seneca Horizon as well as some of the coarse distal debris flows. The felsic flows appear to have been largely constructive in nature, forming domes consisting of a series of superposed alternating flows and breccias. Some of the more massive, near-surface (near paleo-seafloor) sills that lack internal structure or brecciation may in places have emerged through the volcaniclastic cover to form true flows similar to the mechanism described for cryptodomes (McPhie and Allen, 1992). Other intrusions common at all stratigraphic intervals were likely feeders for these and subsequent flows, or were high level sills that did not reach the paleo-seafloor.

Volcaniclastic units have two possible sources: 1) redeposited hyaloclastite from margins of flow-domes, and 2) gravity-settled fallout from pyroclastic eruptions. The nature of the angular, poorly sorted breccias in the lower portions of the stratigraphy favour transportation as a debris flow. The commonly normal graded and well-bedded finer grained beds of the upper volcaniclastic interval favours transportation of volcanic debris as turbidites or deposition of pyroclastic debris by gravity settling. The unbedded volcaniclastic siltstone beds were likely deposited by gravity settling of volcanic ash possibly erupted from a distal pyroclastic source. These beds were likely below wave base since they are often bounded by well laminated beds. The volcaniclastic sequence examined in the Trough Zone is similar to the unwelded subaqueous pyroclastic flows described by Fisher and

Schminke (1984) and portions of the volcaniclastic apron described by Busby-Spera, 1988. These deposits are described as having a single massive coarse-grained lower division up to 300 m thick that lacks internal structure and which is overlain by an upper division composed of thin and often normal-graded fine to coarse-grained ash beds. As such, the entire sequence observed in the Trough Zone may represent a single eruptive event characterized by an initial high energy surge which deposited the coarser massive debris flow material, followed by the deposition of finer volcaniclastic turbidites during the waning stages of the eruption. Such an eruption may have marked the onset of the felsic-dominated extrusive volcanism that is prevalent in the upper parts of the sequence elsewhere on the property. This same eruptive event may have deposited the lava clast breccias that are common in the interval stratigraphically above the mafic lavas. Following, or partly contemporaneous, with this event was a period of more effusive volcanism that formed the felsic flows and breccias common in the Fleetwood and Vent Zones. The intercalation of pumice-bearing fine volcaniclastic beds with the flows suggests that ash and coarser pyroclastic debris continued to rain down during this effusive period, perhaps 'draping' volcaniclastic material over the flows. However, this material may have originated from many kilometres away and may not necessarily reflect the volcanic processes acting in a particular area at that time. The ultimate origin of the fine-grained volcaniclastic beds is purely speculative at this point.

The similarities between the finer-grained volcaniclastic units in the Hangingwall Interval of both the Fleetwood Zone and the Pit Area suggest that these stratigraphic intervals are correlatable; the debris flow and gravity settling processes that deposited these units are favourable for a more areally extensive deposition of volcanic detritus which would account for the occurrence of these units in all areas of the Seneca property. These areas differ in that felsic flows are more common in the Hangingwall Interval of the Fleetwood Zone and the Vent Zone than in the Pit Area; the Pit Area appears to have been more distal and as such does not contain an abundance of extrusive vent to vent

Facies	Rock Type	Facies Classification	Mode of Deposition	Description
Facies 1	**Lavas**			
1.a	Mafic lavas	- vent to vent proximal	- subaqueous lava flows and eruptions	- massive and brecciated basaltic and basaltic andesite lavas ± in-situ hyaloclastite
1.b	Felsic lavas	- vent to vent proximal	- subaqueous flows and flow-domes	- massive, flow-banded and autobrecciated rhyodacitic lavas ± in-situ hyaloclastite
Facies 2	**Volcaniclastic Rocks**			
2.1	Volcanic sandstones, breccias and crystal tuffs	- medial to distal	- debris flows, turbidites, and subaqueous pyroclastic flows.	- massive to well-bedded and normal graded, moderately to poorly sorted, monolithic to heterolithic.
2.2	Volcanic siltstones/ash	- proximal to distal	- subaqueous deposition by gravity settling; products of subaerial or subaqueous eruptions.	- massive to well laminated; thinly to thickly bedded; well sorted.
2.3	Felsic pumice beds	- proximal to distal	- fallback from pyroclastic eruptions (subaqueous or subaerial).	- dacitic to rhyolitic, quartz-feldspar-phyric pumice, often flattened.
2.4	Volcanic sandstone and conglomerate	- distal	- reworked lava debris; possibly deposited in a deltaic setting.	- 'ore zone conglomerate' - angular to lava clasts; moderately to well sorted; only occurs in Pit Area.
Facies 3	**Synvolcanic Intrusions**			
3.a	Dacitic to rhyodacitic FP intrusion	- proximal to medial	- synvolcanic sills and dikes intruded into flows and 'wet' sediments.	- feldspar ± quartz-phyric; massive to weakly brecciated; often chilled at margins.
3.b	Rhyolitic QFP intrusions	- proximal to medial	- synvolcanic sills and dikes intruded into flows and 'wet' sediments.	- quartz-feldspar -phyric; massive to weakly brecciated; often chilled at margins;. occasionally peperitic textured
3.c	Mafic intrusions	- proximal to medial	- synvolcanic sills and dikes intruded into flows and 'wet' sediments.	- basaltic andesite intrusions; variably peperitic and amygdaloidal.
Facies 4	**Argillaceous beds**	- distal marine	- gravity settling of sediments and pumice clasts	- dark brown to black, fine-grained with occasional felsic pumice clasts.

Table 2.1. Summary of the characteristics of the major volcanic facies present at the Seneca property. The facies are subdivided on the basis of their inferred proximity to a volcanic vent and their modes of deposition.

proximal facies rocks. The Trough Zone appears to be more distal than all of the other areas since it lacks the synvolcanic intrusions or feeders that are abundant in the Pit Area. These observations indicate that there is an overall facies change northwest to southeast across the Seneca property from vent to vent-proximal facies rocks in the Fleetwood Zone to distal facies-dominated rocks in the Pit Area and Trough Zone.

CHAPTER 3

PETROLOGY OF THE VOLCANIC SEQUENCE AT SENECA

3.1 INTRODUCTION

Thin section analysis of the volcanic rocks at Seneca proved useful in confirming macroscopic observations, and in outlining subtle igneous textures, mineralogical characteristics and degrees of alteration that allowed for the subdivision of units that were macroscopically indistinguishable. This chapter will outline the petrographic characteristics of the major volcanic units at Seneca and will use geochemical data to infer the tectonic affinity of the rocks and the possible igneous processes that may have led to the variability in the data set.

3.2 PETROGRAPHY OF THE VOLCANIC ROCKS AT SENECA

3.2.1 FACIES 1: LAVA FLOWS AND BRECCIAS

3.2.1.1 MAFIC LAVAS

Basaltic and andesitic lavas are invariably amygdaloidal (Plate 3.1a). The fire fountain debris contains 10 to 20 % calcite and chlorite-filled amygdules that are up to 2 mm in diameter, but generally less than 0.5 mm. The groundmass is essentially aphyric and contains fine plagioclase laths that often display a trachytic texture. The groundmass is strongly chloritic. Large phenocrysts are rare; small euhedral plagioclase laths are present up to 5 %, and ferromagnesian phenocrysts were not observed. Plagioclase phenocrysts from mafic rocks that are in the proximity of the Fleetwood and Vent Zone stockworks are variably altered to sericite ± epidote and calcite. Where the lavas are brecciated, the matrix comprises predominantly angular

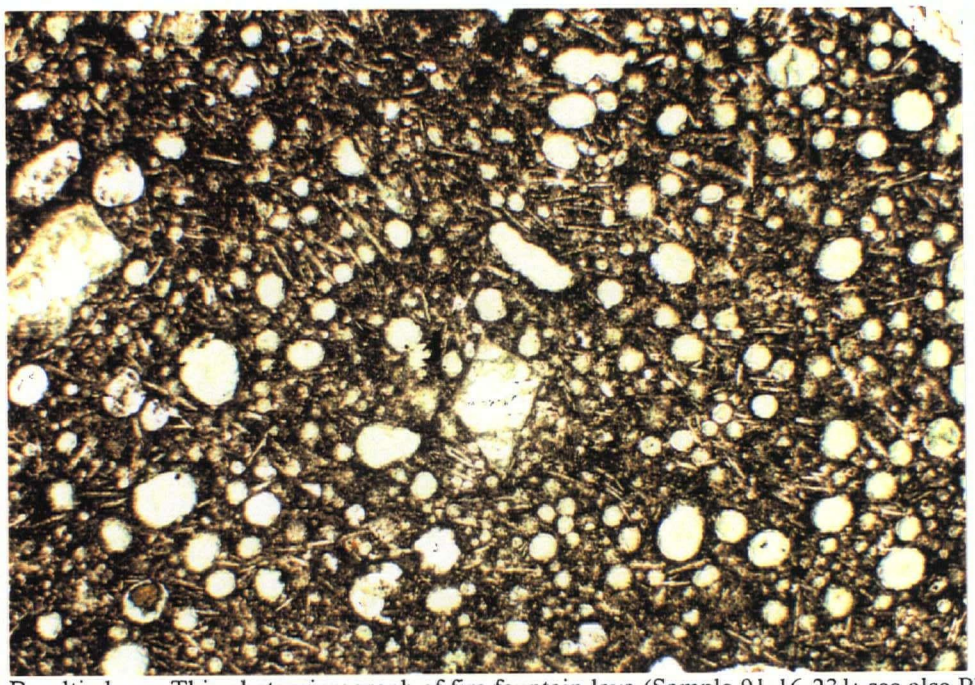

Plate 3.1a: Basaltic lava. This photomicrograph of fire fountain lava (Sample 91-16-231; see also Plate 2.4a) shows the strongly chlorite-calcite amygdaloidal and essentially aphyric nature of these subaqueously erupted basalts. Only fine plagioclase microlites and an occasional larger phenocryst are discernible. (Plane polarized light; Field of view = 5mm).

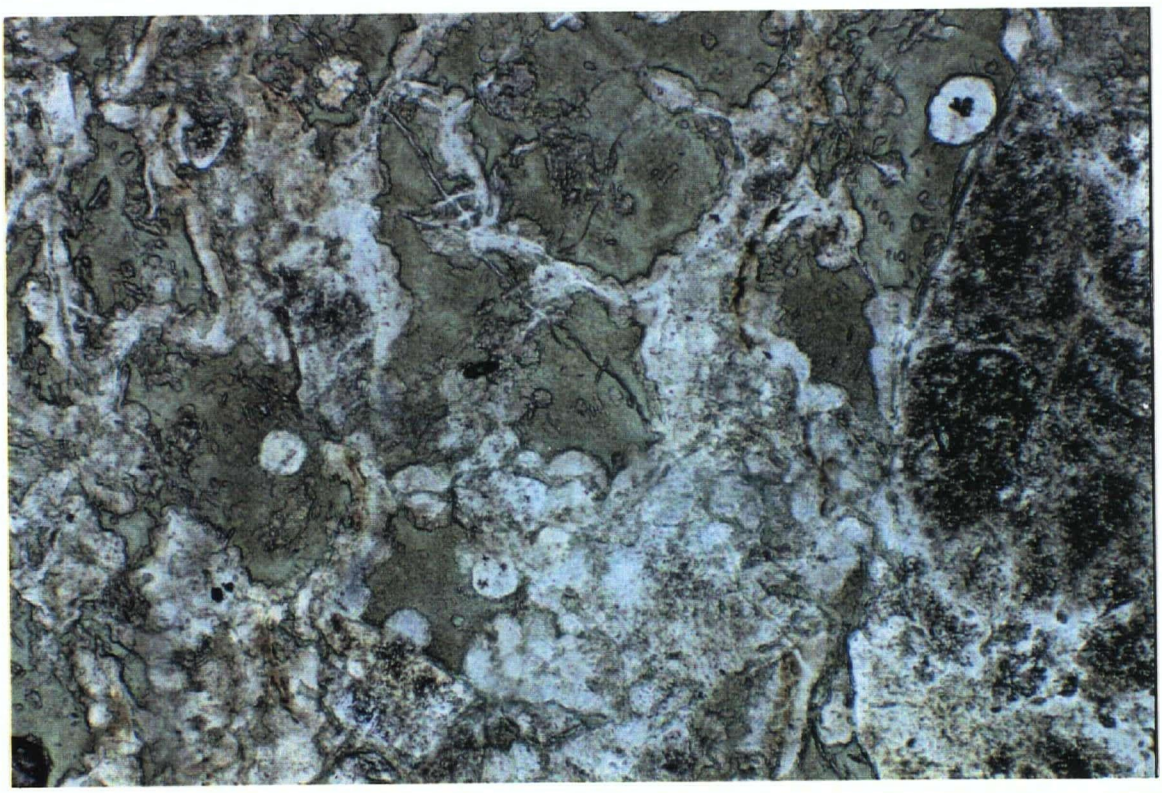

Plate 3.1b: Vesicular glassy rhyolitic lava. This photomicrograph of a chilled and weakly in-situ brecciated rhyolite flow (Sample 92-33-70) shows the vesicular nature of this unit and the typical variable quartz and chlorite alteration of the glass. (Plane polarized light; Field of view = 1.25 mm).

and subangular chloritized glass shards believed to be derived from the lava clasts by spalling of their quenched, glassy rims. The rims of the lava clasts are noticeably finer grained than the massive cores suggesting they were quenched upon contact with the water.

3.2.1.2 FELSIC LAVAS

The felsic lavas contain 5 to 15% subhedral to euhedral plagioclase phenocrysts that are typically 1 to 2 mm long. Quartz phenocrysts are less common, but may comprise up to 7% of the rock. They are generally subrounded and less than 5 mm in diameter. Chloritized laths and euhedral phenocrysts are also usually present (up to 5%, but more commonly <2%) and average 1 to 2 mm in size. These mafic phenocrysts are inferred to be altered hornblende based on some of their crystal forms, but some may also be altered pyroxene.

The felsic lavas are moderately to strongly silicified (Plate 3.1b). The groundmass of the lavas consists of mosaic-textured quartz with lesser sericite and chlorite. Flow banding is visible in thin section and is enhanced by variations in the silica and chlorite alteration. Relict perlitic cracking is common in these rocks suggesting that the groundmass of the lavas were originally glassy. This texture forms in response the volume increase associated with the hydration of glass (McPhie and Allen, 1993). The perlitic fractures are highlighted by chlorite alteration. Both classical and banded perlite are present. Classical perlite consists of arcuate cracks with chloritic cores and is present more commonly in the massive lavas (Plate 3.2a). Banded perlite consists of a network of rectilinear cracks subparallel and oblique to the flow banding (McPhie and Allen, 1993) (Plate 3.2b).

Plate 3.2a: Classic perlite in rhyodacitic glass. Photomicrograph of Sample 91-16-61 shows the arcuate fine cracks that form due to volume expansion associted with the hydration of volcanic glass. The cracks and some of the cores of perlite are accentuated by weak chlorite alteration. (Plane polarized light; Field of view = 1.25 mm).

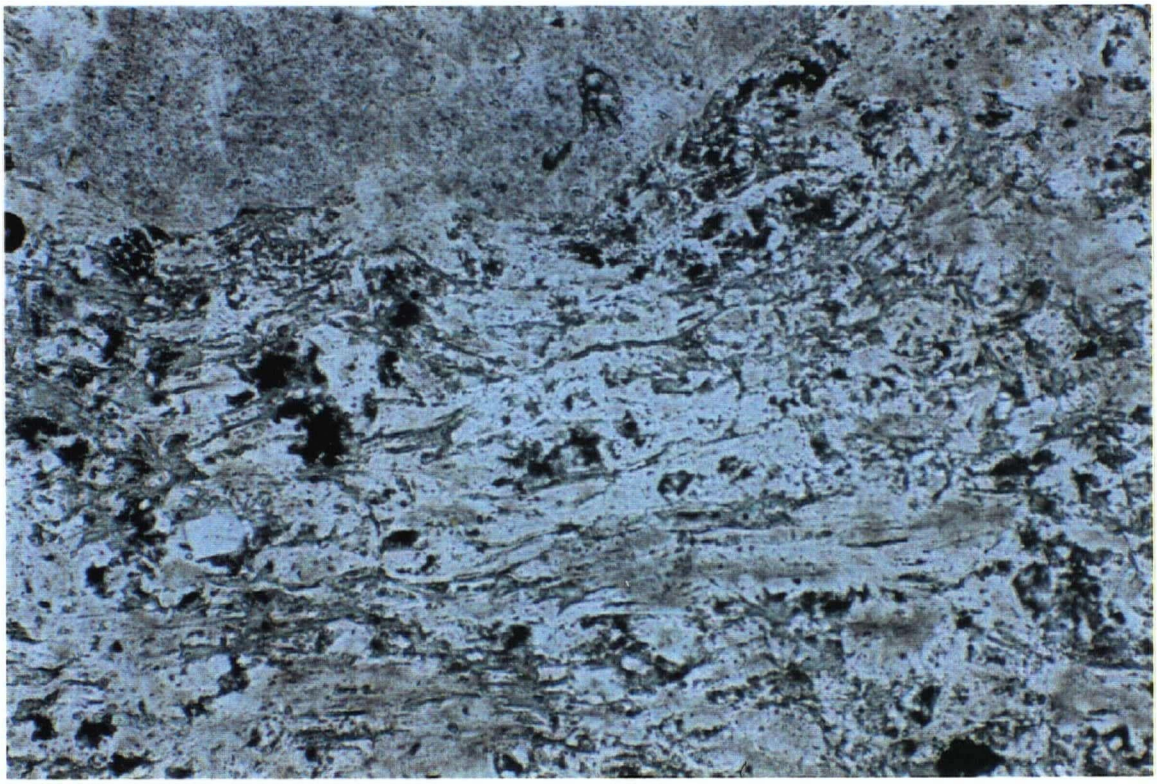

Plate 3.2b: Banded perlite in rhyodacitic flow. Photomicrograph of Sample 91-18-64 shows the rectilinear cracks that form when perlite develops from a flow-banded felsic glass. (Plane polarized light; Field of view = 1.25 mm).

3.2.2 FACIES 2: VOLCANICLASTIC ROCKS

3.2.2.1 FACIES 2.1: VOLCANICLASTIC DEBRIS FLOWS AND TURBIDITES

Coarse grained fragmental rocks are composed of lava clasts, crystal fragments and glassy, hyaloclastic debris (Plate 3.3). Lava clasts are comprised primarily of feldspar and quartz-feldspar-phyric debris. Trachytic mafic clasts are also present, both as discrete beds and in heterolithic beds mixed with felsic clasts (Plate 3.4a). The lava clasts are variably silicified and sericitized and are texturally and mineralogically the same as the lava flows and synvolcanic intrusions. Lava clasts and feldspar phenocrysts in rocks from the Trough Zone tend to be much less altered than those in rocks from the rest of the property. The pumiceous clasts, or fiamme, generally have and elongate, flattened texture and ragged margins (Plate 3.3b). They are also feldspar ± quartz-phyric and have a chloritic groundmass. Although they are spatially associated with the mineralized zones, these coarse units do not contain any sulphide clasts.

3.2.2.2 FACIES 2.2: VOLCANICLASTIC SILTSTONES

The very fine grained volcaniclastic ash beds are generally massive in thin section and textures are not easily discernible. Where present, laminations are defined by subtle grain-size variations. The beds are composed almost entirely of subround to angular glassy shards and finer felsic ash, but they are occasionally interbedded with reworked mafic hyaloclastite. Three types of glass shards are present: platy shards, cuspate or vesicular shards and tube pumice fragments (Plates 3.5 and 3.6a). The cuspate shape of many of the shards is due to quench fragmentation of glass or to the shattering of vesicular glass which leaves the arcuate remnants of the vesicle walls. The tube pumice fragments are composed of glass shards with elongate tube vesicles, and are relatively rare. The shards are surrounded by a matrix of much finer chloritized ash.

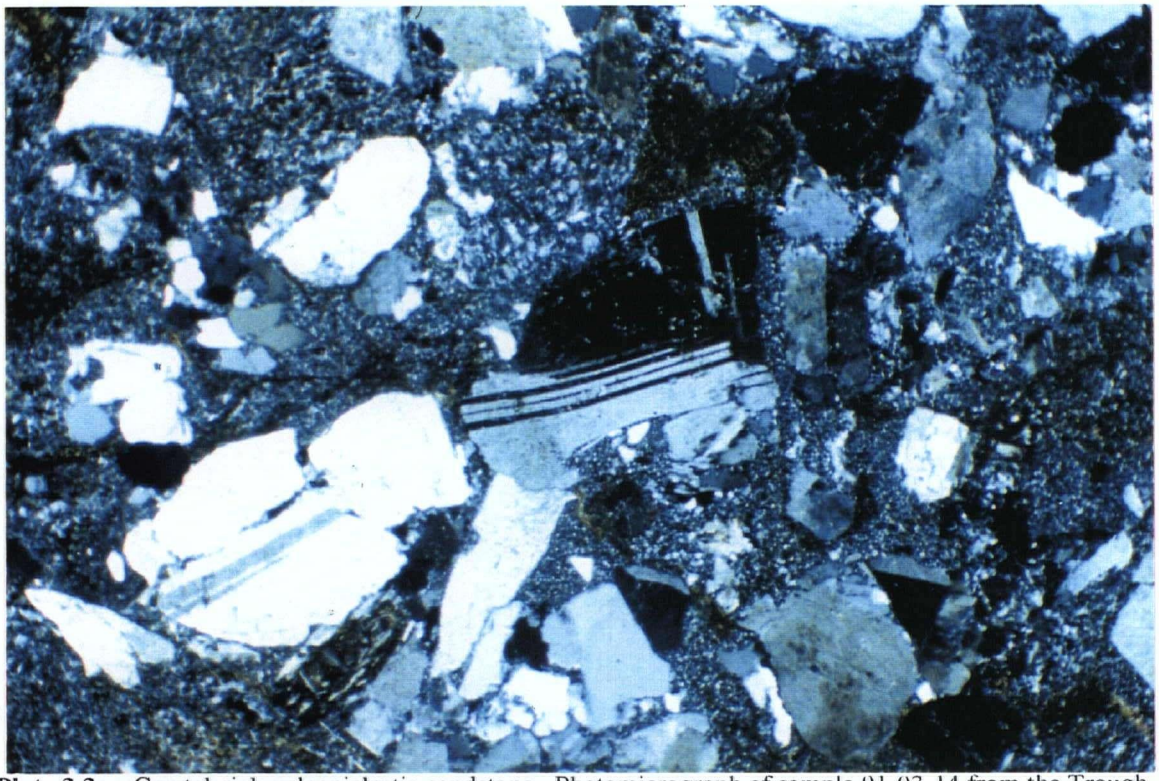

Plate 3.3a: Crystal-rich volcaniclastic sandstone. Photomicrograph of sample 91-03-14 from the Trough Zone shows illustrates the predominance of quartz and plagioclase crystals in these normal graded, turbiditic beds. The lack of lithic lava clasts in this bed may imply a certain degree of density sorting during transportation. (X-Nicols; Field of view = 5 mm).

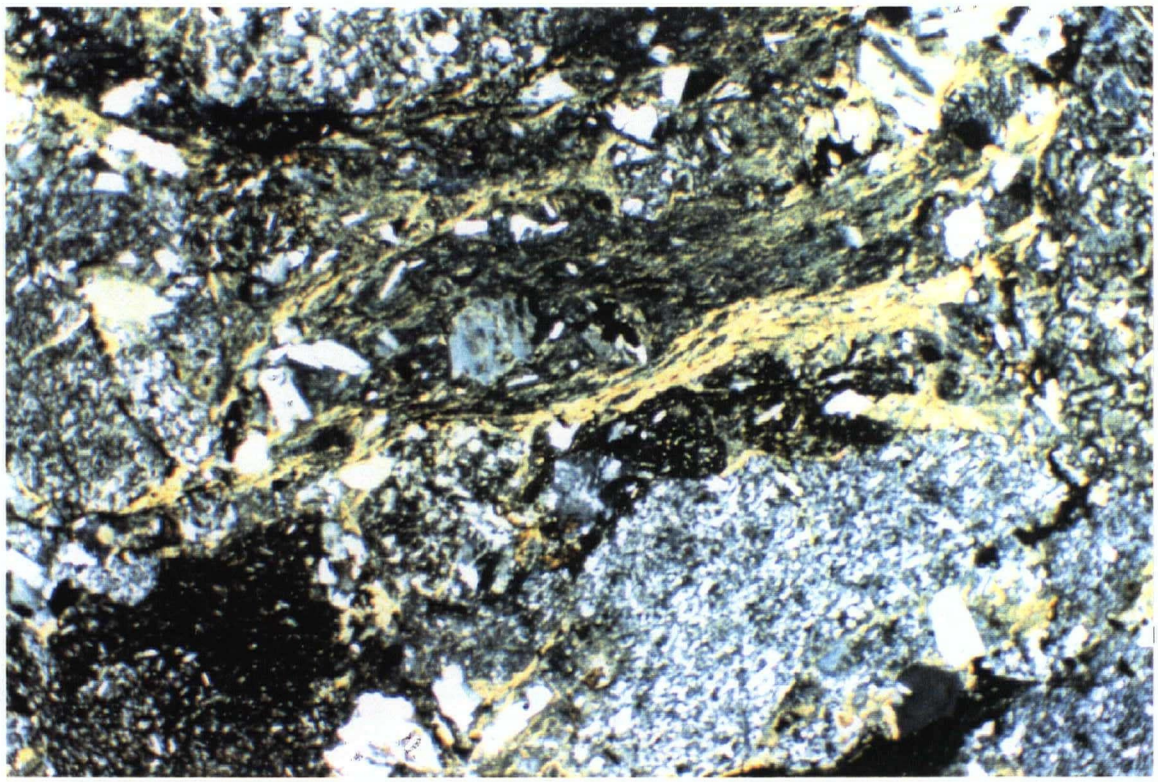

Plate 3.3b: Fiamme in coarse grained debris flow. Photomicrograph of felsic lava clast-dominated unit from the footwall of the Pit Area shows foliated texture of a flattened pumice fragment. The abundance of glassy material in such units may imply eruption as a subaqueous pyroclastic flow. (X-Nicols; Field of view = 5 mm).

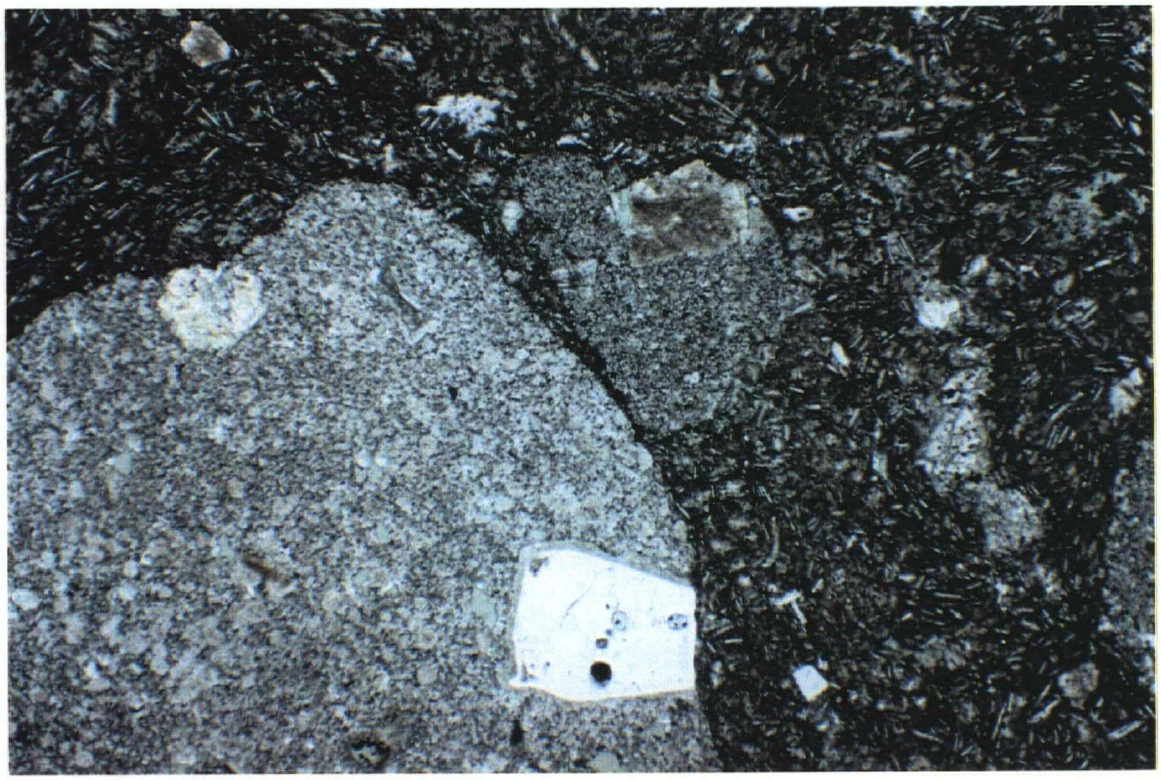

Plate 3.4a: Heterolithic breccia. Photomicrograph of Sample 92-33-166 shows a clast of spherulitic QFP rhyolite (lower left) surrounded by chloritic basaltic andesite debris. (Plane polarized light; Field of view = 5 mm).

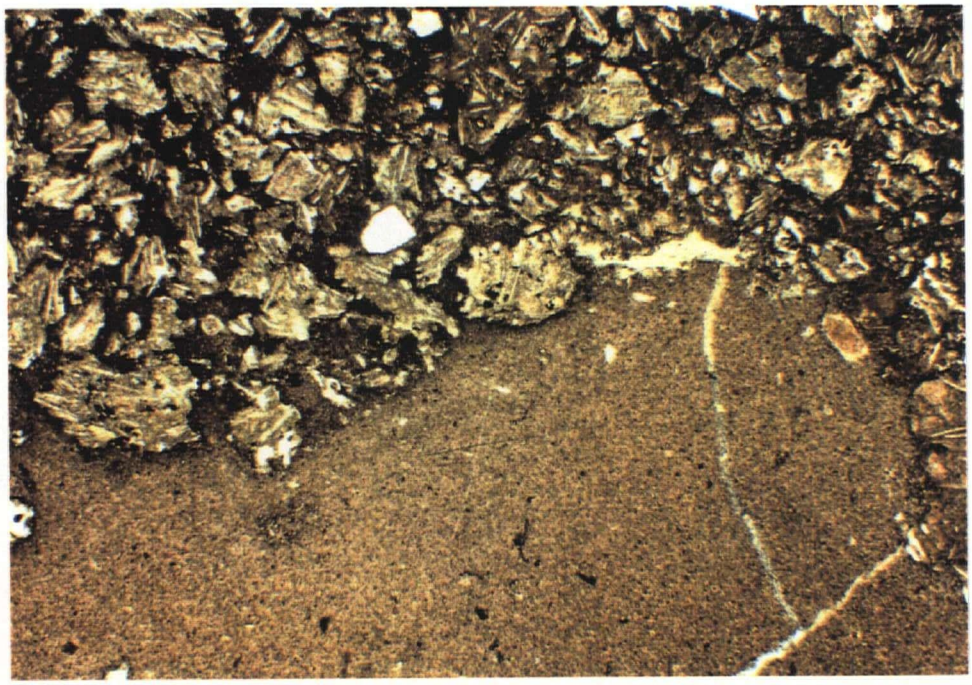

Plate 3.4b: Bedding contact between reworked basaltic hyaloclastite (upper half) and fine grained felsic ash/volcaniclastic siltstone. The mafic material may be a reworked and transported equivalent of the fire fountain debris lower in the sequence. (Plane polarized light; Field of view = 5 mm).

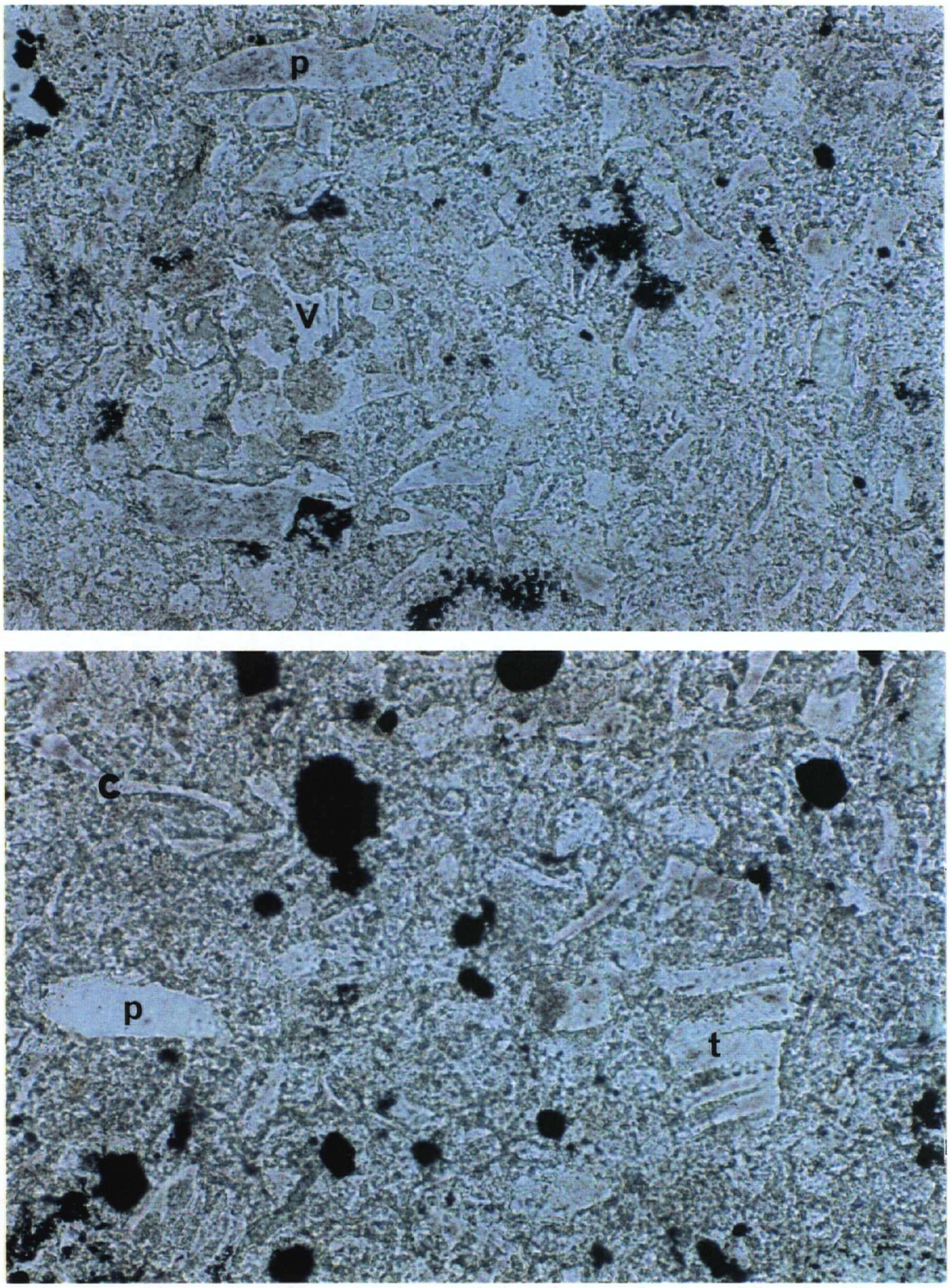

Plate 3.5: Two photomicrographs illustrating the typical glassy fragmental textures of the volcaniclastic siltstones and ashes. The upper photo contains platy shards (labelled p) and vesicular fragments (v). The lower photo contains platy shards (p), cuspate shards (c) and a fragment of tube pumice (t) that has elongate tube-like vesicles. (Plane polarized light; Field of view = 625 μ).

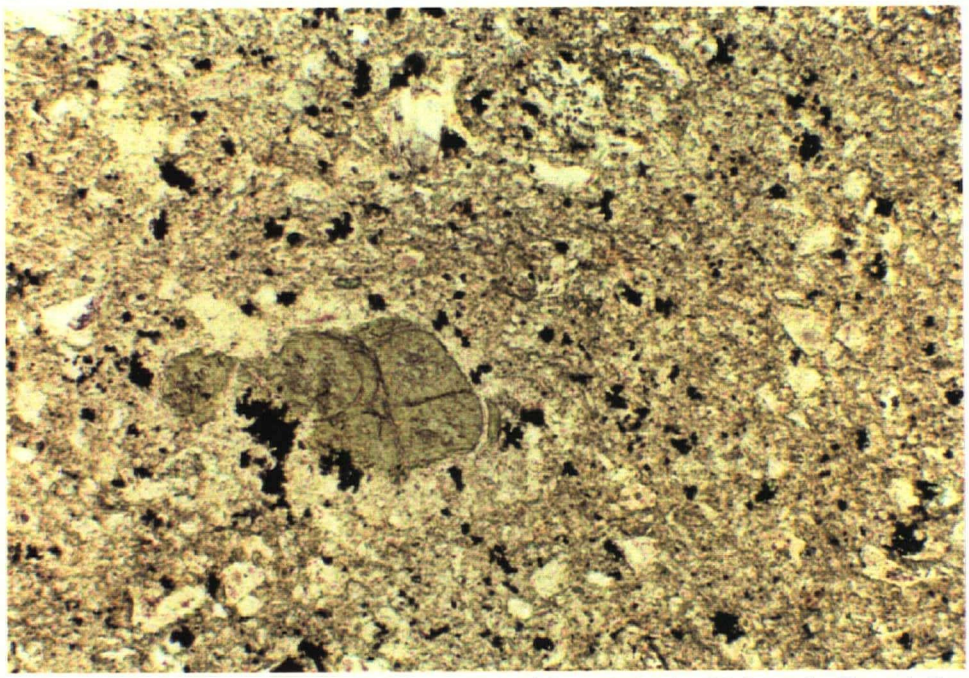

Plate 3.6a: Volcaniclastic siltstone/ash. Photomicrograph of Sample 91-03-75 from the Trough Zone shows a fragment of chlorite altered glass with perlitic cracks surrounded by very fine glass shards. (Plane polarized light; Field of view = 1.25 mm).

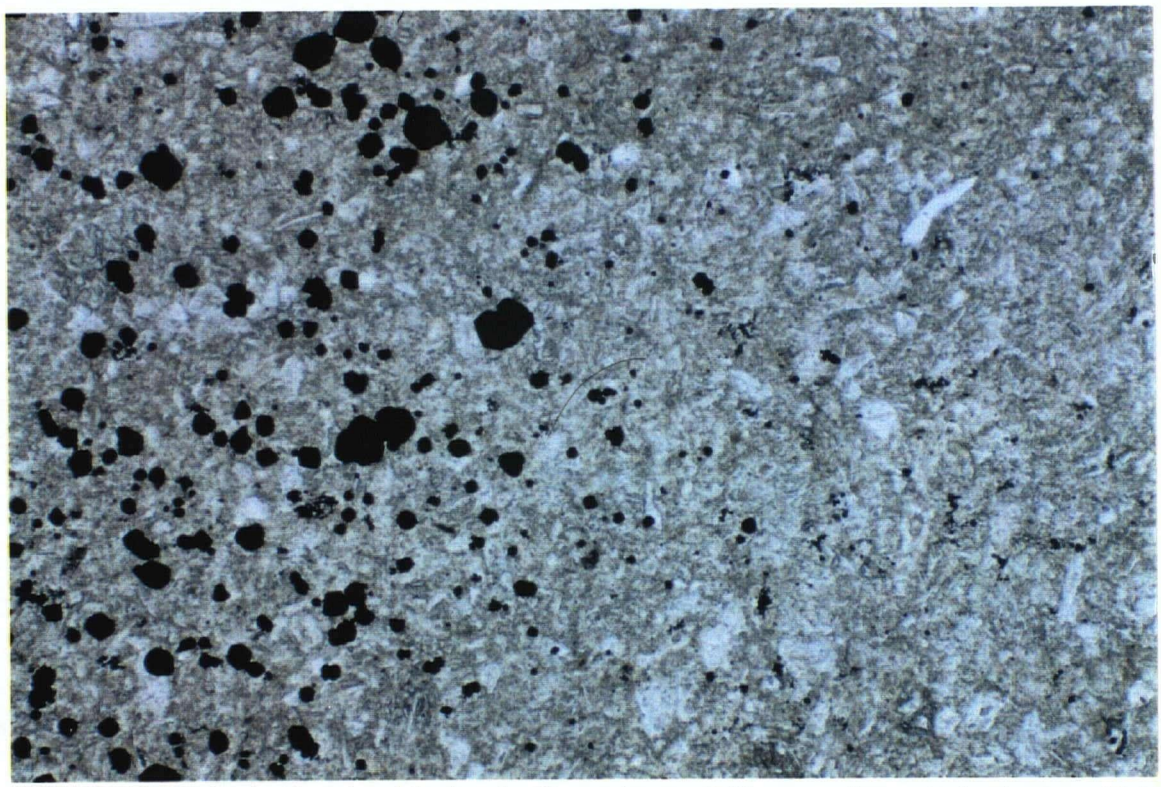

Plate 3.6b: Pyritic lamination in volcaniclastic ash. Photomicrograph illustrates fine pyrite lamination which is a common feature of the volcaniclastic sequence immediately above the stockworks in the Fleetwood and Vent Zones. Left side of photo is up direction. (Plane polarized light; Field of view = 1.25 mm).

Thin pyrite laminations are present in some of the ash beds (Plate 3.6b). They are generally observed in strata close to the mineralized Seneca Horizon. Although in thin section the pyrite appears to possibly have a replacement origin, the laminae themselves do not exhibit any compositional or textural contrast to the adjacent laminae that would favour preferential replacement. The origin of these laminae is not clear.

3.2.3 FACIES 3: SYNVOLCANIC INTRUSIONS

3.2.3.1 MAFIC INTRUSIONS

Mafic intrusions, in contrast to mafic flows, are poorly to non-vesicular. They tend to contain a greater amount of larger euhedral plagioclase phenocrysts and microlites up to 0.5 mm in size (Plate 3.7a). These are often aligned, giving the rock a weakly trachytic texture. Primary ferromagnesian phases were not observed although they may have been present and have since been altered to chlorite. Some of these intrusions are magnetic, suggesting the presence of magnetite although it was not confirmed in thin section. Peperitic textures are common at the contacts between these intrusions and unconsolidated sediments (Plate 3.7b).

3.2.3.2 FELSIC INTRUSIONS

FP Intrusions

Dacitic to rhyodacitic composition feldspar-phyric synvolcanic intrusions (FP) are very common at Seneca. They contain 5 to 15 % sub- to euhedral plagioclase phenocrysts, but more commonly less than 10 % (Plate 3.8a). Small quartz phenocrysts are also occasionally present, but generally make up less than 3 % of the rock. The groundmass of the FP intrusions has a felty, and occasionally weakly trachytic, texture defined by varying abundances of plagioclase microlites.

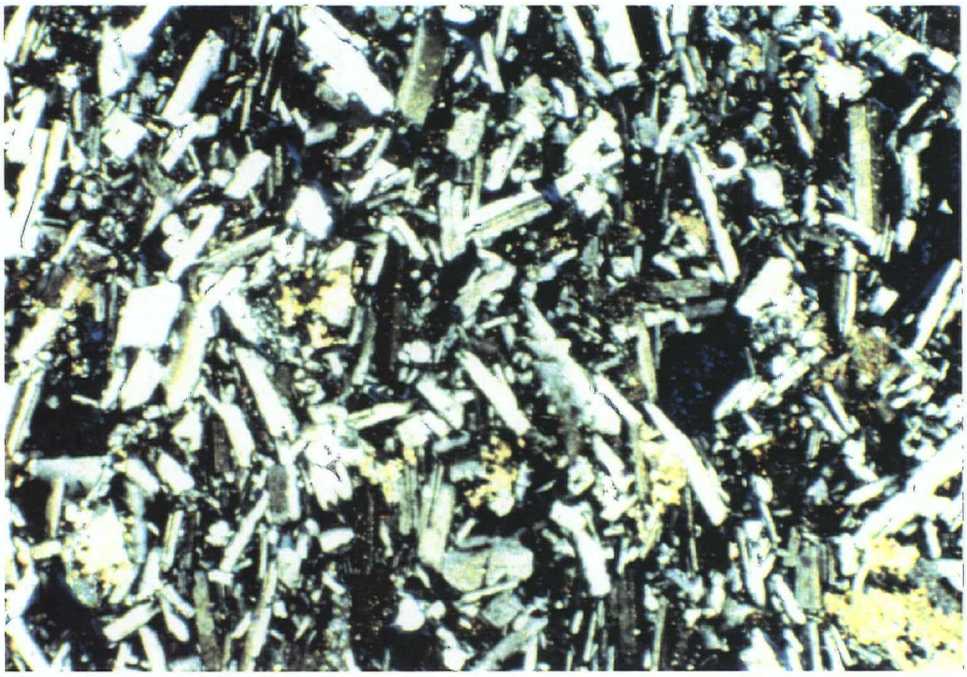

Plate 3.7a: Basaltic andesite. Photomicrograph of Sample 83-17-34 shows the abundance of plagioclase phenocrysts and the poorly vesicular nature of these units which were generally emplaced as sills (see also Plate 2.2b). (X-Nicols; Field of view = 5 mm).

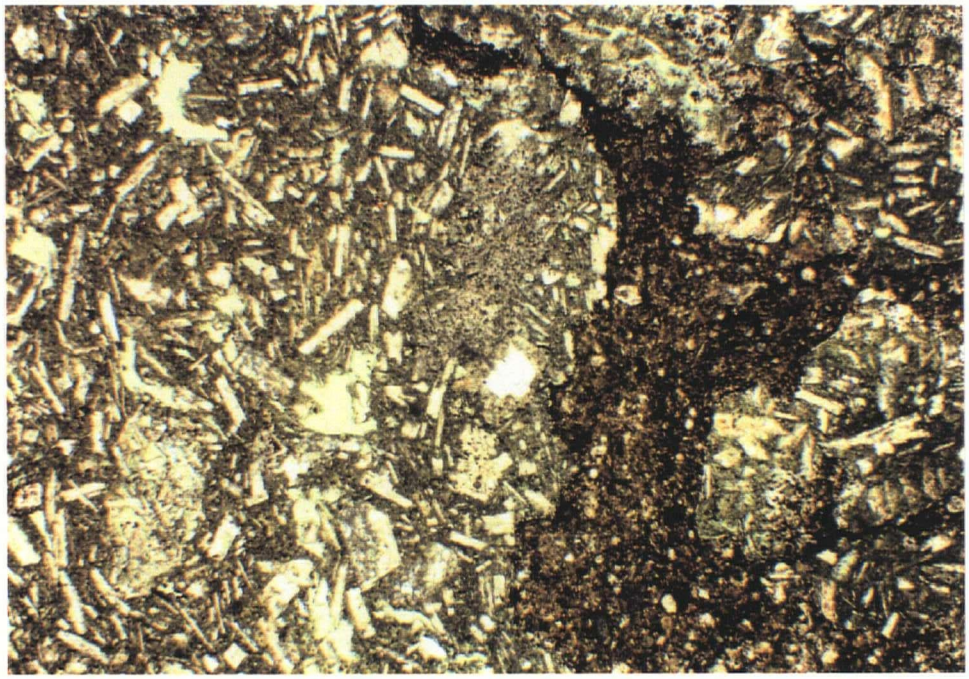

Plate 3.7b: Peperitic basaltic andesite sill. Photomicrograph of Sample 83-10-56 shows the brecciation of the mafic sill that occurs during interaction with wet sandy volcaniclastic material which becomes fluidized and incorporated into the interstices as shown by the brown areas. (Plane polarized light; Field of view = 5 mm).

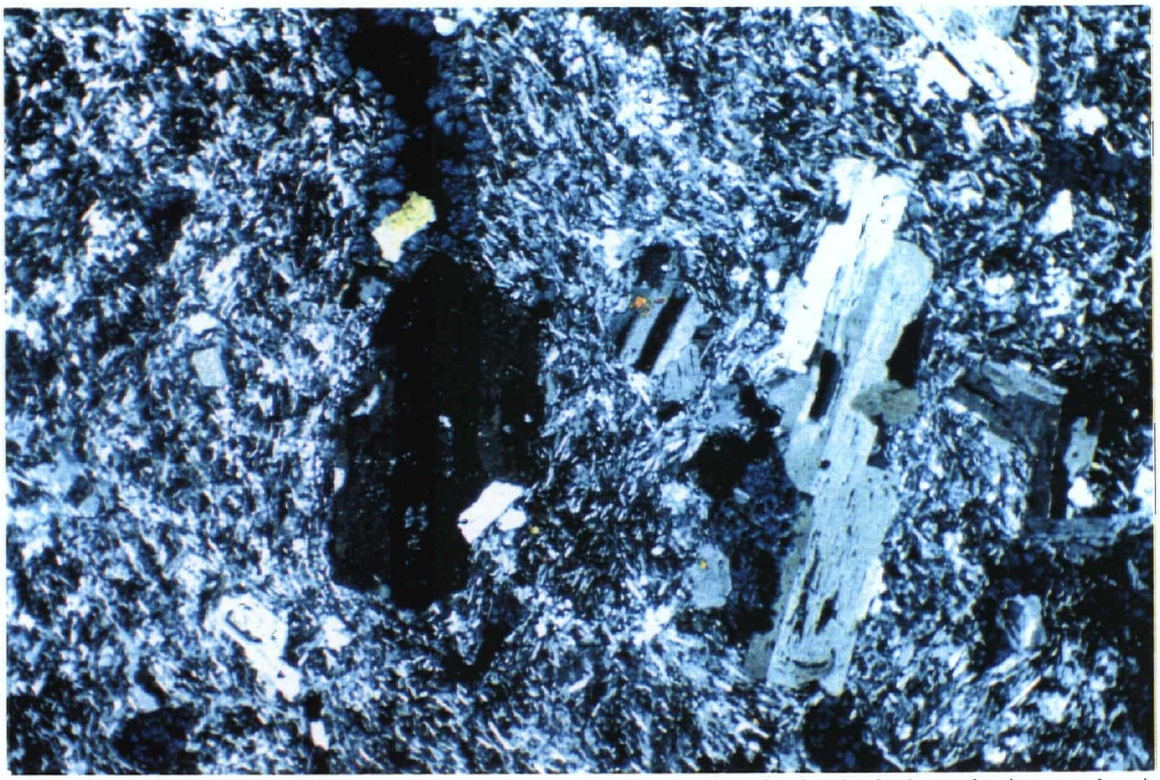

Plate 3.8a: Typical FP dacite intrusion. Photomicrograph of a massive, fresh, plagioclase-phyric synvolcanic intrusion (Sample 92-27-85) with a felted groundmass and no quartz phenocrysts. and scattered chlorite amygdules. (X-Nicols; Field of view = 5mm).

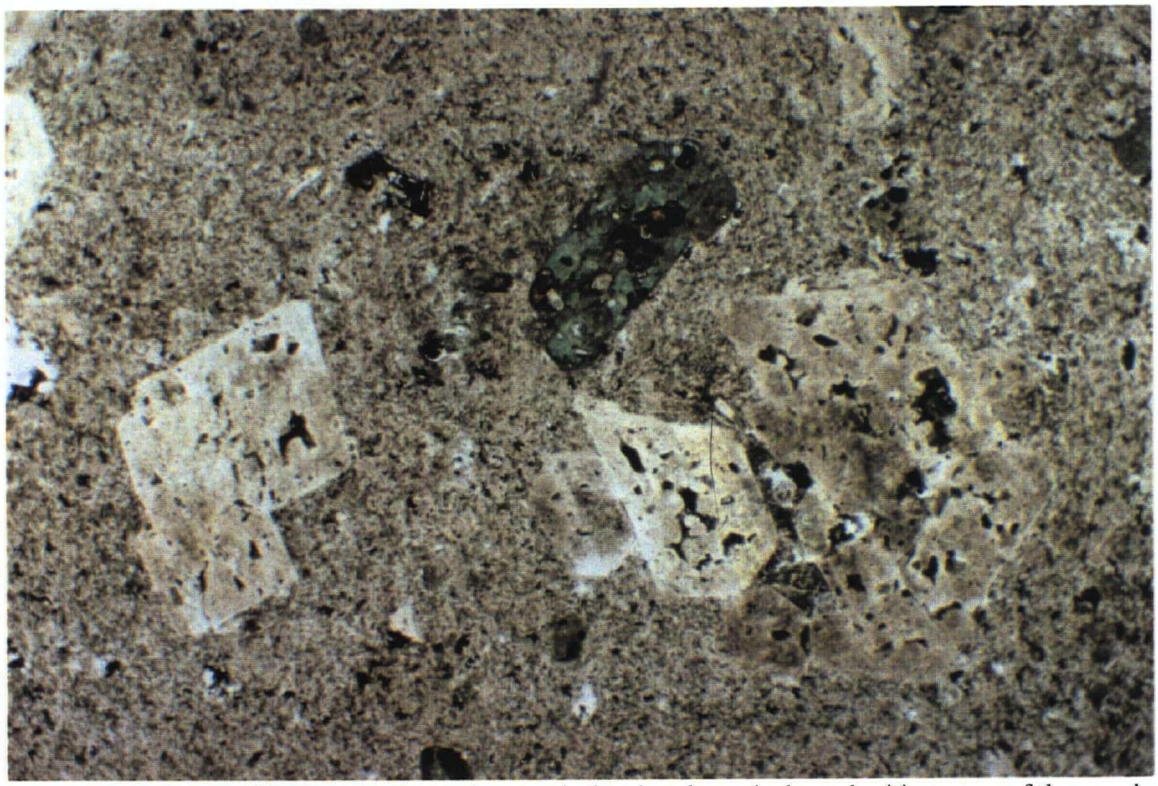

Plate 3.8b: Rhyodacite FP intrusion. Photomicrograph showing the typical porphyritic texture of these rocks with euhedral plagioclase phenocrysts (weakly sericitized) and chloritized mafic phenocrysts (pyroxene/hornblende). (Plane polarized light; Field of view = 5 mm).

The plagioclase phenocrysts are 0.5 to 2 mm in size and commonly display albite twinning. They are variably sericite altered; even the least altered samples display a weak 'dusting' of sericite, whereas the the strongly altered samples from the stockwork zones contain relict phenocrysts that have been completely replaced by sericite. The presence of potassium feldspar phenocrysts was not confirmed petrographically.

Inferred ferromagnesian phases are present, but have been completely altered to chlorite (Plate 3.8b). These relict phenocrysts make up 2 to 5 % of the rocks and are generally less than 1 mm in size. The original mineralogy of these mafic minerals, inferred from the remnant crystal shapes, appears to have been hornblende and clinopyroxene.

The FP intrusions often contain inclusions which display a variably glomeroporphyritic texture. These clusters are up to 2 mm in size and consist of intergrown plagioclase laths and chloritized mafic minerals that can comprise up to 5 % of the rock (Plate 3.10). The origin of these clusters is not clear, but they may represent small 'xenoliths' of a cumulate layer that were carried up close to surface during the emplacement of the sills and dikes. The possible lithogeochemical significance of these clusters will be discussed in the next chapter.

QFP Intrusions

Quartz-feldspar-phyric intrusions contain 7 to 15 % plagioclase phenocrysts and 5 to 10 % quartz phenocrysts. In contrast to the FP units, the groundmass of the QFP rocks is typically spherulitic, indicating it was originally glassy (Plate 3.9a). The spherulites consist of quartz and variably altered feldspar that occasionally shows a radiating texture.

Plagioclase phenocrysts are 1 to 3 mm in size and are sub- to euhedral. They are generally weakly to moderately sericite altered and display albite twinning.

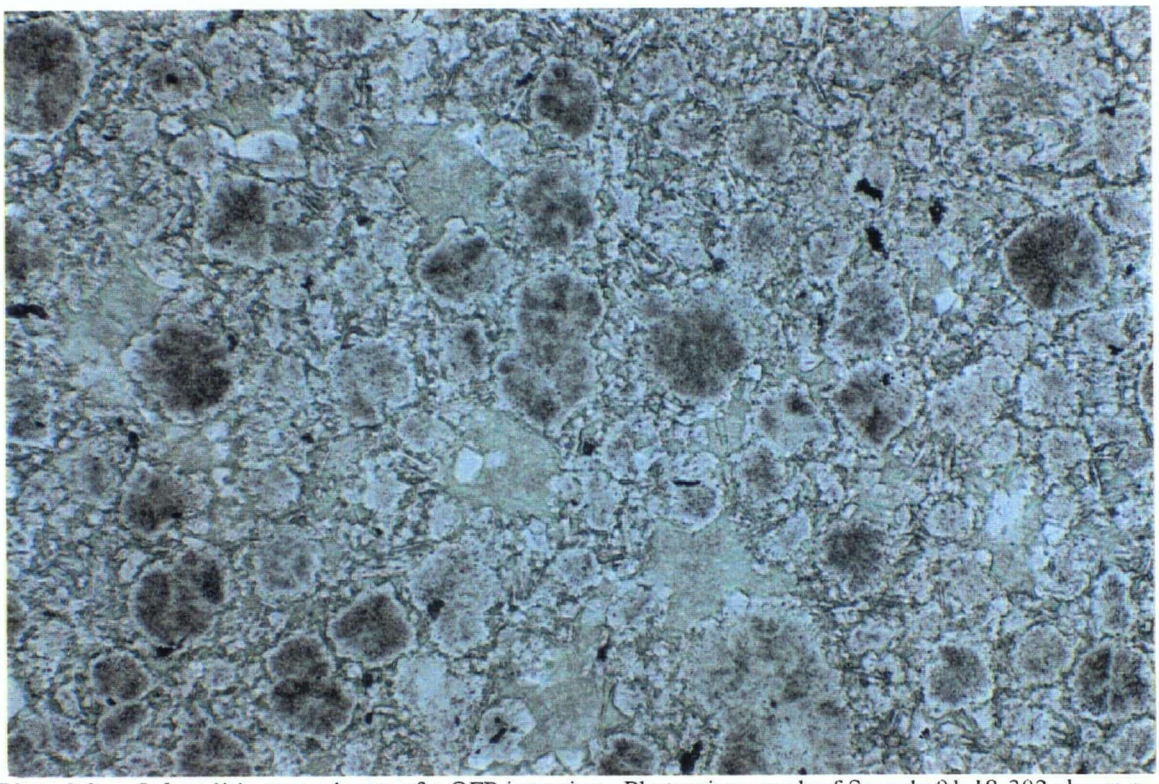

Plate 3.9a: Spherulitic groundmass of a QFP intrusion. Photomicrograph of Sample 91-18-302 shows a typical texture of the rhyolitic synvolcanic sills and dikes which tend to have a more glassy groundmass compared with FP intrusions. (Plane polarized light; Field of view = 1.25 mm).

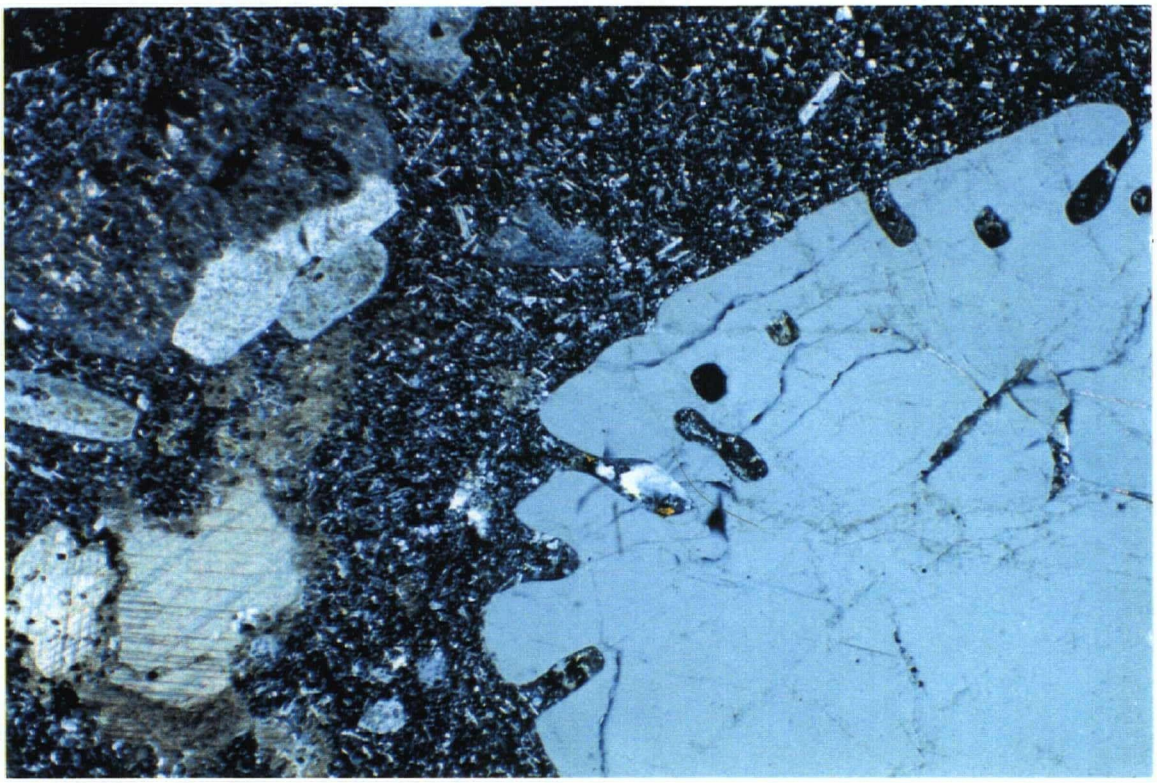

Plate 3.9b: QFP rhyolite intrusion. Photomicrograph of Sample 92-26-227 shows large embayed quartz phenocryst, a common feature of the QFP intrusions, and a weakly sericitized plagioclase phenocryst and some calcite to the left. (X-Nicols; Field of view = 5 mm).

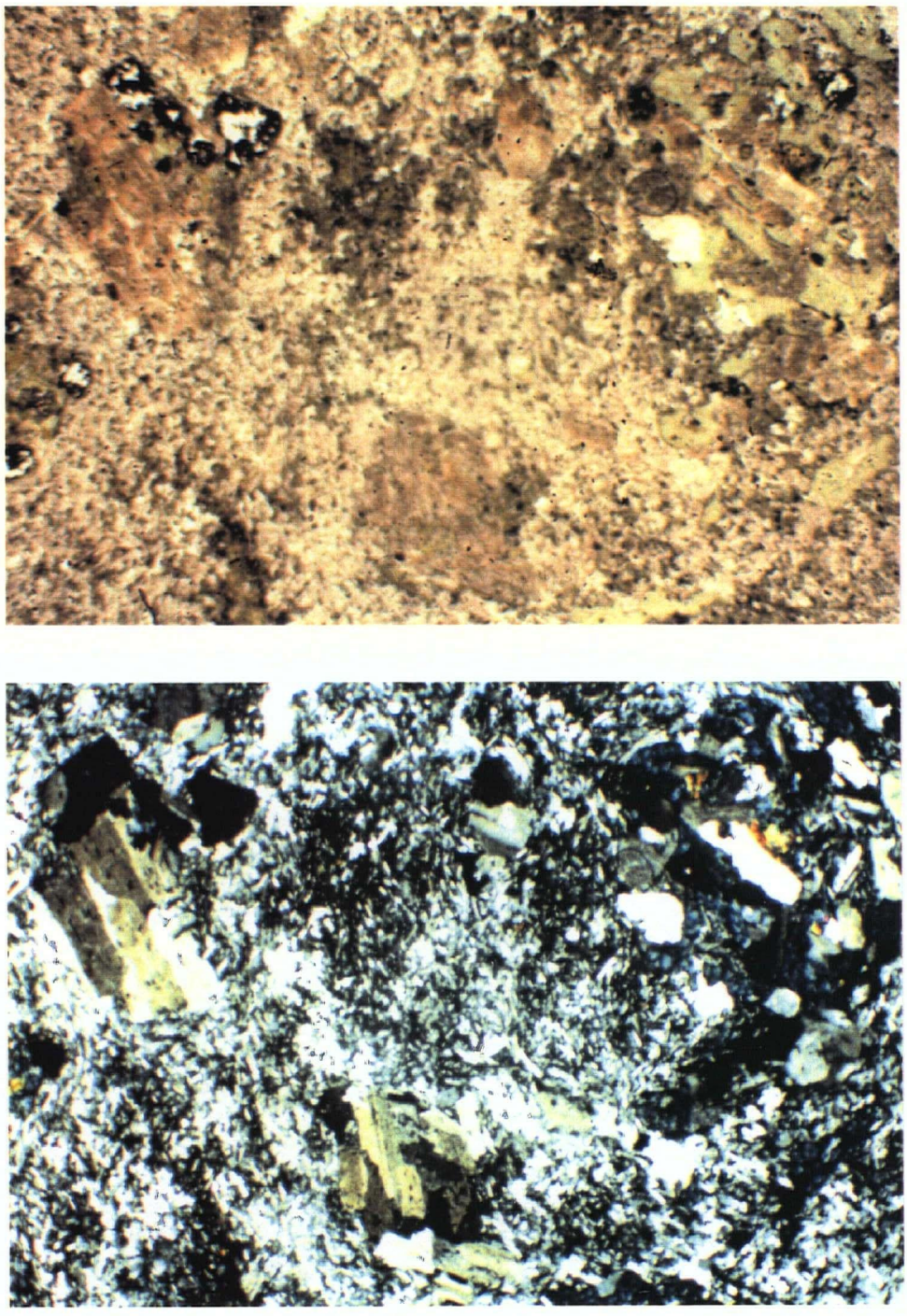

Plate 3.10: Group A felsic unit. Photomicrographs of Sample 92-27-85, an FP dacite that was classified as group A based on its major element chemistry. This more intermediate composition group often contains cumulophyric clusters of minerals (upper right) which contain plagioclase and mafic minerals (now chloritized). The groundmass generally has a felted texture and is less glassy than the more silicic rocks. (Upper: plane polarized light, Lower: X-Nicols; Field of view = 5mm).

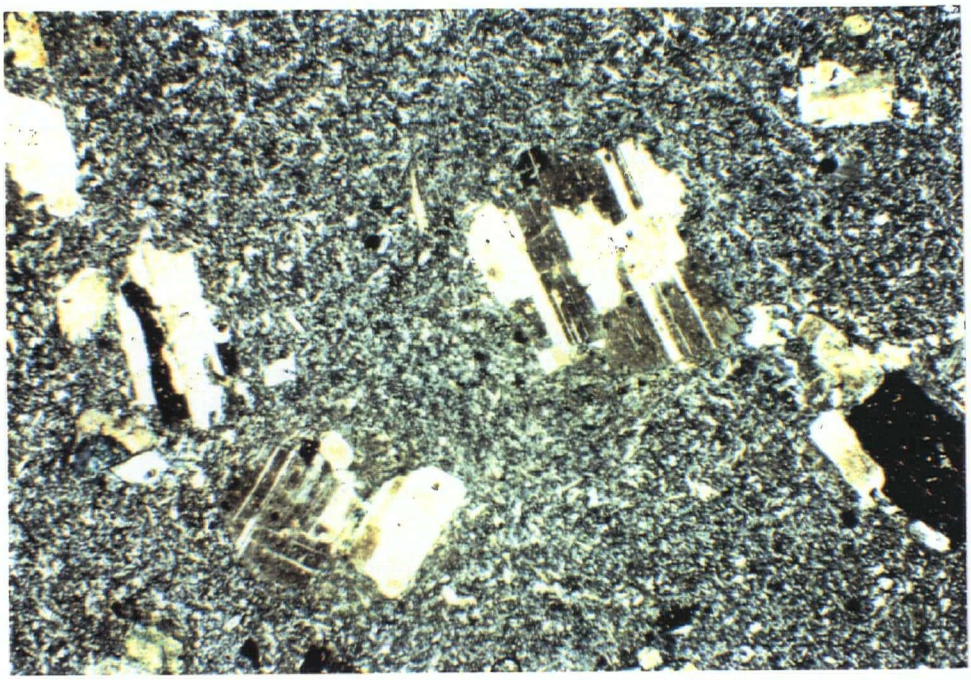

Plate 3.11a: Group C felsic unit. Photomicrograph of Sample83-02-320, an FP rhyodacite, showing plagioclase phenocrysts in an aphanitic groundmass. This compositional group of rocks generally lacks the cumulophyric inclusions seen in groups A and B and the abundant quartz of group D rocks. (X-Nicols; Field of view = 5 mm).

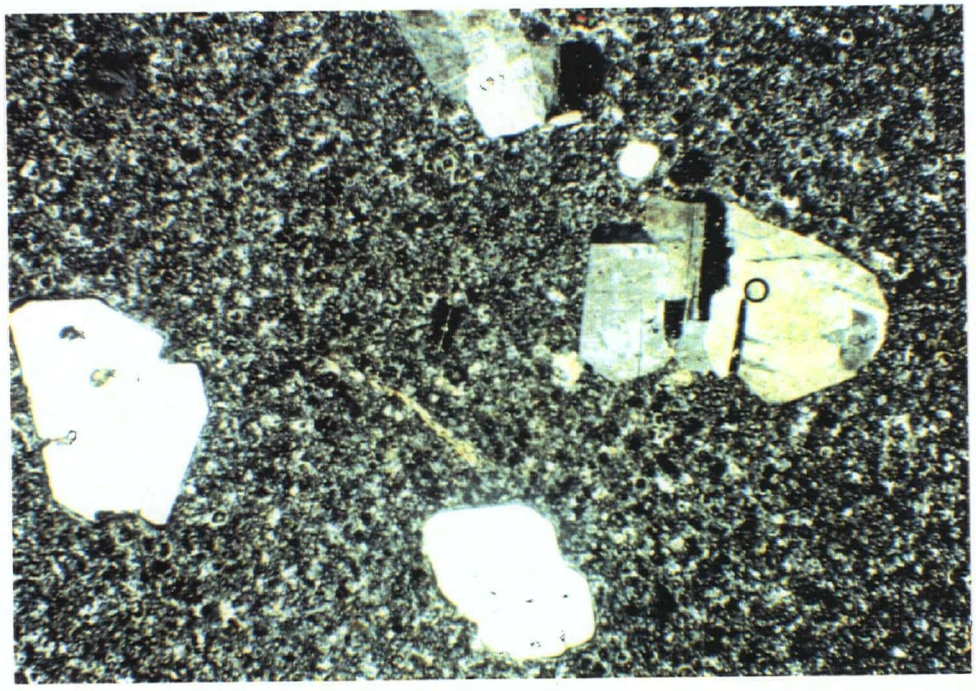

Plate 3.11b: Group D felsic unit. Photomicrograph of sample 91-02-85, a QFP rhyolite dome, showing weakly sericitized plagioclase phenocrysts and euhedral quartz crystals with silica overgrowths. This sample has the glassy, spherulitic groundmass typical of this most silicic compositional group. (X-Nicols; Field of view = 5 mm).

Quartz phenocrysts are up to 5 mm in size, but more commonly 1 to 2 mm (Plates 3.9b and 3.11b). They are commonly rounded or hexagonal in cross-section. The embayments that are common among the larger quartz phenocrysts are indicative of rapid crystal growth (McPhie and Allen, 1993).

Inferred ferromagnesian phenocrysts are present and make up 1 to 2 % of the rocks. They are also completely altered to chlorite, but are inferred to represent relict hornblende and clinopyroxene crystals. However, in contrast to the FP units, the QFP units lack cumulophyric crystal clusters.

3.3 IGNEOUS LITHOGEOCHEMISTRY

Lithogeochemical data is used in this study to distinguish different lithologic units, to determine the tectonic affinity of these units, and to determine possible igneous processes that may have produced the primary, non-hydrothermal chemical variations within the volcanic rocks. Petrography has shown that most samples at the Seneca property have undergone at least a weak sericitic alteration. In this chapter major and trace element data for a subset of *least* altered rocks are used to best determine the primary igneous lithogeochemical trends by minimizing the effects of this ubiquitous alteration. Major and trace element data for these samples are included in Table 3.1. The locations of the sampled drillholes and the geochemical data for the entire sample set is included in Appendix A. Calculations of analytical uncertainty are included in Appendix C.

3.4 METHODOLOGY

Ninety-eight samples of drillcore were analysed in four separate batches between September, 1993 and November, 1994 using X-ray fluorescence at Geochemical Laboratories, Department of Earth and Planetary Sciences, McGill University, Montreal, Quebec. Major

Table 3.1. Chemical composition of least altered volcanic rocks at the Seneca prospect.

Sample	83-02-67	83-02-186	83-02-277	83-02-320	83-06-50	85-03-70	85-03-126	91-02-85	91-02-170	91-10-99	91-10-118	92-26-227	92-27-71
Hole	83-02	83-02	83-02	83-02	83-06	85-03	85-03	91-02	91-02	91-10	91-10	92-26	92-27
Depth	67.0	186.3	277.0	319.6	49.8	70.5	126.2	85.2	170.0	99.1	118.0	227.2	70.9
Depth	219.8	611.1	908.8	1048.7	163.4	231.2	414.1	279.4	557.8	325.1	387.3	745.2	232.5
Unit	FP	FP	FP	FP	FP	FP	FP	QFP	FP	FEL DYK	FEL DYK	FP	QFP
(Wt. %)													
SiO_2	69.43	68.83	70.50	70.06	69.27	69.26	70.35	73.93	69.13	74.25	75.04	73.26	69.59
TiO_2	0.50	0.51	0.43	0.45	0.40	0.41	0.39	0.28	0.50	0.28	0.30	0.29	0.39
Al_2O_3	14.59	14.73	13.95	14.42	14.98	14.94	14.64	13.61	14.40	12.57	12.25	13.64	13.97
Fe_2O_3	3.99	3.90	3.16	3.45	3.77	3.89	3.68	2.34	4.27	2.14	2.16	2.38	3.52
MnO	0.09	0.06	0.17	0.07	0.08	0.08	0.10	0.06	0.10	0.08	0.06	0.08	0.14
MgO	2.23	2.06	1.84	1.94	1.92	2.27	1.54	1.22	2.20	0.55	0.69	0.78	1.45
CaO	0.84	1.13	1.29	0.92	0.78	0.43	0.74	0.34	0.73	1.38	0.85	1.72	2.46
Na_2O	4.72	5.40	4.44	4.65	5.75	5.97	6.01	4.94	5.58	3.48	4.84	5.01	4.51
K_2O	1.89	1.25	1.50	1.88	1.21	0.49	1.08	1.94	0.98	3.29	1.82	1.34	1.03
P_2O_5	0.14	0.15	0.11	0.11	0.13	0.14	0.12	0.05	0.11	0.05	0.05	0.06	0.09
LOI	1.92	1.78	2.58	2.11	1.93	2.05	1.43	1.63	1.83	1.67	1.25	1.69	3.23
Total	100.34	99.80	99.97	100.06	100.22	99.93	100.08	100.34	99.83	99.74	99.31	100.25	100.38
(ppm)													
Cr	106	90	137	193	104	48	98	153	117	36	24	bd	156
Ni	11	8	13	11	6	7	15	6	4	5	3	bd	18
Co	9	3	12	9	10	7	6	6	9	bd	bd	28	7
Sc	11	10	8	10	3	8	7	bd	9	na	na	na	6
V	57	56	47	51	60	52	61	28	73	24	20	40	51
Cu	8	3	8	21	21	7	18	11	25	29	22	36	46
Pb	5	5	4	4	4	4	4	4	8	3	1	na	6
Zn	47	55	69	44	82	57	58	42	207	40	34	49	94
Ba	424	292	263	481	340	17	475	529	426	1539	1272	725	448
Rb	24	13	19	24	11	8	8	17	8	37	18	13	14
Sr	144	126	58	101	108	64	101	73	94	104	113	299	179
Ga	14	14	12	12	13	14	13	11	12	13	12	13	12
Nb	6	5	6	6	5	5	5	5	6	9	9	5	4
Zr	116	115	124	127	110	109	115	119	116	130	131	114	103
Y	28	26	23	24	23	22	21	17	25	25	26	17	21
Th	bd	bd	bd	bd	bd	bd	bd	bd	bd	bd	bd	bd	bd
U	bd	bd	bd	bd	bd	bd	bd	bd	bd	bd	bd	bd	1.0
Cs	na	na	0.2	na	na	na	na	na	na	na	na	na	na
Hf	na	na	2.7	na	na	na	na	na	na	na	na	na	na
La	na	na	11.3	na	na	na	na	na	na	na	na	na	na
Ce	na	na	23	na	na	na	na	na	na	na	na	na	na
Nd	na	na	12	na	na	na	na	na	na	na	na	na	na
Sm	na	na	2.76	na	na	na	na	na	na	na	na	na	na
Eu	na	na	0.87	na	na	na	na	na	na	na	na	na	na
Tb	na	na	0.5	na	na	na	na	na	na	na	na	na	na
Yb	na	na	2.46	na	na	na	na	na	na	na	na	na	na
Lu	na	na	0.35	na	na	na	na	na	na	na	na	na	na
Zr/Y	4.1	4.4	5.4	5.3	4.8	5.0	5.5	7.0	4.6	5.2	5.0	6.7	4.9
La_N/Yb_N	-	-	3.1	-	-	-	-	-	-	-	-	-	-

Analytical method: X-ray fluorescence, induced neutron activation analysis
The major elements plus Cu-Zn-Ni-Cr-V-Sc were analysed using glass beads.
The elements Zr-Y-Nb-Rb-Sr-Ga-Pb were analysed using pressed pellets.
(bd = below detection limit; na = not analysed)

Table 3.1. Chemical composition of least altered volcanic rocks at the Seneca prospect.

Sample	92-27-85	92-27-177	92-29-140	92-29-227	92-39-200	93-VT-01	93-FW-51	83-02-227	83-06-124	83-10-56	83-17-34	85-03-155
Hole	92-27	92-27	92-29	92-29	92-39	86-13	91-06	83-02	83-06	83-10	83-17	85-03
Depth	85.2	177.7	140.3	226.8	200.5	25.0	128.0	227.0	123.9	53.6	34.0	154.8
Depth	279.5	583.0	460.1	744.1	657.9	82.0	419.9	744.8	406.5	175.7	111.7	508.0
Unit	FP	FP	QFP	FP	QFP	FP	FP	MAFIC	MAFIC	MAFIC	MAFIC	MAFIC
(Wt. %)												
SiO_2	64.75	68.95	75.01	63.72	73.53	71.29	74.16	47.28	51.41	51.90	51.83	53.66
TiO_2	0.68	0.51	0.27	0.71	0.31	0.41	0.31	0.68	0.83	0.86	0.83	0.81
Al_2O_3	15.49	14.36	13.04	16.01	13.37	14.32	13.24	19.93	17.50	18.25	17.51	17.45
Fe_2O_3	6.23	4.43	2.41	5.89	2.23	3.48	2.46	9.40	10.10	9.58	10.11	9.02
MnO	0.20	0.15	0.19	0.20	0.10	0.19	0.12	0.17	0.19	0.21	0.31	0.16
MgO	3.03	2.86	1.08	3.49	0.94	2.07	1.30	7.43	6.51	6.16	6.14	5.40
CaO	1.61	1.28	1.46	1.71	1.34	0.54	0.83	4.89	2.97	2.44	2.82	2.93
Na_2O	5.59	4.31	4.80	5.57	3.97	5.22	4.35	3.86	4.79	5.92	5.64	5.57
K_2O	0.05	0.73	0.62	0.28	2.84	0.54	1.80	1.39	0.68	0.10	0.06	0.29
P_2O_5	0.20	0.11	0.06	0.23	0.06	0.09	0.06	0.13	0.19	0.24	0.22	0.23
LOI	2.20	2.39	1.54	2.72	1.52	1.70	1.52	5.13	5.54	4.57	4.98	4.87
Total	100.03	100.08	100.48	100.53	100.21	99.85	100.16	100.29	100.71	100.23	100.45	100.39
(ppm)												
Cr	77	127	1	bd	376	79	15	209	75	30	45	55
Ni	19	18	bd	bd	3	11	37	38	18	21	15	20
Co	12	9	21	15	9	3	25	32	30	34	27	34
Sc	17	5	na	na	6	10	3	29	23	24	22	22
V	99	78	42	56	29	56	39	210	227	215	210	186
Cu	379	6	61	249	609	66	38	45	37	122	69	76
Pb	6	4	na	na	5	3	1	9	9	7	8	8
Zn	184	83	114	171	850	99	57	66	126	190	204	147
Ba	bd	200	251	146	2499	200	1576	753	747	37	6	148
Rb	4	11	8	3	20	8	16	22	18	9	10	10
Sr	118	141	312	224	219	89	165	372	103	119	72	156
Ga	14	13	13	17	9	12	12	15	16	17	16	15
Nb	5	5	5	4	5	5	11	1	4	4	4	4
Zr	96	114	109	94	120	116	126	47	81	77	75	79
Y	26	26	15	36	17	21	26	14	19	21	16	19
Th	bd	bd	bd	bd	bd	bd	bd	1.0	1.0	bd	1.0	bd
U	bd	bd	bd	bd	1.0	bd	bd	bd	bd	bd	bd	bd
Cs	na	na	0.3	na	bd	na	na	na	na	na	bd	bd
Hf	na	na	3.0	na	2.8	na	na	na	na	na	1.2	1.4
La	na	na	9.6	na	11.1	na	na	na	na	na	3.0	5.2
Ce	na	na	21	na	24	na	na	na	na	na	8	13
Nd	na	na	9	na	12	na	na	na	na	na	6	8
Sm	na	na	1.85	na	2.21	na	na	na	na	na	1.58	2.09
Eu	na	na	0.50	na	0.72	na	na	na	na	na	0.52	0.73
Tb	na	na	0.4	na	0.4	na	na	na	na	na	0.3	0.4
Yb	na	na	1.78	na	2.04	na	na	na	na	na	1.66	1.82
Lu	na	na	0.26	na	0.30	na	na	na	na	na	0.24	0.26
Zr/Y	3.7	4.4	7.3	2.6	7.1	5.5	4.8	3.4	4.3	3.7	4.7	4.2
La_N/Yb_N	-	-	3.6	-	3.7	-	-	-	-	-	1.2	1.9

Analytical method: X-ray fluorescence

The major elements plus Cu-Zn-Ni-Cr-V-Sc were analysed using glass beads.

The elements Zr-Y-Nb-Rb-Sr-Ga-Pb were analysed using pressed pellets.

(bd = below detection limit; na = not analysed)

Table 3.1. Chemical composition of least altered volcanic rocks at the Seneca prospect.

Sample	91-08-200	91-16-69	91-16-231	91-16-233	92-27-333	92-28-374	93-SN-47	94-FF-01	
Hole	91-08	91-16	91-16	91-16	92-27	92-28	79-08	-	
Depth	199.8	69.3	231.1	232.9	333.5	374.5	161.0	-	Detection
Depth	655.6	227.5	758.3	764.0	1094.0	1228.6	528.2	-	Limits
Unit	MAFIC	MAFIC	MAFIC	MAFIC	MAFIC	MAFIC	MAFIC	MAFIC	(ppm)
(Wt. %)									
SiO2	48.91	50.95	45.56	43.75	45.33	47.89	52.91	39.42	60
TiO2	0.77	0.77	0.65	0.66	0.77	0.58	1.18	0.75	35
Al2O3	20.55	17.16	15.84	16.10	17.80	20.38	15.18	14.97	120
Fe2O3	9.45	10.67	7.92	9.52	10.79	8.71	13.42	8.38	30
MnO	0.16	0.58	0.29	0.33	0.58	0.41	0.25	0.31	30
MgO	4.17	8.46	6.34	9.04	13.88	10.45	4.39	5.73	95
CaO	9.42	3.11	10.45	8.19	1.29	1.07	4.03	17.42	15
Na2O	2.92	3.79	2.48	3.08	3.21	1.30	4.48	0.93	75
K2O	0.36	0.14	1.24	0.20	0.01	3.09	0.29	0.29	25
P2O5	0.15	0.13	0.14	0.11	0.13	0.13	0.27	0.15	35
LOI	3.58	5.02	9.09	9.34	6.92	6.63	4.06	11.44	100
Total	100.44	100.78	100.00	100.32	100.71	100.64	100.47	88.35	100
(ppm)									
Cr	16	44	150	132	133	92	9	63	2
Ni	19	18	14	23	33	22	bd	10	3
Co	25	31	30	36	48	13	28	24	10
Sc	na	29	32	32	31	na	29	34	10
V	280	235	242	229	264	206	283	273	10
Cu	167	118	94	93	151	35	108	86	15
Pb	bd	8	bd	10	6	na	6	bd	2
Zn	62	286	83	273	479	317	120	86	2
Ba	65	3	1026	88	bd	1249	329	76	50
Rb	4	11	7	12	9	43	2	5	1
Sr	352	196	174	177	78	78	270	350	1
Ga	18	14	13	13	15	16	19	16	1
Nb	6	2	7	1	2	4	7	0	1
Zr	49	63	30	44	48	37	59	47	1
Y	19	17	15	14	16	16	38	17	1
Th	bd	1.0	bd	1.0	bd	bd	bd	0.4	0.1
U	bd	bd	bd	bd	bd	bd	4.8	bd	0.1
Cs	na	na	na	0.4	0.2	na	bd	bd	0.2
Hf	na	na	na	0.7	0.7	na	1.4	0.6	0.2
La	na	na	na	2.5	2.9	na	6.6	3.0	0.1
Ce	na	na	na	6	8	na	19	9	1
Nd	na	na	na	5	6	na	13	7	1
Sm	na	na	na	1.39	1.79	na	3.81	1.99	0.01
Eu	na	na	na	0.52	0.56	na	1.16	0.71	0.05
Tb	na	na	na	0.3	0.4	na	0.8	0.4	0.1
Yb	na	na	na	1.31	1.53	na	3.25	1.52	0.05
Lu	na	na	na	0.18	0.23	na	0.47	0.22	0.01
Zr/Y	2.6	3.7	2.0	3.1	3.0	2.3	1.5	2.8	-
La_N/Yb_N	-	-	-	1.3	1.3	-	1.4	1.3	-

Analytical method: X-ray fluorescence, induced neutron activation analysis
The major elements plus Cu-Zn-Ni-Cr-V-Sc were analysed using glass beads.
The elements Zr-Y-Nb-Rb-Sr-Ga-Pb were analysed using pressed pellets.
(bd = below detection limit; na = not analysed)

elements plus the trace elements Cu, Zn, Ni, Cr, V and Sc were measured using glass beads. The trace element concentrations of Zr, Y, Nb, Rb, Sr, Ga and Pb were measured using pressed pellets. The rare earth elements were analysed by instrumental neutron activation analysis at Activation Laboratories Ltd., Ancaster, Ontario.

The sample set was chosen to approximately reflect both the entire compositional range and the relative abundance of the various synvolcanic intrusive, extrusive and volcaniclastic units observed in the examined stratigraphic interval at Seneca. Fewer volcaniclastic samples were analysed because their geochemistry is more difficult to interpret due to the influence of non-igneous processes such as mixing of various clast compositions during transportation. As such, the volcaniclastic samples in the data set are restricted almost entirely to massive, fine-grained Facies 2.2 volcanic siltstones. These samples are not included in the least altered data subset. All samples were taken from drillcore, except for 94-FF-01 which was collected from an outcrop of mafic lava near Morris Creek, 4 km to the southeast of the property. Petrography and plots of the lithogeochemical data were used to determine which samples have undergone the least alteration. Samples with the least amount of sericitization of feldspars and/or silicification of the groundmass were chosen for the least altered subset. Data for samples on all lithogeochemical plots have been recalculated on an anhydrous basis.

3.5 TECTONIC AFFINITY

Previous studies (Irvine and Baragar, 1971; Winchester and Floyd, 1977; Wood et al., 1979) have illustrated the use of certain major and trace elements to discriminate between rock suites from different tectonic settings. The hydrothermal alteration present around Seneca limits the use of diagrams based on mobile elements. These mobile elements will not be ignored completely, however, and will be discussed in the subsequent chapter dealing with alteration and

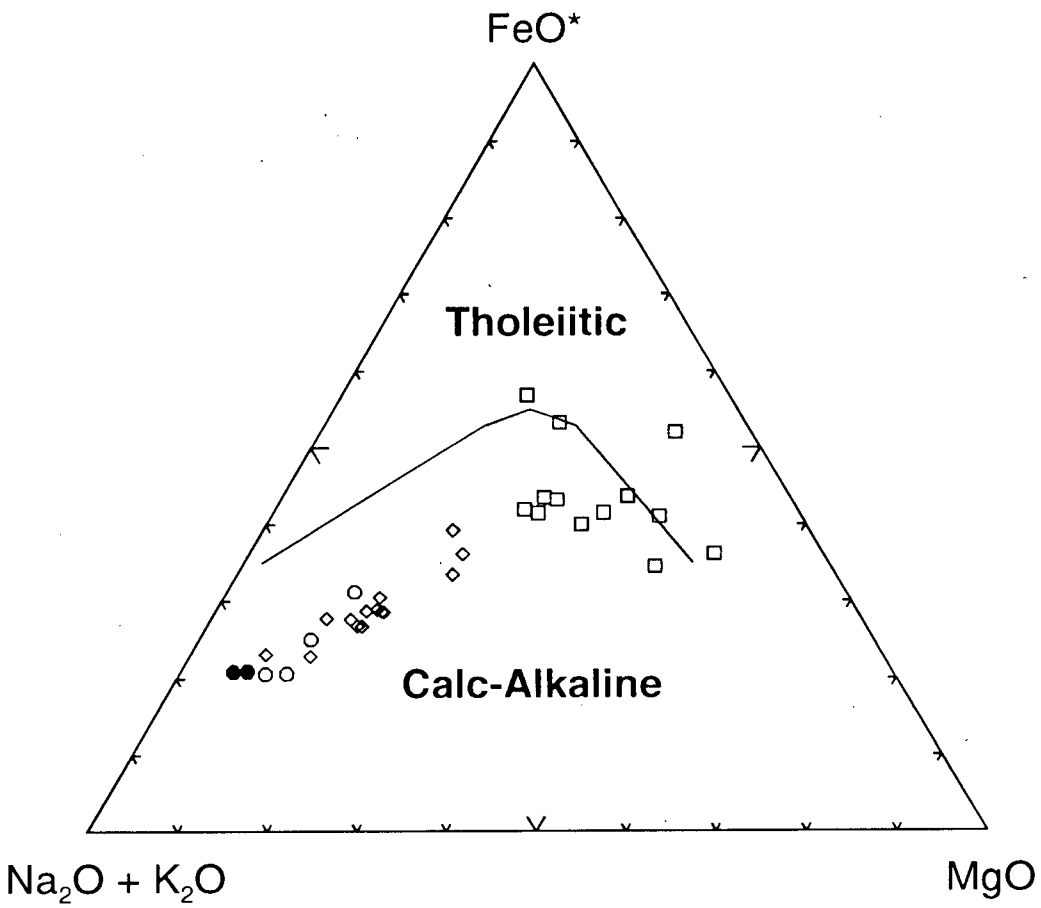

(from Irvine & Baragar, 1971, fig. 2)

LEGEND

- □ Basalts, andesites
- ◇ FP dacites & rhyodacites
- ○ QFP rhyolites
- ● Aphyric rhyolite dikes

Figure 3.1. AFM plot of least altered volcanic rocks from the Seneca property. The plot illustrates the calc-alkaline nature of the volcanic sequence.

a)

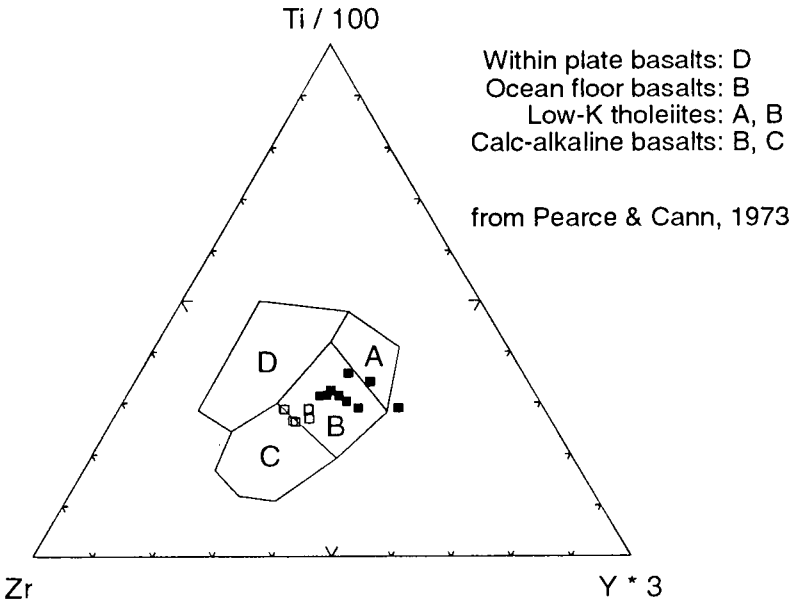

b)

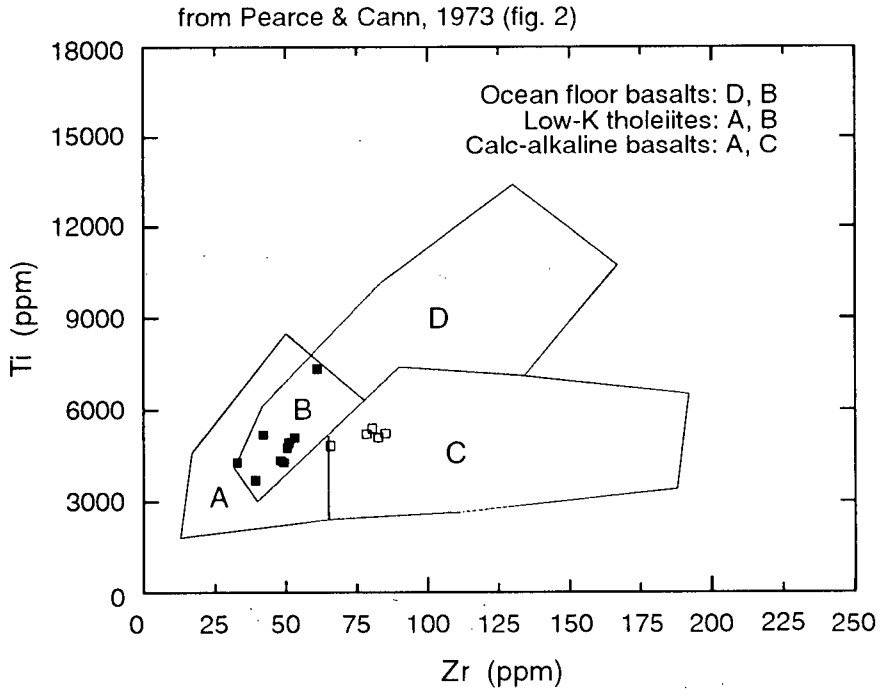

Figure 3.2. Zr-Ti -Y and Zr-Ti discrimination plots for least altered basalts and basaltic andesites at Seneca. These plots illustrate the compositional contrasts among the mafic rocks from low-K tholeiites (basalts) to calc-alkaline basalts (basaltic andesites). Filled squares are basalts and open squares are basaltic andesite.

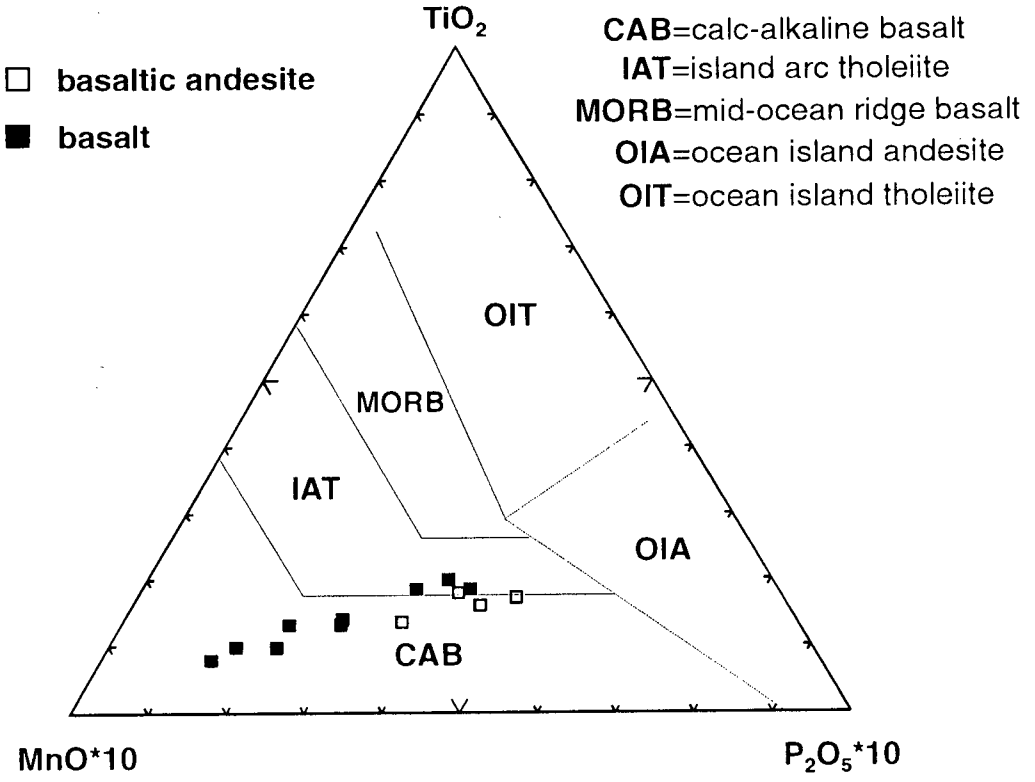

Figure 3.3. TiO_2-(MnO*10)-(P_2O_5*10) discrimination plot for all mafic samples at the Seneca property. Compositional fields are taken from Mullen (1983). This plot demonstrates the calc-alkaline to weakly tholeiitic nature of the basalts and basaltic andesites at Seneca.

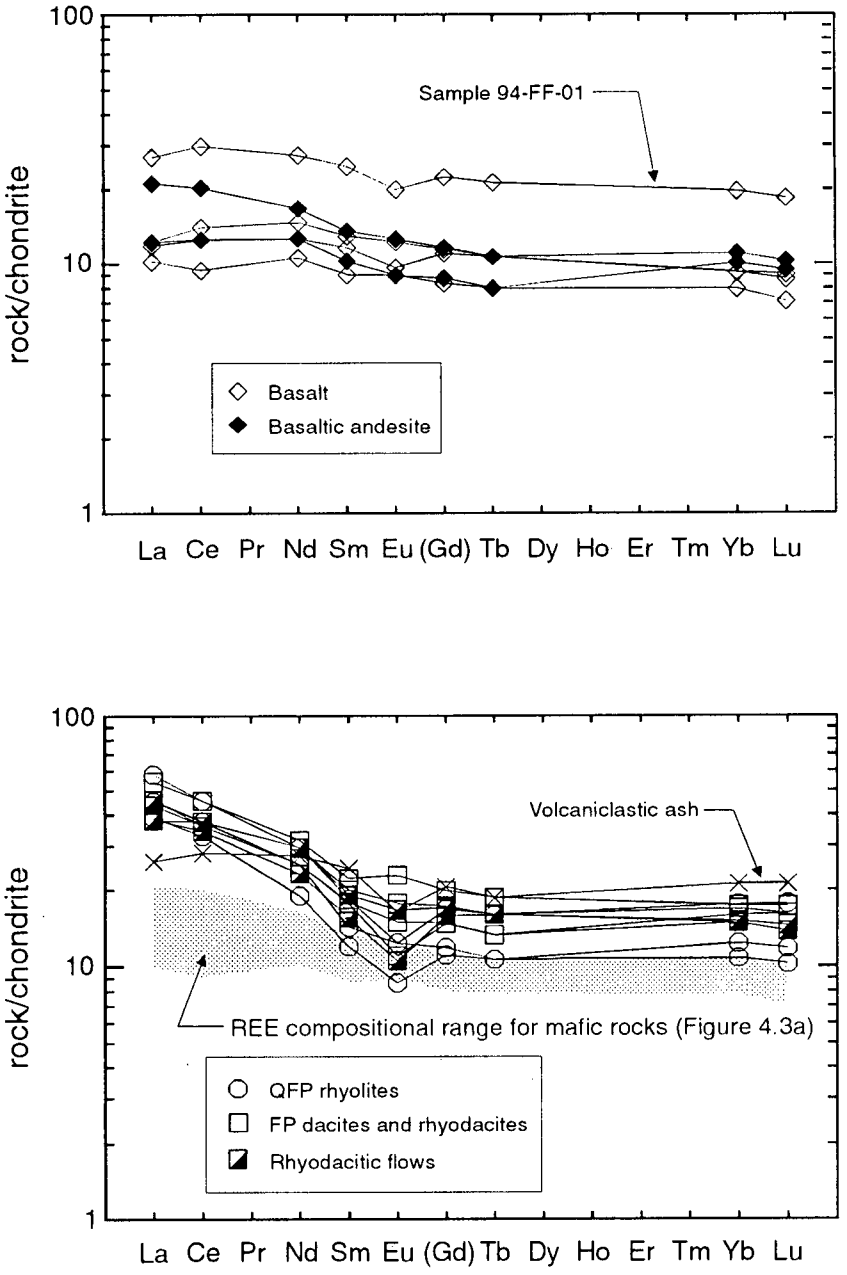

Figure 3.4. Rare earth element patterns of a) basalts and basaltic andesites and b) dacites to rhyolites from the Seneca property. REE abundances are normalized to the chondritic values of Evensen et al. (1978). Gd values have been estimated using the formula Gd = 1/3 Sm+2/3Tb.

mass changes. Also, Harker plots of the major elements versus SiO_2 will be used in this chapter to illustrate the range in the geochemical data. The low overall abundances of some trace elements (eg. Ta, Th, U) in the rocks at Seneca also hinders the use of some of these methods of tectonic discrimination.

The AFM plot of Irvine and Baragar (1971) (Figure 3.1) shows that the volcanic rock samples from Seneca have a calc-alkaline affinity, although some of the mafic samples may have a more tholeiitic nature having less Na_2O and K_2O and more FeO and MgO. Figure 3.2 illustrates that the mafic rocks at Seneca range in composition from low-K tholeiites to calc-alkaline basalts. The mafic samples plot in the fields of calc-alkaline basalts to island arc tholeiites in the TiO_2-(MnO_2*10)-(P_2O_5*10) discrimination plot (Figure 3.3; Mullen, 1983). These trends are consistent with the rocks having been formed in a volcanic island arc setting at or near a destructive plate boundary (Irvine and Baragar, 1971; Pearce and Cann, 1973).

Figure 3.4 depicts the rare earth element abundances relative to chondrite for both mafic and felsic rocks at Seneca. Chondrite values are taken from Evensen et al. (1978). The mafic samples (Figure 3.4a) show flat, chondritic to slightly fractionated, light REE-enriched patterns. La_N/Yb_N ratios range from 1.2 to 1.9 indicating a tholeiitic to transitional affinity (Jakes and Gill, 1970). The felsic rocks (Figure 3.4b) all have an enrichment in the light REE, and La_N/Yb_N ratios range from 2.0 to 3.7 indicating a transitional to calc-alkaline affinity (Jakes and Gill, 1970).

One sample of fine grained volcaniclastic siltstone/ash (Sample 91-16-94, Appendix A.3) was analysed for REEs. This sample has approximately the same overall abundances and the same flat trend amongst the HREEs as the felsic samples (Figure 3.4). However, the volcaniclastic sample does not exhibit the enrichment in LREEs that characterizes the dacitic to rhyolitic lavas and intrusions. The REE pattern of this sample coincides well with the pattern for sample

Zr and Y are immobile elements and are good indicators of the tectonic affinity of a volcanic suite (Pearce and Cann, 1973; MacLean, 1990). Pearce and Cann (1973) and Pearce (1982) summarized the trace element abundances for rocks of different tectonic settings. Their data showed that abundances of Zr and Y for rocks from volcanic arcs were lower than those for rocks from oceanic ridges and basins. Zr and Y abundances for ocean floor basalts range from 64 to 129 ppm and 22 to 47 ppm respectively; Zr and Y abundances for mafic volcanic arc rocks range from 33 to 107 ppm and 15 to 24 ppm respectively (Pearce and Cann, 1973). Using these trace element abundances as a guide, the volcanic rocks at Seneca are consistent with formation in a volcanic arc. The data summarized by Pearce and Cann (1973) also demonstrated that in a volcanic arc setting, rocks with a tholeiitic affinity (lower K_2O, higher Fe/Mg values) had Zr/Y ratios of less than 3.5, whereas rocks of calc-alkaline affinity (higher K_2O) had Zr/Y ratios of greater than 3.5. Using this Zr/Y ratio of 3.5 as a potential boundary between tholeiitic and calc-alkaline rocks in a volcanic arc setting, it is apparent that almost all of the felsic rocks (rhyodacites and rhyolites) at Seneca are calc-alkaline in nature. The mafic rocks (basalts and basaltic andesites) can be subdivided into two groups based on this Zr/Y boundary. The more basaltic composition flows and breccias have Zr/Y ratios of less than 3.5, whereas the more andesitic composition sills have Zr/Y ratios of greater than 3.5.

3.6 GEOCHEMICAL CLASSIFICATION OF UNITS

Using the Zr/TiO_2-SiO_2 discrimination diagram of Winchester and Floyd (1977), it is apparent that the volcanic rocks at Seneca are bimodal with a basaltic to basaltic andesitic population and a dacitic to rhyolitic population which are separated by a 'gap' corresponding to compositions from 53 to 63 wt. % SiO_2 (Fig. 3.5). The bimodal nature of these rocks is also apparent on silica variation diagrams (Figures 3.6 and 3.7). Although bimodal geochemical suites

are not uncommon among rocks of volcanic terranes, this characteristic is not consistent with the data set of Mahoney (1994) which encompassed the entire Harrison Lake Formation of which these rocks are a part. As such, this bimodal signature may simply be a local phenomenon and may not be representative of the entire regional volcanic sequence.

The volcanic rocks at Seneca can be separated into a number of subgroups based on their major and immobile minor and trace element geochemistry. TiO_2, coupled with Zr and Al, is a useful monitor of fractionation and with SiO_2 can be used to subdivide the felsic and mafic composition groups of units.

3.6.1 MAFIC ROCKS

The mafic rocks are subdivided into two subgroups: 1) 'less evolved' basaltic composition rocks with lower TiO_2, Zr and SiO_2 contents and Zr/Y ratios less than 3.5, and 2) 'more evolved' basaltic andesitic composition rocks with higher TiO_2, Zr and SiO_2 contents and Zr/Y ratios between 3.5 and 4.8 (Figures 3.8 and 3.9). TiO_2, P_2O_5, Zr and Y contents all increase through the range from 44 to 56 wt. % SiO_2 suggesting that they are incompatible with minerals crystallizing from mafic composition melts. MgO, Fe_2O_3 and Al_2O_3 all decrease from 44 to 56 wt. % SiO_2 suggesting that they are compatible in this range of melt compositions (Figure 3.6).

3.6.2 FELSIC ROCKS

The least altered felsic samples (dacites to rhyolites) are subdivided into four subgroups (denoted A to D on Figures 3.8 and 3.9) based on their relative TiO_2 contents and their petrographic characteristics such as the presence of the cumulophyric clusters described previously. Groups A, B and C comprise mostly dacitic to rhyodacitic FP rocks whereas group D comprises mostly rhyolitic FP and QFP rocks. These groups have unique, non-overlapping TiO_2

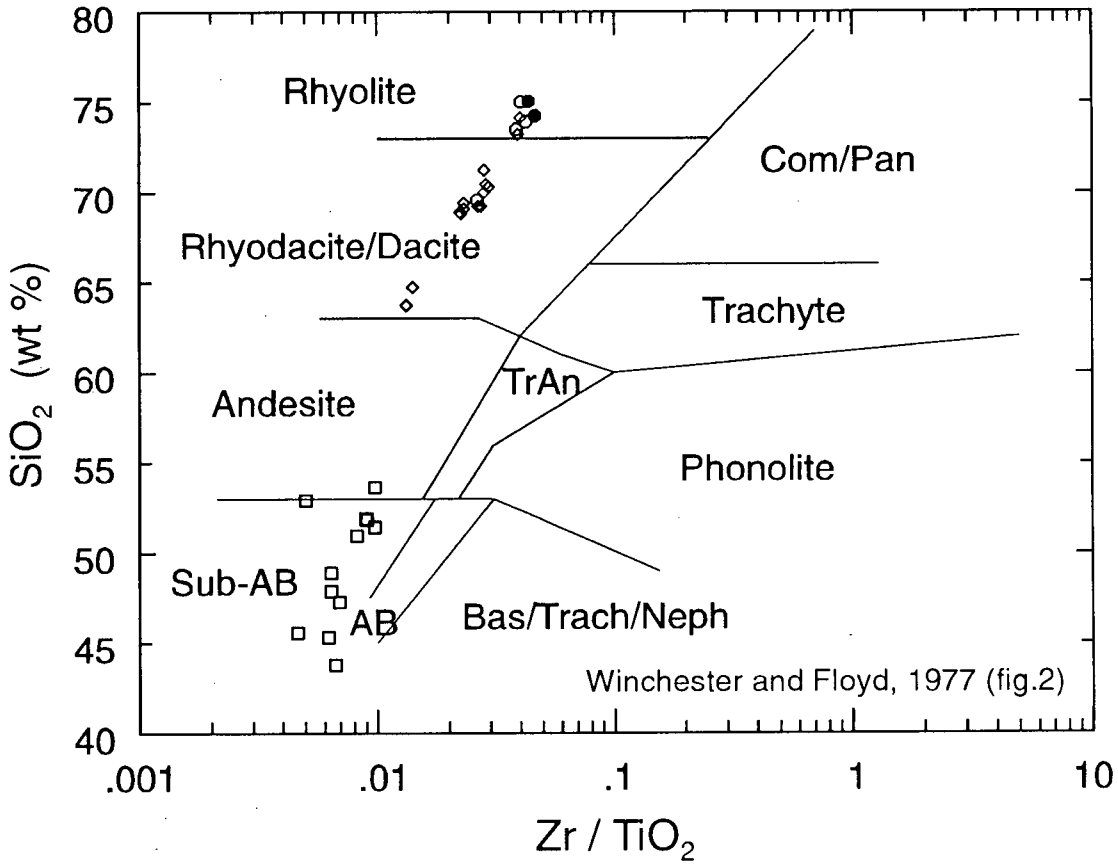

Figure 3.5. Zr/TiO_2 vs. SiO_2 discrimination plot of the least altered volcanic rocks at Seneca. The plot illustrates the range in compositions in the volcanic sequence and highlights the compositional gap that exists from 53 to 63 wt. % SiO_2. The symbols are the same as in Figure 4.1.

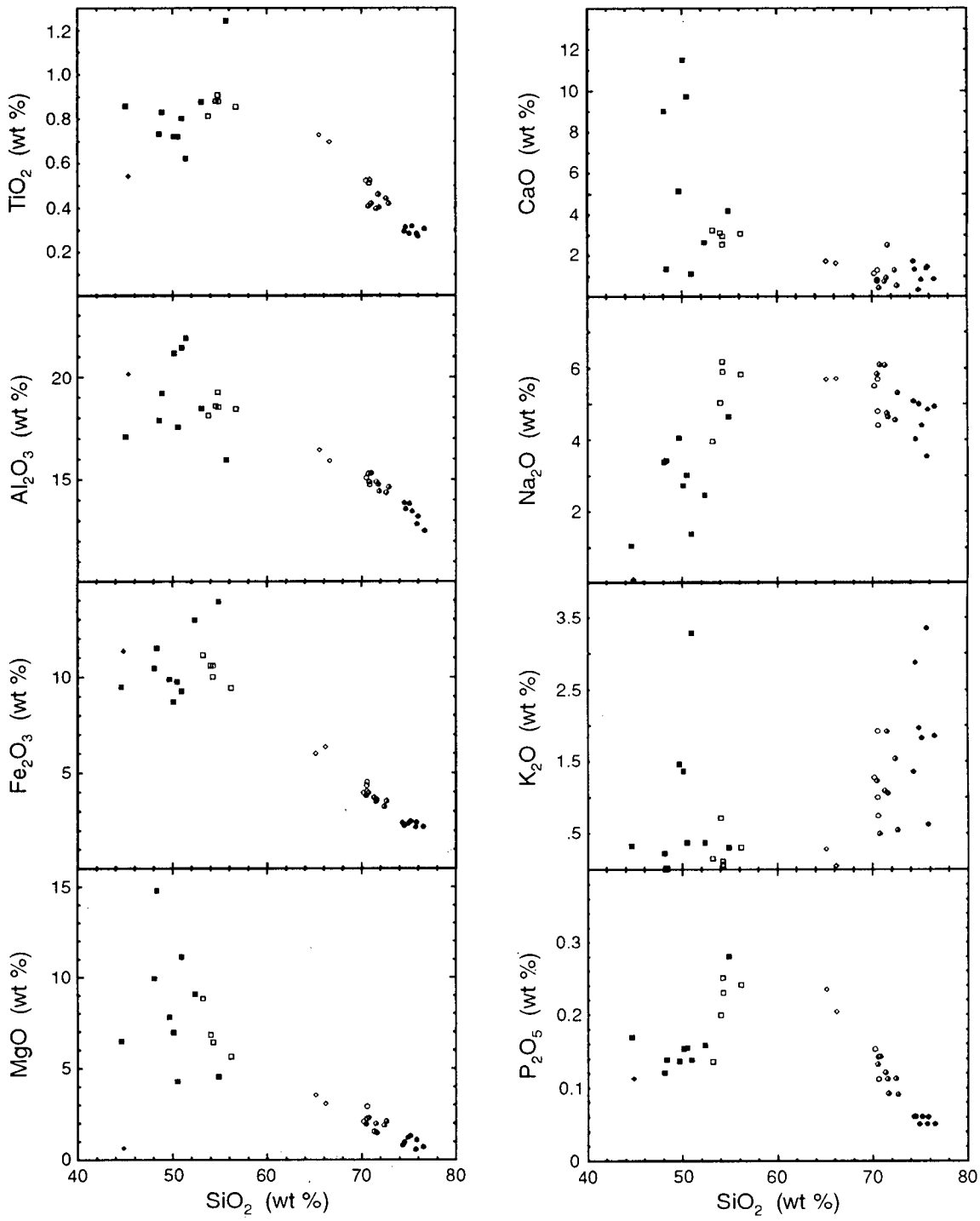

Figure 3.6. Harker-type variation diagrams of the major elements versus SiO_2.

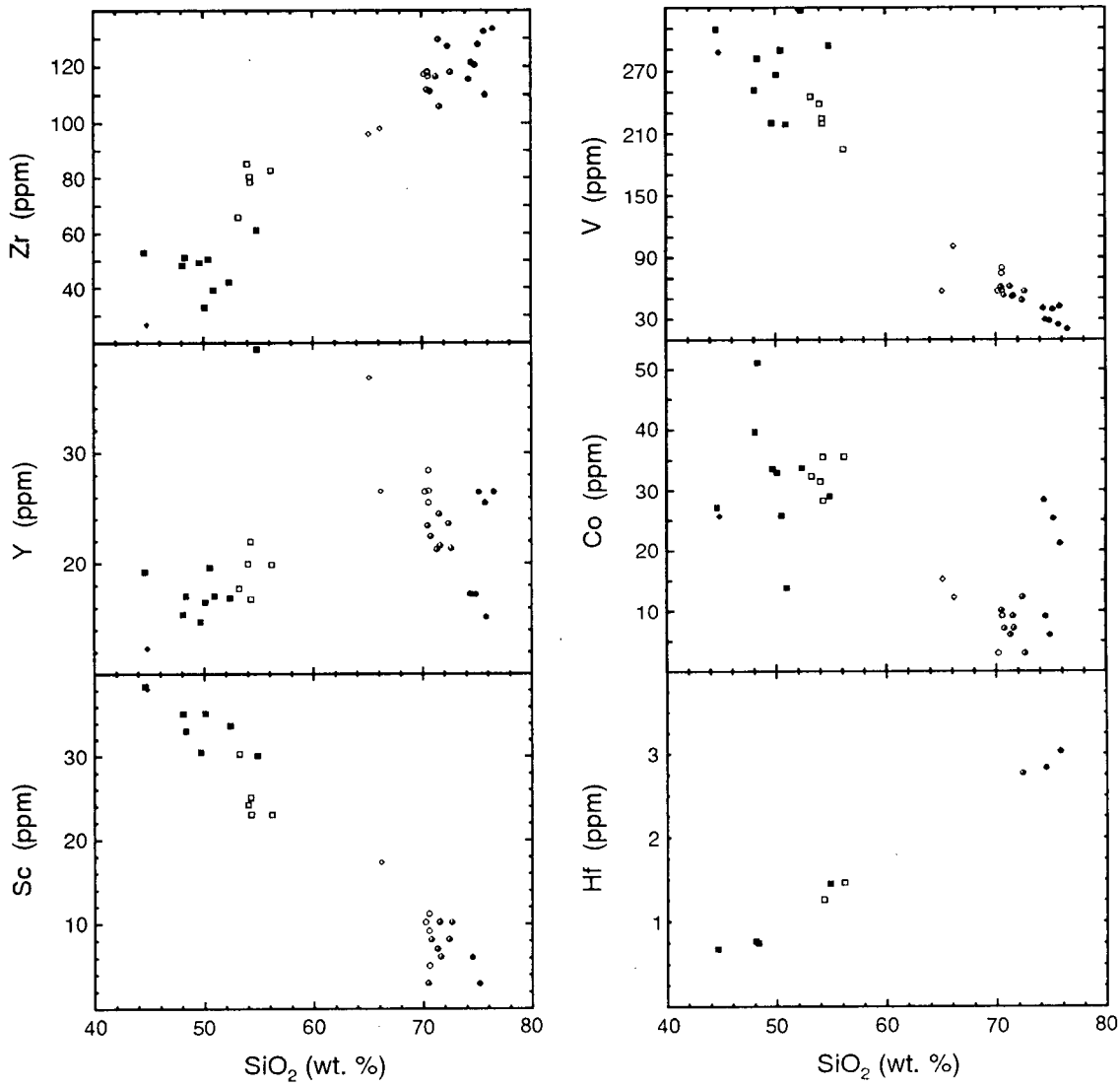

Figure 3.7. Harker-type variation diagrams of selected trace elements versus SiO_2.

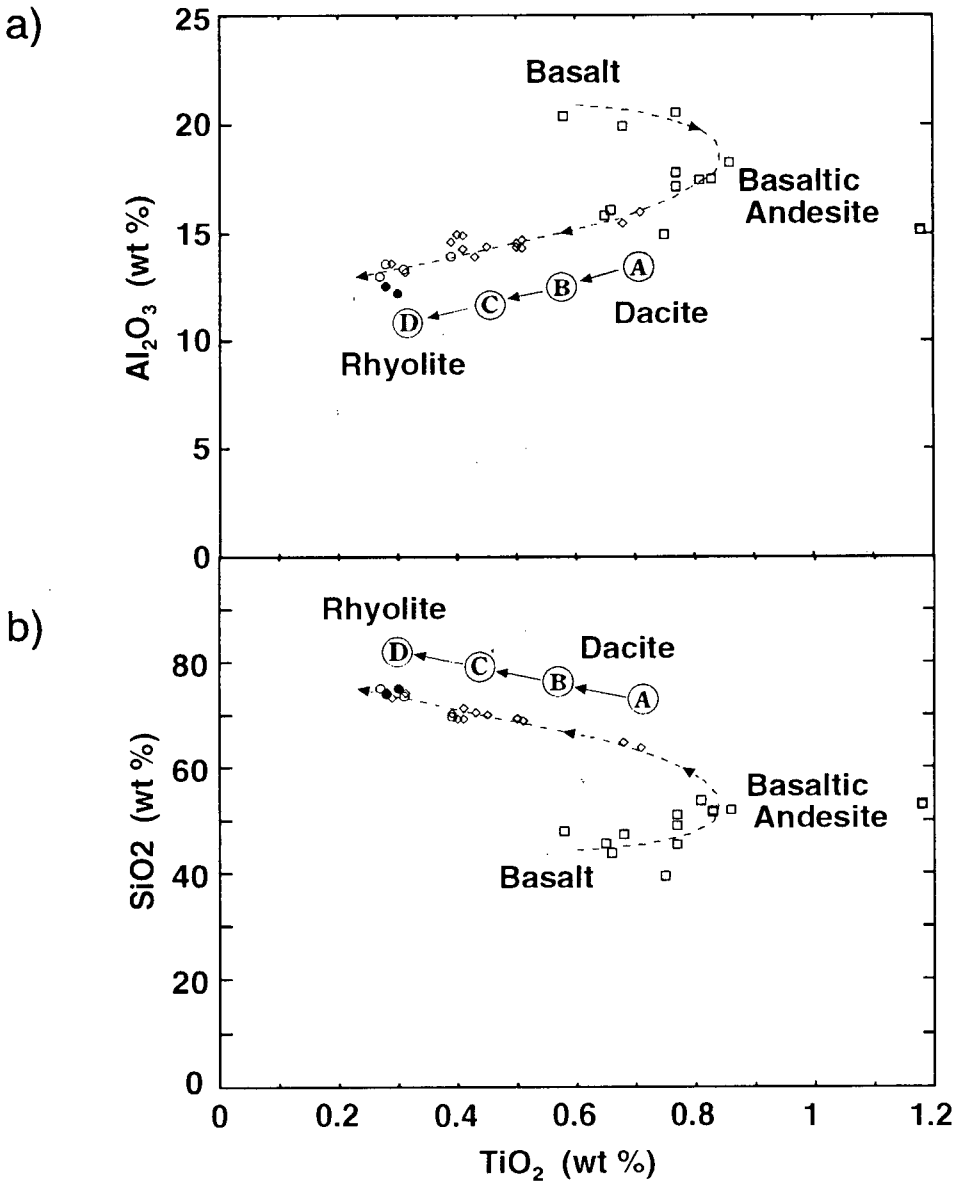

Figure 3.8. a) Binary immobile element plot of Al_2O_3 vs. TiO_2. b) Binary immobile-mobile element plot of SiO_2 vs. TiO_2. Both plots show subdivision of mafic and felsic compositions based on petrographic differences and TiO_2 contents. Mafic rocks are broken down into basalts and basaltic andesites; felsic rocks are divided into 4 groups A to D (see text for discussion).

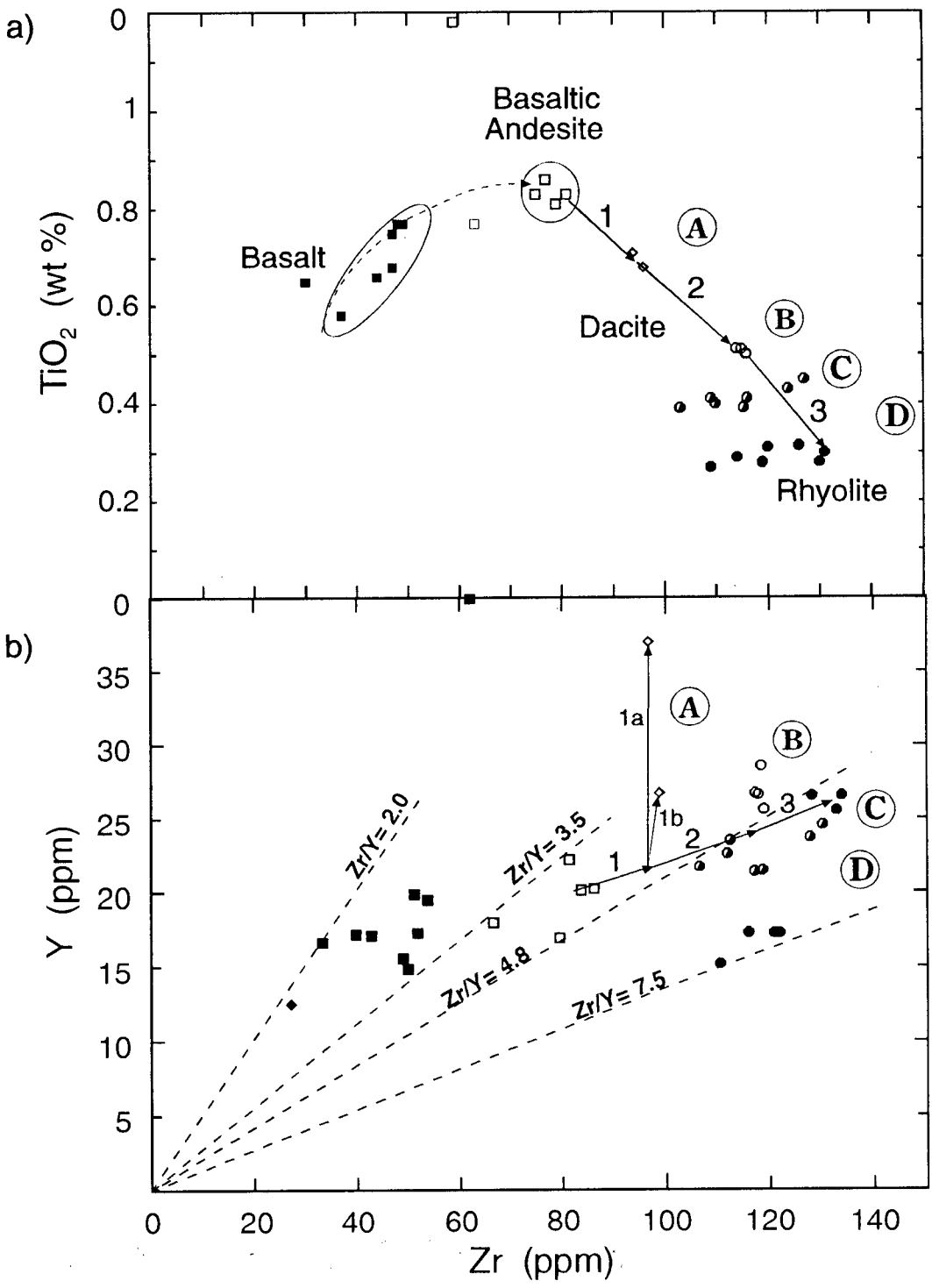

Figure 3.9. a) Zr-TiO_2 plot shows increase in TiO_2 from basalt to basaltic andesite followed by a decrease from basaltic andesite to rhyolite; b) Zr-Y plot illustrating the increase in Zr/Y ratios from basaltic to rhyolitic compositions. Both plots show the felsic subgroups A to D and the fractional crystallization paths 1 to 3 that were modelled and summarized in Table 4.3 (see text for discussion).

contents which decrease from A to D. Al_2O_3 decreases from A to D while SiO_2 increases. There is an overall decrease in all the major element contents, except for possibly K_2O, in the range from dacitic rocks to rhyolitic rocks (Figures 3.6 to 3.8). Zr contents increase over this range. In contrast to the mafic rocks, Y contents decrease with increasing silica content in the dacitic to rhyolitic samples (Figure 3.7), and thus, there is an overall gradual increase in the Zr/Y ratios from dacitic to rhyolitic compositions (Figure 3.9b). On a Zr-TiO_2 plot (Fig. 3.9a), groups A and B form clusters with very little compositional variation, whereas groups C and D form linear to curvilinear trends defined by variations in Zr content and only small variations in TiO_2 content. These groups also have petrographic differences as outlined in the preceding section.

Most of the FP and QFP samples have Zr/Y ratios of greater than 4.2 and are thus classified as calc-alkaline as discussed above (Figure 3.9b). The only two exceptions are the two intermediate, dacitic composition samples which comprise group A. The Zr/Y ratio of 4.8 that forms the upper limit for mafic composition samples also forms a distinct boundary between group B and group C and D felsic rocks. While group C samples have Zr/Y ratios less than 5.4 and plot close to this boundary, group D samples are much more variable and have Zr/Y ratios ranging from 4.8 to 7.5. It is apparent then that the transition from dacitic to rhyodacitic to rhyolitic compositions corresponds to a gradual increase in the Zr/Y ratio controlled by an overall greater increase in Zr contents relative to Y in groups A to C followed by a greater decrease in Y contents relative to Zr in group D.

3.7 IGNEOUS ROCK-FORMING PROCESSES

Trends in the major and trace element geochemistry of volcanic rocks are largely controlled by the fractional crystallization of different mineral phases at different points in the evolution of a body of magma. Elements that are incompatible (i.e. are not partitioned into a

precipitating phase) are enriched in the residual melts during progressive crystallization and will have a positive correlation when plotted against SiO_2 on variation diagrams (Figures 3.6 and 3.7). Zr and Hf show such a positive correlation over the entire compositional range (Figure 3.7). Other elements such as TiO_2, Y and P_2O_5 exhibit a positive correlation with SiO_2 in the range of mafic samples (< 57 wt. % SiO_2), but exhibit negative correlations over the range of felsic compositions (> 65 wt. % SiO_2) suggesting that there are changes in the assemblage of precipitating phases during magmatic evolution such that elements that are initially incompatible are partitioned into later-crystallizing phases.

This study will use Pearce element ratio analysis and fractional crystallization modelling to explain the trends in the major and trace elements. Since it is not clear that the mafic and felsic rocks are *directly* related by fractionation, the petrogenesis of each compositional group will be addressed separately.

Pearce Element Ratio Analysis

Pearce element ratios (PERs) are a useful tool in determining which minerals have contributed to chemical variations in a related suite of volcanic rocks and the extent to which they were involved. PER analysis associates primary chemical variability in a suite of genetically related rocks to the addition or removal of an assemblage of minerals. PERs utilize molar quantities and have a denominator constituent which is conserved by processes of mass transfer. The axes of PER plots are chosen based on the stoichiometry of the minerals involved in the hypothesis that is being tested. The procedure for selecting a conserved element and testing petrologic hypotheses using PERs is described in detail by Russell and Nicholls (1988), Stanley and Russell (1989) and Russell et al. (1990).

Zr was chosen as the best conserved element for the volcanic rocks at Seneca because no other elements were truly conserved (Nb concentrations are quite low and have a greater degree of analytical uncertainty). Zr contents increase steadily between basaltic and rhyolitic compositions suggesting that it is incompatible over the entire compositional range and is being enriched in the increasingly fractionated melts. Ti is only a conserved element in the most basaltic composition rocks and is therefore not used in PER calculations. Since Zr can be partitioned into accessory phases such as hornblende, it is not truly a conserved element. However, the effects of the fractionation of the major minerals such as feldspar and quartz will have the greatest effects on the bulk composition of the rocks. It should be noted that the variability of Zr contents among some of the more silicic rocks (groups C and D, Figure 3.9) may be due to the fractionation of small amounts of zircon. Zircon has only been identified in one sample, but may be present as a minor phase in the aphanitic glassy groundmass of the QFP rhyolites.

3.7.1 MAFIC ROCKS

Pearce element ratio analysis was used to interpret the petrogenesis of the basalts and basaltic andesites. The fractionation of plagioclase, which is the only discernible phenocryst phase in these mafic rocks, is inferred to have had the greatest effect on the bulk geochemistry during magmatic evolution. Thus PERs were used to test petrogenetic models which involve plagioclase fractionation. Figure 3.10a is a PER plot which uses Zr as the conserved element and models the effects of the fractionation of a combination of plagioclase, olivine and clinopyroxene. On such a plot, rocks that are related by the fractionation of these minerals in any proportion will lie along a line having unit slope (i.e. m=1). Displacements in the vertical sense from the linear fractionation trend can be attributed to Ca or Na-metasomatism. It is apparent that the basalts from the Fleetwood Zone are less evolved and can be related to the basaltic andesites from the Pit Area by

a)

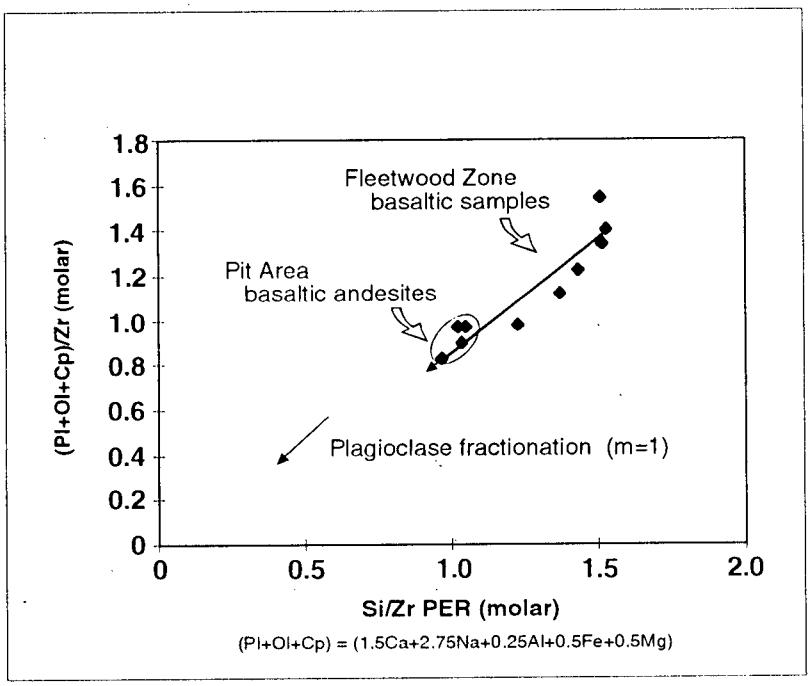

b)

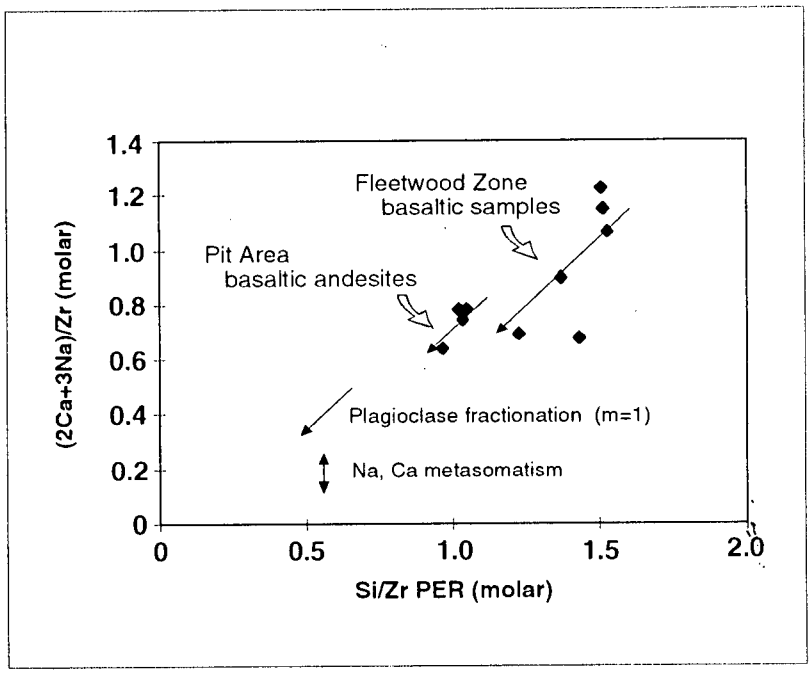

Figure 3.10. PER plots for the least altered mafic samples at Seneca. a) shows the effects of the fractionation of an assemblage of plagioclase, olivine and pyroxene and b) models the effects of plagioclase fractionation alone.

the fractionation of some combination of the assemblage plagioclase, olivine and clinopyroxene. Although olivine and clinopyroxene were not observed in the rocks, it is possible that they have been completely removed by fractionation, but have still influenced the geochemical trends. Figure 3.10b shows the effects of fractionating plagioclase alone; samples related by plagioclase fractionation lie along lines with unit slopes, and, again, vertical displacements from these lines are due to Ca and Na metasomatism. The data points on this plot can be divided into two separate groups each lying along a line of unit slope. These two groups correspond to the basaltic Fleetwood Zone samples and the more andesitic Pit Area samples.

3.7.2 FELSIC ROCKS

Pearce element ratio analysis is used to explain the variation of the major elements in the least altered felsic rocks (dacitic to rhyolitic compositions) while combinations of binary geochemical plots and Rayleigh fractionation modelling are used to explain the variations in trace element contents.

Pearce Element Ratio Analysis

Zr was chosen as the best conserved element among the felsic rocks for use in PER analysis. It is used with caution, however, because it may be a compatible element in the most silicic samples. The compatibility of both TiO_2 and P_2O_5 in the felsic rocks rules them out as possible alternate conserved elements.

Figure 3.11a is a phase discrimination PER plot in which chemical variations in genetically-related rocks can be related to the fractionation of a combination of minerals. The effects of fractionation of various mineral phases are shown as a series of vectors with different slopes. The fractionation of some combination of these minerals will result in a trend which has a

a)

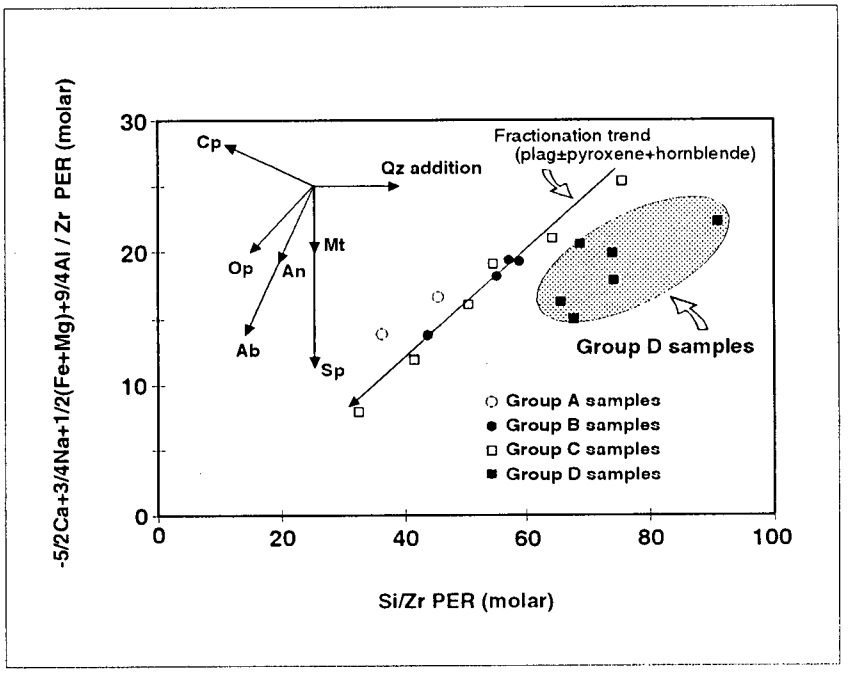

b)

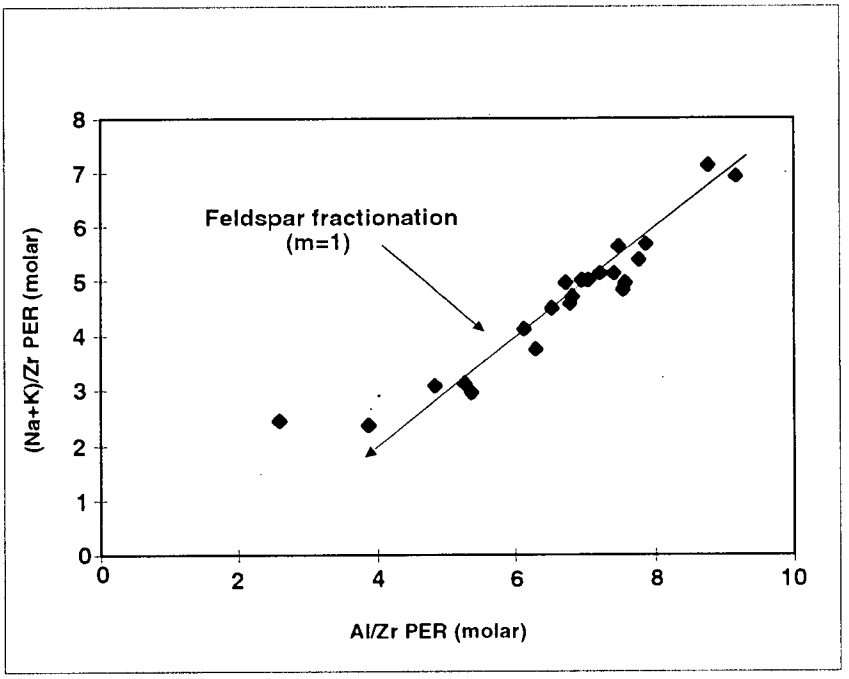

Figure 3.11. PER plots of the least altered felsic samples at Seneca. a) is a phase discrimination diagram which illustrates the effects of quartz addition on the group D samples, and b) demonstrates the modelling of feldspar fractionation on the felsic samples.

slope corresponding to the sum of the vectors of the minerals involved. Plagioclase fractionation alone would yield a trend with a slope of 1 on this plot. In Figure 3.11a, samples in groups A, B and C, which were defined above, lie along a line which has a slope of less than 1. This indicates that an additional phase to plagioclase, such as pyroxene, may be involved in the fractionation process. It is possible, based on this plot alone, to explain the slope of the trend as a result of orthopyroxene fractionation alone, but this is not consistent with results of other PER plots (i.e. modelling feldspar fractionation) and petrographic observations which indicate plagioclase is the most abundant phenocryst phase. Fractionation of hornblende would also cause such a displacement from the plagioclase fractionation line. Since Si is included in the abscissa, addition or removal of quartz to or from the system in the form of small phenocrysts or secondary silicification will result in horizontal displacements on this plot. Group D felsic samples which contain variable amounts of quartz have higher Si/Zr PER values and plot away from the main fractionation trend suggesting quartz has been added to the system.

Figure 3.11b is a PER plot which tests the effects of feldspar fractionation. All but one of the samples plot on or near a trendline of unit slope indicating that plagioclase and K-feldspar fractionation can explain the chemical variation in these rocks. This is in accordance with the trend described above for Figure 3.11a in which the samples also plotted close to the feldspar fractionation line, but were drawn off due to the effects of the cyrstallization of quartz and possibly pyroxene or hornblende, none of which would effect the slope of the trend on Figure 3.11b.

Fractional crystallization modelling of trace elements

The equilibrium distribution of a trace element between mineral and melt is often described by the Nernst distribution (partition) coefficient defined by:

$$K_d = C_{im} / C_{il} \qquad [3.1]$$

Andesitic Melts (<63 wt. % SiO_2)					
	Fs	**Hb**	**Ap**	**Mg**	**CPx**
Zr	0.013	1.40	-	0.20	.162
Y	0.060	2.50	-	0.50	1.50
Ti	0.050	3.00	-	9.00	0.40
Dacitic to Rhyolitic Melts (>63 wt. % SiO_2)					
	Fs	**Hb**	**Ap**	**Mg**	**CPx**
Zr	0.100	4.0	0.1	0.800	0.6
Y	0.100	6.0	40	2.00	4.0
Ti	0.050	7.00	0.1	12.50	0.70

Table 3.2: Mineral/melt partition coefficients for the trace elements Zr, Y and Ti between selected minerals and andesitic and dacitic to rhyolitic composition melts (summarized from Rollinson, 1993 after Pearce and Norry, 1979); Fs=feldspar, Hb=hornblende, Ap=apatite, Mg=magnetite, CPx=clinopyroxene.

where K_d is the Nernst distribution coefficient, C_{im} is the concentration of the trace element *i* in the mineral and C_{il} is the concentration of of the trace element *i* in the liquid (McIntire, 1963). Apatite has a strong affinity for partitioning Y, illustrated by the very high partition coefficient of 40 for Y between apatite and a rhyolitic liquid (Table 3.2). Therefore, the crystallization of even small amounts of apatite will greatly deplete Y from the residual melts. Conversely, the presence of small amounts of apatite in the rocks will yield higher concentrations of Y for those samples. Hornblende will also partition Y, although the effect of hornblende crystallization on the content of Y is not as great as for apatite because of the lower partition coefficient of 6.0 for Y between hornblende and liquid. Zr contents are also affected by the precipitation of hornblende; Zr has a partition coefficient of 4.0 between liquid and hornblende.

The effects of fractional crystallization of several mineral phases on the trace element concentrations of rocks can be modelled using the Rayleigh fractionation equation:

$$C_L = C_0 * F^{(D-1)} \qquad [3.2]$$

where C_L is the weight concentration of trace element in the liquid, C_0 is the weight concentration of the trace element in the parental liquid (before fractionation), F is the weight fraction of melt remaining and D is the bulk distribution coefficient of the fractionating mineral assemblage (Rollinson, 1993). The bulk distribution coefficient is defined by:

$$\mathbf{D_i = x_1Kd_1 + x_2Kd_2 + ...} \qquad \textbf{[3.3]}$$

where x_1 is the percentage proportion of mineral 1 in the rock and Kd_1 is the Nernst partition coefficient for element *i* in mineral 1 (Rollinson, 1993). The model for Rayleigh fractionation assumes that crystallized phases are removed from the melt and that no assimilation or magma replenishment from an external source occurs.

To approximate the effects of fractional crystallization on the overall trace element abundances in the felsic rocks, the fractionation of varying proportions of the assemblage feldspar, hornblende, magnetite and apatite was modelled using the formula for Rayleigh fractionation (Equation [3.2]) and the partition coefficients summarized in Table 3.2. The variability in the trace element contents *within* each of the four felsic subgroups (A to D) will be tested by modelling the fractional crystallization of the minerals hornblende, magnetite and apatite, whereas the overall change in major and trace element abundances from group A to group D is likely controlled by the fractional crystallization of feldspar and quartz. Apatite and hornblende partition Zr and Y in varying proportions and magnetite strongly partitions Ti. The precipitation of even small amounts of these phases will produce distinct changes in the trace element trends. For simplicity, 'feldspar' is used to represent a combination of fractionating plagioclase and K-feldspar; since petrographic evidence suggests that plagioclase is the most abundant feldspar in these rocks and since both plagiocalse and K-feldspar have similar low affinities for the trace elements Zr and Y, the partition

coefficients for Zr and Y between plagioclase and melt are used here to model the effects of total feldspar fractionation.

Fractional crystallization was modelled in three major steps, each with its own initial and final melt compositions. These steps represent stages in the overall magmatic evolution from andesite to dacite and dacite to rhyolite, and are illustrated in Figures 3.8 and 3.9. The results of this modelling are summarized in Table 3.3. Since Ti has been established as a reliable monitor of fractionation (i.e. it shows a systematic variation with respect to SiO_2 and Al_2O_3), the changes in Ti were accounted for first by fractionating magnetite only. Since magnetite fractionation alone does not account for the changes in Zr and Y, various amounts of feldspar, hornblende and apatite were also fractionated. Hornblende must be fractionated to offset the enrichment of Zr brought about by feldspar fractionation (fractionation of feldspar removes Na, Ca, Al and Si, thus enriching Zr, Y and Ti in the melt). Thus, as increasing amounts of feldspar are removed from the system, increasing amounts of hornblende and decreasing amounts of magnetite must be removed to yield the trace element trends observed in the volcanic rocks at Seneca. Apatite is included to balance the effects of fractionation on Y concentrations.

Step 1: Andesite to dacite

Step 1 represents the magmatic evolution from andesitic to dacitic compositions. Initial trace element concentrations of 82 ppm Zr, 21.5 ppm Y and 5280 ppm Ti and 'target' final dacitic concentrations of 98 ppm Zr, 22 ppm Y and 4260 ppm Ti were used. The fractionation of 17.5 % magnetite can account for the bulk of these changes in trace element abundances (Table 3.3), but petrographic evidence suggests that other minerals such as plagioclase and hornblende were likely involved. In addition, fractionation of magnetite *only* does not explain the steady decrease in Al_2O_3 from andesitic to rhyolitic compositions. It appears that the trends can be best accounted for by fractionation of 8 to 15 % feldspar, 7.5 to 12 % hornblende, 5.5 to 9.5 % magnetite and small

amounts of apatite.

The two samples that comprise group A have similar Zr and Ti concentrations, but quite different Y concentrations (Fig. 3.9b). To account for the variability of Y, the effects of accumulation rather than removal of apatite were modelled (Table 3.3, steps 1a and 1b). As such it appears that the Y abundances of these two samples can be accounted for by the accumulation of 1.5 and 4.1 % apatite in the rocks. The presence of apatite, which has been confirmed petrographically, supports such a model since these rocks have higher P_2O_5 contents than rocks that would lie on the inferred fractionation trend from andesite to dacite. In addition, of these two samples, the rock with the higher Y content also contains considerably more apatite.

Step 2: Group A to Group B felsic rocks

The second step of the fractionation modelling represents the transition between dacitic and rhyodacitic composition rocks (group A to group B). Initial concentrations of 98 ppm Zr, 21.5 ppm Y and 4260 ppm Ti and final melt or daughter rock concentrations of 117 ppm Zr, 24 ppm Y and 3120 ppm Ti were used. As with step 1, the change in the trace element abundances modelled in step 2 can be explained by fractionation of magnetite only; in this case 19.5 % magnetite would be required to be removed to yield the observed trace element trends. However, once again this model does not explain the major element trends. It appears that a fractionating assemblage of 5 to 10 % feldspar, up to 10 % hornblende and 10 to 15 % magnetite best explains the observed trace element trends. The variability of Y within group B samples can again be explained by the accumulation of small amounts (<0.5%) of apatite in the rocks.

Step 3: Group B to Groups C and D

Step 3 represents the transition between rhyodacitic and rhyolitic composition rocks (group B to groups C and D). Initial concentrations of 117 ppm Zr, 24 ppm Y and 3120 ppm Ti and final melt/daughter rock concentrations of 133 ppm Zr, 26 ppm Y and 1800 ppm Ti were modelled.

Step	C_0 (ppm)			% mineral fractionated				C_L (ppm)		
	Zr	Y	Ti	Fs	Hb	Mg	Ap	Zr	Y	Ti
1	82	20	5280	-	-	17.5	-	96.8	22.7	4202
				8	7.5	9.5	0.25	98.1	21.5	4286
				15	12	5.5	-	98.3	21.3	4279
1a	82	20	5280	15	12	6	+1.5	97.5	26.5	4214
1b	82	20	5280	15	12	6	+4.1	96.0	36.8	4315
2	98	21.5	4260	-	-	19.5	-	117.7	24.5	3119
				-	2	18	-	116.5	24.1	3124
				7.5	8.4	11	-	117.1	23.4	3147
				10	10	9	-	117.0	23.1	3206
				12	11	8.5	+0.5	117.1	24.5	3121
				20	14.5	4.9	+0.5	117.1	23.9	3113
3	117	24	3120	-	11.5	15.7	+0.7	133.0	26.1	1811
				10	15.5	9.5	-	132.8	22.7	1800
				15	16.5	7.5	+0.8	133.0	25.7	1837

Table 3.3. Summary of the results of the effects of fractional crystallization on the abundances of the trace elements Zr, Y and Ti. The trace element variations are examined for three steps representing magmatic evolution from andesite to dacite to rhyolite (steps 1 to 3 are indicated on Figure 3.9). The effects of fractionating different amounts of the minerals minerals feldspar, hornblende, magnetite and apatite on an initial trace element abundance, C_0, were modelled using Rayleigh fractionation. C_L represents the trace element abundance in the residual liquid or subsequent daughter rock following fractionation. Values marked with + indicate accumulation of a mineral in the daughter rock. (Fs=plagioclase ± K-feldspar, Hb=hornblende, Mg=magnetite, Ap=apatite).

The modelling of the trace element trends of this step was more difficult. This is attributed to the variability in the Zr and Y contents that is present in group C and D samples that is not present in groups A and B (Fig. 3.9). However, the final results showed that a fractionating assemblage similar to steps 1 and 2 can explain the trends (Table 3.3). In contrast to group A and B rocks, quartz is more common as a phenocryst phase in group D rocks, and to a lesser extent in group C rocks, suggesting it too may be a fractionating phase. However, like feldspar, the partition coefficients of the trace elements between quartz and a felsic melt are very low, and thus the effects of quartz fractionation would be very silmilar to those of feldspar fractionation.

3.8 DISCUSSION

Major and trace element discrimination plots and ratios demonstrate that the volcanic rocks at Seneca are of dominantly transitional to calc-alkaline affinity and were formed in a volcanic island arc setting. Variation diagrams indicate that the suite is bimodal with a compositional 'gap' from 53 to 63 wt. % SiO_2. It is not clear whether the volcanics sampled at Seneca are representative of the entire Weaver Lake Member as the data of Mahoney (1994) suggests that intermediate compositions are present elsewhere in the volcanic belt. As such, perhaps the bimodal nature of these rocks is entirely a local phenomenon.

Mafic rocks are subdivided into basalts (<60 ppm Zr, Zr/Y < 3.5) and basaltic andesites (>60 ppm Zr, Zr/Y > 3.5). PER analysis shows that the two groups of mafic rocks can be related to each other by fractionation of the assemblage plagioclase-olivine-clinopyroxene, but that trends *within* the two groups can be explained by plagioclase fractionation alone.

Felsic rocks with dacitic to rhyolitic compositions are subdivided into four subgroups that exhibit decreasing contents of TiO_2 with increasing Zr and SiO_2 contents. PER analysis does not disprove the hypothesis that groups A, B and C are related by the fractionation of the assemblage feldspar-quartz±pyroxene and/or hornblende. The fractionation of feldspar alone can explain most of the major element variation. Trace element trends within the felsic rocks can be accomodated by 30 to 40 % fractional crystallization of the assemblage feldspar-hornblende-magnetite±apatite (feldspar>hornblende>magnetite). Quartz may also be involved, but will have the same effects on the trends as feldspar fractionation (i.e. residual enrichment of Zr, Ti and Y).

The results of the PER analysis and the modelling of trace element fractionation do not produce identical results. The PER analysis suggests that plagioclase fractionation has the greatest effect on the geochemical trends (Figure 3.11b) whereas the fractional crystallization modelling

suggests that the trace element trends can be accomodated by fractionation of similar amounts of plagioclase, hornblende and magnetite. In this modelling, the amounts of fractionated magnetite seem to be reasonable since there are few other minerals if any that can account for the rate of decrease in the Ti contents of the felsic rocks. Magnetite is present in some of these rocks, and where it was not observed petrographically, its presence was inferred by the magnetic nature of some samples. The flaw in the model may be in the assumption that hornblende is the only fractionating mineral that partitions Zr (clinopyroxene also partitions Zr, but to a lesser degree than hornblende). The fractionation of even very small amounts of zircon would greatly deplete Zr in the residual melts and would eliminate the need for hornblende as an abundant fractionating phase. Zircon fractionation could also balance the effects on the Zr contents if greater amounts of feldspar were fractionated. However, the fractionation of much larger amounts of feldspar likely would have caused larger Eu anomalies than are observed in these rocks.

The more silicic samples of groups C and D have more variable Zr contents than the other groups and form two distinct linear trends. It is possible that zircon fractionation has caused these trends. It seems unlikely that this variability is due to alteration because any alteration that might be present would be expected to also effect the samples in groups A and B. If zircon fractionation is the source of these trends, then a change in the physical conditions or composition of the magma body must have occurred between the formation of groups B and C since groups A and B show very little Zr variation. Watson (1979) states that any felsic magma will likely contain zircon crystals since the saturation level of zircon in these composition melts is low and is strongly dependant upon the molar (Na_2O+K_2O/Al_2O_3) of the melts. Watson's experimental studies showed that a change from 1.0 to 2.0 in the molar (Na_2O+K_2O/Al_2O_3) of melts in equilibrium with zircon resulted in a 500-fold increase in the solubility of Zr in these liquids. Therefore, considering the felsic rocks at Seneca, it is possible that the molar (Na_2O+K_2O/Al_2O_3) in groups C and D were

sufficiently different from groups A and B to cause a decreased solubility of Zr in the melts and thus facilitating zircon crystallization in groups C and D. However, it is difficult to reliably calculate and test these molar ratios in the rocks at Seneca due to the mobility of the alkalies even in the least altered samples.

In summary, it is not clear whether or not fractional crystallization alone can explain the relationships between the mafic and felsic rocks and between the four felsic subgroups. Hall (1987) suggests that the derivation of rhyolites from differentiation alone from a basaltic parent is possible, but that only small volumes of rhyolite can be produced. This would not explain the large volumes of felsic rocks present in the study area. Another process such as a continual replenishment of the basaltic parent would have to be invoked. It is also apparent that the PER analysis and fractional crystallization modelling only adequately describe a 'global fractionation trend' for the dacitic to rhyolitic composition rocks. There appears to have been some separation or 'pooling' of different smaller felsic magma batches from a larger source. Fractionation within the source magma body yielded the global fractionation trends. The smaller magma bodies perhaps rose to higher crustal levels at different stages in this global evolutionary trend and subsequently continued to evolve and fractionate further. Such a scenario seems to be necessary to explain the subtrends that are present amongst the minor and trace elements.

CHAPTER 4
ALTERATION

4.1 INTRODUCTION

Strong hydrothermal alteration on the Seneca property is restricted to discordant, laterally discontinuous zones around the mineralized stockworks in the Fleetwood and Vent zones and to the areally extensive ore zone conglomerate in the Pit Area. Quartz-sericite-pyrite is the dominant alteration assemblage with lesser amounts of chlorite, epidote and calcite. This chapter will describe the petrographic and geochemical characteristics of this alteration and will attempt to quantify the effects of the hydrothermal processes using the mass balance method of MacLean (1990).

4.2 DISTRIBUTION OF ALTERATION

Pit Area

The most areally extensive zone of alteration at Seneca occurs in the Pit Area and is associated with the ore zone conglomerate. Moderate to intense silicification and sericitization is the dominant alteration style in this unit. In places the sericite alteration has completely destroyed the matrix material leaving only some of the more resistant lava clasts as evidence of the unit's original fragmental texture. The alteration is confined to a shallowly dipping interval of varying thickness which was intersected in drillholes at depths varying from near surface to a maximum depth of 150 m. The surface projection of this zone an area of approximately 500 m by 500 m around the Pit Area. One drillhole located 1 km to the northeast of the Pit Area intersected a strongly altered and weakly mineralized horizon that is lithologically very similar to the OZC intersected in drillhole 85-03 (Pit Area) suggesting that the Seneca horizon may be much more laterally extensive. The thickness of the altered OZC varies from 2 metres to over 15 metres. Although the alteration in this unit is very strong and is widespread, it is essentially stratabound and there is no apparent stockwork zone immediately

underlying the OZC that could be interpreted as a feeder zone. It appears that the permeability of the coarse, less well sorted OZC provided a more favourable conduit for the hydrothermal fluids compared with its bounding strata of felsic flows and fine grained volcaniclastic rocks.

Fleetwood and Vent Zones

In contrast to the Pit Area, hydrothermal alteration in the Fleetwood and Vent Zones is discordant and is not as areally extensive. Alteration is confined to discrete stockwork zones that can reach over 50 metres in vertical extent. These zones of stockwork-related hydrothermal alteration all lie along a northwest-southeast striking trend; drillholes located to the northeast of this did not intersect any zones of strong alteration. The most extensive individual stockwork outcrops at surface and is intersected by numerous drillholes in the Vent Zone. This area of strong silicification and sericitization extends over an area of 100 to 200 metres in diameter and can be traced to depths of over 100 metres. The stockwork alteration in the Fleetwood Zone to the northwest of the Vent Zone is less extensive both laterally and vertically. Although alteration in the Fleetwood Zone occurs at depths greater than 100 metres below surface, lithological relationships suggest that it occurs at the same stratigraphic interval as the alteration in the Vent Zone which occurs at surface and extends down to over 100m below surface.

The stratabound alteration in the Pit Area is also along strike of the trend of the stockworks in the Fleetwood and Vent Zones suggesting a possible larger-scale structural control on the hydrothermal activity, as well as a possible genetic relationship between the different alteration zones. However, no large-scale controlling structures were recognized in the limited drillcore.

4.3 CHARACTERIZATION OF HYDROTHERMAL ALTERATION

Sericite-quartz ± pyrite is the dominant hydrothermal alteration assemblage at Seneca. This alteration generally causes a bleaching of the rock or the formation of sericitic envelopes around clasts (Plate 4.1). The only real variability is in the intensity of the alteration and in the amounts of chlorite

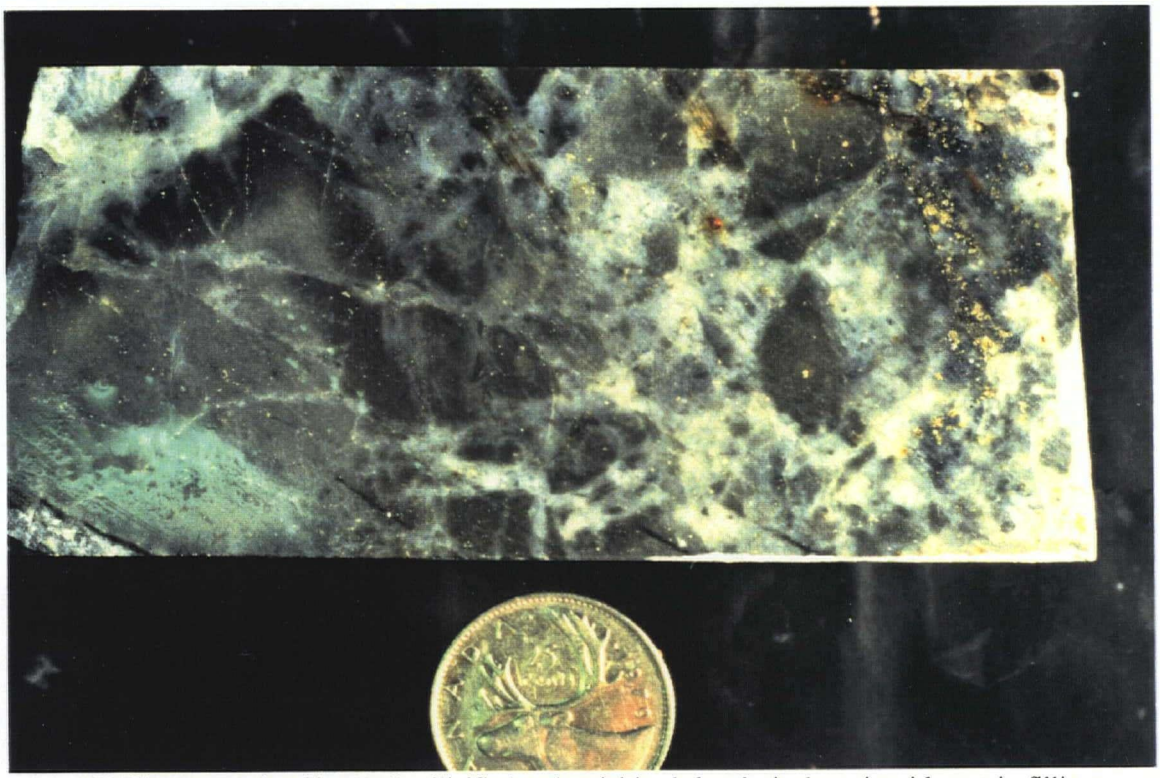

Plate 4.1a: Drillcore sample of intensely silicified and sericitized rhyodacite breccia with matrix-filling quartz and sulphides from the Fleetwood Zone stockwork (DDH 91-16). The late quartz-sulphide phase cuts a previous alteration which formed the altered envelopes around the breccia clasts.

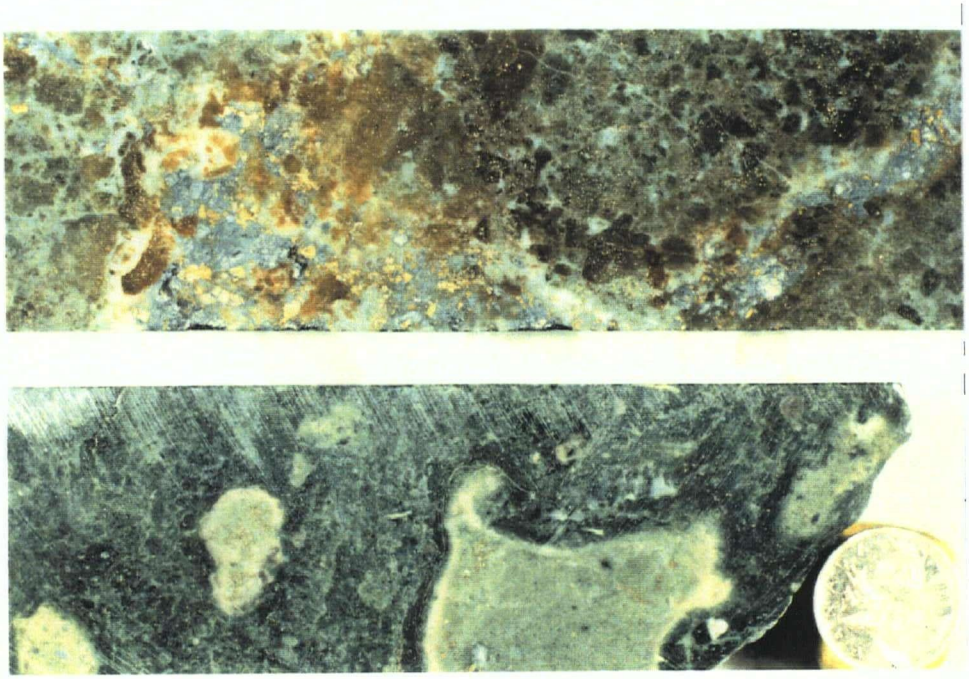

Plate 4.1b: Altered and mineralized basaltic fire fountain debris. This unit underlies the Vent Zone stockwork and has apparently been affected by the same hydrothermal processes that formed the stockwork. It is the position of this unit that allows correlation of the Vent mineralization with the Fleetwood mineralization. (Note the textural similarities with Plates 2.1a and 2.4a).

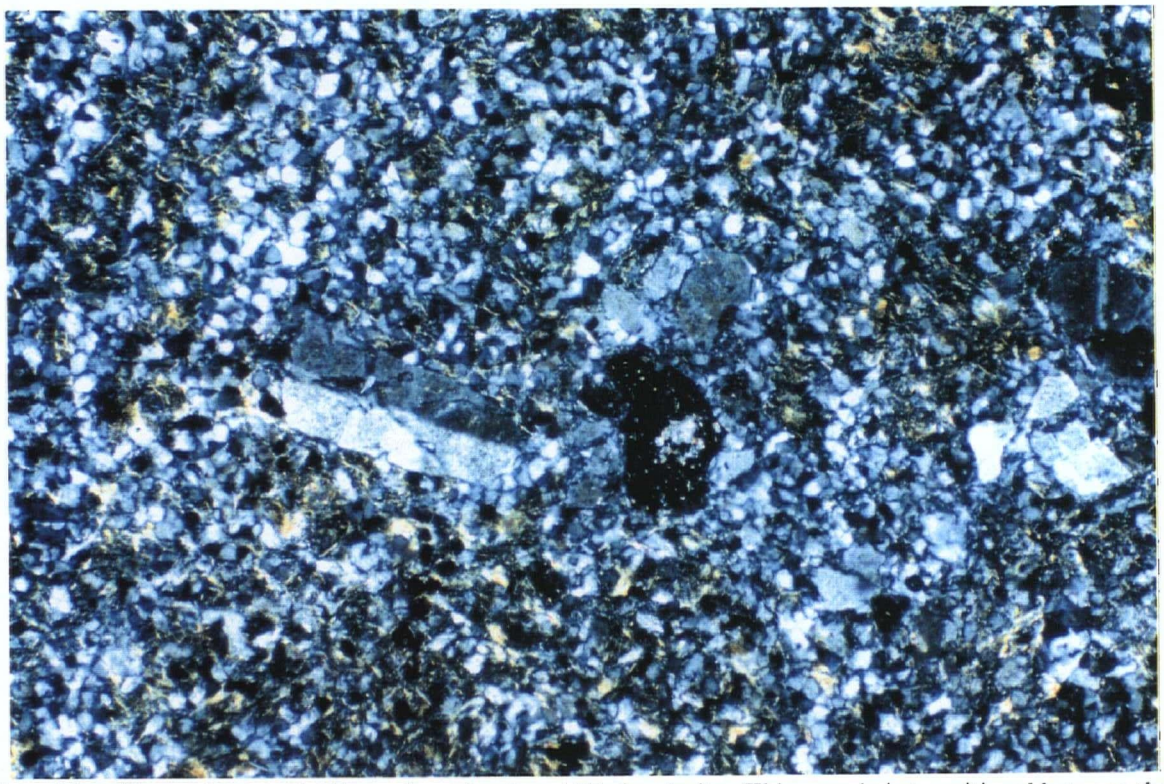

Plate 4.2a: Photomicrograph of a moderately altered FP rhyodacite. This sample is transitional between the least altered samples shown in the previous chapter and the intensely altered rocks such as shown below. The matrix is altered to sericite-quartz, but the phenocrysts remain relatively unaltered. (X-Nicols; Field of view = 1.25 mm).

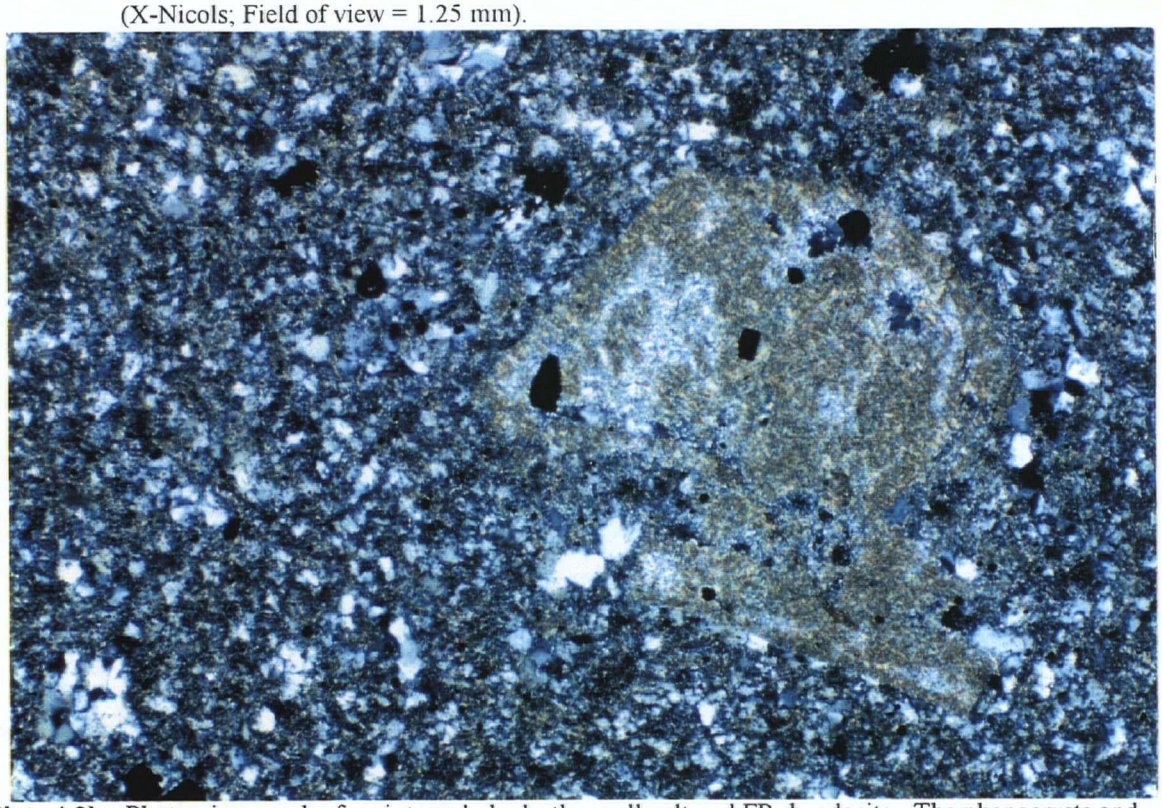

Plate 4.2b: Photomicrograph of an intensely hydrothermally altered FP rhyodacite. The phenocrysts and groundmass have been converted to quartz, sericite and minor chlorite, but the remnant feldspar phenocrysts are still discernible. (X-Nicols; Field of view = 1.25 mm).

and quartz present. Sericitization of feldspar is almost ubiquitous throughout the property and is present to a small degree even in the least altered samples. Least altered samples generally have small amounts of sericite present in the aphanitic groundmass and often the feldspar phenocrysts have a 'dusting' of sericite. As the intensity of alteration increases, the glassy groundmass becomes almost completely converted to a combination of quartz and sericite ± chlorite and the phenocrysts become increasingly sericitized (Plate 4.2). Phenocrysts in the most intensely altered samples from the stockworks are completely converted to sericite ± quartz (Plate 4.2b). However, remnant phenocrysts are still discernible macroscopically and microscopically even in the most strongly altered rocks.

The Fleetwood Zone stockworks in particular have undergone a large degree of silicification, especially in their upper portions. The alteration in upper parts of the Fleetwood stockworks is often associated with flow breccia and hyaloclastite, lithologies that likely favoured movement of hydrothermal fluids. In these zones, the interstices to the angular, hydroclastic fragments are filled by quartz and fragments with altered selvedges are cut by quartz veins (Plate 4.1a). Quartz in the interstices is also often intergrown with sulphides both of which appear to have formed late in the alteration history. The lower parts of these altered stockworks are hosted by more massive rocks in which silicification is not as strong. The rocks are often softer due to sericitization and quartz-sulphide veins are more common.

The host rocks of the Vent Zone stockwork are also quite massive. Quartz-sericite alteation is pervasive, but greater amounts of chlorite are present here than in the Fleetwood Zone. Silicification is also stronger in the upper parts of this zone than in the lower parts. Quartz-sulphide veins are very common in the Vent Zone and often have dark alteration envelopes. (It is not clear petrographically if these selvedges are simply more chloritic than the adjacent rocks). The underlying mafic lavas, where observed, are also often moderately altered. Most commonly these rocks have been bleached by

silicification and are accompanied by disseminated and veinlet sulphides (Plate 4.1b). Some epidote alteration is also present, but it is not clear if this is directly related to the hydrothermal activity.

4.4 QUANTIFICATION OF ALTERATION PROCESSES

The geochemical variability that characterizes the volcanic rocks at Seneca is attributed to a combination of igneous differentiation processes and varying degrees of hydrothermal alteration. The previous chapter outlined possible igneous processes that could account for the variability amongst a set of least altered samples. This chapter will account for the remaining chemical variations by relating the altered samples to this least altered subset by the processes of mass gain and mass loss caused by hydrothermally-induced mineralogical changes and the variable mobility of the major elements. Alteration indices and mass change calculations will be used to characterize the chemical changes and to illustrate variations in alteration effects in different areas of the Seneca property. This chapter will deal entirely with alteration amongst the felsic samples (dacites to rhyolites) since they comprise the greatest portion of the data set and the mafic samples have not undergone a large degree of hydrothermal alteration.

4.4.1 IZAWA ALTERATION DISCRIMINATION DIAGRAM

Changes in the bulk compositions of felsic samples can be related to mineralogical changes represented by the coordinates Al_2O_3-MgO-(CaO+Na_2O+K_2O) where whole rock data have been recalculated as molar proportions (Izawa et al., 1978). On such a diagram least altered samples plot close to the feldspar end-member (Figure 4.1). Increasing degrees of alteration destroys the feldspar and displaces samples away from the feldspar end-member due to the loss of CaO and Na_2O. The most intensely altered samples plot along a tie-line between chlorite and sericite compositions representing maximium loss of CaO and Na_2O and varying gains of MgO (chloritization) and/or K_2O

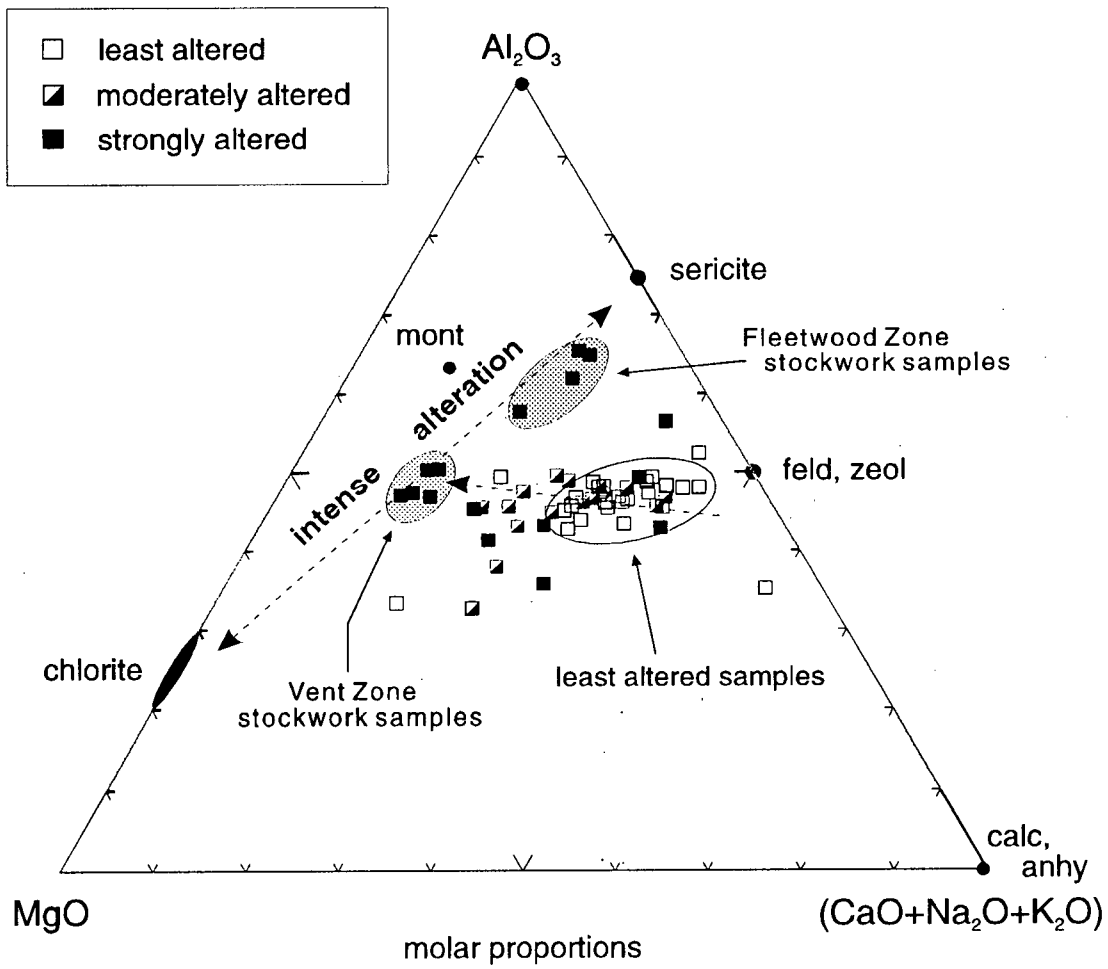

Figure 4.1. Izawa alteration discrimination diagram. The plot illustrates the mineralogical changes that occur within the felsic rocks at Seneca with increasing degrees of alteration. Geochemical data are recalculated as molar proportions. Least altered samples plot close to the feldspar end-member; intensely altered samples plot along a tie-line between chlorite and sericite compositions.

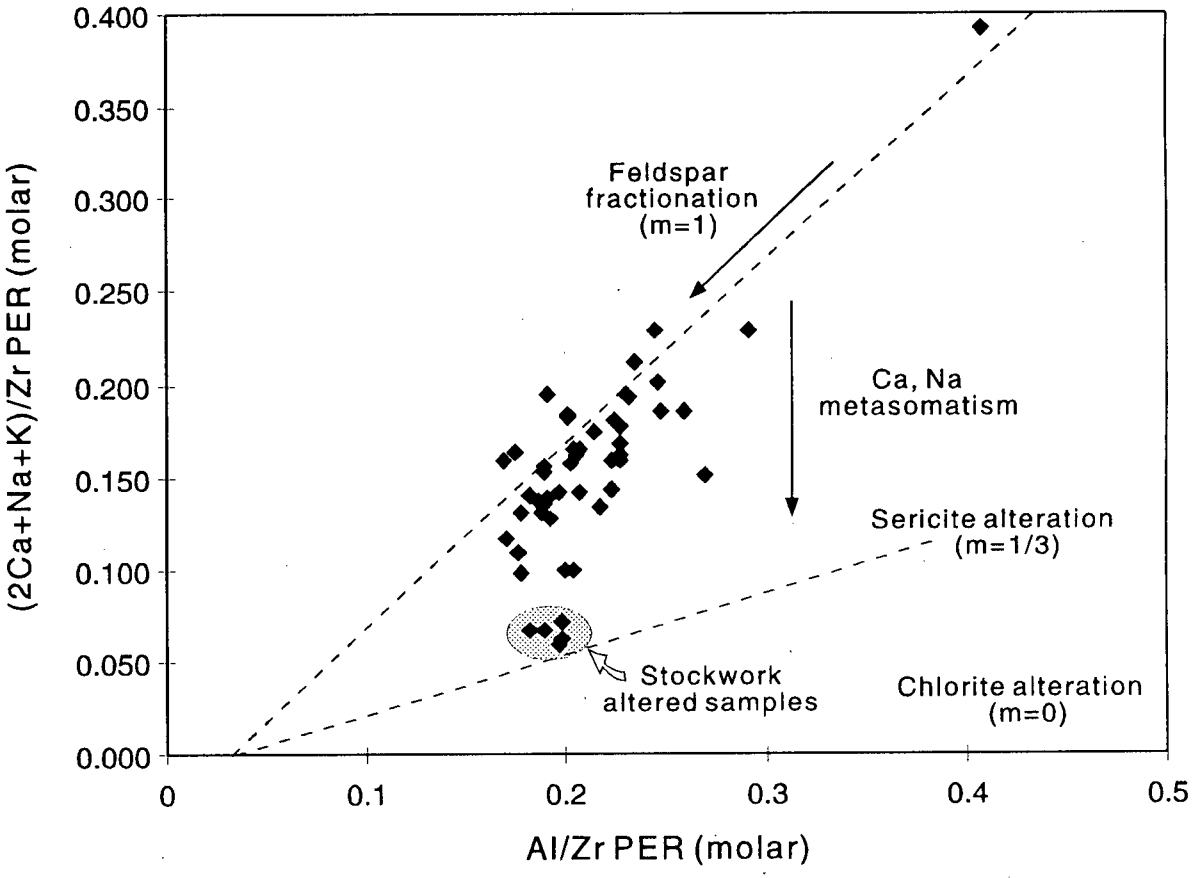

Figure 4.2. (2Ca+Na+K)/Zr vs. Al/Zr PER plot. The diagram illustrates the departure of felsic samples from a fractionation trend with unit slope toward a line with a slope of 1/3 representing the total loss of Na and Ca by the complete sericitization of feldspar. Due to the lack of strong chlorite alteration of felsic rocks at Seneca, samples do not plot below this sericite alteration line.

(sericitization). Such trends are clearly visible on Figure 4.1. The intensely altered stockwork samples (solid symbols on Figure 4.1) can be subdivided into two groups on this plot; one group of samples from the Fleetwood Zone stockworks plots closer to the sericite end-member composition, whereas the second group taken entirely from the Vent Zone stockwork plots closer to the chlorite end-member suggesting a relatively greater involvement of MgO in the hydrothermal processes that formed this stockwork.

Although this diagram is useful in relating some components of the bulk chemistry to mineralogical changes in the rock during alteration, it may be slightly misleading in that it does not consider additions or losses of other elements such as SiO_2 which can be significant in VMS systems.

4.4.2 PER ANALYSIS

An alternative method of illustrating the effects of hydrothermal alteration on the alkali content of the felsic rocks is by using Pearce element ratio analysis. A plot of Al/Zr PER versus (Na+K)/Zr PER was used in the previous chapter to establish a primary trend amongst the least altered samples that can be related to fractionation of dominantly feldspar. A similar plot that has an abscissa of (2Ca+Na+K)/Zr PER (Figure 4.2) can best display the effects of varying degrees of sericitization or chloritization on the composition of the felsic rocks at Seneca. Destruction of feldspar by Ca and Na metasomatism displaces a sample from its unaltered precursor composition on the fractionation trend having a unit slope toward the abscissa (assuming Al_2O_3 is immobile). Samples that have been completely sericitized, such as those from the Fleetwood and Vent Zone stockworks, lie along a line with a slope of 1/3 representing a total loss of Na by the reaction:

$$3NaAlSi_3O_8 + K^+ + 2H^+ \Leftrightarrow KAl_3Si_3O_{10}(OH)_2 + 3Na^+ + 6SiO_2$$

(Stanley and Madeisky, 1994)

Sample	Location	r_{SER}
87-11-75	VENT	39.29
87-12-301	FLEETWD	61.07
87-12-69	FLEETWD	53.63
87-12-147.4	FLEETWD	90.55
91-10-234	FLEETWD	79.56
91-10-210	FLEETWD	30.41
91-10-180	FLEETWD	42.47
91-10-118	FLEETWD	2.13
91-10-99	FLEETWD	16.21
91-16-61	FLEETWD	62.25
91-16-152	FLEETWD	37.96
91-16-159	FLEETWD	90.50
91-16-161	FLEETWD	79.32
91-16-307	FLEETWD	81.31
92-27-71	FLEETWD	45.58
92-27-85	FLEETWD	50.15
92-27-177	FLEETWD	55.19
92-31-281	FLEETWD	23.25
92-31-244	FLEETWD	63.91
92-31-225	FLEETWD	60.47
92-33-75	33-ZONE	38.21
92-39-71	FLEETWD	55.53
92-39-200	FLEETWD	23.36
93-VT-01	VENT	39.00
93-VT-02	VENT	100.29
93-VT-03	VENT	108.11
93-VT-04	VENT	99.05
93-FW-46	FLEETWD	60.51
93-FW-49	FLEETWD	44.98
93-FW-51	FLEETWD	27.44
93-FW-52	FLEETWD	97.78

Sample	Location	r_{SER}
83-02-277	PIT AREA	37.38
83-02-320	PIT AREA	32.00
83-02-186	PIT AREA	30.23
83-02-67	PIT AREA	33.79
83-06-50	PIT AREA	27.19
83-07-27	PIT AREA	21.16
83-07-54	PIT AREA	45.80
83-10-91	PIT AREA	68.88
83-11-24	PIT AREA	44.21
83-11-40	PIT AREA	36.15
85-03-70	PIT AREA	31.75
85-03-126	PIT AREA	19.73
91-02-28	PIT AREA	29.39
91-02-85	PIT AREA	18.15
91-02-170	PIT AREA	26.86
93-SN-44	PIT AREA	61.27
93-SN-45	PIT AREA	40.31
93-SN-46	PIT AREA	42.83

Table 4.1. Summary of the sericitization index (r_{SER}) calculations highlighting the greater average degree of sericitization of feldspar that has occurred in the Fleetwood and Vent Zones relative to the Pit Area. The index is calculated using the formula $r_{SER} = (1 - [(Na + K)/Z) / ((Al/Z) - x_0)]) \times 3/2 \times 100\%$, where Z is the conserved element and x_0 is the abscissa intercept on a (Na + K)/Z vs. (Al/Z) PER plot.

Sericitization Index

Stanley and Madeisky (1994) present a sericite alteration index in which the degree of sericitization is related to the slope of the line between a data point and the abscissa intercept on a (Na+K)/Zr vs. Al/Zr plot and can be calculated using the following equation:

$$r_{SER} = (1 - [(Na + K)/Z) / ((Al/Z) - x_0)]) \times 3/2 \times 100\%$$

where r_{SER} is the relative amount of sericitization of feldspar, Z is the conserved element and x_0 is the abscissa intercept (Stanley and Madeisky, 1994). Although Ca is a component of the ordinate axis in Figure 4.2, Ca has not been incorporated into the sericitization index in this study because of the presence in some of these rocks of minerals such as calcite and epidote which do not appear to have been hydrothermally derived and which would partially obscure the effects of the true hydrothermal alteration. This index has been calculated for a representative set of the FP and QFP flow and intrusion samples from Seneca and the results are included in Table 4.1. The amount of sericitization varies from less than 10 % for the least altered, post-hydrothermal intrusions to greater than 90% for the strongly altered stockwork samples. Although samples such as 91-10-118 and 92-39-200 are close to known areas of hydrothermal alteration, they show relatively small amounts of sericitization. This suggests that either they were intruded into the sequence after the main hydrothermal activity and thus did not experience the degree of alteration of other similar synvolcanic intrusions (e.g. sample 91-16-307), or these intrusions had a lower permeability making them more resistant to alteration. Stockwork samples such as 93-VT-02, -03 and -04 and 91-16-159 have experienced the greatest degree of sericitization.

The sericitization index also highlights the difference in the overall degree of alteration between the Pit Area and the Fleetwood and Vent Zones. The set of samples in Table 4.1 were chosen to represent all of these areas. In general, the Pit Area has lower sericitization indices, less than 40 % (often < 35%), compared to the Fleetwood and Vent Zones where indices are generally greater than 45 % and frequently are > 50 %. The hydrothermal activity that created the stockwork zones also created a zone of moderate to strong sericite alteration throughout the entire Fleetwood and Vent Zone but had a much smaller effect on rocks in the more distal Pit Area.

4.4.3 MASS CHANGE CALCULATIONS

4.4.3.1 METHODOLOGY

The method of MacLean (1990) is used in this section for calculating material changes in altered rock series. The method uses immobile and incompatible elements to determine the precursor compositions of the altered rocks and is described in detail below.

Establishment of fractionation trends

The first and perhaps most critical step in the mass change calculations is the establishment of best fit fractionation lines which represent the primary variability imposed by igneous processes amongst the volcanic series. Immobile element pairs are utilized to establish such trends. Igneous incompatible elements such as Zr or Y are often used in studies such as this as a monitor of fractionation. However, Zr and Y are not used in this study because of their inconsistent behaviour and possible compatibility as demonstrated in the previous chapter. TiO_2 has been chosen instead as the best monitor of fractionation. Although TiO_2 and Al_2O_3 have been shown to be compatible in some units at Seneca, they appear to behave uniformly over the entire range of compositions of the felsic rocks and hence they are useful in monitoring fractionation. MacLean and Kranidiotis (1987) have shown that Al_2O_3 and TiO_2 generally have high degrees of immobility in typical hydrothermal systems and are thus a useful pair of elements with which to establish a regression line or fractionation trend.

Mass change effects on binary plots

Immobile elements are concentrated by processes involving net mass loss and are diluted by processes involving mass gain (MacLean, 1990). The effects of mass changes on a binary plot of immoble elements are illustrated on Figure 4.3. Although these immobile components have not been added to or removed from the system during alteration, the addition or removal of the mobile components such as SiO_2 changes the overall system size and will make it *appear* as though the

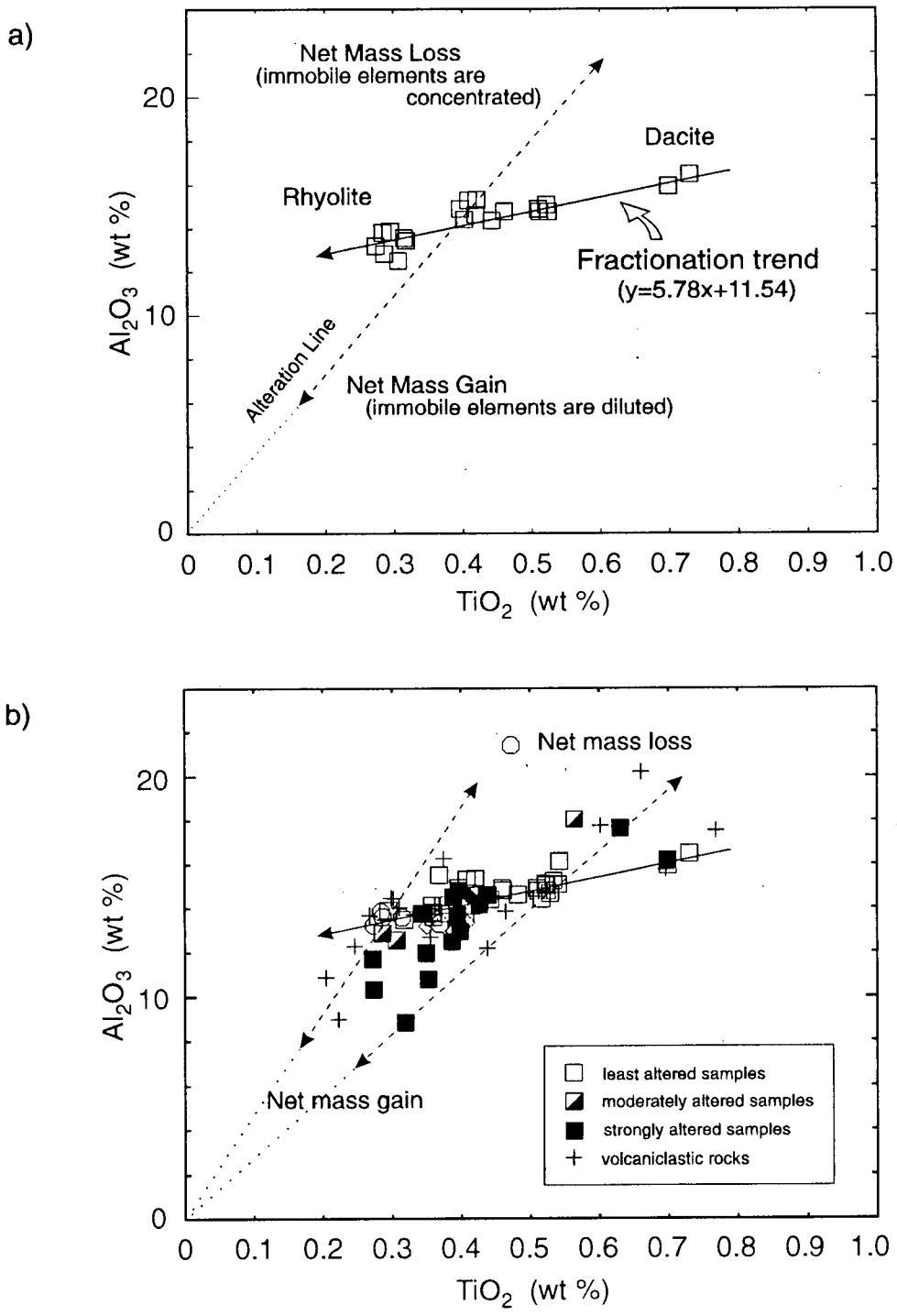

Figure 4.3. Al_2O_3-TiO_2 immobile element binary plot. a) illustrates the use of a set of least altered samples to establish a fractionation trend for the felsic rocks (dacites to rhyolites) at Seneca and the effects of mass gain and mass loss on a binary plot of immobile elements. b) is a plot of all felsic samples and illustrates the effects of the dominant mass gains that have diluted the immobile elements. Figure b) is used to determine the precursor TiO_2 compositions.

quantities of immobile elements have changed. This apparent change is due to whole rock geochemical data being totalled to a sum of 100 wt. %; in reality, the amount of the immobile element has remained fairly constant, but the *system size* has changed by mass loss or mass gain.

Determining precursor compositions

The effect of closure, a mathematical artifact, is a common problem when dealing with geochemical data that are reported as weight percents and are 'forced' to sum to equal 100 %. However, MacLean (1990) presents a simple procedure which circumvents the effects of closure. An altered sample's precursor composition is calculated by determining the intersection of the alteration line with the best fit fractionation line on a binary plot; in essence an altered sample is moved along an alteration line back to its 'original' position on the fractionation trend. The precursor compositions of a series of samples are determined on an element-by-element basis in which each of the mobile elements are plotted individually against the monitor of fractionation and a separate regression line is fit to the least altered samples on each plot. For example, a regression line can be established for the least altered samples on a SiO_2 vs. TiO_2 plot and the mass changes of SiO_2 for the altered samples are related to their relative displacement from this line.

Determining reconstructed compositions

To eliminate the closure effect inherent in the presentation of whole rock geochemical data for altered rocks, MacLean calculates a 'reconstructed composition' which keeps the concentration of the immobile elements constant while adjusting the mobile element concentrations to reflect their changes during alteration. If mass change has occurred, an altered sample would appear to have lost or gained a certain amount of an immobile element due to the fact that whole rock data is totalled to 100%. Since by definition this is not the case, all of the elements need to be readjusted up or down to eliminate this effect. All components in the altered sample are adjusted by a mass factor which is the ratio

between an immobile element concentration in the precursor and its concentration in the altered rock. The reconstructed composition is calculated as follows:

RC = wt. % component (altered rock) * (IM (precursor) / IM (altered rock))

where RC is the reconstructed composition and IM is the immobile element monitor (e.g. TiO_2) (Maclean, 1990). Thus, the reconstructed composition represents the net mass of a rock that has gained or lost mobile components. If a sample has gained mass during alteration, for example by silicification, then the reconstructed composition will total over 100 wt. %. Conversely, if a rock has lost mass by chloritization or sericitization, then the reconstructed composition will total less than 100 wt. %. A mass change in an individual component is the difference between the precursor composition and the reconstructed composition.

4.4.3.2 MASS CHANGE CALCULATIONS FOR FELSIC ROCKS AT SENECA

The step by step calculation of mass changes for the most strongly altered felsic rocks at Seneca using the method of MacLean (1990) as described above is shown in Table 4.2. The procedure for these calculations is described in the following sections.

Fractionation trends

The felsic rocks at Seneca form a continuous compositional trend from dacitic to rhyolitic compositions as illustrated in the previous chapter. As such it is possible for the altered samples to have been derived from multiple precursor compositions. TiO_2 was chosen as the best monitor of fractionation. Al_2O_3 was chosen as the immobile element monitor. Figure 4.3a illustrates the derivation of a regression line or fractionation trend for the least altered samples on an Al_2O_3-TiO_2 binary plot. Figure 4.3b relates all of the felsic samples to the same fractionation trend. This plot is used to determine the concentration of TiO_2 in the precursor for all samples by determining the

Table 4.2. Mass change calculations for strongly altered felsic rocks of the Fleetwood and Vent stockworks.

Analytical Data - Untreated (recalculated on L.O.I.-free basis)

Sample	86-28-67	86-28-103	87-12-147	91-10-180	91-10-210	91-10-234	91-16-159	91-18-252	92-28-132	92-31-244	93-VT-02	93-VT-03	93-VT-04
Hole	86-28	86-28	87-12	91-10	91-10	91-10	91-16	91-18	92-28	92-31	86-13	86-13	86-13
Depth (m)	67	103	147.4	180.37	210.13	234.5	159	252.5	132.5	244.5	50	65	85
Depth (ft)	219.8	337.9	483.6	591.8	689.4	769.3	521.6	828.4	434.7	802.2	164.0	213.3	278.9
Rock Type	ALT FP	ALT FP	ALT FP	ALT FP	FP FLOW	ALT FP	ALT FP	ALT FP	LT FLOW	ALT FP	ALT FP	ALT FP	ALT FP
SiO2	75.72	73.65	78.26	75.25	77.16	74.29	78.75	80.32	71.83	64.90	74.71	73.35	73.92
TiO2	0.39	0.44	0.39	0.34	0.40	0.34	0.26	0.35	0.41	0.63	0.40	0.44	0.43
Al2O3	13.58	14.56	12.41	11.71	13.12	13.74	11.25	10.74	14.55	17.59	12.89	14.53	14.10
FeO*	2.75	2.51	2.74	3.45	1.45	2.67	1.31	3.82	2.60	3.74	4.01	3.00	3.51
MnO	0.11	0.14	0.04	0.01	0.01	0.15	0.01	0.01	0.19	0.13	0.08	0.17	0.08
MgO	3.73	4.81	1.79	0.50	0.47	3.88	0.99	0.67	2.28	5.55	3.95	4.58	3.72
CaO	0.21	0.24	0.22	0.37	1.09	0.65	0.26	0.17	1.56	1.19	0.51	0.54	0.21
Na2O	0.06	0.00	0.15	0.71	4.32	1.94	0.66	0.26	6.03	4.22	0.21	0.00	0.00
K2O	3.19	3.38	3.57	5.47	1.57	2.13	2.69	3.16	0.41	1.63	3.00	3.18	3.75
P2O5	0.11	0.12	0.11	0.10	0.03	0.10	0.10	0.07	0.09	0.19	0.09	0.11	0.09
Total	100.00	100.00	100.00	100.00	100.00	100.00	100.00	100.00	100.00	100.00	100.00	100.00	100.00
- using intersection of fractionation line y=5.7813x + 11.544, and alteration lines y = mx													
Ti precursor	0.40	0.42	0.44	0.41	0.43	0.34	0.31	0.47	0.39	0.52	0.44	0.42	0.42
Al precursor	13.87	13.96	14.07	13.89	14.01	13.49	13.34	14.24	13.80	14.55	14.06	13.99	13.99
Ti mass factor	1.02	0.96	1.13	1.19	1.07	0.98	1.19	1.33	0.95	0.83	1.09	0.96	0.99
- Mass factor = (Ti precursor)/(Ti altered)													

Precursor Values (normalized to 100 %)

SiO2	72.53	72.16	71.73	72.45	71.98	74.06	74.67	71.04	72.83	69.75	71.78	72.08	72.06
TiO2	0.42	0.43	0.45	0.42	0.44	0.35	0.32	0.49	0.40	0.55	0.45	0.44	0.44
Al2O3	14.37	14.48	14.62	14.39	14.54	13.89	13.70	14.83	14.28	15.24	14.60	14.51	14.51
FeO*	3.13	3.27	3.43	3.16	3.34	2.57	2.34	3.68	3.02	4.16	3.41	3.30	3.30
MnO	0.12	0.12	0.12	0.12	0.12	0.10	0.10	0.13	0.11	0.14	0.12	0.12	0.12
MgO	1.78	1.88	2.00	1.80	1.93	1.37	1.20	2.18	1.70	2.53	1.98	1.90	1.91
CaO	1.07	1.09	1.10	1.08	1.09	1.02	1.00	1.12	1.06	1.17	1.10	1.09	1.09
Na2O	5.07	5.11	5.16	5.08	5.13	4.90	4.84	5.23	5.04	5.37	5.15	5.12	5.12
K2O	1.37	1.31	1.23	1.36	1.28	1.63	1.73	1.12	1.42	0.90	1.24	1.29	1.29
P2O5	0.10	0.11	0.12	0.11	0.11	0.08	0.07	0.13	0.10	0.15	0.12	0.11	0.11
Total	100.00	100.00	100.00	100.00	100.00	100.00	100.00	100.00	100.00	100.00	100.00	100.00	100.00

Table 4.2. (continued)

Reconstructed Values - based on untreated data times Ti mass factor

Sample	86-28-67	86-28-103	87-12-147	91-10-180	91-10-210	91-10-234	91-16-159	91-18-252	92-28-132	92-31-244	93-VT-02	93-VT-03	93-VT-04
Hole	86-28	86-28	87-12	91-10	91-10	91-10	91-16	91-18	92-28	92-31	86-13	86-13	86-13
Depth (m)	67	103	147.4	180.37	210.13	234.5	159	252.5	132.5	244.5	50	65	85
Depth (ft)	219.8	337.9	483.6	591.8	689.4	769.3	521.6	828.4	434.7	802.2	164.0	213.3	278.9
Rock Type	ALT FP	ALT FP	ALT FP	ALT FP	FP FLOW	ALT FP	ALT FP	ALT FP	LT FLOW	ALT FP	ALT FP	ALT FP	ALT FP
SiO2	77.33	70.63	88.74	89.31	82.42	72.94	93.36	106.49	68.10	53.71	81.46	70.60	73.34
TiO2	0.40	0.42	0.44	0.41	0.43	0.34	0.31	0.47	0.39	0.52	0.44	0.42	0.42
Al2O3	13.87	13.96	14.07	13.89	14.01	13.49	13.34	14.24	13.80	14.55	14.06	13.99	13.99
FeO*	2.81	2.40	3.10	4.09	1.55	2.62	1.56	5.06	2.47	3.09	4.37	2.89	3.49
MnO	0.12	0.13	0.05	0.01	0.01	0.14	0.01	0.01	0.18	0.10	0.09	0.16	0.08
MgO	3.80	4.61	2.03	0.59	0.50	3.81	1.17	0.89	2.16	4.59	4.30	4.40	3.69
CaO	0.21	0.23	0.25	0.44	1.16	0.64	0.31	0.22	1.48	0.98	0.56	0.52	0.21
Na2O	0.06	0.00	0.17	0.84	4.62	1.91	0.79	0.34	5.71	3.49	0.23	0.00	0.00
K2O	3.25	3.24	4.05	6.49	1.67	2.09	3.19	4.18	0.39	1.35	3.27	3.06	3.72
P2O5	0.12	0.12	0.13	0.12	0.03	0.10	0.12	0.10	0.09	0.16	0.10	0.11	0.09
Total	101.98	95.75	113.03	116.20	106.40	98.08	114.16	132.01	94.77	82.55	108.88	96.15	99.03

-reconstructed values are calculated by multiplying precursor values by Ti mass factor.

Mass Changes (reconstructed values minus precursor values)

SiO2	4.80	-1.53	17.01	16.87	10.44	-1.12	18.69	35.45	-4.73	-16.03	9.68	-1.48	1.28
TiO2	-0.01	-0.02	-0.02	-0.01	-0.02	-0.01	-0.01	-0.02	-0.01	-0.02	-0.02	-0.02	-0.02
Al2O3	-0.50	-0.52	-0.55	-0.50	-0.53	-0.40	-0.36	-0.59	-0.48	-0.68	-0.54	-0.52	-0.53
FeO*	-0.32	-0.86	-0.32	0.93	-1.79	0.05	-0.79	1.38	-0.56	-1.06	0.96	-0.41	0.18
MnO	0.00	0.01	-0.07	-0.10	-0.11	0.04	-0.09	-0.11	0.06	-0.03	-0.03	0.04	-0.04
MgO	2.02	2.73	0.03	-1.21	-1.43	2.44	-0.03	-1.29	0.46	2.06	2.32	2.50	1.78
CaO	-0.86	-0.86	-0.85	-0.63	0.07	-0.38	-0.69	-0.90	0.42	-0.19	-0.54	-0.57	-0.88
Na2O	-5.00	-5.11	-4.99	-4.24	-0.51	-2.99	-4.05	-4.89	0.68	-1.88	-4.92	-5.12	-5.12
K2O	1.88	1.93	2.82	5.13	0.40	0.46	1.45	3.07	-1.03	0.45	2.03	1.76	2.43
P2O5	0.01	0.01	0.01	0.02	-0.08	0.02	0.05	-0.03	-0.01	0.00	-0.01	0.00	-0.02
Total	**2.02**	**-4.21**	**13.07**	**16.24**	**6.44**	**-1.89**	**14.18**	**32.05**	**-5.19**	**-17.40**	**8.93**	**-3.81**	**-0.93**

intersection of the alteration line of each sample with the fractionation trend. Fractionation trends were derived using a least squares regression line for all major elements versus TiO_2 for the least altered sample set. Some of these trends are illustrated in Figure 4.4.

Precursor compositions

Since the precursor TiO_2 concentrations for all the samples were calculated in the previous step, these values can be substituted for x in the equations for the fractionation lines shown in Figure 4.4. This establishes an altered sample's precursor position on the fractionation trend and allows the precursor concentration for each of the elements to be determined by reading off the ordinate axis on each individual binary plot. Once the precursor concentrations of all elements in a sample were determined, the mass factors were calculated and the precursor compositions were normalized to 100%.

Reconstructed compositions and mass change calculations

The reconstructed compositions were calculated by multiplying the untreated data by the Ti mass factor. Finally the actual mass changes for all samples were calculated by subtracting the precursor concentration from the reconconstructed concentration for each component. The net mass changes were calculated by summing the change in each component for each sample. Negative values indicate mass loss while positive values indicate mass gain.

Results

Increasing degrees of alteration in the felsic rocks at Seneca correspond to greater negative mass changes or losses of Na_2O and CaO, but increasing positive mass changes or gains of K_2O. This is due to the conversion of plagioclase to sericite. Changes in other elements such as SiO_2 and MgO are more variable and will be discussed later.

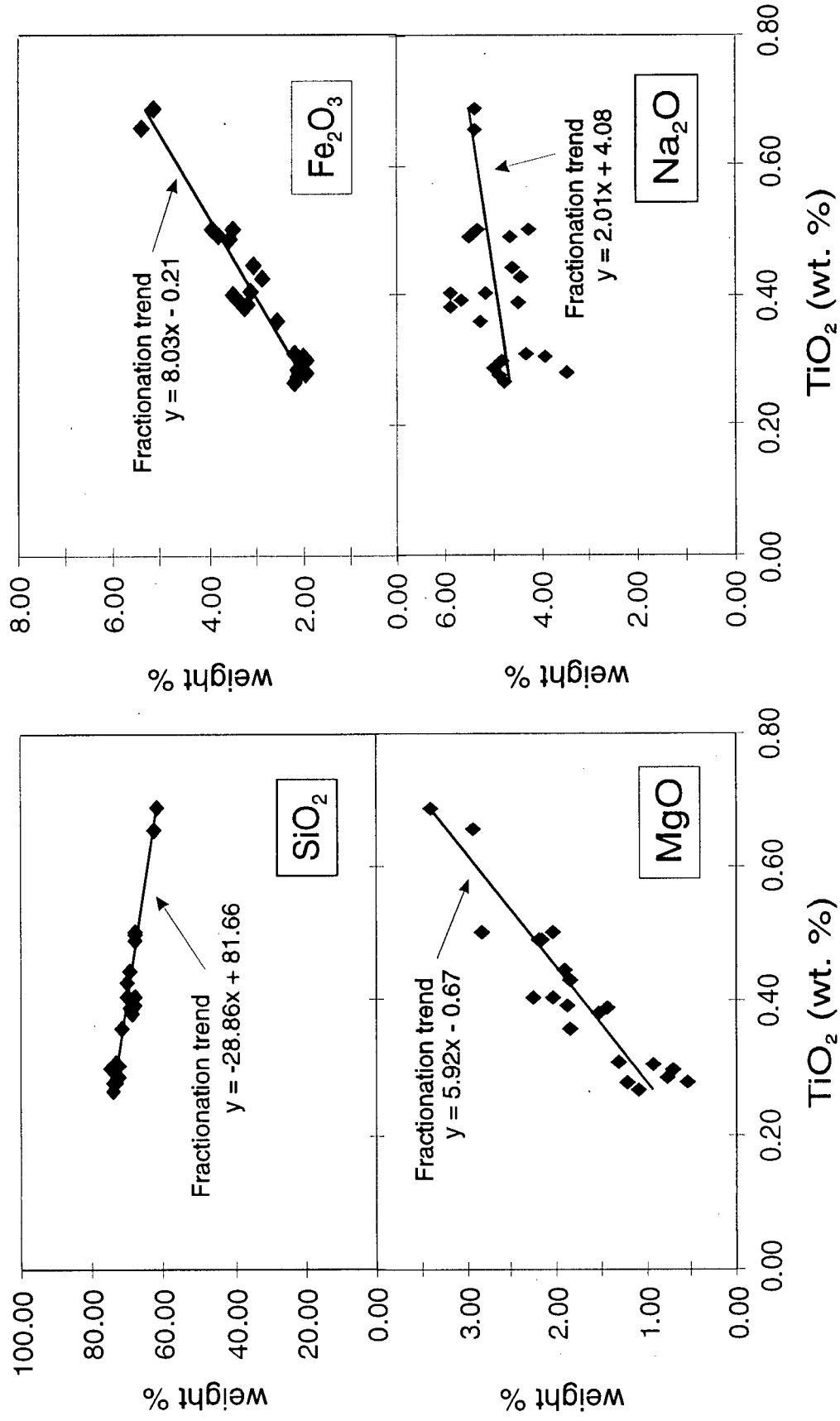

Figure 4.4. Mobile-immobile element plots of least altered felsic samples. These diagrams establish fractionation trends for the major elements. The altered samples are related to these trends in the calculation of the precursor concentrations of the major elements.

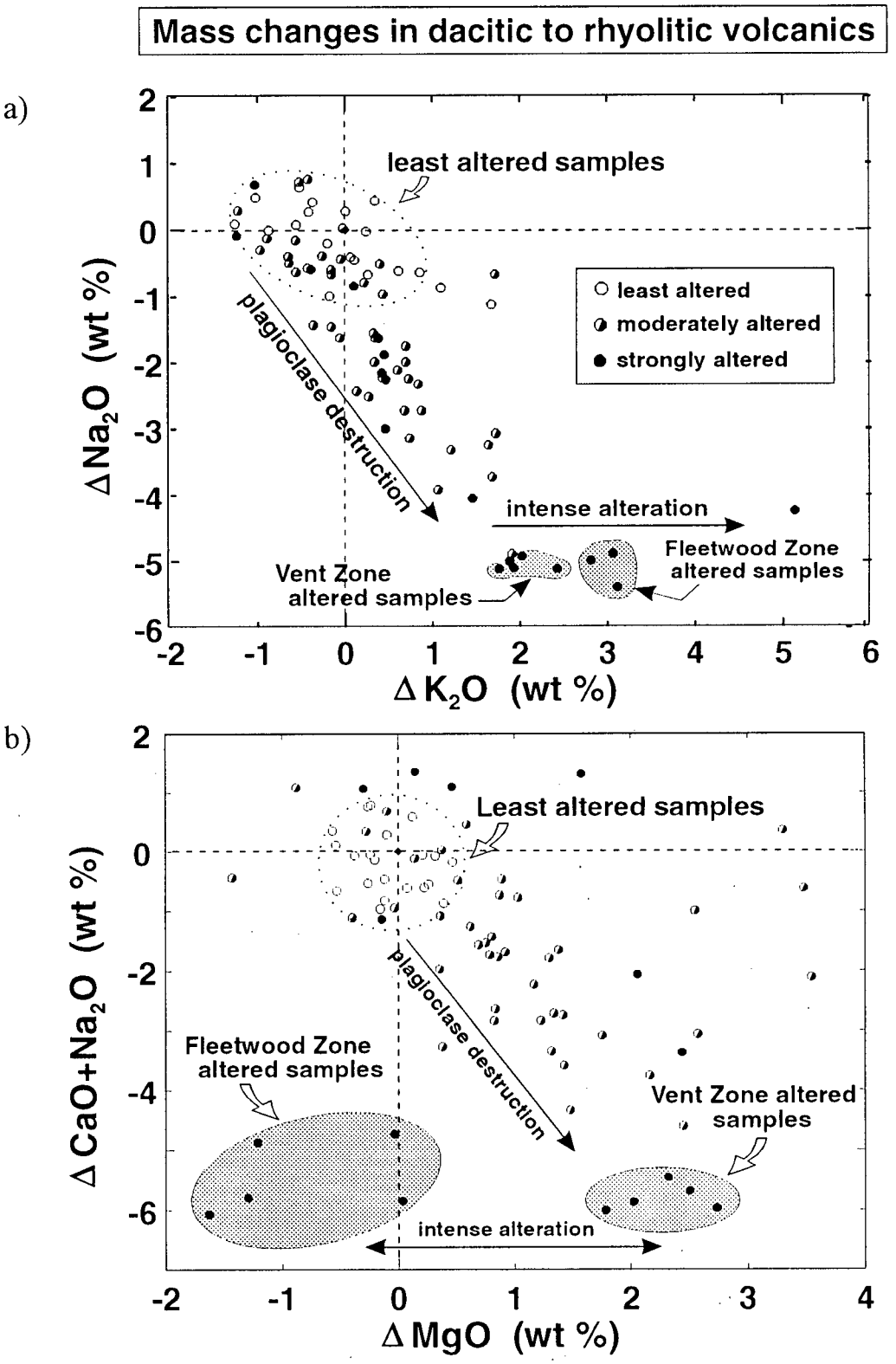

Figure 4.5. Mass change diagrams. These diagrams plot the mass changes in some of the important elements involved in the hydrothermal alteration of the felsic rocks at Seneca. Both plots demonstrate the increasing loss of Na_2O and CaO with increasing alteration. Figure b) illustrates the greater gains of MgO that characterize the Vent Zone stockwork samples.

Figure 4.5 illustrates some of the results of the mass change calculations. The least altered samples (open symbols) cluster around the origin (zero mass change) whereas most of the strongly altered stockwork samples (solid symbols) plot along an approximately horizontal trend representing a complete destruction of plagioclase and, thus, a maximum loss of Na_2O and CaO. Samples cannot plot below this because all of the Na and Ca in the precursor rock has been lost from the system.

Figure 4.5a shows that of the intensely altered samples, all have experienced gains in K2O, but the Fleetwood stockwork has experienced greater gains than the Vent Zone stockwork. A similar split in the intensely altered samples is evident in Figure 4.5b. The Vent Zone samples have undergone gains in MgO whereas the Fleetwood samples have experienced losses in MgO.

Figure 4.6 summarizes some of the mass changes for these stockwork samples. The bars on the graph are arranged from left to right corresponding to the samples' relative locations on Figure 2.1. The actual mass change values are summarized in the table below the graph. It is clear from this figure that changes in SiO_2 have had the greatest overall effect on the net mass changes. Whereas all but one of the samples have had a strong loss of Na_2O and CaO, the samples from the Fleetwood Zone have experienced much greater gains in SiO_2 than the Vent Zone. The Fleetwood Zone, in general, appears to have undergone an overall mass gain, whereas mass losses are more prevalent in the Vent Zone.

The mass changes also appear to vary stratigraphically. For example, the Fleetwood samples that have undergone strong gains in SiO_2 and K_2O (numbers 1, 3, 4 and 7 in Figure 4.6) all occur at a higher stratigraphic level (ie. at a shallower depth), perhaps closer to the paleoseafloor. The samples that have lost SiO_2 while gaining MgO and K_2O (Fig. 4.6, numbers 5 and 6) occur at a lower stratigraphic interval. A similar trend is evident for the Vent Zone samples. Shallower samples (numbers 8 and 10) have had the greatest gains in SiO_2 while the deeper samples have had negative or

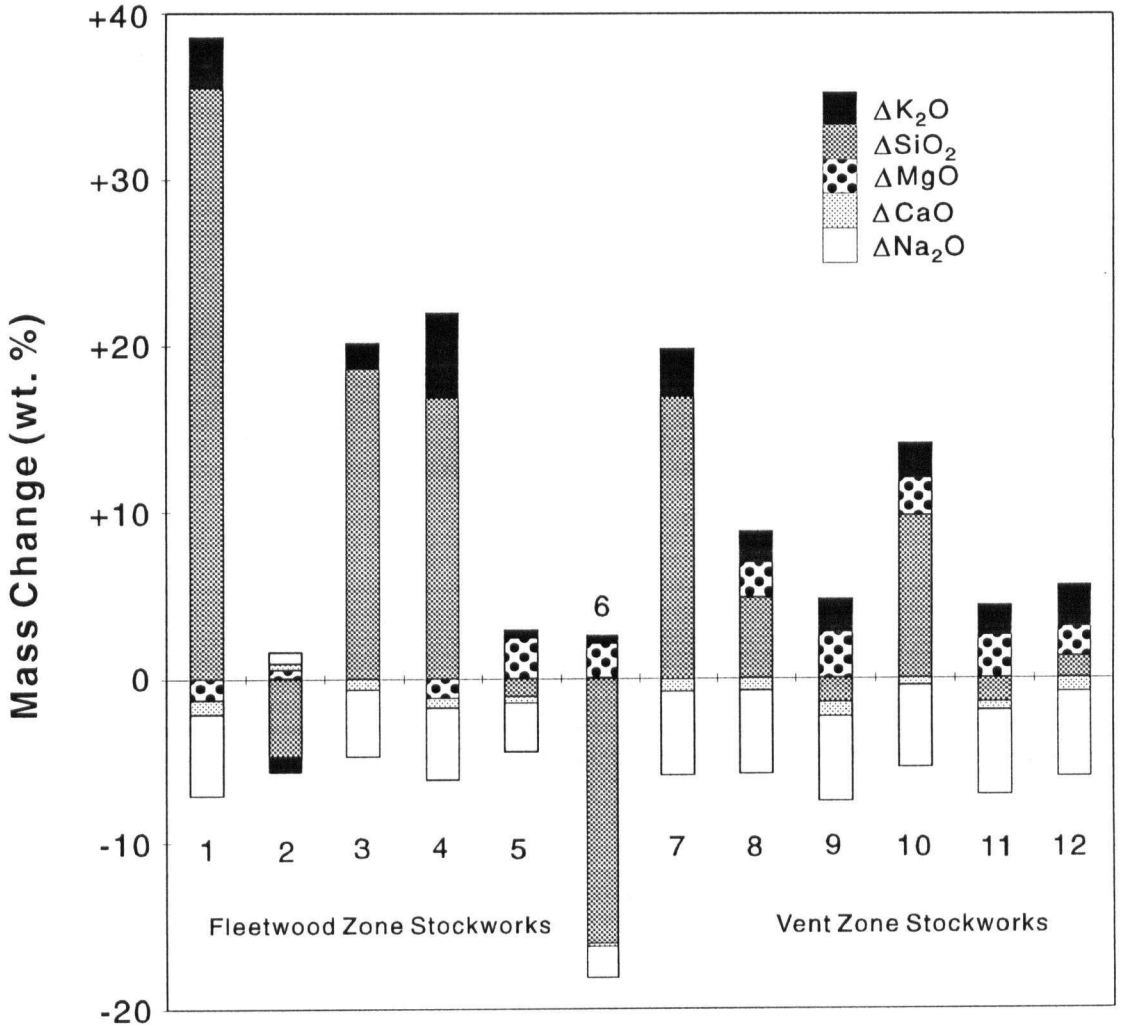

	Fleetwood Zone							Vent Zone				
	1	2	3	4	5	6	7	8	9	10	11	12
	87-12-147	91-10-180	91-10-234	91-16-159	91-18-252	92-28-132	92-31-244	86-28-67	86-28-103	93-VT-02	93-VT-03	93-VT-04
	ALT FP	ALT FP	ALT FP	ALT FP	ALT FP	ALT FLOW	ALT FP	ALT FP	ALT FP	ALT FP	ALT FP	ALT FP
ΔSiO_2	17.01	16.87	-1.12	18.69	35.45	-4.73	-16.03	4.80	-1.53	9.68	-1.48	1.28
ΔTiO_2	-0.02	-0.01	-0.01	-0.01	-0.02	-0.01	-0.02	-0.01	-0.02	-0.02	-0.02	-0.02
ΔAl_2O_3	-0.55	-0.50	-0.40	-0.36	-0.59	-0.48	-0.68	-0.50	-0.52	-0.54	-0.52	-0.53
ΔFeO	-0.32	0.93	0.05	-0.79	1.38	-0.56	-1.06	-0.32	-0.86	0.96	-0.41	0.18
ΔMnO	-0.07	-0.10	0.04	-0.09	-0.11	0.06	-0.03	0.00	0.01	-0.03	0.04	-0.04
ΔMgO	0.03	-1.21	2.44	-0.03	-1.29	0.46	2.06	2.02	2.73	2.32	2.50	1.78
ΔCaO	-0.85	-0.63	-0.38	-0.49	-0.90	0.42	-0.19	-0.86	-0.86	-0.54	-0.57	-0.88
ΔNa_2O	-4.99	-4.24	-2.99	-4.05	-4.89	0.68	-1.88	-5.00	-5.11	-4.92	-5.12	-5.12
ΔK_2O	2.82	5.13	0.46	1.45	3.07	-1.03	0.45	1.88	1.93	2.03	1.76	2.43
ΔP_2O_5	0.01	0.02	0.02	0.05	-0.03	-0.01	0.00	0.01	0.01	-0.01	0.00	-0.02
Total	13.07	16.24	-1.89	14.18	32.05	-5.19	-17.40	2.02	-4.21	8.93	-3.81	-0.98

Figure 4.6. Summary of mass changes for strongly altered stockwork samples. Samples 1 through 7 are from the Fleetwood Zone and samples 8 through 12 are from the Vent Zone. The Fleetwood samples show strong gains in SiO_2 and K_2O in their upper portions and overall mass gains. The Vent samples show similar trends, but have experienced MgO mass gains throughout and have had small positive to negative net mass changes.

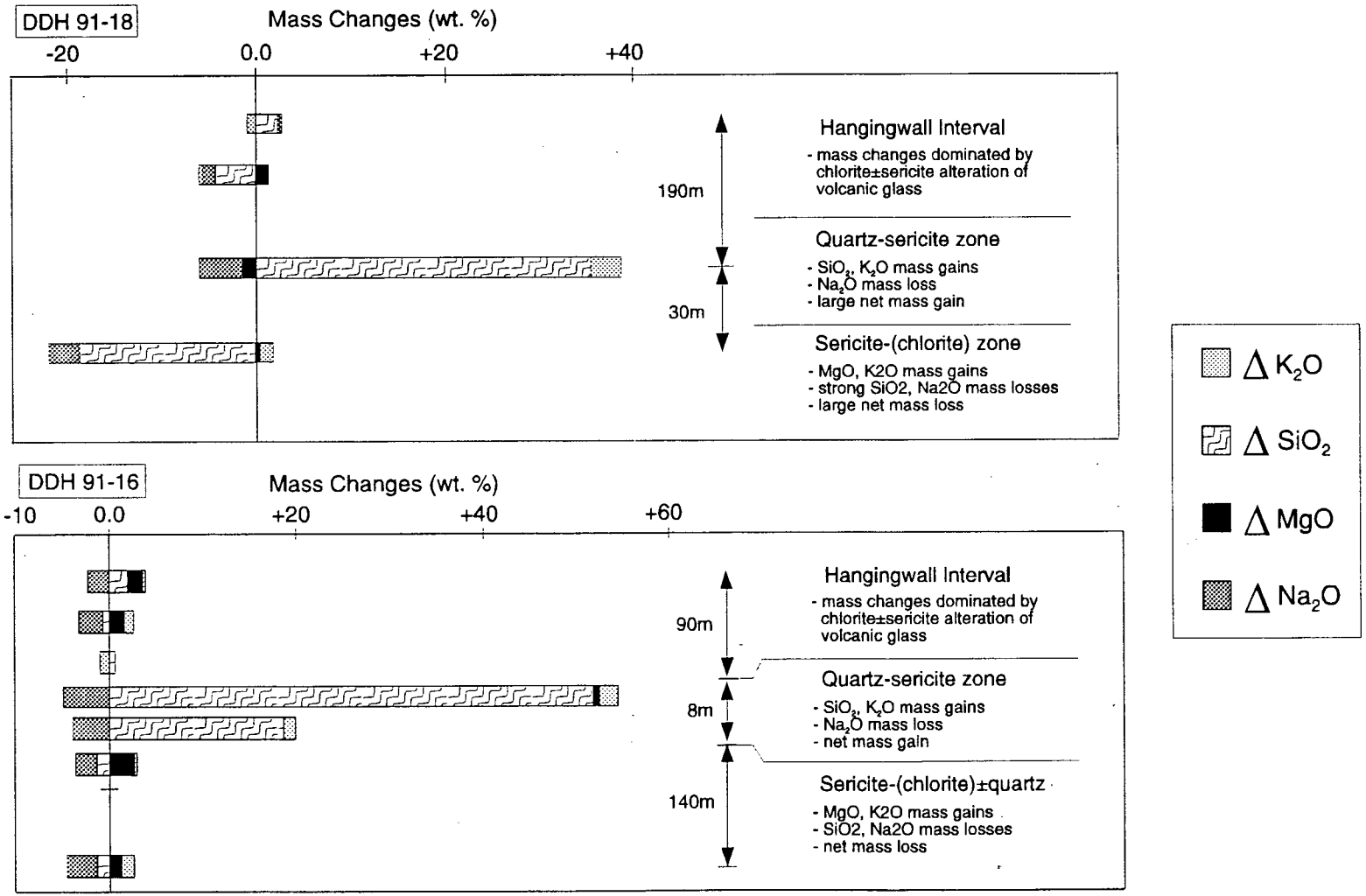

Figure 4.7. Downhole mass changes from drillholes 91-18 and 91-18 in the Fleetwood Zone. These plots show the downhole variations in the alteration assemblages and mass changes that occur in the Fleetwood stockworks. Both drillholes intersect an upper quartz-sericite zone having gains in SiO_2 and K_2O and a lower sericite-chlorite zone having gains in MgO and K_2O.

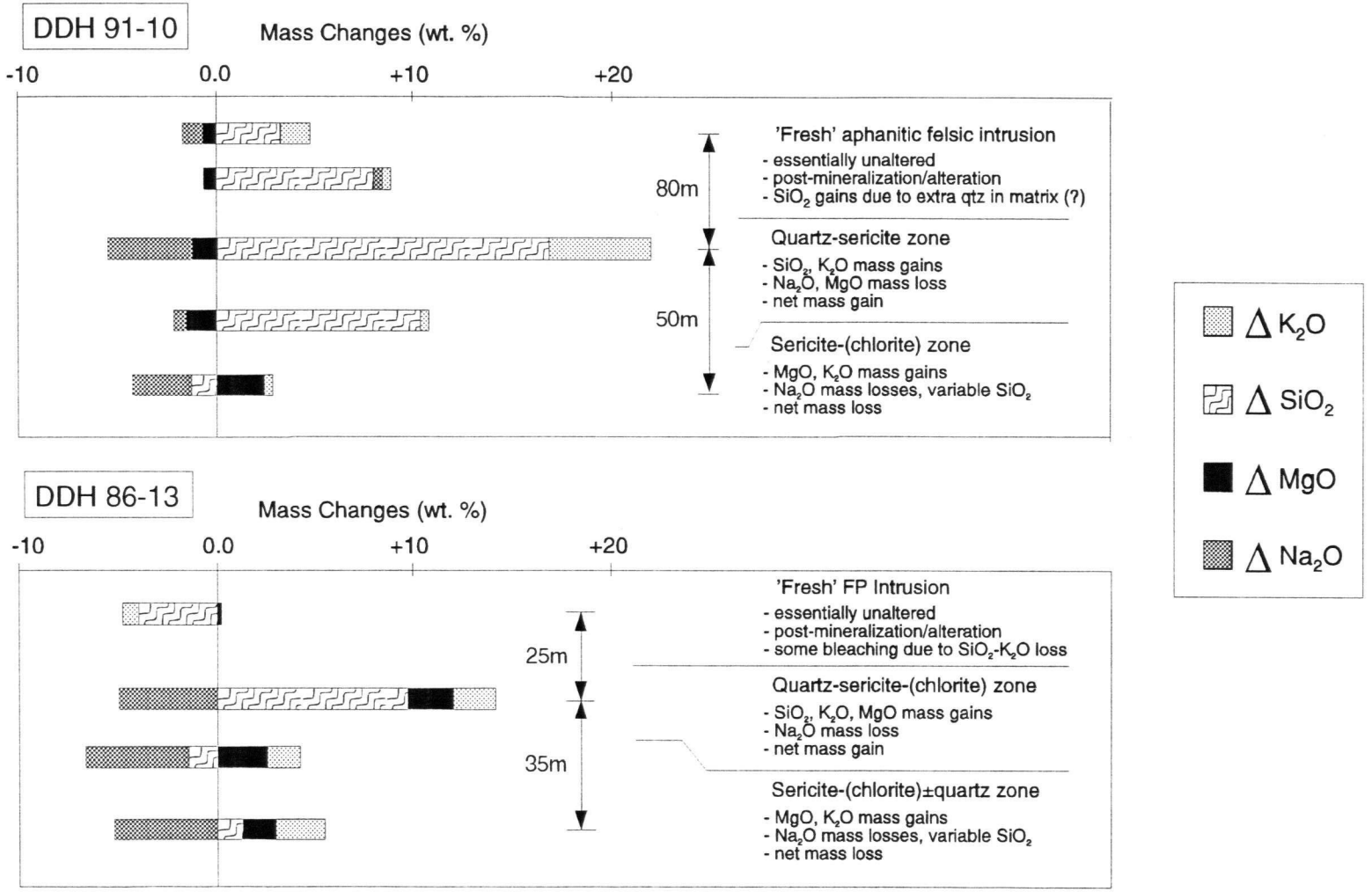

Figure 4.8. Downhole mass changes from drillholes 91-10 in the Fleetwood Zone and 86-13 in the Vent Zone. Both drillholes intersect an upper quartz-sericite zone having gains in SiO_2 and K_2O and losses of Na_2O and a lower sericite-chlorite zone having gains in MgO and K_2O. However, the stockwork in DDH 86-13 has experienced MgO gains throughout and has had smaller net mass changes.

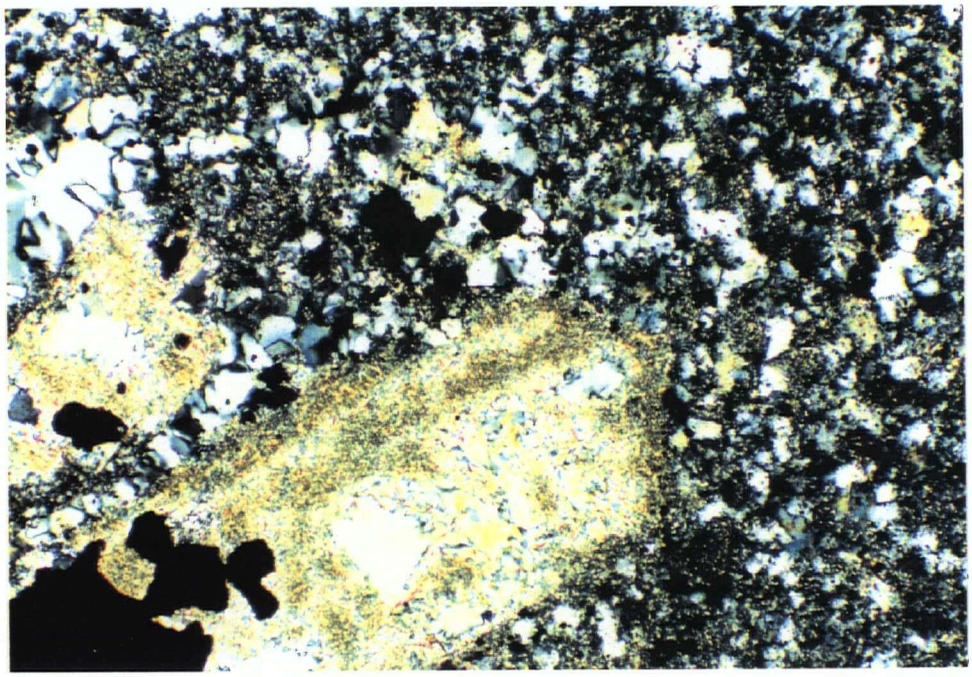

Plate 4.3a: Photomicrograph of Sample 91-10-180, a strongly quartz-sericite altered felsic rock. This alteration assemblage is typical of the upper portion of the Fleetwood Zone. The destruction of feldspar is clearly visible. This sample has experienced an overall mass gain due to the strong addition of silica. (X-Nicols; Field of view = 1.25 mm).

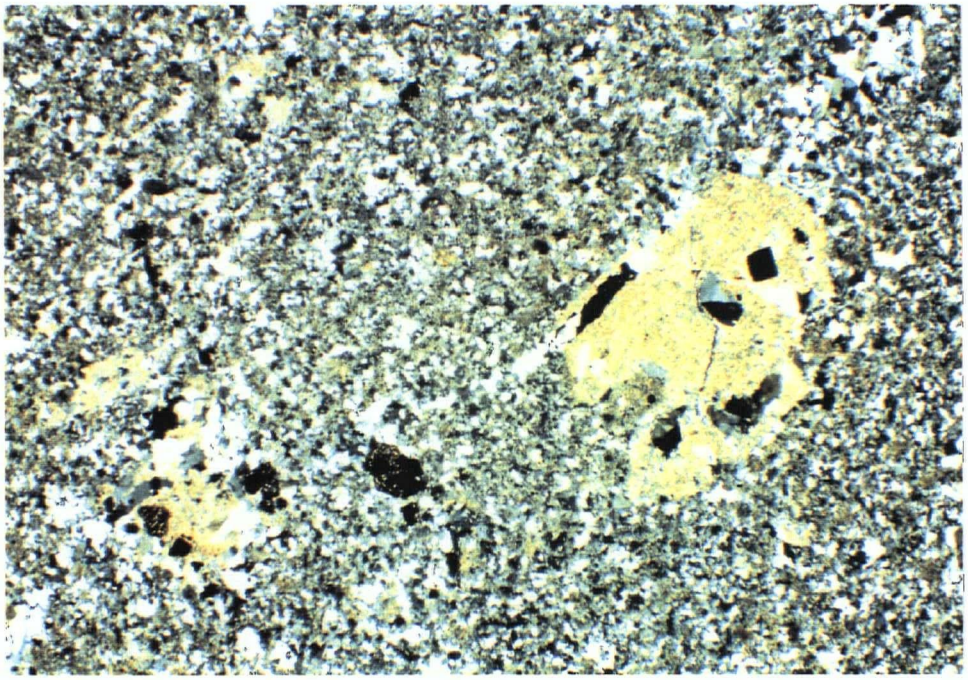

Plate 4.3b: Photomicrograph of Sample 91-18-252, a strongly quartz-sericite altered felsic rock from the Fleetwood Zone. This rock has experienced a similar style of alteration as the sample pictured above, and has also undergone net mass gain. (X-Nicols; Field of view = 5 mm).

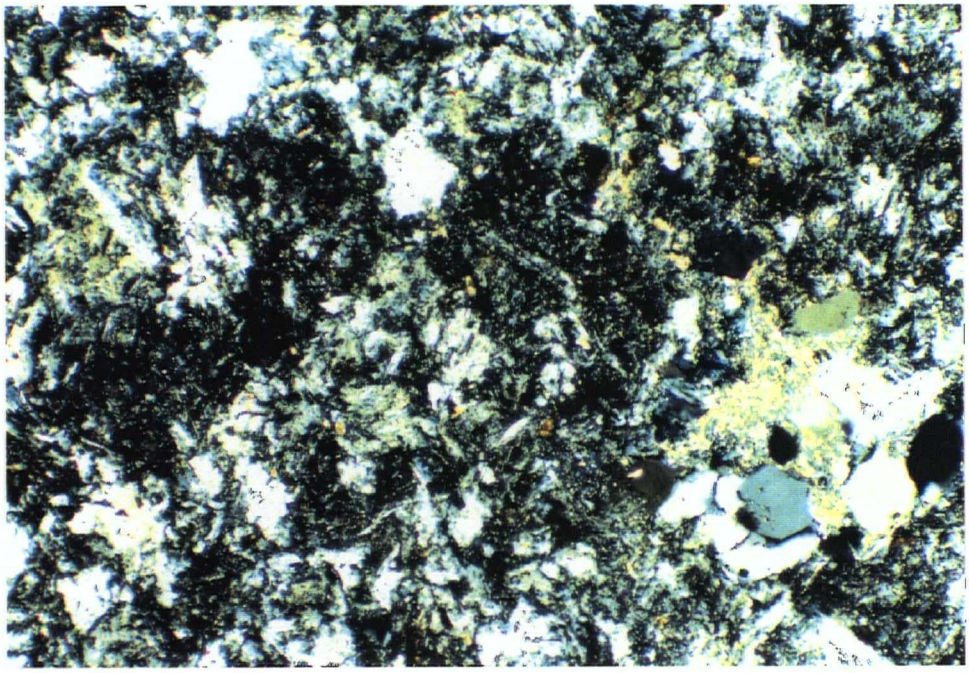

Plate 4.4a: Photomicrograph of Sample 92-31-225, a strongly sericite-chlorite-quartz altered felsic rock. This type of alteration assemblage is typical of the middle to lower parts of the Fleetwood stockwork and parts of the Vent zone stockwork. It is gradational from the assemblage shown in Plate 4.3 and the assemblage pictured below. (X-Nicols; Field of view = 1.25 mm).

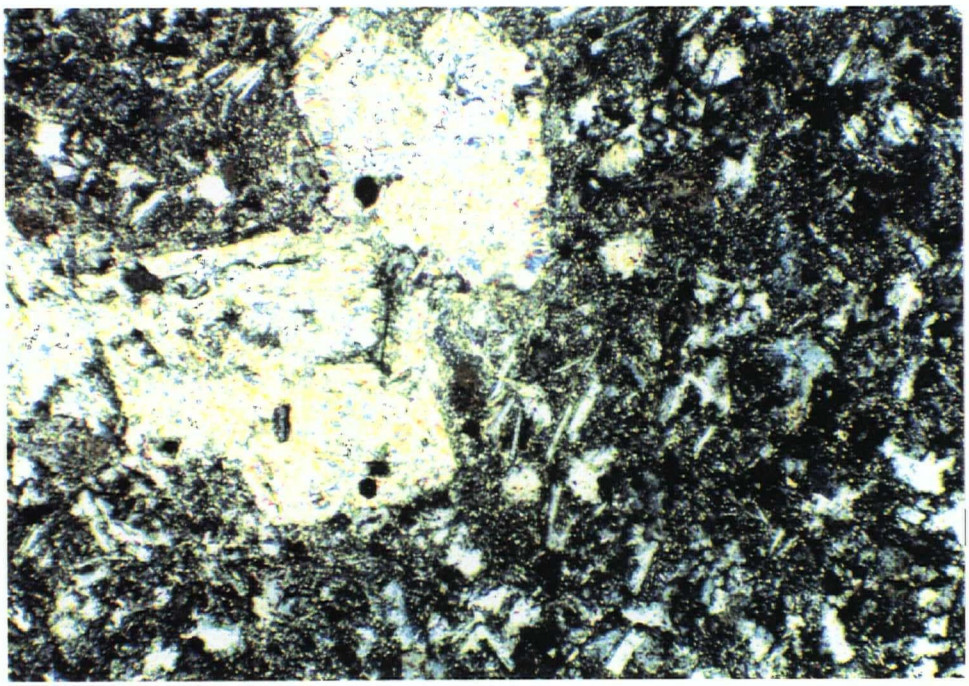

Plate 4.4b: Photomicrograph of Sample 92-31-244, a strongly sericite chlorite altered felsic rock. This type of alteration is typical of the Vent Zone and the lower portions of the Fleetwood stockworks. Such samples have generally experienced mass gains of K_2O and MgO, but net mass losses. (X-Nicols; Field of view = 1.25 mm).

only small positive mass changes in SiO_2 while all samples maintain approximately consistent gains in MgO and K_2O.

This vertical alteration zonation is also illustrated in Figures 4.7 and 4.8 which graphically depict some of the downhole mass changes that have occurred at depth around the Fleetwood and Vent Zone stockworks (see Figure 2.1 for drillhole locations). Drillholes 91-18 and 91-16 on Figure 4.7 have had very strong gains in SiO_2 and K_2O in the upper 10 to 20 metres of their stockwork zones corresponding to an alteration assemblage of quartz and sericite (Plate 4.3). These mass gains decrease downhole while mass gains in MgO become larger. This transition corresponds to a change toward an alteration assemblage dominated by sericite and chlorite (Plate 4.4). Although quartz is sometimes present in varying proportions in this lower zone, SiO_2 has generally been lost from these samples. This SiO_2 loss is particularly strong in the lower part of drillhole 91-18 (Figure 4.7). Mass changes in rocks above the stockwork zones are much smaller and are more variable. They reflect mostly the alteration of volcanic glass to chlorite and sericite. However, the mass losses of Na_2O are not insignificant and may indicate that hydrothermal activity continued after deposition of these units. Drillhole 91-10 (Figure 4.8) has a similar upper quartz-sericite alteration zone and a lower sericite-chlorite zone. SiO_2 gains are much greater in the hangingwall units of this drillhole, but this may be due to excess primary quartz in the groundmass of these aphanitic intrusions. The stockwork zone intersected in drillhole 86-13 from the Vent Zone differs from the others in that MgO gains occur throughout an upper quartz-sericite-chlorite alteration zone and a lower sericite-chlorite zone.

Another common style of alteration present at Seneca is the variable silicification and chloritization that gives the felsic flows their distinctive banding. Although this alteration appears quite strong, it does not result in large mass changes. Despite the amount of chlorite present, the mass changes in MgO are quite small (<0.75 wt. %). The only significant mass gains that have occurred in these rocks are for SiO_2 which has increased usually by less than 10 weight percent. These samples

also have not experienced large losses of Na_2O or CaO. This type of alteration occurs in all areas of the Seneca property, even in areas that are relatively distant from the stockwork zones. The widespread distribution, the limited mass change and the relatively constant Na_2O and CaO suggest that this alteration is not related to hydrothermal activity. It may reflect the interaction of felsic flows with seawater.

4.5 SUMMARY

The alteration at Seneca is dominated by an assemblage of quartz and sericite with varying amounts of chlorite. Calculated sericitization indices for the felsic rocks across the property suggest that alteration is stronger and more pervasive to the northwest than in the Pit Area to the southeast. Rocks from the Fleetwood and Vent Zone have undergone an average of over 50 % sericite alteration of feldspar, whereas similar rocks in the Pit Area have undergone an average of less than 35 % sericitization of feldspar.

Strong alteration in the Pit Area is confined mostly to the ore zone conglomerate, an extensive coarse grained unit of debris flows and turbidites of varying thickness that has undergone moderate to intense silicification and sericitization. This unit and its characteristic alteration can be traced to almost 1 km from the open pit. The conformable nature of the alteration and the lack of a stockwork feeder zone in the immediate area suggests that hydrothermal fluids flowed laterally through the permeable OZC unit strongly altering it while the bounding strata remained essentially unaltered and unmineralized.

Alteration in the Fleetwood and Vent Zones is related to a roughly linear, northwest-southeast trending series of mineralized stockworks. This alteration is discordant and can be subdivided into two principal alteration zones. The upper zone is up to 25 metres thick, has a typical assemblage of quartz and sericite alteration and has undergone a net mass gain (SiO_2 and K_2O mass gains; Na_2O and CaO

mass losses). The lower zone varies from 30 to over 100 metres in thickness, has a typical assemblage of sericite-chlorite±quartz and has generally undergone a net mass loss (MgO and K_2O mass gains; Na_2O, CaO and SiO_2 mass losses). SiO_2 has been leached from the lower zone while MgO was added. The leached silica may be added to rocks higher in the sequence forming a 'cap' of quartz with additional sericite. It appears that at least a portion of this silica addition which fills the interstices of the breccia in the stockworks in the Fleetwood Zone has occurred late in the hydrothermal history and is partially contemporaneous with sulphide deposition (i.e. quartz-sulphide veins occur in Fleetwood-Vent Zone; Plate 4.1a).

The Vent Zone stockwork displays a similar alteration zonation as described above, but has experienced gains in MgO throughout. This may be due in part to a greater involvement of MgO from seawater in this part of the hydrothermal system. Seawater contains relatively high amounts of Mg (1280 mg Mg/gram seawater, Janecky and Seyfried, 1984). Bischoff and Seyfried (1978) have demonstrated that Mg from seawater is incorporated into precipitating mineral phases once the fluids are heated to over approximately 200° C. Thus, if there is a greater mixing of the seawater with hot hydrothermal fluids then one would expect more Mg to be added to the altered rocks. However, the exposed portion of this stockwork may only represent part of a larger zone that has since been partially eroded, and thus we may be only observing the lowermost portion or perhaps the margins of the overall hydrothermal system.

CHAPTER 5
MINERALIZATION

5.1 INTRODUCTION

Previous studies of the Seneca prospect by Pride (1973), Gannicott et al. (1979), Armbrust and Gannicott (1980) and Urabe et al. (1984) were focussed around the discovery site at the small open pit. These authors described the prospect as a small Zn-Cu-Pb-barite massive sulphide deposit that is similar in many aspects to the Kuroko deposits of Japan. Unfortunately, the exposures in the pit that provided the basis for some of their observations have since been obscured. However, more recent diamond drilling in the mid-1980s and early 1990s resulted in discoveries of additional mineralized intersections in the Pit Area and in the Vent and Fleetwood Zones that provided new insights into the genesis of the deposit. This study will subdivide the description of the mineralized zones on the basis of their geographic locations since the different styles of mineralization are generally unique to a particular area of the property.

5.2 PIT AREA

Pride (1973) and Urabe at al. (1984) recognized the strong association of mineralization in the Pit Area with a dominantly felsic fragmental footwall unit which is now referred to as the ore zone conglomerate (OZC) (Plate 5.1a). Their studies describes a zoned massive sulphide body with a chalcopyrite and pyrite-rich base which is overlain by a sphalerite-barite-galena-rich ore. These zones are analagous to the yellow and black ores respectively that occur in the typical Japanese Kuroko deposits. Such a zonation was not as readily discernible in drillcore, although many of the cores examined in this study were 100 to 200 m away from the main sulphide zone in the pit. Pride (1973) also documented fragmental sulphides which suggest that the mineralization formed at or close to the paleoseafloor allowing some some slumping and reworking to occur.

Plate 5.1a: Representative drillcore samples of the mineralized ore zone conglomerate (OZC) from the Pit Area. From left to right, a downward succession is represented from massive sphalerite-pyrite chalcopyrite-barite, to semi-massive pyrite, to strongly altered felsic conglomerate. The sample to the right is typical of the alteration and texture of most of the OZC.

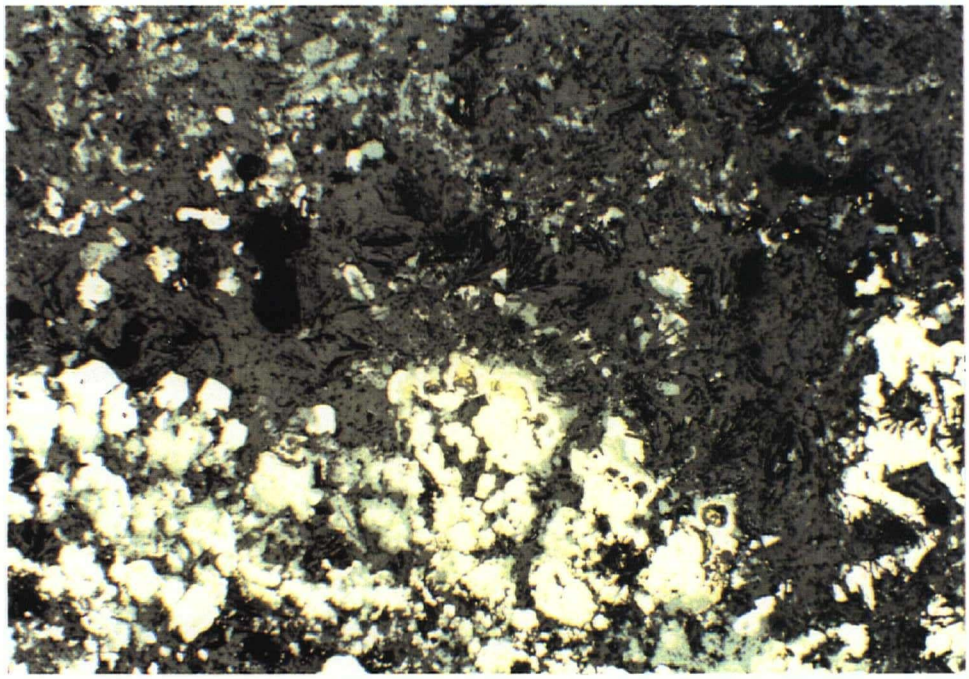

Plate 5.1b: Photomicrograph of massive sulphides and barite in the upper part of the OZC (Sample 85-03-104). An interpreted earlier-formed 'crust' of pyrite-sphalerite-chalcopyrite-barite is shown at the bottom. The remaining space in this sulphide-sulphate framework was filled in by an inferred later bladed barite in the middle of the photo. (Reflected light; Field of view = 5 mm).

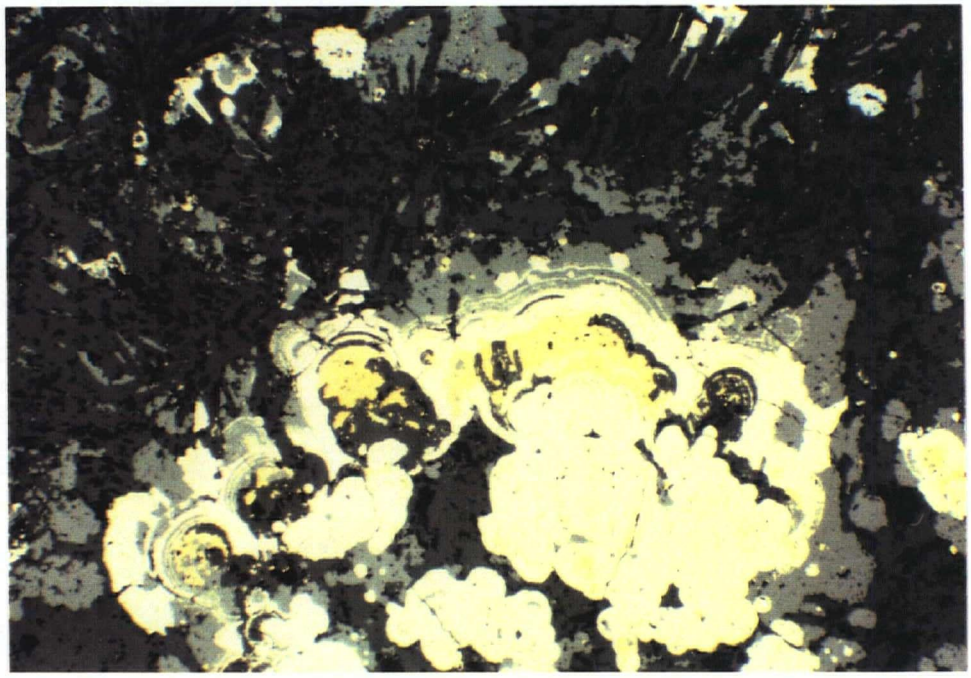

Plate 5.2a: Photomicrograph of massive sulphides and barite from OZC (Sample 85-03-104). Earlier formed colloform sphalerite-pyrite-barite appear to have been partially replaced by chalcopyrite and pyrite and then infilled by a later, bladed barite (upper portion of photo). Triple junction intersections between some pyrite grains suggests recrystallization. (Reflected light; Field of view = 1.25 mm).

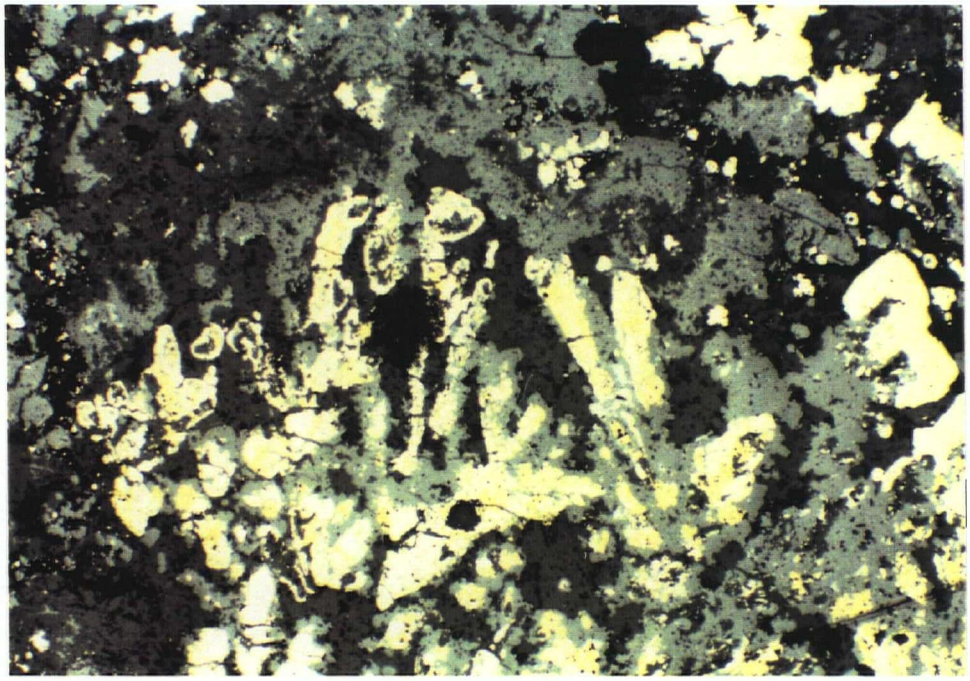

Plate 5.2b: Photomicrograph of Sample 85-03-104 massive sulphides and barite. The sulphides display a bladed texture similar to the barite texture pictured above suggesting that perhaps the sulphides replaced an earlier-formed barite or precipitated on a barite±silica framework. Some lighter grey galena is visible to the right of centre of the photo. (Reflected light; Field of view = 2.5 mm).

			Assay Values					
Drillhole	Depth (m)	Length (m)	Zn %	Cu %	Pb %	Ag g/t	Au g/t	Comments
75-41	141.3	1.0	1.15	0.01	0.85	6.17	0.34	- mineralized OZC
	142.3	1.3	6.30	0.05	0.10	44.57	0.34	- mineralized OZC
	143.6	0.8	2.60	0.30	0.05	14.06	0.34	- mineralized OZC
83-06	121.4	1.3	17.70	5.11	0.04	144.3	6.96	- massive cpy-sph-py
83-07	61.5	4.0	5.25	1.29	0.08	32.83	1.67	- upper Cu-rich zone
83-11	76.8	4.1	5.20	0.70	0.09	47.60	1.47	- upper Zn-rich zone
85-03	104.2	4.2	1.62	0.06	0.12	45.58	0.98	- semi-massive pyrite
	114.0	1.8	0.52	0.012	0.01	2.06	0.17	- typical OZC interval

Table 5. 1. Summary of some typical assay results for some mineralized intervals associated with the ore zone conglomerate in the Pit Area.

Sulphide mineralization associated with the OZC is dominated by disseminated to semi-massive and stringer pyrite. Massive and semi-massive sulphides are generally restricted to the middle and upper parts of the unit and reach thicknesses of up to 2 metres, but are more commonly around 0.5 metres. These intervals are composed of locally 20 to 50 % sphalerite, up to 75 % pyrite, less than 15 % chalcopyrite, up to 15 % barite and generally at least 10 % felsic fragmental material. Galena is also present in small amounts, but is only discernible in polished thin section. The massive sulphides are discontinuous and usually cannot be correlated between adjacent drillholes and some intersections of the OZC contain nothing more than disseminated pyrite. Some assay data from these mineralized zones are summarized in Table 5.1.

More commonly pyrite is the dominant sulphide mineral and occurs as disseminated euhedral grains or as matrix-filling material interstitial to felsic clasts of the OZC. Pyrite also rims the lava clasts in places. Stringers of sulphides (py>cpy>sph) up to 2 cm wide are also observed to crosscut the OZC below the massive sulphides. Some typical assays from such less well mineralized parts of the OZC are the samples from drillhole 85-03 in Table 5.1.

Interpretation of sulphide textures

In polished thin section, sphalerite, pyrite and chalcopyrite occur both as subhedral to euhedral granular aggregates and colloform-textured intergrowths. The colloform sulphides generally exhibit a zonation consisting of chalcopyrite-pyrite±barite cores surrounded by concentric growth zones of pyrite and sphalerite (Plate 5.1b and Plate 5.2a). Pyrite is often rimmed by sphalerite. Some of the finer micron-scale growth bands contain both pyrite and sphalerite, and in places it appear as though the pyrite is replacing the sphalerite. The colloform sulphides occur as isolated globules, but more commonly as coalesced masses. The more granular sulphide aggregates do not have such a zonation and consist of blebs and irregular masses of sphalerite, pyrite and chalcopyrite with small amounts of galena.

Barite occurs in two different forms. Anhedral barite blebs are associated with the granular sulphides. This type of barite is interstitial to the sulphides and can occur at the cores of the colloform spheroids associated with chalcopyrite and pyrite. The barite often appears to be 'corroded' by the surrounding sulphides. Coarser bladed barite is more common and occurs between the masses of granular and colloform sulphides. In places 'bladed' sulphides are also associated with the barite and mimic the texture of the euhadral barite. It is possible that the sulphides have totally replaced the original bladed barite, perhaps first by coating it and then by replacing it from the inside out. Such a scenario may explain the coexistence of barite, a lower temperature mineral with chalcopyrite, a higher temperature mineral.

In general, the massive sulphides and interstitial barite form irregular masses and encrustations. The space around these masses has been infilled by coarser, bladed barite. Chalcopyrite commonly appears to be replacing earlier formed sphalerite and pyrite. However, in places chalcopyrite, pyrite and sphalerite±galena appear to have formed together with little or no apparent

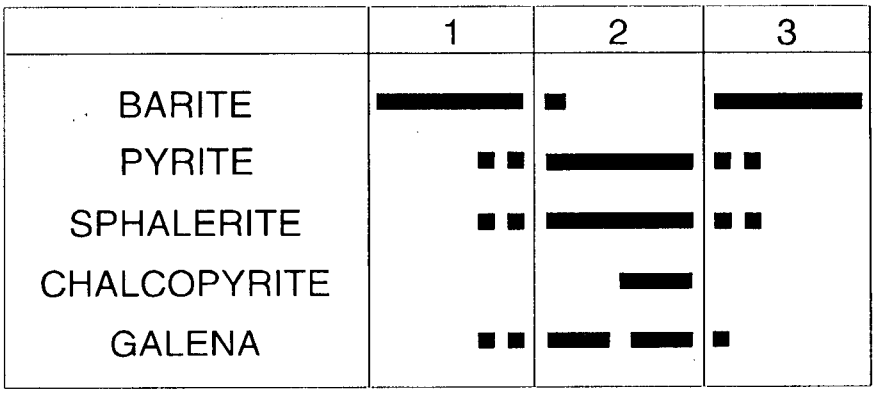

Figure 5. 1. Mineral paragenesis for the massive sulphide zones associated with the ore zone conglomerate at the Pit Area. Solid bars indicate major minerals; broken bars indicate minor minerals.

replacement occurring. These observations led to the formation of the mineral paragenesis summarized in Figure 5.1. Stage 1 involved the precipitation of principally barite with smaller amounts of sphalerite, pyrite and galena. The second stage involved the precipitation of the colloform sphalerite and pyrite. The sulphide spheroids coalesced and likely formed a crust around the earlier barite and sulphides. As the hydrothermal system evolved, and perhaps heated up, chalcopyrite began to precipitate and replace some of the early barite 'framework' increasing the permeability in the sulphide layer and enabling the hydrothermal fluids access to the cores of the colloform masses. It appears that sphalerite, pyrite and galena continued to precipitate while this replacement occurred. It is possible that pulses rather than a steady influx of hotter hydrothermal fluids led to this precipitation of chalcopyrite. Finally, as the system waned and cooled stage 3 minerals were precipitated. These late stage minerals consist of principally bladed barite and lesser sulphides that filled in the remaining pore space in the sulphide layer.

5.3 VENT ZONE

Mineralization in the Vent Zone consists entirely of stockwork veins hosted by a strongly altered massive dacite porphyry intrusion (Plate 5.3). The veins are 1 to 10 mm wide and are

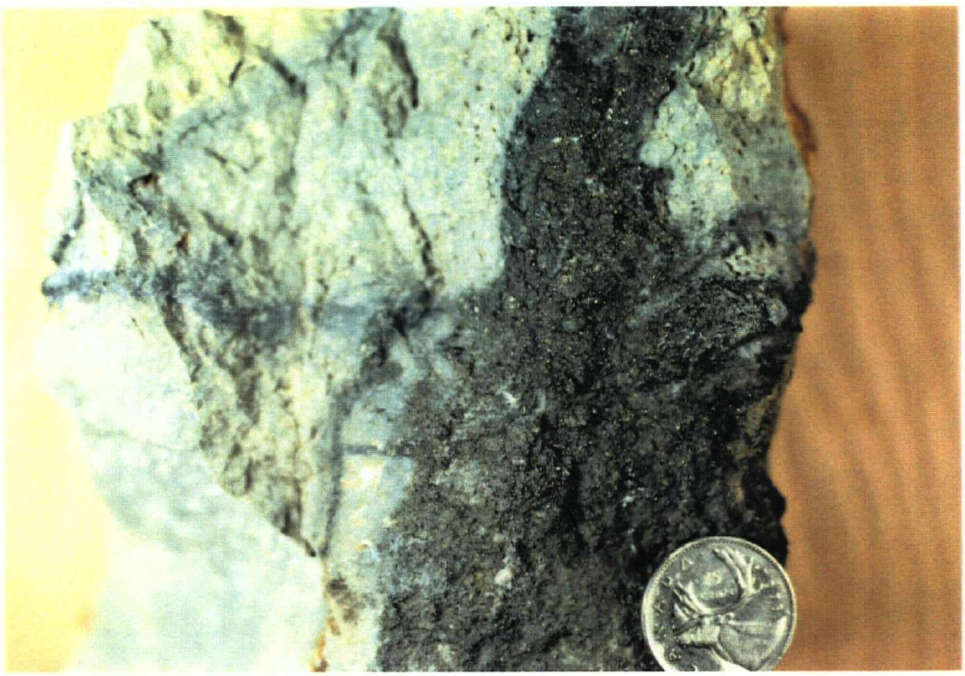

Plate 5.3a: Grab sample from the Vent Zone stockwork outcrop. Sphalerite-pyrite-quartz±chalcopyrite veins are hosted by an intensely altered FP rhyodacite.

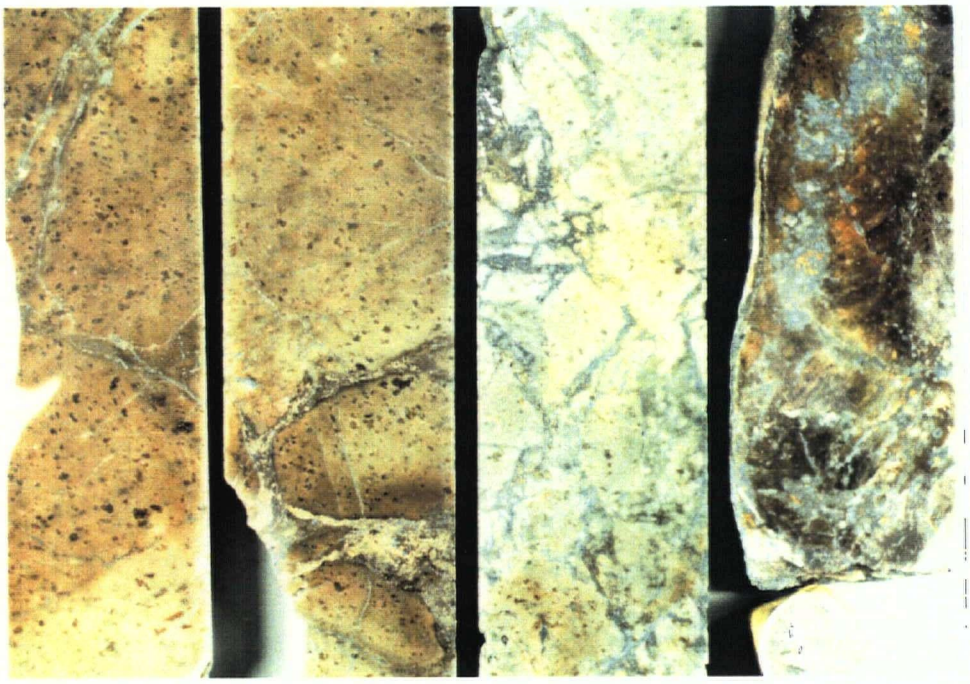

Plate 5.3b: Drillcore samples from DDH 86-28 in the Vent Zone. These samples show the varying intensity of veining throughout the stockwork. The relict feldspar phenocrysts of the host FP rhyodacite are still discernible as darker spots in these rocks.

			Assay Values					
Drillhole	Depth (m)	Length (m)	Zn %	Cu %	Pb %	Ag g/t	Au g/t	Comments
91-16	153.4	1.1	1.54	0.09	0.01	17.0	0.07	- sulphide blebs
	154.5	1.1	5.56	0.38	0.37	162.1	2.37	- massive sulphides
	155.6	1.0	2.10	0.15	0.04	15.4	0.07	- stockwork sulphides
	156.6	1.0	4.74	0.31	0.02	12.7	0.07	- stockwork sulphides
	168.0	0.4	19.3	2.34	0.05	20.5	0.07	- massive sulphides
	177.0	1.5	2.69	0.36	0.07	8.5	0.04	- stockwork sulphides
Average		34.25	2.15	0.30	0.11	13.30	0.14	- from 153 to 184 m

Table 5.2. Summary of selected assay data from the main Fleetwood zone stockwork intersected in drillhole 91-16. Mineralization is dominantly disseminated and stockwork vein sulphides (sphalerite, pyrite, chalcopyrite±galena) with patches of semi-massive to massive sulphides hosted by felsic flows and flow breccias.

composed of principally quartz, pyrite and sphalerite with scattered blebs of chalcopyrite . Locally, the veins comprise 10 to 15 % of the rock, but more commonly make up less than 5 % of the rock. Although the vein mineralization is relatively extensive, the metal grades are generally quite low. Typical assays for the zone are less than 0.50 % and less than 0.20 % Cu with only trace amounts of precious metals. Higher grade zones reach up to 4 % Zn and 0.75 % Cu over 2 metres, but such zones are sparsely distributed. The basaltic breccias that form the immediate footwall to the main stockwork zone contain disseminated and stringer sulphides and in places contain over 3 % Zn and up to 1 % Cu over a 2 metre interval.

5.4 FLEETWOOD ZONE

Mineralization in the Fleetwood Zone in the nortwestern portion of the property is hosted by rhyodacitic flows, flow breccias and synvolcanic intrusions. Sulphides occur as disseminations, veins and as irregular semi-massive patches within the breccias (Plate 5.4). Sphalerite and pyrite are the dominant sulphide minerals with lesser amounts of chalcopyrite and galena variably present. Table 5.2 summarizes some of the assay data from drillhole 91-16 which intersected 34.2 metres of mineralized

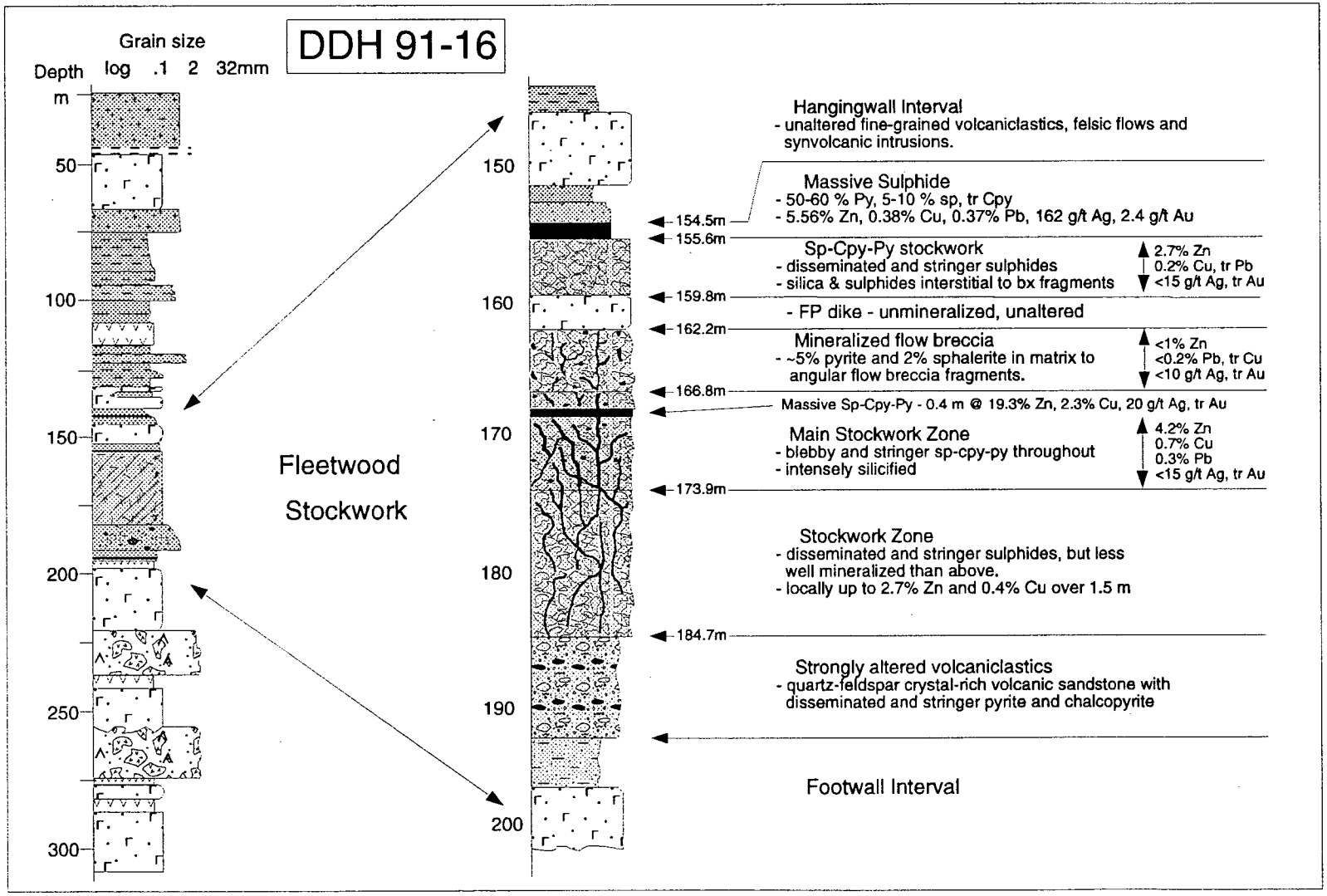

Figure 5.2. Graphic geological log of drillhole 91-16 showing a detailed enlargement of the 34 m wide intersection of the Fleetwood stockwork. The different styles of sulphide mineralization are shown with some accompanying assay data. (see Plate 5.4 for illustrations) (py=pyrite, sp=sphalerite, cpy=chalcopyrite, bx=breccia, tr=trace).

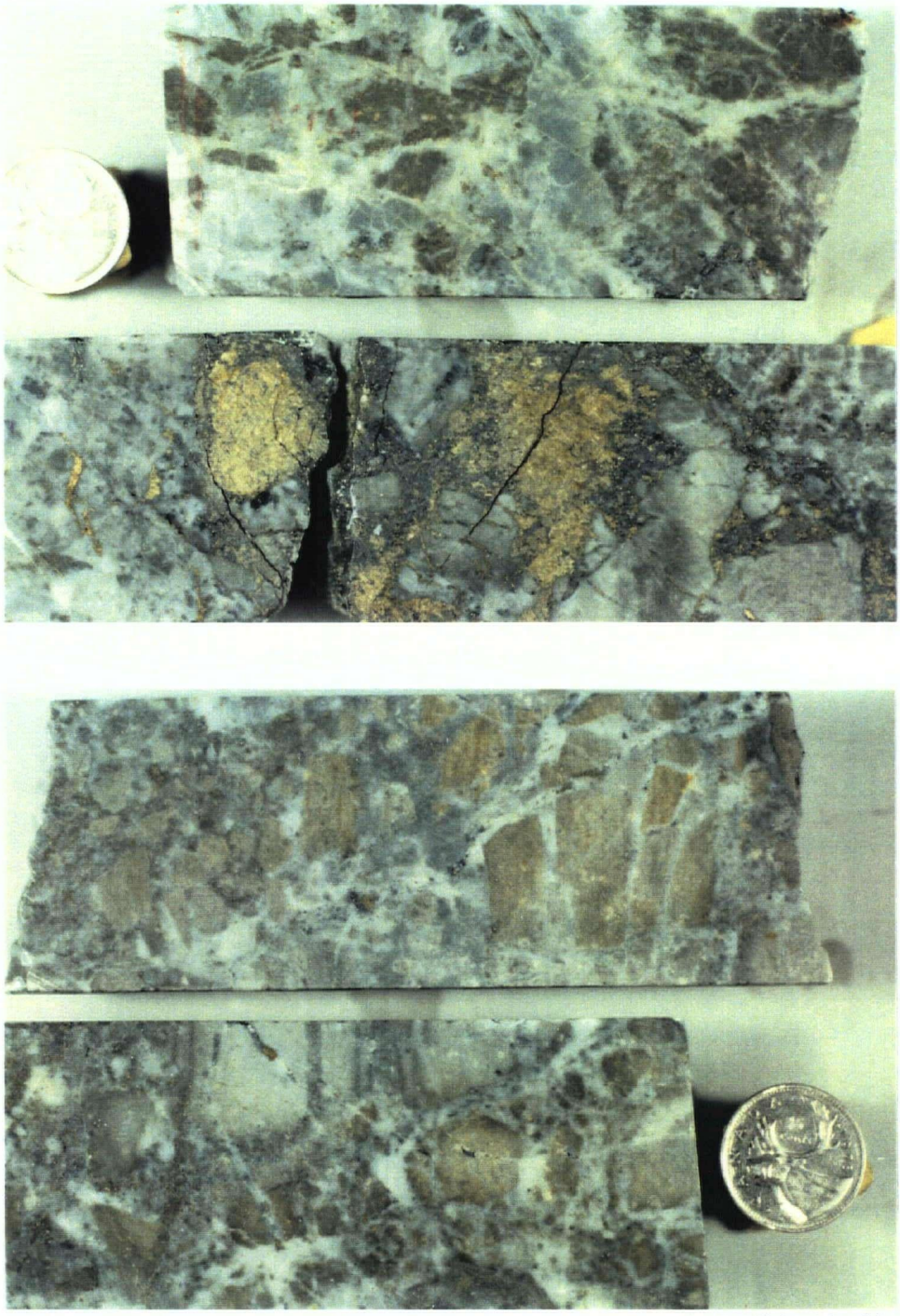

Plate 5.4: Representative drillcore samples from the Fleetwood Zone stockwork (DDH 91-16). Upper photo: samples are from the main stockwork zone in the upper portion of the mineralized zone; they consist of disseminated to semi-massive sphalerite-pyrite-chalcopyrite hosted by a strongly altered felsic breccia. Lower photo: samples are from the lower stockwork zone which contains only disseminated and stringer sulphides. The brecciation is interpreted to be a primary hydroclastic fragmentation as opposed to a phreatic brecciation. (see Figure 5.2 for locations of these zones).

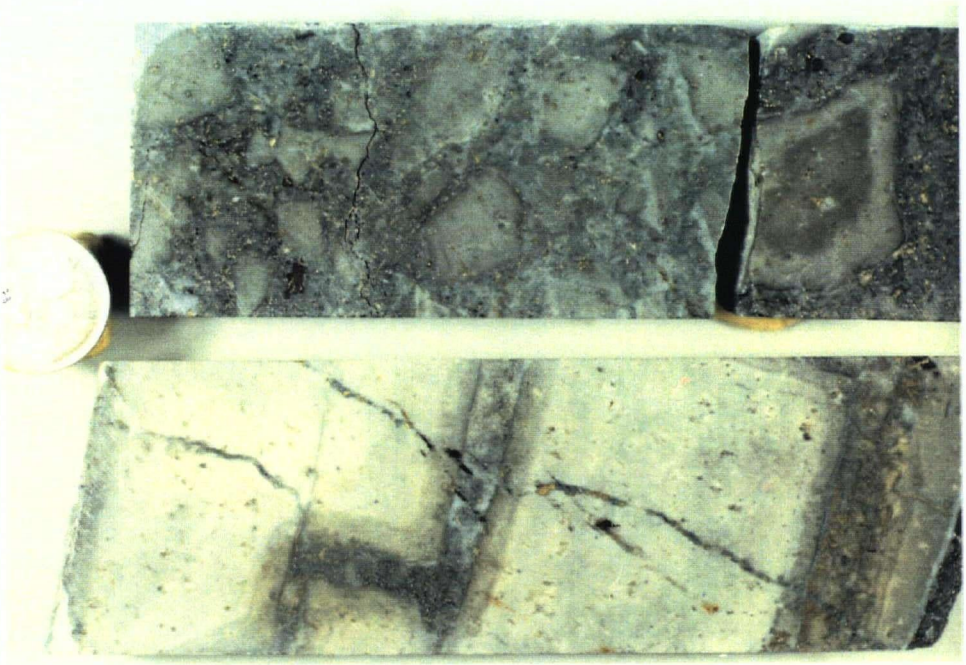

Plate 5.5a: Mineralized flow breccia from a Fleetwood Zone stockwork (DDH 91-18). This stockwork, although less extensive than in DDH 91-16, shows similar features. The host rocks grade downwards into massive felsic flow rocks. Brecciation has preceded alteration and mineralization, and mineralization is strongest where the rock is most brecciated (upper zone).

Plate 5.5b: 33-Zone massive sulphides. This zone consists of massive sphalerite and chalcopyrite with lesser amounts of pyrite and barite. The chalcopyrite appears to be replacing the sphalerite.

flow breccia grading 2.15 % Zn, 0.30 % Cu, 0.11 % Pb and 8.1 g/t Ag. This stockwork interval is illustrated in Figure 5.2. Most of the sulphides occur interstitially to the flow breccia fragments (Plate 5.5a) and are associated with abundant quartz which fills in the remaining space (Plate 5.4). This style of mineralization and the base metal grades are typical for this area of the Seneca property. However, DDH 91-16 represents the thickest such intersection. The stockwork intersected by DDH 91-18 (Figure 2.1) is of comparable thickness, but does not contain as strong mineralization. Other stockwork zones (such as in DDH 87-12) have been intruded by felsic sills. The strong prevalence of synvolcanic intrusions makes it difficult to correlate the stockwork zones between drillholes. As such, it is not clear whether these zones are part of a widespread continuous mineralized interval or if they are each individual stockworks. The similarities in geological associations, stratigraphic position and style of mineralization and alteration in all the stockwoks in the Fleetwood Zone suggests they are all part of a continuous zone.

33 Zone

A zone of massive sulphides, termed the 33 Zone was intersected in drillhole 92-33 located 350 metres to the southwest of drillhole 91-16. This zone is situated at an equivalent stratigraphic position to the mineralization in the rest of the Fleetwood Zone. It consists of 2 metres of massive sphalerite and galena with minor pyrite and galena that is underlain by 1 metre of quartz and chlorite with 1 to 2 % disseminated chalcopyrite and patches of semi-massive pyrite (Plate 5.5b). The massive sulphides are composed of approximately 75 % sphalerite, 5 to 10 % chalcopyrite with the remainder being barite, galena and pyrite. The chalcopyrite appears to be replacing the sphalerite.

The massive sulphides are immediately overlain a cherty sulphide layer that is less than 1 metre thick and is composed of massive to finely laminated chert or siliceous fine ash. Up to 5 % sphalerite and 3 % chalcopyrite are present throughout as 3 mm thick 'beds'. Overlying this layer is a

3 metre thick interval of strongly chloritized rocks. Alteration has obscured the textures, but this unit appears to have had an original fragmental texture. A 10 centimetre wide layer of massive pyrite occurs at the top of this zone. Less than 5 % sphalerite and chalcopyrite are also present.

Two additional holes were drilled to test the 33 Zone. They intersected the same stratigraphic interval 50 metres on either side of DDH 92-33, but failed to intersect any significant mineralization. Therefore, the massive sulphides must either be part of a rather small lens or a part of a larger lens which has been fault-offset or has been disrupted by intrusions. It is also possible, however, that this zone is part of a steeply dipping sulphide vein of zone of replacement. Drillcore observations were not conclusive in determining whether an exhalitive or a vein/replacement origin was more feasible for the 33 Zone mineralization.

5.5 DISCUSSION

The different styles of mineralization at Seneca appear to be strongly controlled by the nature of the host lithologies. The most extensive areas of massive and semi-massive sulphides (Pit Area and Fleetwood Zone) are associated with coarse volcaniclastic rocks and breccias whereas vein-type mineralization (Vent Zone) is hosted by massive synvolcanic intrusions and unbrecciated flows. The interpreted paragenesis of the sulphide minerals agrees with the interpretations of other sulphide deposits: an early formation of a barite ± silica framework onto which grows an encrustation of colloform pyrite and sphalerite all of which are recrystallized and/or replaced by later sulphides (cf. Hannington and Scott, 1988; Paradis et al., 1988).

All sulphide mineralization at the Seneca deposit is essentially Zn-rich. Lydon (1988) states that the upward and outward increase in Zn:Cu ratio in the massive sulphide lens as well as in the stockwork feeder is one of the most definitive features of volcanogenic massive sulphide deposits. Although the Zn:Cu ratios at Seneca are highly variable they are generally in the order of 10:1 around

most mineralized zones in the Pit Area and in the Fleetwood Zone. However, mineralized rocks in the Vent Zone stockwork and the lower portion of the Fleetwood stockwork intersected in DDH 91-16 are more Cu-rich and have Zn:Cu ratios commonly around 6:1 and as low as 2:1. The predominance of Zn over Cu in the mineralized zones is possibly indicative of a cooler hydrothermal system. Halbach et al. (1988) suggest that the formation of galena and sphalerite follows an early stage of deposition of framboidal Fe-sulphides and marks the transition to 'main stage', chalcopyrite-forming mineralization. This transition corresponds to an increase in temperature and a replacement of earlier deposited minerals. Eldridge et al. (1983) document a similar scheme of ore formation for some of the Japanese kuroko deposits with a period of increasing temperature followed by a waning of the hydrothermal system. Framboidal pyrite and sphalerite are abundant in the semi-massive and massive sulphides in the Pit Area. The small amounts of galena and chalcopyrite throughout the property and the high Zn:Cu ratios suggest that the Seneca hydrothermal system never made the transition to 'main stage' mineralization.

CHAPTER 6
DISCUSSION AND CONCLUSIONS

6.1 INTRODUCTION

The Seneca deposit is hosted by Middle Jurassic age volcanic rocks of the Harrison Terrane. This chapter will discuss the significance of the stratigraphic relationships and geochemical trends of these rocks and compare them with modern and ancient volcanic settings. Patterns within the hydrothermally altered zones will also be compared with those associated with known volcanic-hosted deposits in order to establish a geological and geochemical model for the formation of the Seneca deposit.

6.2 STRATIGRAPHY AND GEOCHEMISTRY

6.2.1 STRATIGRAPHIC SUBDIVISIONS

The volcanic stratigraphy at the Seneca property can be subdivided into three major intervals based upon different combinations of lithologies and volcanic facies. These have been termed the Footwall Interval, the Seneca Horizon and the Hangingwall Interval. The Footwall Interval is characterized by basaltic lavas overlain by very coarse, poorly sorted and often heterolithic breccias and mass flows. The Seneca Horizon is a narrower and more discontinuous interval that is composed of felsic flows, breccias and coarse volcaniclastics, and is the host to the mineralization and zones of strongest hydrothermal alteration. The Hangingwall Interval is also composed of felsic flows and volcaniclastics, but the interval is unmineralized and essentially unaltered and the volcaniclastic rocks are dominated by sand and silt/ash-sized detritus; conglomerates and breccias are also less common than in the underlying sequence.

6.2.2 FACIES INTERPRETATIONS

Felsic flows and breccias are much more common in the Fleetwood and Vent Zones than in the Pit Area where synvolcanic sills are the dominant type of porphyritic rock. Dacitic to rhyolitic sills and dikes are common in almost all areas of the property and at all stratigraphic levels. Mafic intrusions are also ubiquitous, but are less common than felsic intrusions. Andesitic sills are intimately associated with the Seneca Horizon in the Pit Area. The greater prevalence of felsic flows suggests that the Fleetwood and Vent Zones are proximal to an inferred volcanic vent. The Pit Area to the southeast of the property is interpreted to be more distal. The volcaniclastic sequences in both areas are quite similar, consisting of coarse, poorly sorted, felsic lava clast-dominated debris flows overlain by massive to well-bedded volcaniclastic sandstones and ashes of felsic composition. However, this sequence is punctuated by felsic flows in the Fleetwood and Vent Zones, but more commonly by sills in the Pit Area. The section of the Trough Zone that was examined in this study (DDH 91-03), located further to the southeast of the Pit Area, contains a similar fining upward volcaniclastic sequence, but contains no flows or intrusive rocks. As well as lacking extrusive lavas and breccias, this section of the Trough Zone also lacks the very coarse debris flows of the Seneca Horizon. Therefore, it appears that the Trough Zone represents a distal equivalent of the Hangingwall Interval.

The uninterrupted volcaniclastic sequence observed in the Trough Zone may represent one continuous eruptive event. The lower massive fine to coarse-grained volcaniclastic sandstone that comprises the lower 70 to 80 metres of the examined drillcore may have been deposited as a single fallback from a pyroclastic eruption which may have originated from a subaerial portion of the volcanic edifice. This eruption also would have likely deposited debris on the more proximal flanks of the edifice. As the volcanic activity waned, this debris would have been washed into the Trough Zone basin as debris flows and turbidites forming the well-bedded, crystal-rich deposits which occur in the upper section of the Trough Zone sequence. This stage of deposition appears to have been punctuated

by periods of relative quiescence during which thin dark brown to black argillaceous beds were deposited. These beds also occur at and above the Seneca Horizon in the Pit Area and may reflect normal, non-volcanic sedimentation in this area.

A similar depositional history seems to have occurred in the Fleetwood Zone and the Pit Area. However, in these areas the lowermost part of the sequence which represents the initial felsic eruption is characterized by very coarse-grained and poorly sorted volcanic breccias deposited by debris flows or subaqueous lahars. This initial high energy event was followed by lower energy deposition by turbidites and gravity settling forming a similar upper volcaniclastic sequence to the Trough Zone. However, in the Fleetwood and Vent Zones, and to a lesser extent in the Pit Area, this deposition was contemporaneous with the formation of the felsic flows and domes. Thus, in these areas coarser beds of flow-derived hyaloclastite are also common.

6.2.3 GEOCHEMISTRY OF THE VOLCANIC SEQUENCE AT SENECA

The volcanic rocks which host the Seneca deposit are bimodal with a basaltic to andesitic composition group of rocks and a dacitic to rhyolitic compositional group. There is a lack of samples at Seneca in the range of 53 to 63 wt. % SiO_2. Dacitic to rhyolitic composition rocks in the form of flows, breccias, synvolcanic intrusions and volcaniclastic rocks are volumetrically dominant in this part of the stratigraphy. The mafic rocks have flat to slightly light rare earth element enriched patterns and are tholeiitic to transitional in nature (La_N/Yb_N = 1.2-1.9, $Zr/Y \leq 3.5$). The felsic rocks are LREE enriched and are transitional to calc-alkaline in nature (La_N/Yb_N = 2.0-3.7, $Zr/Y \geq 3.5$). The mafic lavas referred to as 'fire fountain' rocks are the most primitive rocks in the sequence (low TiO_2, Zr and SiO_2; high MgO and Al_2O_3). The compositions of the more evolved andesitic rocks which were emplaced mostly as synvolcanic sills can be related to these rocks by fractionation of plagioclase,

olivine and clinopyroxene. The geochemical trends amongst the dacitic to rhyolitic rocks can be attributed to the fractionation of feldspar, quartz and pyroxene and/or hornblende.

6.2.4 COMPARISONS OF THE SENECA VOLCANIC ROCKS WITH MODERN SETTINGS

Previous authors (Mahoney et al., 1995; Arthur et al., 1993) have established that the Harrison Lake Formation represents a Middle Jurassic calc-alkaline volcanic arc, but did not speculate extensively as to the possible paleo-tectonic setting of the area or to the geochemical evolution of the volcanic rocks. The stratigraphic and lithogeochemical observations of this study suggest that the Seneca area has experienced a similar but slightly different evolution than the rest of the Weaver Lake Member. An examination of similar geological settings of Miocene and younger ages where the tectonic regimes are fairly well constrained allows for analogies to be made as to the possible evolution of the Seneca stratigraphy.

Lau Basin, southwest Pacific

Clift et al. (1995) present a model for volcanism and sedimentation in narrow sub-basins in the Lau Basin in the southwest Pacific based on drillcores recovered during Leg 135 of the Ocean Drilling Program. The Lau Basin, located 500 km to the north of New Zealand, is the back-arc system to the modern Tofua Arc. Volcanic and tectonic activity in this region is related to the west-northwest subduction of the Pacific plate. The Lau Basin has been formed by extensional tectonism and is bounded to the west by the Lau Ridge and to the east by the Tonga Platform and the Tofua Arc.

Clift et al. (1995) argue that the remote location of the Lau Basin and Tonga Platform precludes significant volcaniclastic input from any source other than the Lau Ridge or Tofua Arc. Most of the sub-basins that were drilled during ODP Leg 135 were constructed on older rifted arc crust and have similar sedimentary characteristics. Most of the sections recovered consisted of overall fining upward sequences of volcaniclastic conglomerates to coarse sands thick-bedded sands and silts topped

by dark brown nanofossil oozes. This sequence overlies basaltic basement rocks. The coarse conglomerates and sandstones contain clasts ranging in composition from rhyolite to basaltic andesite, but are dominated by angular to subrounded dacitic clasts up to 5 cm across. These basal units were deposited by sediment gravity flows, in the case of the massive beds, and as turbidites in the case of the normal-graded coarse sand beds. The finer volcaniclastic sands and silts consist of graded turbidite layers and are dominated by dacitic glass shards. Clift et al. (1995) suggest that the texture and freshness of the glass in these units requires a relatively proximal source such as seamounts within the basin or the flanking volcanic arc.

Volcanic glass fragments from the ODP drillcores were analysed for major and trace elements by electron microprobe and were dated by interpreting the sedimentation rates in the sub-basins. Figure 6.1 summarizes the variations in SiO_2 contents of these glasses with time for Site 840 located in the forearc area of the modern Tofua arc. This material corresponds to volcanic activity during the formation of the Lau arc (~ 5-7 Ma) and the construction of the modern Tofua arc on the Tonga Platform (~ 3 Ma to present). There was an intervening period of basin rifting and extension between the formation of these two arcs with a corresponding relative quiescence in volcanic activity (~ 3-5 Ma). The glass compositions reveal a period of bimodal volcanism during the early history of the Tofua arc with a gap in the data set between approximately 60 and 65 wt. % SiO_2. During this early period of arc development basalts and basaltic andesite lavas were erupted into the rifted sub-basins and were followed by the eruption of felsic lavas. There also appears to be a shorter period of bimodal volcanism during the earliest stages in the formation of the Lau arc during which more primitive basaltic rocks were erupted. The rocks of the more mature arcs are non-bimodal and cover the entire spectrum of compositions from basalts to rhyolites although they lack basaltic compositions of less than 50 wt. % SiO_2.

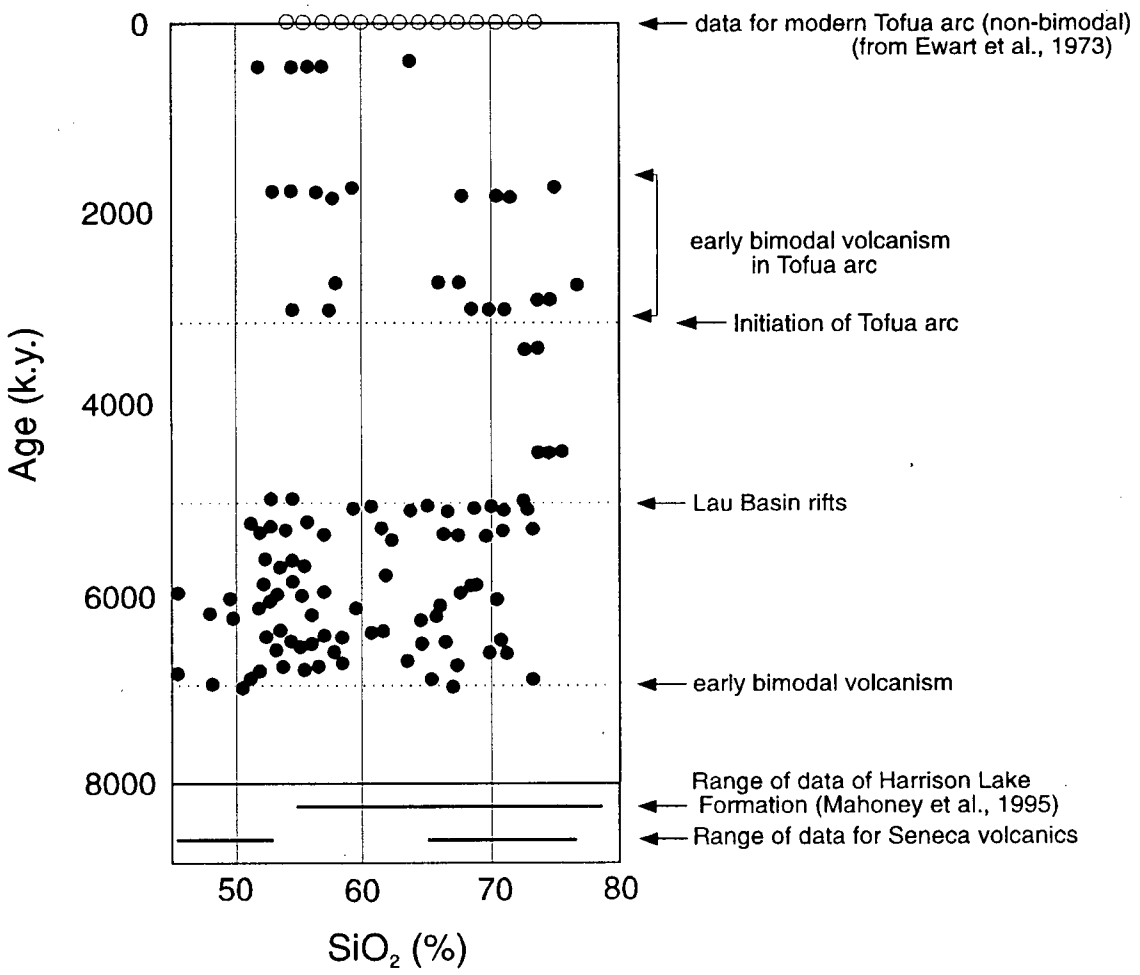

Figure 6.1. Diagram showing the variation in total silica content with age for volcanic glasses from the Tonga Platform east of the Lau Basin, SW Pacific. Data is from Clift et al. (1995) and was collected at ODP Site 840 (ODP Leg 135). This diagram illustrates that the early stages of arc volcanism were bimodal in composition in both the older Lau arc (although less pronounced) and the younger, post-rifting Tofua arc. Data ranges for the Harrison Lake Formation, an interpreted Middle Jurassic arc, and the Seneca volcanic rocks within that same belt are shown for comparison.

Figure 6.1 also shows the compositional range for data from both the Seneca volcanic rocks (this study) and volcanic rocks from the Weaver Lake Member of the Harrison Lake Formation (Mahoney et al., 1995) of which the Seneca stratigraphy is a part. There is a strong similarity between the compositional ranges of both the Seneca rocks and the rocks from the earliest volcanic activity in the Lau arc. The non-bimodal data set from the rest of the Weaver Lake Member corresponds more closely to the younger parts of the Lau arc (post-6 Ma) or perhaps to the compositions of the modern Tofua arc (Ewart et al., 1973) which are also shown on Figure 6.1.

The data and interpretations of Mahoney et al. (1995) for the Middle Jurassic Harrison arc imply that those rocks are representative of a mature arc analogous to the modern Tofua arc. The Seneca volcanic rocks, however, appear to have formed in a slightly different setting within that arc. A strong similarity exists between the stratigraphy of the sub-basins drilled in the Lau Basin and the stratigraphy in the lower parts of the Fleetwood and Vent Zones. In both locations, more primitive basaltic rocks were erupted (the fire fountain rocks in the case of the Fleetwood Zone) and were overlain by very coarse, felsic composition debris flows which were in turn overlain by further felsic volcanic rocks within an overall increasingly well-bedded and finer grained turbiditic volcaniclastic sequence. The stratigraphic similarities and the bimodal compositions of the Seneca rocks suggest that they may have formed in a similar setting to the younger Lau arc and Tofua arc rocks - rifted sub-basins in an intra-arc setting. This comparison is supported by the trace element data for both areas; both are enriched in large ion lithophile elements (LILEs; e.g. K, Rb, Ba)) and have relatively low abundances of incompatible high field strength elements (HFSEs; e.g. Zr, Hf) relative to MORB compositions. Figures 6.2a and 6.2b compare the REE trends of the Seneca basalts and basaltic andesites with those of the mafic glasses of different ages from Site 840 on the Tonga Platform. Both data sets have similar flat, MORB-like REE patterns, overall REE abundances and slight LREE enrichments. The Seneca mafic rocks correspond more closely to the younger latest Miocene rocks

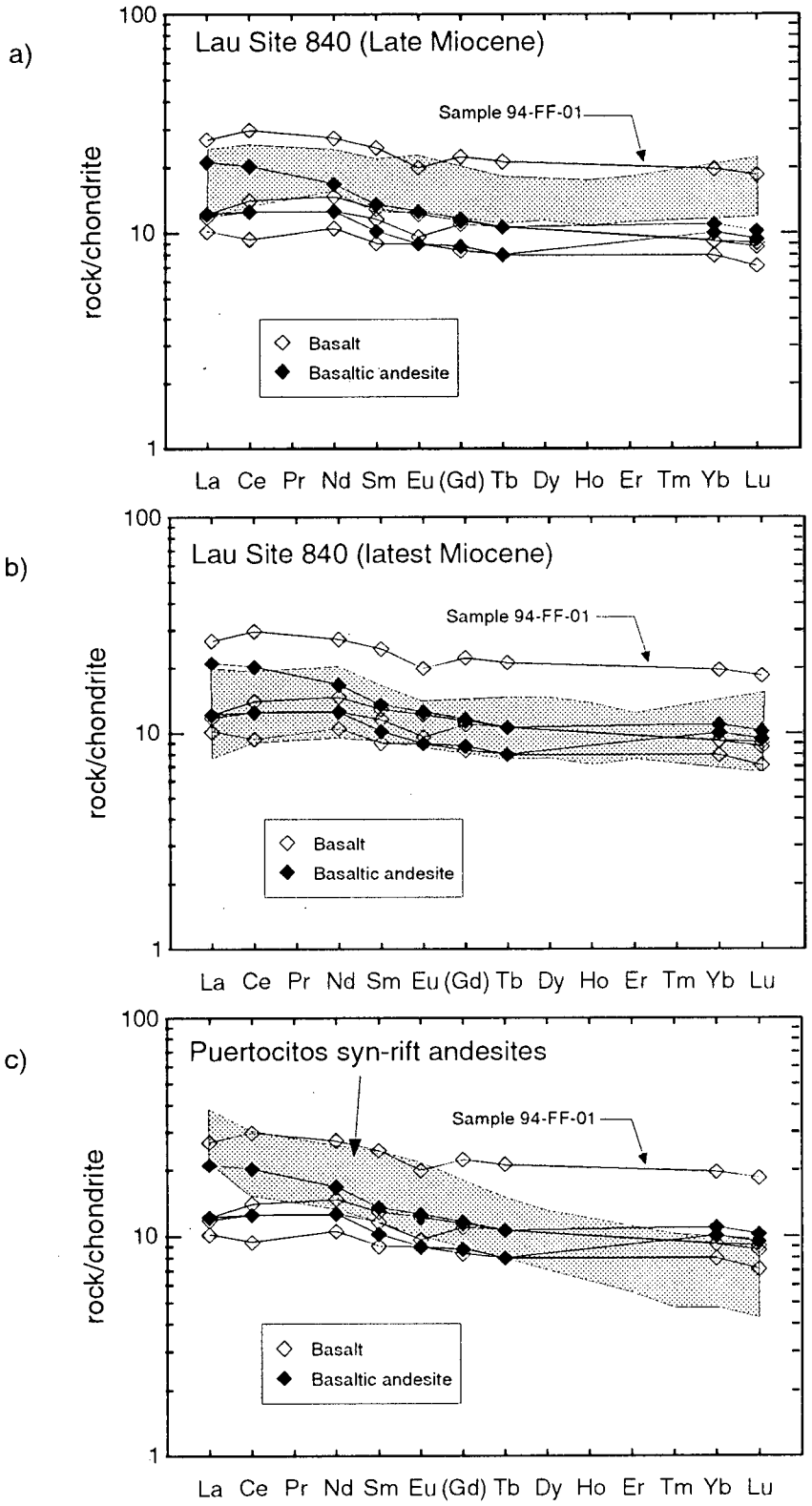

Figure 6.2. Comparison of the REE patterns of the Seneca basalts and basaltic andesites with those from the a) Late Miocene and b) uppermost late Miocene of the Lau Basin (Clift and Dixon, 1994) as well as the c) Puertocitos Volcanic Province, Baja, California (Martin-Barajas et al., 1995). These comparative data are shown as the shaded areas.

from Site 840 (Figure 6.2b). However, considering that the up to 10 % calcite in the amygdules of the Seneca basaltic rocks would uniformly lower REE patterns, the more primitive rocks may actually correspond to the slightly older Miocene rocks in a less developed rifted sub-basin. In either case, it is clear that the Seneca rocks have experienced a similar history to the Tonga Platform rocks and may be related to intra-arc rifting.

Puertecitos Volcanic Province, northeastern Baja California, Mexico

To further test the possibility that the Seneca volcanic rocks formed in a rift setting, another rifted arc sequence will be discussed; in this case the comparison will be made with rocks in a continental margin setting as opposed to the oceanic setting of the Lau Basin rocks discussed above. Martín-Barajas et al. (1995) describe the geology and geochemical trends in the Neogene Puertecitos Volcanic Province of Baja California, Mexico. These rocks are divided into three volcanic sequences - a lower interval of arc-related andesitic lavas and two syn-rift rhyolitic sequences which discordantly overlie the arc-related rocks. The transition from arc volcanism to rift volcanism is related to the opening of the Gulf of California at around 11-6 Ma (Martín-Barajas et al., 1995). Although all of these rocks are calc-alkaline in nature, trends in the trace element contents are different between the three groups. The arc-related rocks are light REE-enriched and have greater amounts of the incompatible elements (e.g. Rb, K, Zr, Hf) than syn-rift rocks. The syn-rift volcanic rocks are also light REE-enriched, but to a lesser degree than the arc-related rocks, and have lower overall abundances in the REEs and the other incompatible elements. The younger of the two syn-rift andesitic sequences is the least evolved lava and, thus, contains lower concentrations of the incompatible elements.

The REE trends of the Puertocitos syn-rift andesites are compared with those form the Seneca area in Figure 6.2c. The Puertocitos rocks show a much more negative sloping REE pattern with

stronger LREE enrichments and relatively more depleted HREEs. These trends suggest that the Puertocitos rocks have experienced a relatively strong influence by continental crust. Martín-Barajas et al. (1995) suggest that the extension during rifting created a high geothermal gradient which caused melting of lithospheric, MORB-type mantle. The resulting andesitic melts were contaminated by crustal melts and eventually produced dacitic to rhyolitic rocks. The strong difference in REE trends between the Puertocitos syn-rift rocks and the Seneca rocks, as well as the lower relative LILE and HFSE abundances of the Seneca rocks, suggest that the composition of the Seneca volcanic rocks are not consistent with formation in a rift setting with a continental crustal influence. However, a possible explanation for the disparate HREE trends in the two areas will be presented below.

Medicine Lake Volcanic Center, northern California

The results of the investigations of a study of the Medicine Lake volcanic centre in northern California, another example of a bimodal calc-alkaline suite of rocks, by Condie and Hayslip (1975) will be discussed here for the purpose of a drawing further comparison with the Seneca area. The Medicine Lake shield volcano, part of the Cascades volcanic system, is composed mainly of basaltic andesite and andesite flows and was formed during the late Pleistocene and has been active most recently 200-300 years ago. These rocks formed from melts produced as a result of the subduction of the Juan de Fuca Ridge beneath continental North America. Condie and Hayslip (1975) studied a bimodal suite of volcanic rocks that is related to the formation of a caldera prior to 10 000 years ago. Some of the REE trends of their data set are compared with the Seneca REE trends in Figure 6.3. The mafic rocks from the Medicine Lake area are more LREE-enriched and contain slightly greater overall abundances of REEs than the Seneca mafic rocks (Figure 6.3a). Condie and Hayslip (1975) also report a basaltic sample that has a flat, slightly LREE-depleted pattern (not shown here) that is very similar to the REE patterns of the Seneca fire fountain rocks suggesting that a less abundant, more primitive batch of lavas also erupted at Medicine Lake, perhaps in a similar fashion to those at Seneca.

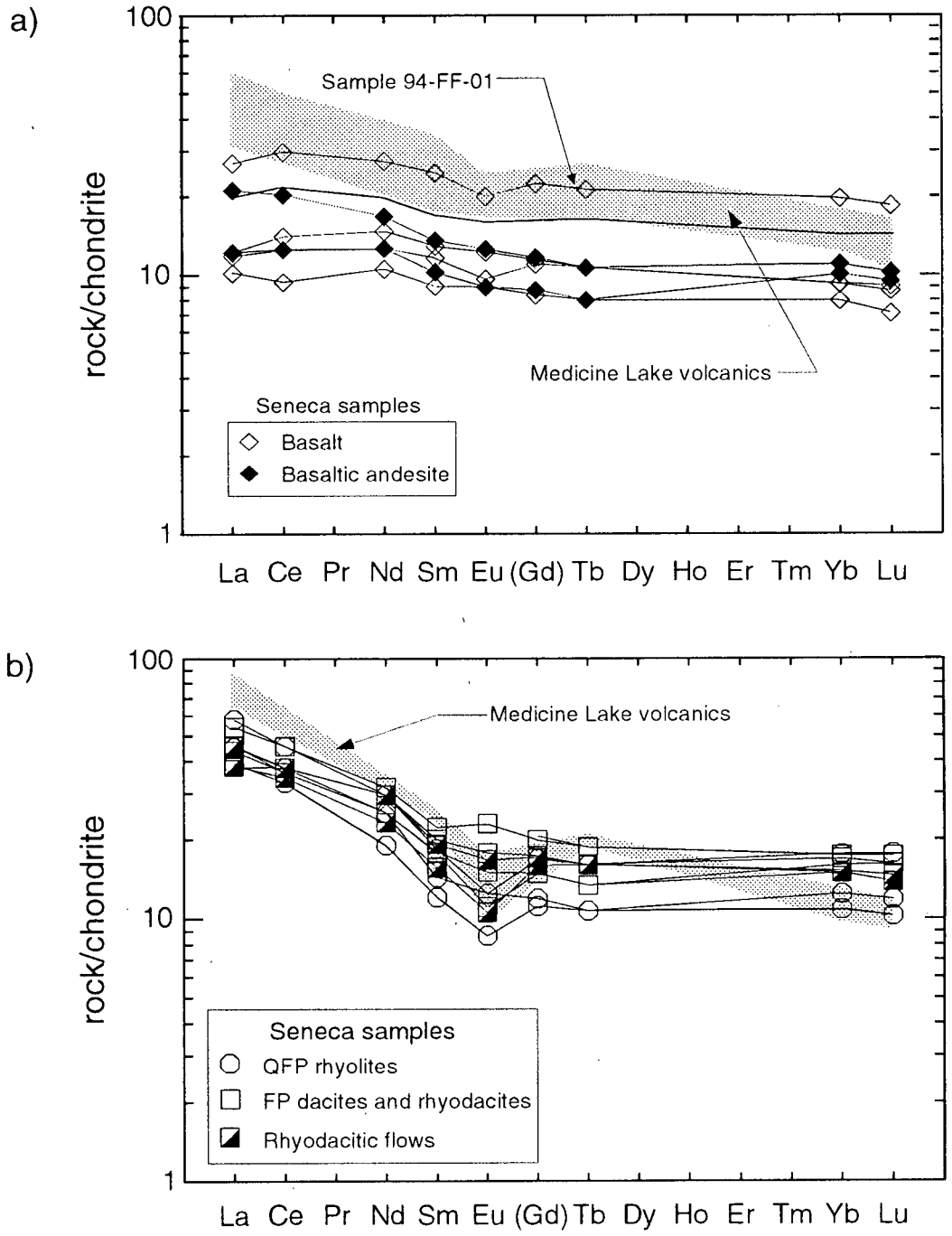

Figure 6.3. Comparison between the REE trends of the Seneca volcanic rocks and the Medicine Lake volcanics, northern California. The upper diagram compares basaltic andesitic rocks and the lower plot compares dacites and rhyolites from both areas. Data for Medicine Lake volcanics is taken from Condie and Hayslip (1975).

The felsic rocks from Medicine Lake, on the other hand, show a better correlation in REE contents with the rhyodacites and rhyolites from Seneca. Both sets of felsic rocks have similar LREE enrichments and negative Eu anomalies (Figure 6.3b). However, the Medicine Lake rocks again have HREE depletions whereas the Seneca rocks have fairly flat HREE patterns.

Condie and Hayslip (1975) propose that the mafic and intermediate composition volcanic rocks at Medicine Lake were derived from the partial melts of the subducting Juan de Fuca Plate which were later modified by magma mixing and fractional crystallization. They suggest that the siliceous lavas were derived by 20 to 50 % partial melting of continental crust of granodiorite composition due to the emplacement of mafic magmas at depth. These interpretations are consistent with the trends in the rare earth element data.

Condie and Hayslip (1975) suggest that the dacite lavas were derived by a mixing of rhyolitic and andesitic magmas. This interpretation of magma mixing may have an application for the more intermediate composition rocks at Seneca. The glomerocrysts that are present in the group A and group B dacites and rhyodacites, and that are absent in the group C and D rhyodacites and rhyolites described in Chapter 3, could be part of a cumulate phase from a mafic magma which was incorporated into these rocks upon mixing with a more silicic magma. The texture of these inclusions is similar to the texture of the basaltic andesitic rocks.

In summary, the REE trends of the Medicine Lake volcanics are quite similar to those in the rocks at Seneca. As such, a similar complex model of magma evolution involving partial melting of an oceanic slab, fractional crystallization involving plagioclase, melting of continental crust and magma mixing could possibly account for the trace element trends in the rocks at Seneca. A problem with this model is the relatively low abundances of incompatible elements in the Seneca volcanics which would only allow a smaller degree of melting of continental crust. Another problem is the flat, non-depleted

HREE patterns at Seneca. Such a pattern, however, can be explained by fractional crystallization of amphibole which, in some cases, can even create a concave-up HREE pattern (Cao et al., 1993; Arculus et al., 1995).

Hokuroku Basin, northern Honshu, Japan

The Miocene volcanic rocks of the Hokuroku Basin in northern Honshu, Japan host perhaps the most famous series of volcanogenic massive sulphide deposits - the Kuroko deposits. These rocks have geochemical similarities to the volcanic rocks at Seneca and, thus, provide an even more relevant comparison. Dudas et al. (1983) describe these rocks as a bimodal suite consisting of tholeiitic to calc-alkaline basalts and calc-alkaline felsic rocks (dacites and rhyolites). The ore-associated stratigraphic interval consists of basal basalts which are overlain predominantly by felsic lavas and tuffs.

A comparison of the REE patterns of the Seneca and the Hokuroku volcanic rocks is illustrated in Figure 6.4. Of the various data sets evaluated here, this Kuroko data set appears to match the Seneca data the best for both mafic and felsic compositions. The flat mafic pattern, the LREE-enriched felsic pattern and the flat to enriched HREE patterns are consistent between both data sets indicating that both sets of rocks could have undergone similar styles of magmatic evolution. Dudas et al. (1983) do not ascribe the Kuroko trace element trends to a particular tectonic setting, but they do state that the trace element signatures of the silicic volcanic rocks lie below those of typical calc-alkaline series and most closely resemble silicic lavas of the Tonga-Kermadec arc which includes the Tofua arc and Lau Basin rocks discussed above.

Lockwood deposit, western Washington State, U.S.

The Lockwood deposit located east of Everett in western Washington State, U.S. is a Cu-rich volcanogenic massive sulphide deposit that is hosted by Jurassic age mafic rocks of predominantly basaltic andesite composition (C.D. Spence, personal communication). A REE plot of one of these

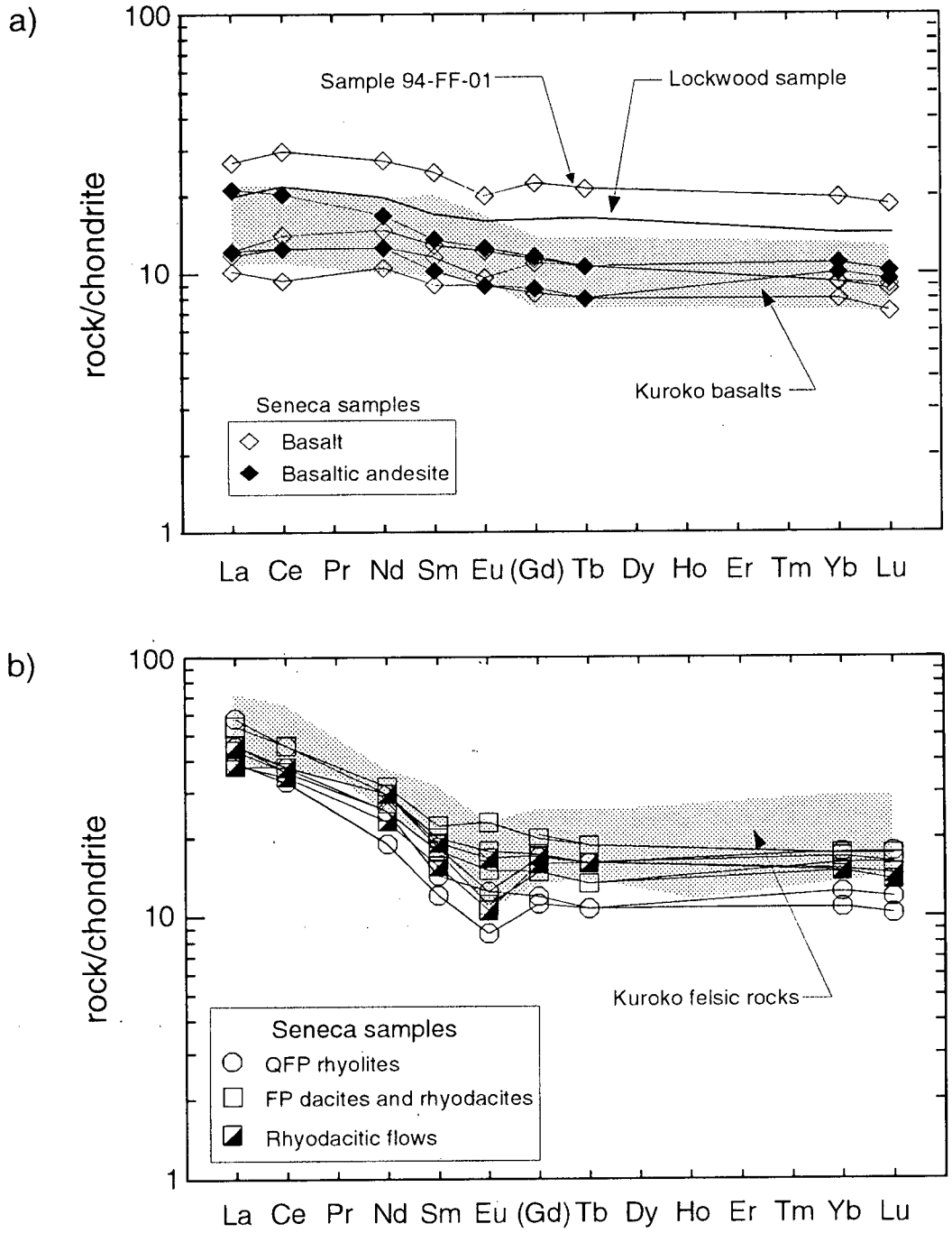

Figure 6.4. Comparison between the REE trends of the Seneca volcanic rocks and Hokuroku Basin volcanic rocks, northern Honshu, Japan. The upper diagram compares mafic rocks and the lower plot compares felsic rocks from both areas. The Lockwood sample indicated on this plot is from the Lockwood deposit in western Washington, U.S. Data for the the Kuroko rocks is from Dudas et al. (1983).

basaltic andesites is included in Figure 6.4a. The strong similarity between this pattern and the patterns for the Seneca mafic rocks, although it is only one sample, as well as their similar ages suggests that the Lockwood volcanic rocks may be correlatable with the Seneca stratigraphy to the north.

6.2.5 SUMMARY

The similarities between the major element chemistry (i.e. bimodal suites) and trace element signatures of the Seneca, the Lau Basin/Tonga Platform and the Hokuroku Basin volcanic rocks suggests they may have formed in similar tectonic environments. The geochemistry of these three areas is neither typical of island arcs nor a true rift setting such as a back-arc basin. It appears that these different packages of rocks formed in an environment that was transitional between a calc-alkaline arc and a rift setting. Such a setting could be an intra-arc rift formed in an extensional environment such as described by Clift et al. (1995). The formation of sub-basins appears to be a prerequisite for the eruption of the more primitive basaltic lavas present in all areas discussed. Perhaps the lack of large amounts of such basalts in these island arc terrains is indicative of the localized nature of the intra-arc sub-basins.

It is not clear at what point in the formation of the Harrison Lake arc that the intra-arc rifting occurred. However, the occurrence of the outcrop at Morris Creek of fire fountain basalts which are essentially the same as those intersected by drilling in the Fleetwood-Vent Zone is coincident with the contact between the Weaver Lake Member and the overlying Echo Island Member. The similar geochemical compositions and the relative topographic positions of both occurrences suggests that the fire fountain localities represent contemporaneous volcanism and that, by inference, rifting must have occurred late in the formation of the arc (i.e. within the youngest rocks of the Weaver Lake Member). Alternatively, based on the distribution of the Echo Island Member flanking the volcanic rocks of the

Weaver Lake Member (*cf* Mahoney et al., 1995), both members may be at least partially lateral facies equivalents. In this case, the timing of the intra-arc rifting becomes more difficult to constrain

The geological observations outlined above (unit distributions, volcanic facies changes, etc.), geochemical trends and geochronological data for the volcanic rocks, and comparisons of the Seneca stratigraphy with other volcanic sequences in well constrained tectonic settings (e.g. the Lau Basin) have been combined in the formation of a geological model for the Seneca area (Figures 6.5 a and b). The early history of the Seneca stratigraphy is marked by the formation of intra-arc sub-basins in both the Fleetwood-Vent Zone and the Pit Area. Basalts were erupted into the sub-basins in the Fleetwood-Vent Zone, but apparently not in the Pit Area. Coarse rhyodacite-dominated breccias were deposited next in all areas, perhaps reflecting the onset or resumption of extrusive felsic volcanism in the area or the redeposition of coarse detritus into the sub-basins from the surrounding areas. The subsequent period of volcanism was dominated by the formation of felsic flows and domes in the Fleetwood-Vent Zone, and by the deposition of volcaniclastic material and lesser flows in the Pit Area. It was during this period that the mineralized zones were formed in both areas. Continued volcanic activity resulted in the deposition and reworking of volcanic debris in the form of volcaniclastic turbidites and ash beds in all areas. The entire sequence is intruded by synvolcanic sills and dikes.

6.3 ALTERATION AND MINERALIZATION

A model for the formation of the stockwork alteration zones of the Fleetwood and Vent Zones has been devised through a combination of petrographic data and mass change calculations. This model is illustrated in Figure 6.6. Alteration occurs almost entirely within massive to brecciated rhyodacite flows and sills. The underlying mafic lavas are variably altered in some places. The Fleetwood and Vent Zone stockwork zones can essentially be divided into two zones with different alteration assemblages: 1) an upper quartz-sericite zone characterized principally by mass gains in SiO_2 and K_2O, mass losses in $Na_2O \pm CaO$ and overall net mass gains, and 2) a lower sericite-

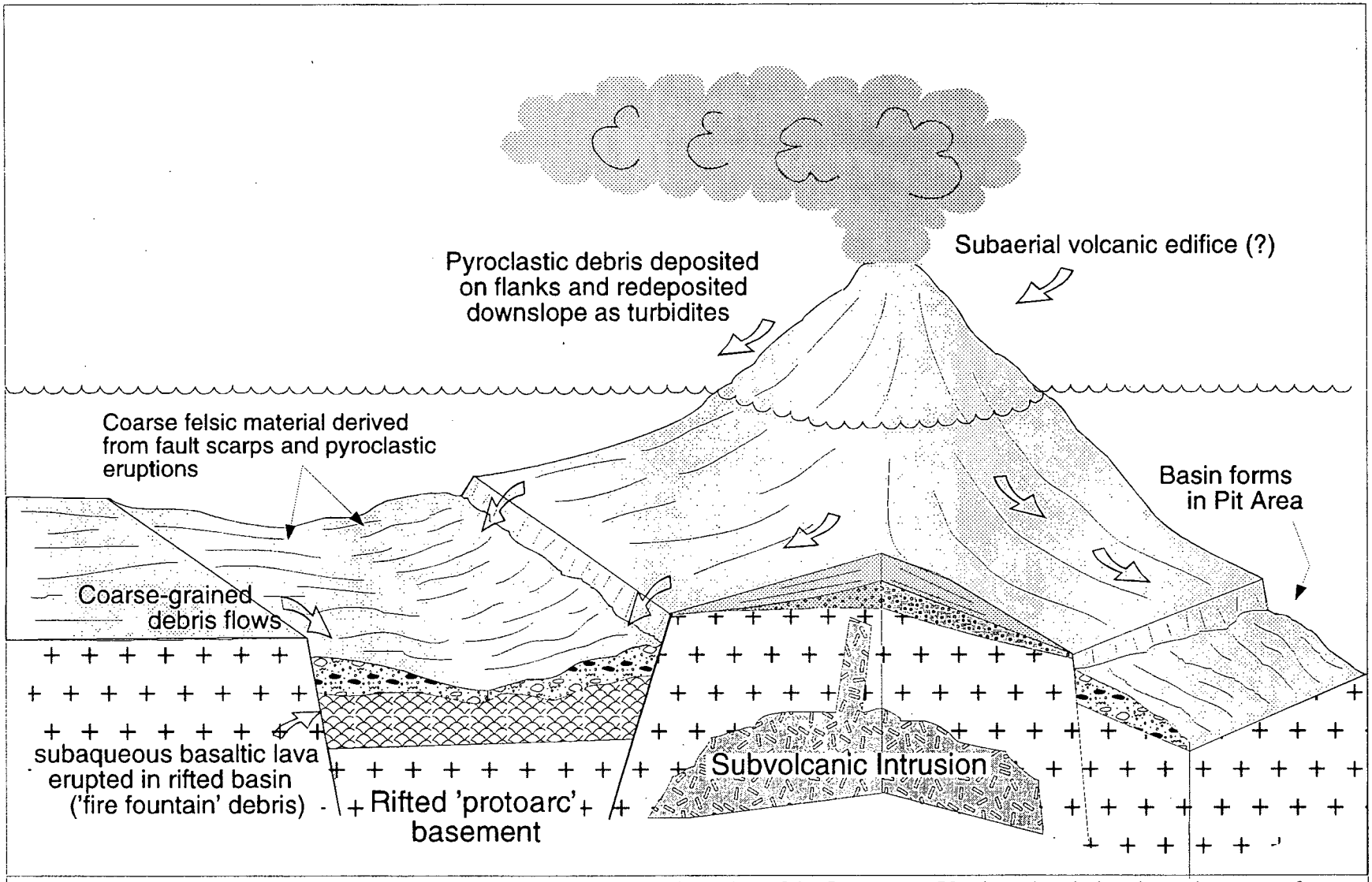

Figure 6.5a. Schematic diagram representing the interpreted volcanic setting of the Seneca area/Harrison Arc during the early stages of formation of the Seneca stratigraphic package. This period is marked by extensional tectonism which forms intraarc subbasins into which are erupted primitive basalts. Felsic pyroclastic activity is occurring simultaneously.

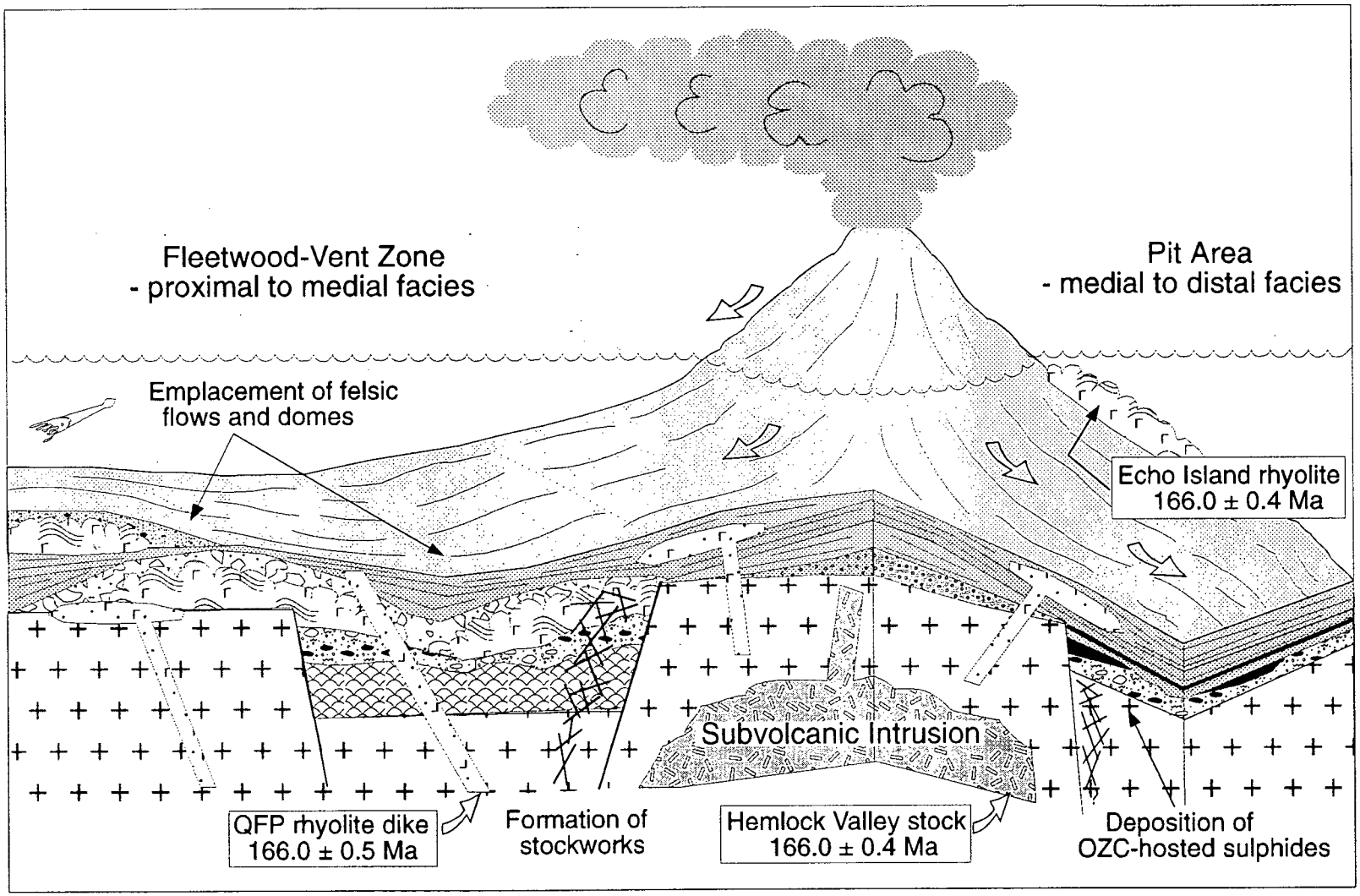

Figure 6.5b. Schematic diagram illustrating the later stages in the formation of the volcanic sequence in the Seneca area. This period is dominated by the formation of felsic flows, breccias and domes and by the deposition of volcaniclastics in the upper part of the sequence. Mineralization is contemporaneous with this deposition. Geochron dates are from Mahoney et al. (1995) and F. Childe (pers. comm.).

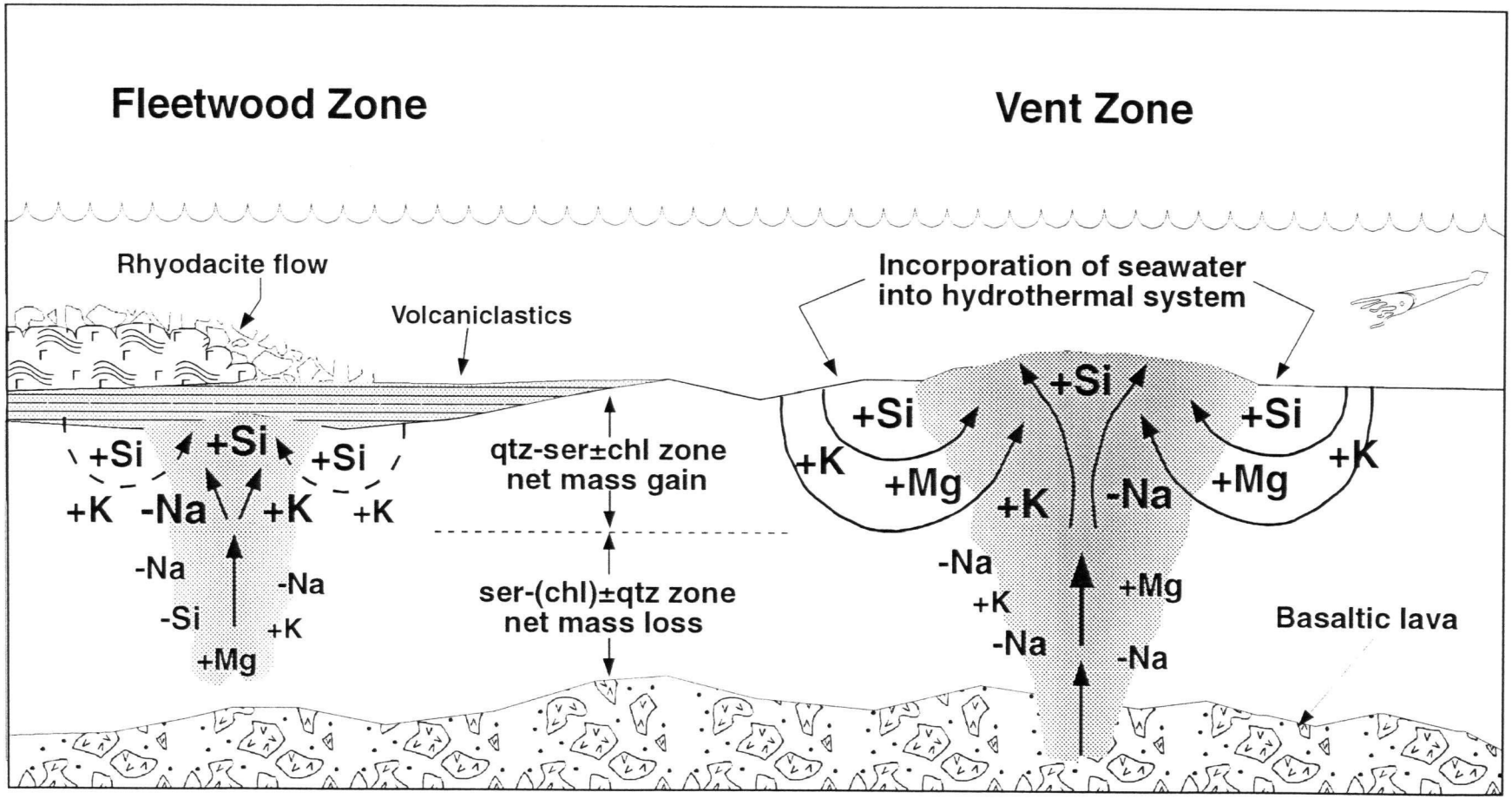

Figure 6.6. Schematic model for the formation of the hydrothermally altered stockwork zones of the Fleetwood and Vent Zones. Mass gains (+) and mass losses (-) of various elements are indicated and correspond to different alteration assemblages discussed in the text. The fine grained volcaniclastics and/or flows may have acted as a cap on the system in the Fleetwood zone inhibiting incorporation of seawater into the hydrothermal system.

chlorite±quartz alteration zone characterized by mass gains in K_2O and MgO, mass losses in SiO_2 and Na_2O and overall net mass losses. Net mass losses have generally occurred throughout the entire Vent Zone stockwork in contrast to the Fleetwood Zone stockworks in which net mass gains are more prevalent. However, since the Vent Zone stockwork is now exposed at surface it is possible that an upper quartz-sericite zone with no MgO gains existed at one time but has since been eroded. Overall, the Vent Zone represents a larger hydrothermal system that may have been more efficient at incorporating Mg in seawater into the alteration minerals (i.e. chlorite).

The vertical and lateral zonation of alteration assemblages is similar to other volcanic hosted massive sulphide deposits such as the Millenbach deposit (Knuckey et al., 1982) and the Delbridge deposit (Barrett et al., 1993) in the Noranda camp, Quebec, and some of the Japanese Kuroko deposits such as the Uwamuki deposit (Urabe et al., 1983). Larson (1984) describes a similar alteration system associated with the Bruce deposit in Arizona. Larson (1984) suggests that the more laterally extensive upper sericite alteration formed due to a change in hydrothermal fluid composition. He proposes that chlorite was the early alteration phase, but that as chlorite was produced the composition of the fluids shifted such that sericite became stable in the upper alteration zone; sericite replaced the earlier chlorite in the upper zone while chlorite continued to form in deeper zones. The magnesium content of the chlorites is greatest in the cores of the alteration pipe and decreases gradually outwards. Larson (1984) also demonstrates that a decrease in the activity of water below 1 greatly expands the stability field of sericite. Larson's model appears to be somewhat applicable to alteration at Seneca. This model would suggest that the predominance of sericite alteration over chlorite alteration at Seneca is indicative of a lower activity of water in the hydrothermal fluids and/or a lesser degree of interaction between the fluids and the rocks.

Strong similarities exist between the Furutobe massive sulphide deposit in Japan and the mineralized zones in the Pit Area at Seneca. The Furutobe deposit is a typical Kuroko-style deposit

comprising three zones of alteration and mineralization (Kuroda, 1983): 1) a lower siliceous ore zone consisting of disseminated and stringer sulphides hosted by altered dacite, 2) an upper siliceous ore zone consisting of stringer and interstice-filling sulphides hosted by dacitic pyroclastic rocks and 3) a stratiform ore zone consisting of pyrite, sphalerite, chalcopyrite, galena, barite and gypsum which overlies the dacitic pyroclastic rocks. The stratiform and siliceous ore zones have gradational boundaries and the abundance of sulphate minerals increases upwards. The sulphides and sulphates formed by the cooling and mixing of hydrothermal fluids with seawater both within the permeable pyroclastic rocks and at the paleoseafloor (Kuroda, 1983). The existence of massive sulphide bodies at the top of an interval of altered and mineralized felsic pyroclastic rocks, the upward gradation from stringer and disseminated sulphides to massive stratiform sulphides as well as the prevalence of barite and colloform-textured sulphides in the upper portions of the mineralized zones in both the Pit Area at the Seneca prospect and at the Furutobe deposit suggests that both they may have formed by similar processes at or near the paleoseafloor. Although a stockwork-style feeder zone was not observed directly below the OZC at Seneca, the Vent Zone stockwork or a similar unexposed zone would be analogous to the lower siliceous ore zone of the Furutobe deposit.

6.4 CONCLUSIONS

The preceding discussion outlined the geological and geochemical characteristics of the volcanic sequence that hosts the Seneca Zn-Cu-Pb prospect and drew some analogies with modern settings to provide some insight to the possible origins of the Seneca stratigraphy and the mineralization and alteration therein. The following sections will summarize the major conclusions of this study.

Volcanic Stratigraphy and Facies Distribution

The 300 to 400 metre-thick package of volcanic rocks that host the Seneca deposit comprises a portion of the Middle Jurassic age Weaver Lake Member of the Harrison Lake Formation in the Harrison Terrane located in southwestern British Columbia.

The Seneca property is divided into four different areas from northwest to southeast: the Fleetwood Zone, the Vent Zone, the Pit Area and the Trough Zone. The predominance of certain lithologies in each area has facilitated the following volcanological interpretations:

- The abundance of mafic and felsic flows and associated breccias in the Fleetwood and Vent Zones is indicative that these areas represent vent to vent-proximal facies.
- The Pit Area stratigraphy contains abundant turbiditic volcaniclastic sandstones and siltstones, abundant synvolcanic sills and dikes with lesser amounts of felsic flows indicating that this area represents medial to distal facies.
- The Trough Zone sequence, although less well constrained, consists entirely of volcaniclastic turbidites and lesser argillaceous beds indicative of a distal subaqueous volcanic facies.

Thus, the volcanic rocks at Seneca correspond to an approximate northwest to southeast transition from vent proximal facies to distal or basinal facies.

The volcanic sequence at Seneca is divided into three stratigraphic intervals described from lowermost to uppermost as follows:

1. Footwall Interval. This interval is characterized by the presence of subaqueously-deposited basaltic lavas, which are spatially restricted to the Fleetwood and Vent Zones, and by coarse, poorly-sorted rhyodacite dominated debris flows.

2. Seneca Horizon. This interval is discontinuous and of variable thickness and is characterized by the presence of stockwork and massive sulphide mineralization and/or strong hydrothermal alteration hosted by massive to brecciated rhyodacitic flows, synvolcanic intrusions and coarse volcaniclastics.

3. Hangingwall Interval. This interval, the thickest package examined, consists of felsic flows and breccias interlayered with massive to well bedded volcaniclastic sandstones and siltstones deposited by turbidites and by gravity settling.

The lateral discontinuity of the Footwall Interval units suggests that they were deposited within sub-basins. The linear trend and stratigraphic continuity of the mineralized and hydrothermally altered zones of the Seneca Horizon suggest that they formed within a structural zone, possibly a growth fault bounding the sub-basins into which the Footwall units were deposited.

Geochemistry

The volcanic rocks at Seneca form a bimodal suite comprising basaltic to basaltic andesitic rocks and volumetrically more abundant dacitic to rhyolitic rocks. The low ratios of Zr/Y and La_N/Yb_N amongst the mafic rocks are indicative of a tholeiitic to transitional affinity. Chemical variations within the mafic rocks can be attributed to the fractional crystallization of plagioclase, olivine and clinopyroxene. The higher Zr/Y and La_N/Yb_N ratios of the felsic rocks are indicative of a transitional to calc-alkaline affinity. Chemical variations in the major element concentrations amongst the felsic rocks can be explained by the fractionation of dominantly plagioclase with lesser amounts of quartz and hornblende and/or pyroxene. Variations in trace element abundances of the felsic rocks can be attributed to the fractionation of varying amounts of plagioclase, magnetite, hornblende and apatite.

Alteration

The strongly altered stockwork zones in the Fleetwood and Vent Zones are divided into two alteration zones as follows:

1. Upper quartz-sericite alteration zone. This zone has experienced net mass gain corresponding to strong mass gains of SiO_2 and K_2O and mass losses of Na_2O and CaO with variable mass changes of MgO.

2. Lower sericite-chlorite ± quartz alteration zone. This zone has experienced net mass loss corresponding to mass losses of Na_2O, CaO and variably SiO_2 and mass gains of K_2O and MgO.

The greater gains of MgO present in the Vent Zone stockwork relative to the Fleetwood Zone suggest that this zone was part of a larger hydrothermal system that was more efficient at incorporating seawater magnesium into the alteration mineral assemblage (i.e. chlorite), or perhaps that overlying volcaniclastic units or flows in the Fleetwood Zone restricted the passage of seawater into the stockwork zones in that area.

Mineralization

The similarities in the inferred stratigraphic locations of the different mineralized zones at Seneca suggests that the stockwork sulphide veins in the Fleetwood and Vent Zones and the disseminated to massive sulphides hosted by the ore zone conglomerate in the Pit Area formed contemporaneously. The nature of the host rock was an important control on the styles of mineralization observed. Veins and stringers of pyrite, sphalerite, chalcopyrite and quartz are the dominant form of mineralization where the host rocks are massive rhyodacite flows and sills, such as in the Vent Zone, whereas disseminated, semi-massive and massive pyrite, sphalerite, chalopyrite and barite are more prevalent where the host lithologies are flow breccias, such as in parts of the Fleetwood Zone, or coarse volcaniclastic sandstone or conglomerate such as in the Pit Area. Although no potential feeder zone was observed as a source for the alteration and mineralization in the Pit Area, a

stockwork zone such as that in the Vent Zone likely served as a conduit for the hydrothermal fluids. Upon intercepting the permeable OZC unit, these fluids would have likely been dispersed laterally forming the extensive zone of conformable alteration and associated mineralization. The hich Zn:Cu ratios in all mineralized zones at Seneca are indicative of an overall cooler hydrothermal system, although the greater amount of chlorite alteration and lower Zn:Cu ratios in the Vent Zone suggest that that zone may have been altered and mineralized by slightly hotter fluids with a greater degree of water-rock interaction. The strong net mass gains, particularly in SiO_2, that characterize the Fleetwood Zone may have 'sealed off' the hydrothermal system and as such the stockworks in this zone are lees extensive than in the Vent Zone where mass losses predominate. This interpretation also provides a possible explanation as to the apparent lack of a massive sulphide lens above the Fleetwood stockworks.

6.5 CLOSING REMARKS

This study succeeded in outlining spatial, volcanological and geochemical characteristics of the lithologic units at the Seneca providing the basis for the interpretation of the tectonic setting of the volcanic rocks and building a geological framework for the interpretation of the formation of the hydrothermally altered and mineralized zones. Comparing the observations of this study with those from other more recently formed geologic settings proved to be useful by providing a more modern context with which to judge the geological and geochemical characteristics of the volcanic rocks at Seneca. This study revealed that a bimodal suite of volcanic rocks may occur within a sequence of related rocks which on the whole does not have a bimodal geochemical signature. This has important implications for mineral exploration within the Harrison Lake Formation, and perhaps within other volcanic belts, since it is these bimodal rocks which host the mineralization at the Seneca property. The identification of sub-basins within older volcanic arc rocks and the recognition of more primitive

composition basalts within these sub-basins also appears to be important since the stockwork-mineralized zones at Seneca are hosted by rocks which directly overlie such basalts. The existence of the sub-basins may indicate that intra-arc rifting or extension has occurred allowing perhaps the tapping of a deeper, more primitive magmatic source and providing the conduits or 'space' required for the upward movement and circulation of the hydrothermal fluids which formed the mineralized zones. The mineralized zones at Seneca are intimately associated with vent-proximal to medial facies volcanic rocks perhaps suggesting that the structures which focussed the hydrothermal activity also focussed the centres of extrusive volcanism. Therefore, the identification of such facies appears to be an additional important criterion for exploration in volcanic settings such as the Seneca property.

REFERENCES

Allen, R.L. (1993). Subaqueous volcanism, facies analysis and ore deposits; *in* Volcanoes and Ore Deposits: MDRU Short Course Notes SC-14, *Mineral Deposit Research Unit*, The University of British Columbia, April, 1993, Vancouver, B.C.

Armbrust, G.A. and Gannicott, R.A. (1980). K/Rb ratios as a source indicator for hydrothermal fluids at the Seneca volcanogenic massive sulfide deposit, British Columbia; *Economic Geology*, volume 75, pages 466-470.

Arthur, A.J. (1986). Stratigraphy along the west side of Harrison Lake, southwestern British Columbia; *in* Current Research, Part B, *Geological Survey of Canada*, Paper 86-1B, pages 715-720.

Arthur, A.J., Smith, P.L., Monger, J.W.H., and Tipper, H.W. (1993). Mesozoic stratigraphy and Jurassic paleontology west of Harrison Lake, southwestern British Columbia; *Geological Association of Canada*, Bulletin 441, 62 pages.

Barrett, T.J., Cattalani, S., and MacLean, W.H. (1993). Volcanic lithogeochemistry and alteration at the Delbridge massive sulfide deposit, Noranda, Quebec; *Journal of Geochemical Exploration*, volume 48, pages 135-173.

Bischoff, J.L. and Seyfried, W.E. (1978). Hydrothermal chemistry of seawater from 25 °C to 350 °C; *American Journal of Science*, volume 278, pages 838-860.

Branney, M.J. (1991). Eruption and depositional facies of the Whorneyside Tuff Formation, English Lake District: An exceptionally large-magnitude phreatoplinian eruption; *Geological Society of America Bulletin*, volume 103, pages 886-897.

Busby-Spera, C.J. (1988). Evolution of a Middle Jurassic back-arc basin, Cedros Island, Baja California: Evidence from a marine volcaniclastic apron; *Geological Society of America Bulletin*, volume 100, pages 218-233.

Carlisle, D. (1963). Pillow breccias and their aquagene tuffs, Quadra Island, British Columbia; *Journal of Geology*, volume 70, pages 48-71.

Cas, R.A.F., Allen, R.L., Bull, S.W., Clifford, B.A., and Wright, J.V. (1990). Subaqueous, rhyolitic dome-top cones: a model based on the Devonian Bunga Beds, southeastern Australia and a modern analogue; *Bulletin of Volcanology*, volume 52, pages 159-174.

Clift, P.D. and Dixon, J.E. (1994). Variations in arc volcanism and sedimentation related to rifting of the Lau Basin (southwest Pacific); in Hawkins, J.W., Parson, A.L., and Allan, J.F. (eds.) *Proceedings of the Ocean Drilling Program, Scientific Results*, volume 135, pages 23-49.

Clift, P.D. and ODP Leg 135 Scientific Party (1995). Volcanism and sedimentation in a rifting island-arc terrain: an example from Tonga, SW Pacific; in *Volcanism Associated with extension at Consuming Plate Margins*, Smellie, J.L., ed., Geological Society Special Publication No. 81, pages 29-51.

Condie, K.C. and Hayslip, D.L. (1975). Young bimodal volcanism at Medicine Lake volcanic center, northern California; *Geochimica et Cosmochimica Acta*, volume 39, pages 1165-1178.

de Rosen-Spence, A.F., Provost, G., Dimroth, E., Gochnauer, K., and Owen, V. (1980). Archean subaqueous felsic flows, Rouyn-Noranda, Quebec, and their Quaternary equivalents; *Precambrian Research*, volume 12, pages 43-77.

Dimroth, E., Cousineau, P., Leduc, M., and Sanschagrin, Y. (1978). Structure and organization of Archean basalt flows, Rouyn-Noranda area, Quebec, Canada; *Canadian Journal of Earth Sciences*, volume 15, pages 902-918.

Dudás, F.Ö., Campbell, I.H., and Gorton, M.P. (1983). Geochemistry of igneous rocks in the Hokuroku district, northern Japan; *in* The Kuroko and Related Volcanogenic Massive Sulfide Deposits: *Economic Geology*, Monograph 5, pages 115-133.

Eldridge, C.S., Barton Jr.,P.B., and Ohmoto, H. (1983). Mineral textures and their bearing on formation of the Kuroko orebodies; *in* The Kuroko and Related Volcanogenic Massive Sulfide Deposits: *Economic Geology*, Monograph 5, pages 241-281.

Evensen, N.M., Hamilton, P.J., and O'Nions, R.K. (1978). Rare earth element abundances in chondritic meteorites; *Geochimica et Cosmochimica Acta*, volume 42, pages 1199-1212.

Ewart, A., Bryan, W.B., and Gill, J.B. (1973). Minerlaogy and geochemistry of the younger volcanic islands of Tonga, SW Pacific; *Journal of Petrology*, volume 14, pages 429-465.

Fisher, R.V. (1966). Rocks composed of volcanic fragments; *Earth-Science Reviews*, volume 1, pages 287-298.

Fisher, R.V. and Schminke, H.-U. (1984). *Pyroclastic Rocks*. Springer-Verlag, Berlin, 472 pages.

Fraser, T.M. (1994). Geology, Alteration and Origin of Hydrothermal Breccias at the Mount Polley Alkalic Porphyry Copper-Gold Deposit, south-central British Columbia; unpublished M.Sc. thesis, *University of British Columbia*, 261 pages.

Friedman, R.M. and Armstrong, R.L. (1994). Jurassic and Cretaceous geochronology of the southern Coast Belt, southern British Columbia, 49-50 degrees N; *Geological Society of America Memoir*.

Gannicott, R.A., Armbrust, G.A., and Agterberg, F.P. (1979). Use of trend surface analysis to delimit hydrothermal alteration patterns; *Canadian Mining and Metallurgy Bulletin*, volume 72, number 806, pages 82-89.

Halbach, P., Pracejus, B., and Marten, A. (1988). Geology and mineralogy of massive sulfide ores from the central Okinawa trough, Japan; *Economic Geology*, volume 88, pages 2210-2225.

Hall, A. (1987). *Igneous Petrology*, Longman Group Ltd., 572 pages.

Hanson, R.E. (1991). Quenching and hydroclastic disruption of andesitic to rhyolitic intrusions in a submarine island-arc sequence, northern Sierra Nevada, California; *Geological Society of America Bulletin*, volume 103, pages 804-816.

Hannington, M.D. and Scott, S.D. (1988). Mineralogy and geochemistry of a hydrothermal silica-sulfide-sulfate spire in the caldera of Axial Seamount, Juan de Fuca Ridge; *Canadian Mineralogist*, volume 26, pages 603-625.

Hawkins, J.W. (1994). Petrologic synthesis: Lau Basin transect (Leg 135); in Hawkins, J.W., Parson, A.L., and Allan, J.F. (eds.) *Proceedings of the Ocean Drilling Program, Scientific Results*, volume 135, pages 879-905.

Hoy, T. (1991). Volcanogenic massive sulphide (VMS) deposits in British Columbia; *in* Ore deposits, tectonics and metallogeny in the Canadian Cordillera, *B.C. Ministry of Energy, Mines and Petroleum Resources*, Paper 1991-4, pages 89-123.

Irvine, T.N. and Baragar, W.R.A. (1971). A guide to the classification of the common volcanic rocks; *Canadian Journal of Earth Sciences*, volume 8, pages 523-548.

Izawa, E., Yoshida, T., and Saito, R. (1978). Geochemical characteristics of hydrothermal alteration around the Fukazawa Kuroko deposit, Akita, Japan; *Mining Geology*, volume 28, pages 325-335.

Jakes, P. and Gill, J. (1970). Rare earth elements and the island arc tholeiitic series; *Earth and Planetary Science Letters*, volume 9, pages 17-28.

Janecky, D.R and Seyfried, Jr., W.E. (1985). Formation of massive sulfide deposits on oceanic ridge crest: Incremental reaction models for mixing between hydrothermal solutions and seawater; *Geochimica et Cosmochimica Acta*; volume 48, pages 2723-2738.

Journeay, J.M. and Csontos, L. (1989). Preliminary report on the structural setting along the southeast flank of the Coast Belt, British Columbia; *in* Current Research, Part E, *Geological Survey of Canada*, Paper 89-1E, pages 177-187.

Kano, K., Takeuchi, K., Yamamoto, T., and Hoshizumi, H. (1991). Subaqueous rhyolite block lavas in the Miocene Ushikiri Formation, Shimane Peninsula, southwest Japan; *Journal of Volcanology and Geothermal Research*, volume 46, pages 241-253.

Knuckey, M.J., Comba, C.D.A., and Riverin, G. (1982). Structure, metal zoning and alteration at the Millenbach deposit, Noranda, Quebec; *in* Precambrian Sulphide Deposits, *Geological Society of Canada*, Special Paper 25, pages 255-295.

Kokelaar, B.P. (1982). Fluidization of wet sediments during the emplacement and cooling of various igneous bodies; *Journal of the Geological Society of London*, volume 139, pages 21-33.

Kuroda, H. (1983). Geologic characteristics and formation environments of the Furutobe and Matsuki Kuroko deposits, Akita Prefecture, northeast Japan; *in* The Kuroko and Related Volcanogenic Massive Sulfide Deposits: *Economic Geology*, Monograph 5, pages 149-166.

Ledbetter, M.T. and Sparks, R.S.J. (1979). Duration of large-magnitude explosive eruptions deduced from graded bedding in deep-sea ash layers; *Geology*, volume 7, pages 240-244.

Lowe, D.R. (1982). Sediment gravity flows: II. Depositional models with special reference to the deposits of high density turbidity currents; *Journal of Sedimentary Petrology*, volume 52, pages 279-297.

Lydon, J.W. (1988). Volcanogenic massive sulphide deposits, Part 2: Genetic models; *in* Ore deposit models, *Geoscience Canada Reprint Series 3*, Roberts, R.G. and Sheahan, P. (Eds.), 318 pages.

MacLean, W.H. (1990). Mass change calculations in altered rock series; *Mineralium Deposita*, volume 25, pages 44-49.

MacLean, W.H. and Kranidiotis, P. (1987). Immobile elements as monitors of mass transfer in hydrothermal alteration: Phelps Dodge massive sulfide deposit, Matagami, Quebec; *Economic Geology*, volume 82, pages 951-962.

Mahoney, J.B. (1994): Nd Isotopic Signatures and Stratigraphic Correlations: Examples from Western Pacific Marginal Basins and Middle Jurassic Rocks of the Southern Canadian Cordillera; unpublished Ph.D. thesis, *University of British Columbia*, 289 pages.

Mahoney, J.B., Friedman, R.M., and McKinley, S.D. (1995). Evolution of a Middle Jurassic volcanic arc: stratigraphic, isotopic and geochemical characteristics of the Harrison Lake Formation, southwestern British Columbia; *Canadian Journal of Earth Science*, volume 32, pages 1759-1776.

Martín-Barajas, A., Stock, J.M., Layer, P., Hausback, B., Renne, P., and López-Martinez, M. (1995). Arc-rift transition volcanism in the Puertecitos Volcanic Province, northeastern Baja California, Mexico; *Geological Society of America Bulletin*, volume 107, number 4, pages 407-424.

McIntire, W.L. (1963). Trace element partition coefficients - a review of theory and applications to geology; Geochimica et Cosmochimica Acta, volume 27, pages 1209-1264.

McKinley, S.D., Thompson, J.F.H., and Barrett, T.J. (1995). Volcanic stratigraphy and lithogeochemistry of the Seneca prospect, southwestern British Columbia (92H/5W); *in* Geological Fieldwork 1994, Grant, B., and Newell, J.M., editors, *B.C. Ministry of Energy, Mines and Petroleum Resources*, Paper 1995-1, pages 503-512.

McPhie, J. and Allen, R.L. (1992). Facies architecture of mineralized sequences: Cambrian Mount Read Volcanics, Western Tasmania; *Economic Geology*, volume 87, pages 587-596.

McPhie, J., Doyle, M., and Allen, R. (1993). Volcanic Textures: a guide to the interpretation of textures in volcanic rocks; *Centre for Ore Deposit and Exploration Studies*, University of Tasmania, 198 pages.

Monger, J.W.H. (1970). Hope Map-area, west half, British Columbia; *Geological Survey of Canada*, Paper 69-47.

Mullen, E.D. (1983). $MnO/TiO_2/P_2O_5$: a minor element discriminant for basaltic rocks of oceanic environments and its implications for petrogenesis; *Earth and Planetary Science Letters*, volume 62, pages 53-62.

Paradis, S., Jonasson, I.R., Le Cheminant, G.M., and Watkinson, D.H. (1988). Two zinc-rich chimneys from the Plume Site, southern Juan de Fuca Ridge; *Canadian Mineralogist*, volume 26, pages 637-654.

Pearce, J.A. (1982). Trace element characteristics of lavas from destructive plate boundaries; in *Andesites*, Thorpe, R.S. (ed.), John Wiley and Sons.

Pearce, J.A. and Cann, J.R. (1973). Tectonic setting of basic volcanic rocks determined using trace element analyses; *Earth and Planetary Science Letters*, volume 19, pages 290-300.

Pearce, J.A. and Norry, M.J. (1979). Petrogenetic implications of Ti, Zr, Y and Nb variations in volcanic rocks; *Contributions to Mineralogy and Petrology*, volume 69, pages 33-47.

Pearson, D.E. (1973). Harrison, Lucky Jim; *in* Geology, Exploration and Mining in British Columbia 1973, *B.C. Ministry of Energy, Mines and Petroleum Resources*, pages 125-128.

Pride, K.R. (1973). A Mineralographic Study of Selected Sulfide Samples from the Seneca Property, near Harrison Mills, British Columbia, unpublished B.Sc. thesis, *University of British Columbia*, 44 pages.

Rollinson, H.R. (1993). Using geochemical data: evaluation, presentation, interpretation. Longman Group Ltd., 352 pages.

Russell, J.K. and Nicholls, J. (1988). Analysis of petrologic hypotheses with Pearce element ratios; *Contributions to Mineralogy and Petrology*, volume 99, pages 25-35.

Russell, J.K., Nicholls, J., Stanley, C.R., and Pearce, T.H. (1990). Pearce element ratios: a paradigm for the testing of petrologic hypotheses; EOS, volume 71, number 5, pages 234-247.

Stanley, C.R. and Madeisky, H.E. (1994). Lithogeochemical exploration for hydrothermal ore deposits using Pearce element ratio analysis; *in* Alteration and Alteration Processes associated with Ore-forming Systems, Lentz, D.R., ed., *Geological Association of Canada*, Short Course Notes, volume 11, pages 193-211.

Stanley, C.R. and Russell, J.K. (1989). Petrologic hypothesis testing with Pearce element ratio diagrams: derivation of diagram axes; *Contributions to Mineralogy and Petrology*, volume 103, pages 78-89.

Thompson, R.I. (1972). Report on Harrison, Lucky Jim Property; *in* Geology, Exploration and Mining in British Columbia 1972, *B.C. Ministry of Energy, Mines and Petroleum Resources*, pages 102-114.

Urabe, T., Scott, S.D., and Hattori, K. (1983). A comparison of footwall-rock alteration and geothermal systems beneath some Japanese and Canadian volcanogenic massive sulfide deposits, *in* The Kuroko and Related Volcanogenic Massive Sulfide Deposits: *Economic Geology*, Monograph 5, pages 345-364.

Walker, R.G. (1984). Turbidites and associated coarse clastic deposits; *in* Walker, R.G. (ed.), Facies Models, 2nd Edition, *Geological Association of Canada Reprint Series1*, pages 171-188.

Watson, E.B. (1979). Zircon saturation in felsic liquids: experimental results and applications to trace element geochemistry; *Contributions to Mineralogy and Petrology*, volume 70, pages 407-419.

Winchester, J.A. and Floyd, P.A. (1977). Geochemical discrimination of different magma series and their differentiation products using immobile elements; *Chemical Geology*, volume 20, pages 325-343.

Wood, D.A., Joron, J.-L., and Treuil, M. (1979). A reappraisal of the use of trace elements to classify and discriminate between magma series erupted in different tectonic settings; Earth and Planetary Science Letters, volume 45, pages 326-336.

APPENDIX A

LITHOGEOCHEMICAL DATA

All of the samples analysed as part of this study were taken from diamond drillcores, except for Sample 94-FF-01 which was sampled from an outcrop at Morris Creek, 5 km to the southeast of the property. As such, most samples are numbered using a combination of their drillhole number and depth. The locations of the sampled drillholes are shown on Figure A.1. Care was taken to avoid sampling vein material in the rocks. All samples were analysed using X-ray flourescence at Geochemical Laboratories, McGill University, Montreal, Quebec. All major elements and Cu, Zn, Ni, Cr, V, Sc were analysed using glass beads. The trace elements Zr, Y, Nb, Rb, Sr, Ga and Pb were analysed using pressed pellets. All rare earth elements were analysed by induced neutron activation analysis at Activation Laboratories, Ancaster , Ontario. All geochemical data is included in the following tables and has been subdivided on the basis of composition. Detection limits are given at the end of Appendix A.3. The following abbreviations have been used in the data tables:

FP = feldspar porphyry (dacite to rhyodacite)

QFP = quartz-feldspar porphyry (rhyodacite to rhyolite)

FL = flow

FEL DYK = felsic dike (aphanitic)

VCLT = volcaniclastic (siltstone/ash)

ALT = altered

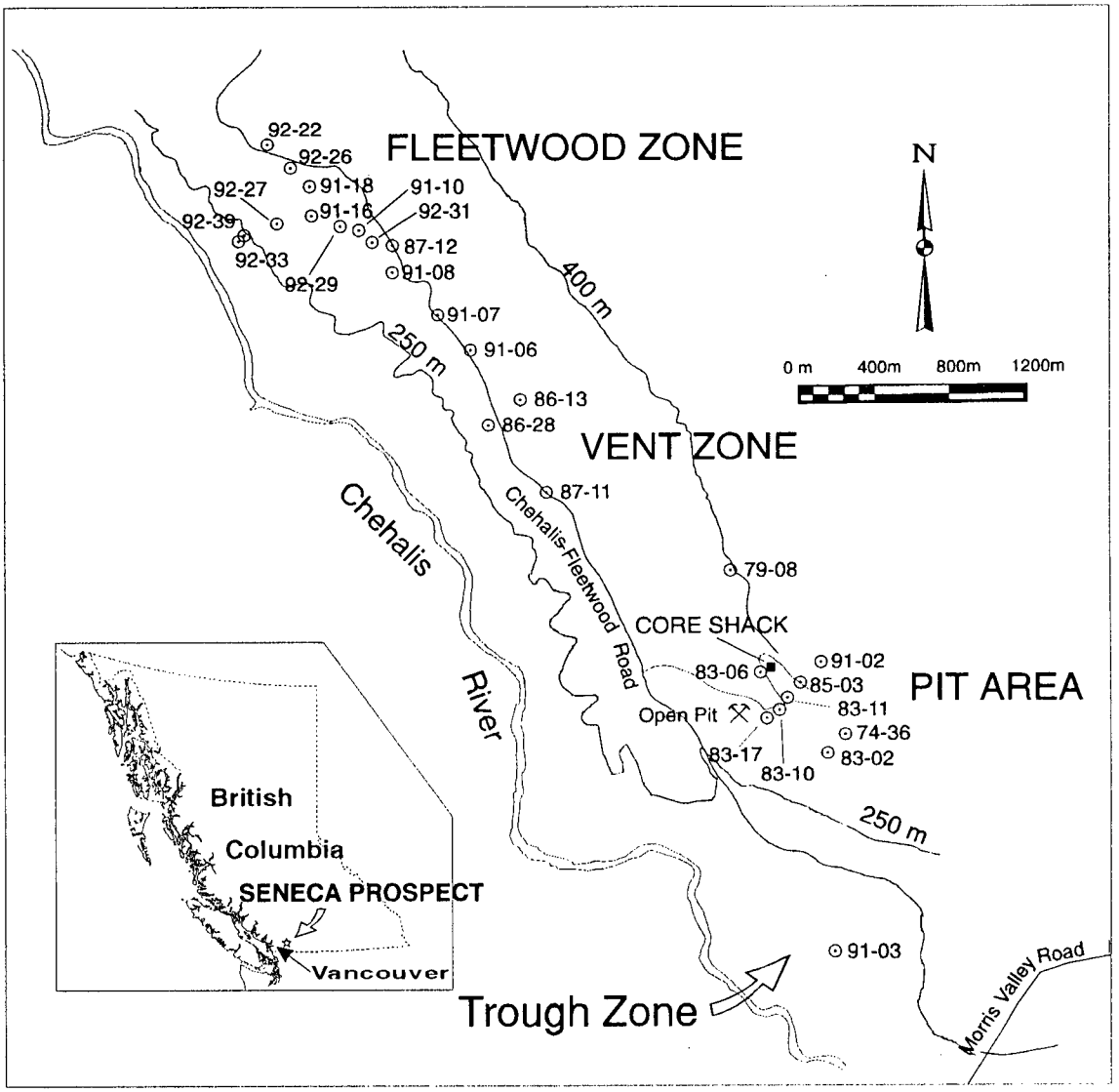

Figure A.1. Map of the Seneca property showing the locations of the drillholes from which the lithogeochemical samples were taken for this study.

Appendix A.1. Chemical composition of felsic volcanic rocks at Seneca.

Sample	83-02-67	83-02-186	83-02-277	83-02-320	83-06-50	83-07-27	83-07-54	83-10-91	83-11-24
Hole	83-02	83-02	83-02	83-02	83-06	83-07	83-07	83-10	83-11
Depth	67.0	186.3	277.0	319.6	49.8	26.1	53.0	91.3	28.1
Depth	219.8	611.1	908.8	1048.7	163.4	85.6	173.9	299.6	92.0
Rock Type	FP	FP	FP	FP	FP	FP	FP	FP	FP
(Wt. %)									
SiO_2	69.43	68.83	70.50	70.06	69.27	72.67	67.51	66.53	69.95
TiO_2	0.50	0.51	0.43	0.45	0.40	0.36	0.51	0.52	0.47
Al_2O_3	14.59	14.73	13.95	14.42	14.98	13.47	14.55	15.54	14.22
Fe_2O_3	3.99	3.90	3.16	3.45	3.77	2.86	4.58	4.22	3.75
MnO	0.09	0.06	0.17	0.07	0.08	0.07	0.11	0.12	0.08
MgO	2.23	2.06	1.84	1.94	1.92	1.86	3.48	3.81	2.83
CaO	0.84	1.13	1.29	0.92	0.78	0.55	0.77	0.68	0.67
Na_2O	4.72	5.40	4.44	4.65	5.75	5.31	4.97	3.19	4.43
K_2O	1.89	1.25	1.50	1.88	1.21	1.12	0.71	2.05	1.31
P_2O_5	0.14	0.15	0.11	0.11	0.13	0.08	0.13	0.16	0.12
LOI	1.92	1.78	2.58	2.11	1.93	1.44	2.37	3.20	2.49
Total	100.34	99.80	99.97	100.06	100.22	99.79	99.68	100.03	100.32
(ppm)									
Cr	106	90	137	193	104	11	18	25	90
Ni	11	8	13	11	6	bd	bd	40	6
Co	9	3	12	9	10	36	21	5	10
Sc	11	10	8	10	3	8	16	10	6
V	57	56	47	51	60	31	82	50	60
Cu	8	3	8	21	21	30	30	91	6
Pb	5	5	4	4	4	bd	1	1	4
Zn	47	55	69	44	82	37	60	91	81
Ba	424	292	263	481	340	468	557	418	463
Rb	24	13	19	24	11	12	8	29	15
Sr	144	126	58	101	108	70	78	56	63
Ga	14	14	12	12	13	13	15	17	13
Nb	6	5	6	6	5	11	10	10	5
Zr	116	115	124	127	110	114	101	104	113
Y	28	26	23	24	23	27	31	32	26
Th	bd	bd	bd	bd	bd	bd	bd	bd	bd
U	bd	bd	bd	bd	bd	bd	bd	bd	bd
Cs	na	na	0.2	na	na	na	na	na	0.6
Hf	na	na	2.7	na	na	na	na	na	2.4
La	na	na	11.3	na	na	na	na	na	9.3
Ce	na	na	23	na	na	na	na	na	24
Nd	na	na	12	na	na	na	na	na	14
Sm	na	na	2.76	na	na	na	na	na	3.08
Eu	na	na	0.87	na	na	na	na	na	1.03
Tb	na	na	0.5	na	na	na	na	na	0.6
Yb	na	na	2.46	na	na	na	na	na	2.79
Lu	na	na	0.35	na	na	na	na	na	0.41
Zr/Y	4.1	4.4	5.4	5.3	4.8	4.2	3.3	3.3	4.3
La_N/Yb_N			3.1						2.2

Analytical method: X-ray fluorescence, induced neutron activation analysis
The major elements plus Cu-Zn-Ni-Cr-V-Sc were analysed using glass beads.
The elements Zr-Y-Nb-Rb-Sr-Ga-Pb were analysed using pressed pellets.
(bd = below detection limit; na = not analysed)

Appendix A.1 (continued). Chemical composition of felsic volcanic rocks at Seneca.

Sample	83-11-40	85-03-70	85-03-126	86-28-67	86-28-103	87-11-75	87-12-69	87-12-147	87-12-301
Hole	83-11	85-03	85-03	86-28	86-28	87-11	87-12	87-12	87-12
Depth	85.2	70.5	126.2	67.0	103.0	75.5	69.2	147.4	301.4
Depth	279.4	231.2	414.1	219.8	337.9	247.7	227.1	483.6	988.8
Rock Type	FP	FP	FP	ALT FP	ALT FP	FP FL	FP	ALT FP	FP FL
SiO_2	71.17	69.26	70.35	72.97	70.86	73.94	70.57	75.11	71.50
TiO_2	0.45	0.41	0.39	0.38	0.42	0.38	0.37	0.37	0.39
Al_2O_3	14.57	14.94	14.64	13.09	14.01	12.63	13.73	11.91	12.76
Fe_2O_3	3.03	3.89	3.68	2.95	2.68	2.92	3.57	2.92	2.65
MnO	0.07	0.08	0.10	0.11	0.13	0.17	0.10	0.04	0.12
MgO	2.02	2.27	1.54	3.59	4.63	2.04	2.96	1.72	2.40
CaO	0.61	0.43	0.74	0.20	0.23	0.55	1.04	0.21	1.50
Na_2O	4.88	5.97	6.01	0.06	0.00	4.08	3.36	0.14	2.75
K_2O	1.24	0.49	1.08	3.07	3.25	1.03	1.86	3.43	1.70
P_2O_5	0.10	0.14	0.12	0.11	0.12	0.11	0.10	0.11	0.11
LOI	2.17	2.05	1.43	3.81	4.05	1.92	2.30	3.61	3.61
Total	100.31	99.93	100.08	100.34	100.38	99.77	99.96	99.57	99.49
Cr	67	48	98	bd	bd	28	32	23	44
Ni	6	7	15	1	bd	6	8	3	9
Co	9	7	6	7	9	bd	bd	3	bd
Sc	6	8	7	na	na	na	na	na	na
V	43	52	61	44	40	29	49	45	35
Cu	3	7	18	473	12	30	19	65	49
Pb	4	4	4	na	na	1	3	7	3
Zn	46	57	58	198	164	75	66	2057	86
Ba	143	17	475	557	1400	265	528	873	497
Rb	16	8	8	47	52	15	20	45	21
Sr	65	64	101	8	10	68	137	18	121
Ga	13	14	13	16	14	14	14	17	14
Nb	6	5	5	7	7	9	8	8	7
Zr	134	109	115	108	117	122	120	118	122
Y	29	22	21	26	25	30	26	27	29
Th	bd	bd	bd	bd	bd	bd	bd	bd	bd
U	bd	bd	bd	bd	bd	bd	bd	bd	bd
Cs	na	na	na	na	na	0.3	na	na	na
Hf	na	na	na	na	na	2.7	na	na	na
La	na	na	na	na	na	11.2	na	na	na
Ce	na	na	na	na	na	24	na	na	na
Nd	na	na	na	na	na	14	na	na	na
Sm	na	na	na	na	na	2.95	na	na	na
Eu	na	na	na	na	na	0.97	na	na	na
Tb	na	na	na	na	na	0.6	na	na	na
Yb	na	na	na	na	na	2.46	na	na	na
Lu	na	na	na	na	na	0.35	na	na	na
Zr/Y	4.6	5.0	5.5	4.2	4.7	4.1	4.6	4.4	4.2
La_N/Yb_N						3.1			

Analytical method: X-ray fluorescence, induced neutron activation analysis
The major elements plus Cu-Zn-Ni-Cr-V-Sc were analysed using glass beads.
The elements Zr-Y-Nb-Rb-Sr-Ga-Pb were analysed using pressed pellets.
(bd = below detection limit; na = not analysed)

Appendix A.1 (continued). Chemical composition of felsic volcanic rocks at Seneca.

Sample	91-02-28	91-02-85	91-02-170	91-03-40	91-10-99	91-10-118	91-10-180	91-10-210	91-10-234
Hole	91-02	91-02	91-02	91-03	91-10	91-10	91-10	91-10	91-10
Depth	28.1	85.2	170.0	39.9	99.1	118.0	180.4	210.1	234.5
Depth	92.0	279.4	557.8	130.9	325.1	387.3	591.8	689.4	769.3
Rock Type	QFP	QFP	FP	QFP	FEL DYK	FEL DYK	ALT FP	FP FL	ALT FP
SiO_2	73.72	73.93	69.13	56.48	74.25	75.04	72.51	75.36	71.48
TiO_2	0.28	0.28	0.50	0.44	0.28	0.30	0.33	0.39	0.33
Al_2O_3	13.28	13.61	14.40	19.92	12.57	12.25	11.28	12.81	13.22
Fe_2O_3	2.35	2.34	4.27	3.74	2.14	2.16	3.69	1.57	2.85
MnO	0.06	0.06	0.10	0.18	0.08	0.06	0.01	0.01	0.14
MgO	1.88	1.22	2.20	2.86	0.55	0.69	0.48	0.46	3.73
CaO	0.18	0.34	0.73	2.33	1.38	0.85	0.36	1.06	0.63
Na_2O	3.82	4.94	5.58	4.21	3.48	4.84	0.68	4.22	1.87
K_2O	2.32	1.94	0.98	3.22	3.29	1.82	5.27	1.53	2.05
P_2O_5	0.05	0.05	0.11	0.09	0.05	0.05	0.10	0.03	0.10
LOI	2.03	1.63	1.83	5.99	1.67	1.25	3.21	2.24	3.57
Total	99.97	100.34	99.83	99.46	99.74	99.31	97.92	99.68	99.97
Cr	129	153	117	0	36	24	0	40	16
Ni	5	6	4	5	5	3	5	10	2
Co	7	6	9	bd	bd	bd	8	3	5
Sc	2	bd	9	na	na	na	na	na	na
V	26	28	73	58	24	20	20	30	29
Cu	5	11	25	30	29	22	406	67	77
Pb	4	4	8	5	3	1	94	208	3
Zn	57	42	207	90	40	34	13967	1428	239
Ba	445	529	426	5392	1539	1272	6220	2047	665
Rb	18	17	8	48	37	18	49	18	23
Sr	54	73	94	275	104	113	40	181	52
Ga	11	11	12	22	13	12	16	14	14
Nb	7	5	6	8	9	9	6	8	8
Zr	141	119	116	193	130	131	106	122	117
Y	26	17	25	38	25	26	30	24	23
Th	bd	bd	bd	bd	bd	bd	bd	bd	bd
U	bd	bd	bd	bd	bd	bd	2.0	bd	bd
Cs	bd	na	na	na	na	na	na	na	na
Hf	3.1	na	na	na	na	na	na	na	na
La	14.2	na	na	na	na	na	na	na	na
Ce	29	na	na	na	na	na	na	na	na
Nd	14	na	na	na	na	na	na	na	na
Sm	2.83	na	na	na	na	na	na	na	na
Eu	0.72	na	na	na	na	na	na	na	na
Tb	0.6	na	na	na	na	na	na	na	na
Yb	2.90	na	na	na	na	na	na	na	na
Lu	0.45	na	na	na	na	na	na	na	na
Zr/Y	5.4	7.0	4.6	5.1	5.2	5.0	3.5	5.1	5.1
La_N/Yb_N	3.3								

Analytical method: X-ray fluorescence, induced neutron activation analysis
The major elements plus Cu-Zn-Ni-Cr-V-Sc were analysed using glass beads.
The elements Zr-Y-Nb-Rb-Sr-Ga-Pb were analysed using pressed pellets.
(bd = below detection limit; na = not analysed)

Appendix A.1 (continued). Chemical composition of felsic volcanic rocks at Seneca.

Sample	91-16-61	91-16-152	91-16-159	91-16-161	91-16-307	91-18-64	91-18-252	91-18-284	92-26-227
Hole	91-16	91-16	91-16	91-16	91-16	91-18	91-18	91-18	92-26
Depth	61.2	151.8	159.0	161.3	307.5	64.3	252.5	284.6	227.2
Depth	200.8	498.0	521.6	529.2	1008.9	211.0	828.4	933.7	745.2
Rock Type	FP	FP	ALT FP	FP	FP	FP FL	ALT FP	FP	FP
SiO_2	73.22	73.17	78.18	63.50	67.91	74.06	77.62	64.94	73.26
TiO_2	0.35	0.35	0.26	0.49	0.52	0.35	0.34	0.54	0.29
Al_2O_3	13.21	13.41	11.17	13.55	14.48	13.31	10.38	17.30	13.64
Fe_2O_3	2.71	2.37	1.45	4.22	4.39	2.71	4.10	2.70	2.38
MnO	0.13	0.10	0.01	0.12	0.20	0.11	0.01	0.13	0.08
MgO	2.85	1.60	0.98	4.76	3.95	1.97	0.65	2.94	0.78
CaO	0.51	1.03	0.26	2.50	0.89	0.69	0.16	1.32	1.72
Na_2O	2.65	4.75	0.66	2.67	2.05	4.69	0.25	2.36	5.01
K_2O	1.90	0.66	2.67	1.06	2.09	0.96	3.05	3.52	1.34
P_2O_5	0.07	0.07	0.10	0.11	0.13	0.08	0.07	0.12	0.06
LOI	2.63	1.97	0.00	6.58	3.54	1.59	3.86	4.27	1.69
Total	100.23	99.48	95.74	99.56	100.15	100.52	100.49	100.14	100.25
Cr	121	438	250	160	68	11	bd	bd	bd
Ni	10	10	10	7	4	2	bd	4	bd
Co	3	4	2	7	10	17	23	3	28
Sc	3	2	1	12	5	na	na	na	na
V	30	38	36	79	72	32	44	46	40
Cu	bd	91	909	23	25	53	870	103	36
Pb	3	3	671	5	4	na	na	na	na
Zn	79	150	12525	235	125	110	2592	103	49
Ba	453	4068	24702	1063	374	302	676	1723	725
Rb	27	6	10	15	28	15	43	45	13
Sr	53	242	302	100	63	120	18	74	299
Ga	11	10	2	12	13	12	17	15	13
Nb	7	5	bd	5	7	7	6	8	5
Zr	135	120	72	108	131	128	103	168	114
Y	24	18	16	20	28	23	29	42	17
Th	bd	bd	bd	bd	bd	bd	bd	bd	bd
U	bd	1.0	6.4	bd	bd	bd	bd	bd	bd
Cs	na	na	bd	na	0.4	bd	bd	na	na
Hf	na	na	3.2	na	2.9	2.8	2.8	na	na
La	na	na	5.8	na	13.3	9.4	11.9	na	na
Ce	na	na	12	na	29	22	28	na	na
Nd	na	na	8	na	15	11	17	na	na
Sm	na	na	1.65	na	3.43	2.40	3.16	na	na
Eu	na	na	0.40	na	1.33	0.61	0.51	na	na
Tb	na	na	0.4	na	0.7	0.6	0.7	na	na
Yb	na	na	1.97	na	2.86	2.49	3.09	na	na
Lu	na	na	0.32	na	0.44	0.37	0.44	na	na
Zr/Y	5.6	6.7	4.6	5.4	4.7	5.6	3.6	4.0	6.7
La_N/Yb_N			2.0		3.1	2.5	2.6		

Analytical method: X-ray fluorescence, induced neutron activation analysis
The major elements plus Cu-Zn-Ni-Cr-V-Sc were analysed using glass beads.
The elements Zr-Y-Nb-Rb-Sr-Ga-Pb were analysed using pressed pellets.
(bd = below detection limit; na = not analysed)

Appendix A.1 (continued). Chemical composition of felsic volcanic rocks at Seneca.

Sample	92-27-71	92-27-85	92-27-177	92-28-35	92-28-132	92-28-185	92-29-140	92-29-227	92-31-281
Hole	92-27	92-27	92-27	92-28	92-28	92-28	92-29	92-29	92-31
Depth	70.9	85.2	177.7	35.4	132.5	185.0	140.3	226.8	281.4
Depth	232.5	279.5	583.0	116.1	434.7	606.9	460.1	744.1	923.0
Rock Type	QFP	FP	FP	FP FL	ALT FL	QFP	QFP	FP	FP
SiO_2	69.59	64.75	68.95	74.13	69.83	74.14	75.01	63.72	68.44
TiO_2	0.39	0.68	0.51	0.34	0.40	0.36	0.27	0.71	0.52
Al_2O_3	13.97	15.49	14.36	12.78	14.15	12.94	13.04	16.01	14.81
Fe_2O_3	3.52	6.23	4.43	2.37	2.81	1.95	2.41	5.89	3.93
MnO	0.14	0.20	0.15	0.13	0.18	0.13	0.19	0.20	0.14
MgO	1.45	3.03	2.86	2.82	2.22	2.27	1.08	3.49	1.61
CaO	2.46	1.61	1.28	0.41	1.52	1.03	1.46	1.71	1.56
Na_2O	4.51	5.59	4.31	1.16	5.86	3.25	4.80	5.57	6.19
K_2O	1.03	0.05	0.73	3.01	0.40	1.67	0.62	0.28	0.43
P_2O_5	0.09	0.20	0.11	0.07	0.09	0.07	0.06	0.23	0.15
LOI	3.23	2.20	2.39	3.18	2.93	2.67	1.54	2.72	2.12
Total	100.38	100.03	100.08	100.40	100.39	100.48	100.48	100.53	99.90
Cr	156	77	127	bd	bd	bd	1	bd	17
Ni	18	19	18	1	bd	1	bd	bd	5
Co	7	12	9	10	15	9	21	15	2
Sc	6	17	5	na	na	na	na	na	na
V	51	99	78	29	29	29	42	56	70
Cu	46	379	6	73	21	27	61	249	44
Pb	6	6	4	na	na	na	na	na	2
Zn	94	184	83	120	100	125	114	171	104
Ba	448	bd	200	1814	139	495	251	146	286
Rb	14	4	11	38	5	24	8	3	5
Sr	179	118	141	64	109	64	312	224	162
Ga	12	14	13	12	13	13	13	17	15
Nb	4	5	5	8	8	8	5	4	8
Zr	103	96	114	129	152	147	109	94	133
Y	21	26	26	22	28	33	15	36	32
Th	bd	bd	bd	bd	bd	bd	bd	bd	bd
U	1.0	bd	bd	bd	bd	bd	bd	bd	bd
Cs	na	na	na	na	na	na	0.3	na	na
Hf	na	na	na	na	na	na	3.0	na	na
La	na	na	na	na	na	na	9.6	na	na
Ce	na	na	na	na	na	na	21	na	na
Nd	na	na	na	na	na	na	9	na	na
Sm	na	na	na	na	na	na	1.85	na	na
Eu	na	na	na	na	na	na	0.50	na	na
Tb	na	na	na	na	na	na	0.4	na	na
Yb	na	na	na	na	na	na	1.78	na	na
Lu	na	na	na	na	na	na	0.26	na	na
Zr/Y	4.9	3.7	4.4	5.9	5.4	4.5	7.3	2.6	4.2
La_N/Yb_N							3.6		

Analytical method: X-ray fluorescence, induced neutron activation analysis
The major elements plus Cu-Zn-Ni-Cr-V-Sc were analysed using glass beads.
The elements Zr-Y-Nb-Rb-Sr-Ga-Pb were analysed using pressed pellets.
(bd = below detection limit; na = not analysed)

Appendix A.1 (continued). Chemical composition of felsic volcanic rocks at Seneca.

Sample	92-31-244	92-31-225	92-33-75	92-39-71	92-39-200	93-VT-01	93-VT-02	93-VT-03	93-VT-04
Hole	92-31	92-31	92-33	92-39	92-39	86-13	86-13	86-13	86-13
Depth	244.5	224.9	75.0	71.1	200.5	25.0	50.0	65.0	85.0
Depth	802.2	737.9	245.9	233.2	657.9	82.0	164.0	213.3	278.9
Rock Type	ALT FP	FP	FP	FP	QFP	FP	ALT FP	ALT FP	ALT FP
SiO_2	61.89	68.41	69.73	72.52	73.53	71.29	71.15	70.22	70.44
TiO_2	0.60	0.50	0.36	0.35	0.31	0.41	0.38	0.42	0.41
Al_2O_3	16.77	13.91	15.13	13.77	13.37	14.32	12.28	13.91	13.43
Fe_2O_3	3.96	4.54	3.28	3.45	2.23	3.48	4.24	3.19	3.72
MnO	0.12	0.17	0.13	0.12	0.10	0.19	0.08	0.16	0.08
MgO	5.29	3.68	2.43	2.24	0.94	2.07	3.76	4.38	3.54
CaO	1.13	0.98	0.95	0.75	1.34	0.54	0.49	0.52	0.20
Na_2O	4.02	3.57	5.15	3.54	3.97	5.22	0.20	bd	bd
K_2O	1.55	1.21	0.83	1.26	2.84	0.54	2.86	3.04	3.57
P_2O_5	0.18	0.13	0.07	0.07	0.06	0.09	0.09	0.11	0.09
LOI	4.06	2.95	2.36	2.14	1.52	1.70	4.90	4.28	4.57
Total	99.57	100.05	100.42	100.21	100.21	99.85	100.43	100.23	100.05
Cr	3	26	165	178	376	79	87	84	157
Ni	4	5	9	4	3	11	13	8	45
Co	6	8	7	6	9	3	7	10	6
Sc	na	na	3	7	6	10	10	6	5
V	76	80	40	37	29	56	47	34	46
Cu	69	47	37	22	609	66	223	28	86
Pb	282	4	5	4	5	3	12	6	14
Zn	338	176	57	48	850	99	430	160	607
Ba	1680	263	261	405	2499	200	546	739	830
Rb	18	16	10	15	20	8	41	36	53
Sr	136	90	173	114	219	89	8	8	9
Ga	16	15	12	13	9	12	14	13	14
Nb	8	8	8	7	5	5	6	6	6
Zr	140	113	154	142	120	116	117	128	123
Y	40	32	27	26	17	21	24	27	20
Th	bd	bd	bd	bd	bd	bd	2.0	bd	2.0
U	bd	bd	2.0	1.0	1.0	bd	bd	bd	bd
Cs	na	na	bd	na	bd	na	na	0.9	0.3
Hf	na	na	3.2	na	2.8	na	na	3.0	2.9
La	na	na	10.7	na	11.1	na	na	11.2	8.6
Ce	na	na	23	na	24	na	na	26	21
Nd	na	na	12	na	12	na	na	14	11
Sm	na	na	2.73	na	2.21	na	na	2.87	2.23
Eu	na	na	0.64	na	0.72	na	na	0.51	0.37
Tb	na	na	0.5	na	0.4	na	na	0.6	0.5
Yb	na	na	2.63	na	2.04	na	na	2.95	2.26
Lu	na	na	0.41	na	0.30	na	na	0.49	0.33
Zr/Y	3.5	3.5	5.7	5.5	7.1	5.5	4.9	4.7	6.2
La_N/Yb_N			2.7		3.7			2.6	2.6

Analytical method: X-ray fluorescence, induced neutron activation analysis
The major elements plus Cu-Zn-Ni-Cr-V-Sc were analysed using glass beads.
The elements Zr-Y-Nb-Rb-Sr-Ga-Pb were analysed using pressed pellets.
(bd = below detection limit; na = not analysed)

Appendix A.1 (continued).

Sample	93-SN-44	93-SN-45	93-SN-46	93-FW-46	93-FW-49	93-FW-51	93-FW-52	
Hole	79-08	79-08	79-08	91-06	91-06	91-06	91-06	
Depth	200.0	199.0	179.5	22.2	46.5	128.0	204.6	Detection
Depth	656.2	652.9	589.0	72.8	152.6	419.9	671.2	Limits
Rock Type	ALT FP	ALT FP	FP	ALT FP	ALT FP	FP	ALT FP	(ppm)
SiO_2	78.57	67.68	72.10	58.00	69.29	74.16	80.87	60
TiO_2	0.27	0.37	0.35	0.67	0.38	0.31	0.31	35
Al_2O_3	10.01	13.86	13.45	15.48	14.33	13.24	8.50	120
Fe_2O_3	2.24	3.38	3.11	7.89	4.02	2.46	3.69	30
MnO	0.17	0.29	0.14	0.41	0.20	0.12	0.01	30
MgO	1.02	1.72	2.32	5.08	1.31	1.30	0.56	95
CaO	1.51	3.04	0.92	3.47	2.31	0.83	0.29	15
Na_2O	2.07	4.44	4.26	4.93	5.13	4.35	bd	75
K_2O	1.43	1.14	1.00	0.41	0.29	1.80	2.32	25
P_2O_5	0.06	0.09	0.08	0.13	0.11	0.06	0.09	35
LOI	2.62	3.75	2.31	3.96	2.13	1.52	3.53	100
Total	99.96	99.76	100.05	100.44	99.51	100.16	100.17	100
Cr	7	2	4	40	bd	15	bd	2
Ni	bd	bd	bd	6	bd	37	bd	3
Co	23	18	9	30	31	25	22	10
Sc	6	12	9	27	7	3	3	10
V	32	41	45	195	40	39	41	10
Cu	35	19	23	64	23	38	547	15
Pb	6	6	2	4	1	1	49	2
Zn	79	118	69	202	98	57	715	2
Ba	436	400	355	453	1586	1576	1677	50
Rb	19	16	16	4	4	16	34	1
Sr	49	70	70	174	261	165	22	1
Ga	10	13	13	15	14	12	13	1
Nb	11	11	11	8	9	11	10	1
Zr	99	131	128	69	111	126	77	1
Y	23	29	27	26	28	26	19	1
Th	bd	bd	bd	bd	bd	bd	bd	0.1
U	bd	bd	bd	0.8	bd	bd	0.9	0.1
Cs	na	na	na	na	na	na	na	0.2
Hf	na	na	na	na	na	na	na	0.2
La	na	na	na	na	na	na	na	0.1
Ce	na	na	na	na	na	na	na	1
Nd	na	na	na	na	na	na	na	1
Sm	na	na	na	na	na	na	na	0.01
Eu	na	na	na	na	na	na	na	0.05
Tb	na	na	na	na	na	na	na	0.1
Yb	na	na	na	na	na	na	na	0.05
Lu	na	na	na	na	na	na	na	0.01
Zr/Y	4.2	4.5	4.7	2.6	4.0	4.8	4.0	
La_N/Yb_N								

Analytical method: X-ray fluorescence, induced neutron activation analysis
The major elements plus Cu-Zn-Ni-Cr-V-Sc were analysed using glass beads.
The elements Zr-Y-Nb-Rb-Sr-Ga-Pb were analysed using pressed pellets.
(bd = below detection limit; na = not analysed)

Appendix A.2. Chemical composition of mafic volcanic rocks at Seneca.

Sample	83-02-227	83-06-124	83-10-56	83-17-34	85-03-155	91-08-200	91-16-69	91-16-231	91-16-233
Hole	83-02	83-06	83-10	83-17	85-03	91-08	91-16	91-16	91-16
Depth	227.0	123.9	53.6	34.0	154.8	199.8	69.3	231.1	232.9
Depth	744.8	406.5	175.7	111.7	508.0	655.6	227.5	758.3	764.0
Rock Type	MAFIC	MAFIC	MAFIC	MAFIC	MAFIC	MAFIC	MAFIC	MAFIC	MAFIC
SiO_2	47.28	51.41	51.90	51.83	53.66	48.91	50.95	45.56	43.75
TiO_2	0.68	0.83	0.86	0.83	0.81	0.77	0.77	0.65	0.66
Al_2O_3	19.93	17.50	18.25	17.51	17.45	20.55	17.16	15.84	16.10
Fe_2O_3	9.40	10.10	9.58	10.11	9.02	9.45	10.67	7.92	9.52
MnO	0.17	0.19	0.21	0.31	0.16	0.16	0.58	0.29	0.33
MgO	7.43	6.51	6.16	6.14	5.40	4.17	8.46	6.34	9.04
CaO	4.89	2.97	2.44	2.82	2.93	9.42	3.11	10.45	8.19
Na_2O	3.86	4.79	5.92	5.64	5.57	2.92	3.79	2.48	3.08
K_2O	1.39	0.68	0.10	0.06	0.29	0.36	0.14	1.24	0.20
P_2O_5	0.13	0.19	0.24	0.22	0.23	0.15	0.13	0.14	0.11
LOI	5.13	5.54	4.57	4.98	4.87	3.58	5.02	9.09	9.34
Total	100.29	100.71	100.23	100.45	100.39	100.44	100.78	100.00	100.32
Cr	209	75	30	45	55	16	44	150	132
Ni	38	18	21	15	20	19	18	14	23
Co	32	30	34	27	34	25	31	30	36
Sc	29	23	24	22	22	na	29	32	32
V	210	227	215	210	186	280	235	242	229
Cu	45	37	122	69	76	167	118	94	93
Pb	9	9	7	8	8	bd	8	bd	10
Zn	66	126	190	204	147	62	286	83	273
Ba	753	747	37	6	148	65	3	1026	88
Rb	22	18	9	10	10	4	11	7	12
Sr	372	103	119	72	156	352	196	174	177
Ga	15	16	17	16	15	18	14	13	13
Nb	1	4	4	4	4	6	2	7	1
Zr	47	81	77	75	79	49	63	30	44
Y	14	19	21	16	19	19	17	15	14
Th	1.0	1.0	bd	1.0	bd	bd	1.0	bd	1.0
U	bd	bd	bd	bd	bd	bd	bd	bd	bd
Cs	na	na	na	bd	bd	na	na	na	0.4
Hf	na	na	na	1.2	1.4	na	na	na	0.7
La	na	na	na	3.0	5.2	na	na	na	2.5
Ce	na	na	na	8	13	na	na	na	6
Nd	na	na	na	6	8	na	na	na	5
Sm	na	na	na	1.58	2.09	na	na	na	1.39
Eu	na	na	na	0.52	0.73	na	na	na	0.52
Tb	na	na	na	0.3	0.4	na	na	na	0.3
Yb	na	na	na	1.66	1.82	na	na	na	1.31
Lu	na	na	na	0.24	0.26	na	na	na	0.18
Zr/Y	3.4	4.3	3.7	4.7	4.2	2.6	3.7	2.0	3.1
La_N/Yb_N				1.2	1.9				1.3

Analytical method: X-ray fluorescence, induced neutron activation analysis
The major elements plus Cu-Zn-Ni-Cr-V-Sc were analysed using glass beads.
The elements Zr-Y-Nb-Rb-Sr-Ga-Pb were analysed using pressed pellets.
(bd = below detection limit; na = not analysed)

Appendix A.2 (continued).

Sample	92-27-333	92-28-374	93-SN-47	93-FW-48	93-FW-50	94-FF-01	
Hole	92-27	92-28	79-08	91-06	91-06	-	
Depth	333.5	374.5	161.0	37.3	95.1	-	Detection
Depth	1094.0	1228.6	528.2	122.4	312.0	-	Limits
Rock Type	MAFIC	MAFIC	MAFIC	ALT MAF	ALT MAF	MAFIC	(ppm)
SiO_2	45.33	47.89	52.91	43.47	49.65	39.42	60
TiO_2	0.77	0.58	1.18	0.52	0.82	0.75	35
Al_2O_3	17.80	20.38	15.18	19.34	17.27	14.97	120
Fe_2O_3	10.79	8.71	13.42	11.02	12.29	8.38	30
MnO	0.58	0.41	0.25	0.44	0.82	0.31	30
MgO	13.88	10.45	4.39	0.63	8.60	5.73	95
CaO	1.29	1.07	4.03	21.29	2.51	17.42	15
Na_2O	3.21	1.30	4.48	0.10	2.33	0.93	75
K_2O	0.01	3.09	0.29	bd	0.35	0.29	25
P_2O_5	0.13	0.13	0.27	0.11	0.15	0.15	35
LOI	6.92	6.63	4.06	3.46	5.42	11.44	100
Total	100.71	100.64	100.47	100.37	100.21	88.35	100
Cr	133	92	9	144	179	63	2
Ni	33	22	bd	1	50	10	3
Co	48	13	28	25	32	24	10
Sc	31	na	29	37	32	34	10
V	264	206	283	279	310	273	10
Cu	151	35	108	22	472	86	15
Pb	6	na	6	7	bd	bd	2
Zn	479	317	120	33	363	86	2
Ba	bd	1249	329	134	183	76	50
Rb	9	43	2	bd	2	5	1
Sr	78	78	270	699	181	350	1
Ga	15	16	19	19	18	16	1
Nb	2	4	7	4	8	0	1
Zr	48	37	59	26	40	47	1
Y	16	16	38	12	16	17	1
Th	bd	bd	bd	bd	bd	0.4	0.1
U	bd	bd	4.8	bd	bd	bd	0.1
Cs	0.2	na	bd	na	na	bd	0.2
Hf	0.7	na	1.4	na	na	0.6	0.2
La	2.9	na	6.6	na	na	3.0	0.1
Ce	8	na	19	na	na	9	1
Nd	6	na	13	na	na	7	1
Sm	1.79	na	3.81	na	na	1.99	0.01
Eu	0.56	na	1.16	na	na	0.71	0.05
Tb	0.4	na	0.8	na	na	0.4	0.1
Yb	1.53	na	3.25	na	na	1.52	0.05
Lu	0.23	na	0.47	na	na	0.22	0.01
Zr/Y	3.0	2.3	1.5	2.1	2.5	2.8	
La_N/Yb_N	1.3		1.4			1.3	

Analytical method: X-ray fluorescence, induced neutron activation analysis
The major elements plus Cu-Zn-Ni-Cr-V-Sc were analysed using glass beads.
The elements Zr-Y-Nb-Rb-Sr-Ga-Pb were analysed using pressed pellets.
(bd = below detection limit; na = not analysed)

Appendix A.3. Chemical composition of volcaniclastic rocks at Seneca.

Sample	83-10-20	83-17-19	85-03-92	87-11-144	87-11-160	87-12-115	91-03-14	91-03-35	91-03-75
Hole	83-10	83-17	85-03	87-11	87-11	87-12	91-03	91-03	91-03
Depth	20.8	19.3	91.8	144.8	160.3	114.9	14.0	35.2	75.1
Depth	68.3	63.5	301.2	475.1	525.8	377.0	45.9	115.5	246.4
Rock Type	VCLT	VCLT	VCLT	VCLT	VCLT	VCLT	VCLT	VCLT	VCLT
SiO_2	48.22	63.73	73.62	74.98	53.80	72.90	71.71	69.48	72.12
TiO_2	0.61	0.44	0.26	0.43	0.73	0.32	0.30	0.29	0.41
Al_2O_3	18.76	13.08	13.25	11.95	16.64	13.22	13.50	13.82	13.42
Fe_2O_3	8.47	5.90	2.52	2.99	8.45	2.95	2.51	2.96	2.80
MnO	0.20	0.30	0.04	0.15	0.53	0.08	0.08	0.10	0.11
MgO	7.45	5.32	1.82	1.87	7.38	2.10	1.51	1.66	1.48
CaO	3.62	1.91	0.75	0.62	2.50	0.61	1.44	2.03	0.63
Na_2O	3.93	2.01	3.29	5.03	5.50	2.58	4.48	4.47	4.27
K_2O	2.43	2.54	1.82	0.38	0.10	2.11	1.17	1.29	2.86
P_2O_5	0.11	0.08	0.04	0.11	0.16	0.07	0.08	0.07	0.13
LOI	6.24	4.70	3.04	1.44	4.57	2.76	3.51	3.85	1.79
Total	100.05	100.01	100.45	99.95	100.36	99.70	100.29	100.02	100.02
Cr	241	257	32	12	37	21	28	34	25
Ni	38	38	7	4	18	6	2	7	9
Co	28	20	6	2	24	bd	bd	1	bd
Sc	25	11	5	na	na	na	na	na	na
V	210	113	40	27	228	36	32	29	34
Cu	76	43	10	67	98	30	29	25	56
Pb	bd	24	10	2	4	7	2	2	8
Zn	67	198	58	58	303	76	33	39	53
Ba	1455	1630	88	39	15	690	84	348	639
Rb	20	25	30	5	1	28	15	17	31
Sr	133	67	82	45	113	102	66	105	64
Ga	14	11	12	12	15	14	13	14	14
Nb	8	4	5	9	6	8	8	8	9
Zr	39	90	117	117	61	150	100	112	157
Y	15	21	20	36	26	24	20	22	43
Th	bd	6.0	bd	bd	bd	bd	bd	bd	bd
U	bd	bd	bd	bd	bd	bd	bd	bd	bd
Cs	na	na	na	na	na	na	na	na	na
Hf	na	na	na	na	na	na	na	na	na
La	na	na	na	na	na	na	na	na	na
Ce	na	na	na	na	na	na	na	na	na
Nd	na	na	na	na	na	na	na	na	na
Sm	na	na	na	na	na	na	na	na	na
Eu	na	na	na	na	na	na	na	na	na
Tb	na	na	na	na	na	na	na	na	na
Yb	na	na	na	na	na	na	na	na	na
Lu	na	na	na	na	na	na	na	na	na
Zr/Y	2.5	4.3	5.9	3.3	2.3	6.3	5.0	5.1	3.7
La_N/Yb_N									

Analytical method: X-ray fluorescence, induced neutron activation analysis
The major elements plus Cu-Zn-Ni-Cr-V-Sc were analysed using glass beads.
The elements Zr-Y-Nb-Rb-Sr-Ga-Pb were analysed using pressed pellets.
(bd = below detection limit; na = not analysed)

Appendix A.3 (continued). Chemical composition of volcaniclastic rocks at Seneca.

Sample	91-03-116	91-03-150	91-08-167	91-08-184	91-08-194	91-16-94	91-16-153	91-18-181	92-29-164
Hole	91-03	91-03	91-08	91-08	91-08	91-16	91-16	91-18	92-29
Depth	116.8	150.1	166.9	184.8	194.5	93.9	152.8	181.4	163.9
Depth	383.0	492.4	547.7	606.2	638.1	308.2	501.3	595.1	537.7
Rock Type	VCLT	VCLT	VCLT	VCLT	VCLT	VCLT	VCLT	VCLT	VCLT
SiO_2	73.48	69.60	63.99	73.15	66.00	63.71	79.01	69.60	76.79
TiO_2	0.34	0.48	0.58	0.29	0.36	0.67	0.21	0.35	0.24
Al_2O_3	12.11	14.08	17.10	13.98	15.59	15.15	8.46	13.57	11.95
Fe_2O_3	2.53	2.99	4.27	1.78	4.39	6.67	1.26	5.54	1.78
MnO	0.06	0.07	0.15	0.08	0.18	0.23	0.03	0.09	0.04
MgO	3.38	3.60	3.18	2.44	4.40	5.24	1.37	2.62	3.07
CaO	0.39	0.41	1.10	0.37	0.43	0.92	1.93	0.43	0.25
Na_2O	1.66	3.23	4.20	2.15	2.81	3.01	0.00	3.30	0.73
K_2O	1.91	1.68	2.06	2.73	2.20	1.07	2.23	1.52	2.73
P_2O_5	0.09	0.12	0.13	0.07	0.08	0.14	0.01	0.08	0.04
LOI	4.09	3.79	3.30	2.62	3.60	3.64	5.18	3.41	2.95
Total	100.04	100.05	100.06	99.66	100.04	100.45	99.69	100.51	100.57
Cr	20	29	18	25	37	17	264	bd	bd
Ni	1	3	4	3	13	19	10	3	bd
Co	5	8	7	5	11	10	6	27	12
Sc	na	na	na	na	na	14	1	na	na
V	22	42	60	22	56	123	20	62	27
Cu	33	23	33	19	16	16	7	18	27
Pb	4	3	4	1	3	6	5	na	na
Zn	51	62	100	49	109	91	52	72	81
Ba	121	372	382	489	439	222	2832	450	627
Rb	22	18	30	39	31	18	26	20	40
Sr	49	63	126	41	58	67	34	70	37
Ga	14	14	18	16	17	16	5	14	13
Nb	9	9	8	10	9	5	5	7	8
Zr	147	129	129	176	134	102	109	117	140
Y	34	41	35	31	25	34	15	25	21
Th	bd	bd	bd	bd	bd	bd	bd	bd	bd
U	bd	bd	bd	bd	bd	bd	bd	bd	bd
Cs	na	na	na	na	na	0.3	na	na	na
Hf	na	na	na	na	na	2.4	na	na	na
La	na	na	na	na	na	6.4	na	na	na
Ce	na	na	na	na	na	18	na	na	na
Nd	na	na	na	na	na	13	na	na	na
Sm	na	na	na	na	na	3.77	na	na	na
Eu	na	na	na	na	na	0.95	na	na	na
Tb	na	na	na	na	na	0.7	na	na	na
Yb	na	na	na	na	na	3.50	na	na	na
Lu	na	na	na	na	na	0.54	na	na	na
Zr/Y	4.3	3.1	3.7	5.7	5.4	3.0	7.3	4.7	6.7
La_N/Yb_N						1.2			

Analytical method: X-ray fluorescence, induced neutron activation analysis
The major elements plus Cu-Zn-Ni-Cr-V-Sc were analysed using glass beads.
The elements Zr-Y-Nb-Rb-Sr-Ga-Pb were analysed using pressed pellets.
(bd = below detection limit; na = not analysed)

Appendix A.3 (continued).

Sample	92-39-237	92-33-172	92-33-173	92-33-176	
Hole	92-39	92-33	92-33	92-33	
Depth	237.4	171.7	173.0	175.4	Detection
Depth	778.8	563.2	567.6	575.4	Limits
Rock Type	VCLT	OTHER	OTHER	OTHER	(ppm)
SiO_2	79.51	25.64	93.99	95.49	60
TiO_2	0.20	0.20	0.06	0.07	35
Al_2O_3	10.61	13.64	2.42	1.49	120
Fe_2O_3	1.05	12.77	2.17	1.15	30
MnO	0.02	0.39	0.01	0.01	30
MgO	0.57	10.40	0.44	0.18	95
CaO	1.10	0.62	0.17	0.23	15
Na_2O	4.06	8.42	2.20	bd	75
K_2O	0.63	0.60	0.39	0.29	25
P_2O_5	0.04	0.10	0.05	bd	35
LOI	2.29	11.63	0.00	1.11	100
Total	100.08	84.41	101.90	100.02	100
Cr	291	0	292	602	2
Ni	9	39	9	8	3
Co	7	31	1	5	10
Sc	4	6	0	3	10
V	19	118	69	17	10
Cu	81	10029	2294	88	15
Pb	4	94	4450	10	2
Zn	67	166362	42166	300	2
Ba	692	bd	bd	1971	50
Rb	5	74	bd	1	1
Sr	120	75	106	38	1
Ga	5	0	36	1	1
Nb	5	6	bd	1	1
Zr	125	118	bd	37	1
Y	21	10	3	5	1
Th	bd	56.0	bd	bd	0.1
U	1.0	bd	24.8	bd	0.1
Cs	na	na	na	na	0.2
Hf	na	na	na	na	0.2
La	na	na	na	na	0.1
Ce	na	na	na	na	1
Nd	na	na	na	na	1
Sm	na	na	na	na	0.01
Eu	na	na	na	na	0.05
Tb	na	na	na	na	0.1
Yb	na	na	na	na	0.05
Lu	na	na	na	na	0.01
Zr/Y	6.0	11.8	0.0	7.4	
La_N/Yb_N					

Analytical method: X-ray fluorescence, induced neutron activation analysis
The major elements plus Cu-Zn-Ni-Cr-V-Sc were analysed using glass beads.
The elements Zr-Y-Nb-Rb-Sr-Ga-Pb were analysed using pressed pellets.
(bd = below detection limit; na = not analysed)

APPENDIX B

MASS CHANGE CALCULATIONS

The following tables contain the results of the mass change calculations that are discussed in Chapter 4 of this study. All samples in the data set are included in these calculations. A complete description of the theory and methodology of such calculations can be found in MacLean and Kranidiotis (1987) and MacLean (1990). Data in these tables are reported as *weight percent* changes. Negative values correspond to mass loss and positive values correspond to mass gain. The apparent mass changes in Al_2O_3, although small, may indicate that Al is slightly mobile, or that the fractionation trends are not perfectly constrained.

Appendix B. Mass change calculations for major elements.

Sample	83-02-67	83-02-186	83-02-277	83-02-320	83-06-50	83-07-27	83-07-54	83-10-20	83-10-91	83-11-24	83-11-40
Hole	83-02	83-02	83-02	83-02	83-06	83-07	83-07	83-10	83-10	83-11	83-11
Depth	67.01	186.26	277.00	319.64	49.82	26.08	53.01	20.82	91.33	28.05	85.17
Depth	219.85	611.08	908.78	1048.67	163.45	85.56	173.91	68.31	299.63	92.03	279.42
Rock Type	FP	FP	FP	FP	FP	FP	FP	VCLT	FP	FP	FP
wt. % change											
SiO_2	-1.89	-2.81	-0.83	-3.24	-10.30	0.44	-3.08	-34.45	-9.30	-0.71	-3.15
TiO_2	-0.02	-0.02	-0.02	-0.02	-0.01	-0.01	-0.02	-0.02	-0.02	-0.02	-0.02
Al_2O_3	-0.64	-0.65	-0.54	-0.55	-0.44	-0.44	-0.65	-0.59	-0.62	-0.60	-0.54
FeO*	-0.37	-0.53	-0.53	-0.42	0.29	-0.23	0.09	2.11	-0.32	-0.34	-0.77
MnO	-0.04	-0.08	0.05	-0.05	-0.03	-0.04	-0.03	0.03	-0.02	-0.05	-0.05
MgO	-0.15	-0.38	-0.12	-0.12	0.21	0.32	1.04	3.48	1.23	0.62	-0.03
CaO	-0.32	-0.04	0.20	-0.20	-0.33	-0.49	-0.39	1.62	-0.51	-0.46	-0.51
Na_2O	-0.64	-0.02	-0.67	-0.62	0.27	0.41	-0.39	-2.25	-2.33	-0.80	-0.44
K_2O	0.86	0.24	0.26	0.61	-0.42	-0.37	-0.26	0.72	0.84	0.22	-0.05
P_2O_5	0.00	0.00	-0.01	-0.01	0.03	-0.01	-0.01	-0.05	0.01	-0.01	-0.02
Total	**-3.23**	**-4.29**	**-2.21**	**-4.62**	**-10.74**	**-0.41**	**-3.72**	**-29.40**	**-11.03**	**-2.15**	**-5.59**

Sample	83-17-19	85-03-70	85-03-92	85-03-126	86-28-67	86-28-103	87-11-75	87-11-144	87-11-160	87-12-69	87-12-115
Hole	83-17	85-03	85-03	85-03	86-28	86-28	87-11	87-11	87-11	87-12	87-12
Depth	19.34	70.46	91.80	126.22	67.00	103.00	75.50	144.80	160.26	69.21	114.90
Depth	63.45	231.16	301.18	414.10	219.81	337.92	247.70	475.06	525.78	227.06	376.96
Rock Type	VCLT	FP	VCLT	FP	ALT FP	ALT FP	FP FLOW	VCLT	VCLT	FP	VCLT
wt. % change											
SiO_2	-0.84	-9.53	-3.58	-7.87	4.80	-1.53	9.69	21.80	-15.92	-3.05	-0.32
TiO_2	-0.02	-0.01	-0.01	-0.01	-0.01	-0.02	-0.02	-0.02	-0.04	-0.01	-0.01
Al_2O_3	-0.62	-0.46	-0.29	-0.44	-0.50	-0.52	-0.52	-0.69	-0.96	-0.44	-0.38
FeO*	2.00	0.31	0.35	0.29	-0.32	-0.86	-0.38	-0.91	1.50	0.36	0.23
MnO	0.20	-0.04	-0.05	-0.01	0.00	0.01	0.07	0.04	0.32	-0.01	-0.02
MgO	3.55	0.47	0.92	-0.10	2.02	2.73	0.37	-0.27	3.30	1.38	0.84
CaO	0.96	-0.66	-0.22	-0.35	-0.86	-0.86	-0.48	-0.41	1.03	-0.01	-0.39
Na_2O	-3.07	0.48	-1.47	0.63	-5.00	-5.11	-0.60	0.76	-0.67	-1.63	-2.25
K_2O	1.73	-1.02	-0.16	-0.52	1.88	1.93	-0.16	-0.42	-0.16	0.35	0.46
P_2O_5	-0.05	0.03	-0.01	0.02	0.01	0.01	0.01	-0.02	-0.07	0.01	0.00
Total	**3.83**	**-10.43**	**-4.50**	**-8.36**	**2.02**	**-4.21**	**7.99**	**19.85**	**-11.67**	**-3.06**	**-1.85**

Appendix B (continued). Mass change calculations for major elements.

Sample	87-12-147	87-12-301	91-02-28	91-02-85	91-02-170	91-03-14	91-03-35	91-03-40	91-03-75	91-03-116	91-03-150
Hole	87-12	87-12	91-02	91-02	91-02	91-03	91-03	91-03	91-03	91-03	91-03
Depth	147.40	301.40	28.05	85.17	170.02	14.00	35.20	39.90	75.10	116.75	150.10
Depth	483.59	988.83	92.03	279.42	557.80	45.93	115.48	130.90	246.39	383.03	492.45
Rock Type	ALT FP	FP FLOW	QFP	QFP	FP	VCLT	VCLT	QFP	VCLT	VCLT	VCLT
SiO_2	17.01	6.64	-2.45	-4.43	-0.87	-4.68	-9.42	-37.56	3.41	10.72	0.60
TiO_2	-0.02	-0.02	-0.01	-0.01	-0.02	-0.01	-0.01	-0.01	-0.02	-0.01	-0.02
Al_2O_3	-0.55	-0.53	-0.32	-0.31	-0.65	-0.34	-0.32	-0.34	-0.53	-0.47	-0.63
FeO*	-0.32	-0.73	0.03	0.03	-0.13	0.01	0.48	0.04	-0.72	-0.40	-1.14
MnO	-0.07	0.01	-0.03	-0.03	-0.03	-0.02	0.00	0.03	-0.01	-0.04	-0.06
MgO	0.03	0.69	0.86	0.22	-0.20	0.38	0.59	0.81	-0.40	2.17	1.34
CaO	-0.85	0.55	-0.79	-0.64	-0.42	0.43	0.96	0.56	-0.44	-0.62	-0.72
Na_2O	-4.99	-2.11	-0.97	0.02	0.28	-0.40	-0.50	-1.99	-0.67	-3.14	-1.99
K_2O	2.82	0.60	0.43	-0.02	0.01	-0.65	-0.64	0.33	1.72	0.74	0.69
P_2O_5	0.01	0.01	-0.01	0.00	-0.03	0.02	0.01	0.00	0.02	0.00	-0.02
Total	**13.07**	**5.11**	**-3.25**	**-5.17**	**-2.08**	**-5.26**	**-8.84**	**-38.13**	**2.37**	**8.94**	**-1.96**

Sample	91-08-167	91-08-184	91-08-194	91-10-99	91-10-118	91-10-180	91-10-210	91-10-234	91-16-61	91-16-94	91-16-152
Hole	91-08	91-08	91-08	91-10	91-10	91-10	91-10	91-10	91-16	91-16	91-16
Depth	166.93	184.78	194.50	99.10	118.04	180.37	210.13	234.50	61.20	93.94	151.80
Depth	547.66	606.22	638.11	325.13	387.26	591.76	689.39	769.34	200.78	308.20	498.02
Rock Type	VCLT	VCLT	VCLT	FEL DYK	FEL DYK	ALT FP	FP FLOW	ALT FP	FP	VCLT	FP
SiO_2	-16.81	-6.91	-18.33	3.25	8.14	16.87	10.44	-1.12	2.06	-0.52	0.54
TiO_2	-0.02	-0.01	-0.01	-0.01	-0.01	-0.01	-0.02	-0.01	-0.01	-0.04	-0.01
Al_2O_3	-0.63	-0.31	-0.36	-0.34	-0.39	-0.50	-0.53	-0.40	-0.43	-0.97	-0.42
FeO*	-0.64	-0.52	1.05	-0.19	-0.37	0.93	-1.79	0.05	-0.26	0.51	-0.56
MnO	-0.01	-0.01	0.06	-0.01	-0.03	-0.10	-0.11	0.04	0.03	0.06	0.00
MgO	0.36	1.32	2.57	-0.53	-0.56	-1.21	-1.43	2.44	1.42	1.76	0.14
CaO	-0.22	-0.62	-0.63	0.47	-0.08	-0.63	0.07	-0.38	-0.51	-0.36	0.01
Na_2O	-1.76	-2.72	-2.43	-1.13	0.43	-4.24	-0.51	-2.99	-2.23	-2.72	-0.13
K_2O	0.69	0.68	0.14	1.67	0.34	5.13	0.40	0.46	0.43	0.87	-0.89
P_2O_5	-0.03	0.01	0.00	-0.01	-0.02	0.02	-0.08	0.02	-0.02	-0.08	-0.01
Total	**-19.05**	**-9.09**	**-17.94**	**3.18**	**7.44**	**16.24**	**6.44**	**-1.89**	**0.47**	**-1.50**	**-1.35**

Appendix B (continued). Mass change calculations for major elements.

Sample	91-16-153	91-16-159	91-16-161	91-16-307	91-18-64	91-18-181	91-18-252	91-18-284	92-26-227	92-27-71	92-27-85
Hole	91-16	91-16	91-16	91-16	91-18	91-18	91-18	91-18	92-26	92-27	92-27
Depth	152.81	159.00	161.29	307.52	64.30	181.40	252.50	284.60	227.15	70.86	85.20
Depth	501.34	521.64	529.16	1008.91	210.95	595.13	828.40	933.71	745.23	232.48	279.52
Rock Type	VCLT	ALT FP	FP	FP	FP FLOW	VCLT	ALT FP	FP	FP	QFP	FP
SiO_2	51.76	18.69	-1.18	-1.36	2.18	-4.18	35.45	-18.79	-4.68	-4.39	-1.24
TiO_2	-0.01	-0.01	-0.03	-0.02	-0.01	-0.01	-0.02	-0.02	-0.01	-0.01	-0.04
Al_2O_3	-0.40	-0.36	-0.69	-0.69	-0.43	-0.42	-0.59	-0.55	-0.32	-0.47	-0.96
FeO*	-0.74	-0.79	-0.13	-0.20	-0.25	2.30	1.38	-1.47	-0.02	0.15	0.03
MnO	-0.05	-0.09	-0.01	0.06	0.01	-0.01	-0.11	-0.02	-0.01	0.03	0.03
MgO	0.83	-0.03	2.55	1.43	0.52	1.17	-1.29	0.38	-0.26	-0.24	-0.54
CaO	2.06	-0.69	1.52	-0.27	-0.33	-0.60	-0.90	-0.03	0.68	1.37	0.31
Na_2O	-4.90	-4.05	-2.51	-3.31	-0.16	-1.64	-4.89	-3.24	0.07	-0.58	-0.20
K_2O	1.91	1.45	0.27	1.21	-0.57	-0.06	3.07	1.64	-0.56	-0.43	-0.20
P_2O_5	-0.06	0.05	-0.04	-0.02	-0.01	0.00	-0.03	-0.02	0.00	-0.01	-0.02
Total	**50.40**	**14.18**	**-0.25**	**-3.19**	**0.94**	**-3.44**	**32.05**	**-22.12**	**-5.10**	**-4.58**	**-2.84**

Sample	92-27-177	92-28-35	92-28-132	92-28-185	92-29-140	92-29-164	92-29-227	92-31-281	92-31-244	92-31-225	92-33-75
Hole	92-27	92-28	92-28	92-28	92-29	92-29	92-29	92-31	92-31	92-31	92-33
Depth	177.70	35.40	132.50	185.00	140.25	163.90	226.80	281.35	244.50	224.92	74.95
Depth	583.00	116.14	434.70	606.95	460.13	537.72	744.08	923.05	802.15	737.91	245.89
Rock Type	FP	FP FLOW	ALT FLOW	QFP	QFP	VCLT	FP	FP	ALT FP	FP	FP
SiO_2	-0.11	5.67	-4.73	5.82	-0.13	8.15	-3.90	-3.10	-16.03	1.99	-12.80
TiO_2	-0.02	-0.01	-0.01	-0.01	-0.01	-0.01	-0.04	-0.02	-0.02	-0.02	-0.01
Al_2O_3	-0.67	-0.44	-0.48	-0.47	-0.31	-0.30	-0.98	-0.66	-0.68	-0.69	-0.37
FeO*	-0.08	-0.51	-0.56	-1.09	0.16	-0.19	-0.51	-0.59	-1.06	0.10	0.20
MnO	0.01	0.03	0.06	0.03	0.10	-0.04	0.02	0.00	-0.03	0.04	0.02
MgO	0.39	1.48	0.46	0.76	0.12	2.45	-0.24	-0.88	2.06	1.30	0.90
CaO	0.13	-0.60	0.42	0.04	0.50	-0.69	0.36	0.37	-0.19	-0.14	-0.17
Na_2O	-1.00	-3.73	0.68	-1.56	0.09	-3.92	-0.41	0.71	-1.88	-1.64	-0.30
K_2O	-0.18	1.68	-1.03	0.32	-1.26	1.06	0.06	-0.53	0.45	0.38	-0.97
P_2O_5	-0.04	-0.01	-0.01	-0.02	0.01	-0.01	0.00	0.00	0.00	-0.02	-0.01
Total	**-1.57**	**3.56**	**-5.19**	**3.81**	**-0.72**	**6.52**	**-5.65**	**-4.70**	**-17.40**	**1.30**	**-13.51**

Appendix B (continued). Mass change calculations for major elements.

Sample	92-39-71	92-39-200	92-39-237	93-VT-01	93-VT-02	93-VT-03	93-VT-04	93-SN-44	93-SN-45	93-SN-46	93-FW-46
Hole	92-39	92-39	92-39	86-13	86-13	86-13	86-13	79-08	79-08	79-08	91-06
Depth	71.07	200.53	237.39	25.00	50.00	65.00	85.00	200.00	199.00	179.53	22.20
Depth	233.17	657.90	778.83	82.02	164.04	213.25	278.87	656.16	652.88	589.00	72.83
Rock Type	FP	QFP	VCLT	FP	ALT FP	ALT FP	ALT FP	ALT FP	ALT FP	FP	ALT FP
SiO_2	-2.63	-1.39	20.91	-3.82	9.68	-1.48	1.28	33.59	-6.65	-0.90	-8.60
TiO_2	-0.01	-0.01	-0.01	-0.01	-0.02	-0.02	-0.02	-0.01	-0.01	-0.01	-0.04
Al_2O_3	-0.41	-0.36	-0.27	-0.49	-0.54	-0.52	-0.53	-0.44	-0.44	-0.42	-0.94
FeO*	0.42	-0.33	-0.63	-0.05	0.96	-0.41	0.18	-0.04	0.18	0.13	1.62
MnO	0.01	0.00	-0.06	0.07	-0.03	0.04	-0.04	0.12	0.17	0.04	0.24
MgO	0.79	-0.26	-0.10	0.26	2.32	2.50	1.78	-0.14	0.15	0.88	1.58
CaO	-0.29	0.34	0.40	-0.55	-0.54	-0.57	-0.88	1.02	1.95	-0.10	2.17
Na_2O	-1.44	-0.87	0.29	-0.01	-4.92	-5.12	-5.12	-2.15	-0.60	-0.64	-0.85
K_2O	-0.36	1.09	-1.22	-0.88	2.03	1.76	2.43	0.42	-0.39	-0.56	0.10
P_2O_5	-0.01	-0.01	0.01	-0.02	-0.01	0.00	-0.02	-0.01	0.00	0.00	-0.08
Total	**-3.93**	**-1.79**	**19.30**	**-5.48**	**8.93**	**-3.81**	**-0.93**	**32.36**	**-5.64**	**-1.59**	**-4.80**

Sample	93-FW-49	93-FW-51	93-FW-52	92-33-172	92-33-173	92-33-176
Hole	91-06	91-06	91-06	92-33	92-33	92-33
Depth	46.50	128.00	204.60	171.67	173.00	175.40
Depth	152.56	419.94	671.25	563.21	567.58	575.45
Rock Type	ALT FP	FP	ALT FP	OTHER	OTHER	OTHER
SiO_2	-7.34	0.36	69.39	-53.81	449.27	951.39
TiO_2	-0.01	-0.01	-0.03	0.00	-0.01	-0.05
Al_2O_3	-0.44	-0.37	-0.70	-0.20	-0.40	-1.09
FeO*	0.63	-0.16	1.47	9.33	8.33	4.84
MnO	0.09	0.03	-0.13	0.29	-0.05	-0.08
MgO	-0.30	0.08	-1.63	9.18	1.10	-2.09
CaO	1.16	-0.17	-0.68	-0.33	-0.07	1.10
Na_2O	-0.09	-0.45	-5.39	3.26	7.36	-5.96
K_2O	-1.24	0.11	3.12	-1.66	0.53	3.11
P_2O_5	0.02	-0.01	0.00	0.07	0.20	-0.25
Total	**-7.52**	**-0.60**	**65.45**	**-33.87**	**466.26**	**950.93**

APPENDIX C

ESTIMATES OF PRECISION AND ACCURACY

A number of Mineral Deposit Research Unit in-house standards were submitted at different times with the various batches of samples analysed for this study to examine the accuracy of analytical data. Three different standards were used: ALB-1 - Ajax albitite, P-1 - Porteau Cove granodiorite and QGRM-100 - gabbro. The MDRU-compiled data from previous analyses of these standards was taken from Fraser (1994). The mean values of this data were used as the accepted values reported in the following tables. It should be noted that these previous analyses were carried out at a different laboratory (X-RAL, Don Mills, Ontario) than that used in this study. As such, these standards only provide an approximate guide to the accuracy of analyses of the samples in this study. The standards were submitted in different batches and were analysed more than once in two of the batches. Several batches of samples from other studies were submitted at the same time as well as between the batches from this study. These other batches included duplicate samples and the same MDRU standards as used in this study and thus provided an additional means of assessing analytical variability both during the analysis of a single batch of samples and between several batches of samples.

There was little analytical variation both within a single batch of analyses as well as between batches. Based on the standards, percent errors were low (<5 %, and often < 1.5 %) for the major elements. The trace elements, however, showed a wide range in errors, although the elements most commonly used in this study (e.g. Zr and Y) generally showed relatively low degrees of error (<10 % error for Zr, 7 to 13 % error for Y). The samples analysed at McGill University usually have smaller associated errors than those analysed at XRAL Labs. Different analytical techniques (e.g. XRF using glass beads versus pressed pellets) can account for some of the disparity in trace element concentrations between the different labs. Comparative accepted versus measured binary plots illustrate the relationship between the various analyses (Figures C.1 to C.3).

Five duplicate samples of rocks collected for this study were also submitted to test precision. This data is included in Appendix C.2 and is summarized in a series of plots in Figures C.4 and C.5.

In general, precision was excellent for the major elements (<5 % deviation) except for possibly Na_2O and K_2O. Some of the trace elements show some scatter, but generally lie within 1 standard deviation of 1:1 line.

Appendix C.1. Analyses of in-house standards.

	ALB-1 Accepted				ALB-1 Measured				P-1 Accepted				P-1 Measured			
Element	Mean	1 St. Dev	% Error	n	Mean	1 St. Dev	% Error	n	Mean	1 St. Dev	% Error	n	Mean	1 St. Dev	% Error	n
SiO_2	55.02	0.25	0.45	14	55.51	0.19	0.34	8	69.65	0.35	0.50	15	70.91	0.37	0.52	8
TiO_2	0.61	0.28	1.50	14	0.61	0.01	0.88	8	0.41	0.02	4.19	15	0.38	0.01	1.35	8
Al_2O_3	18.92	0.01	1.63	14	19.00	0.17	0.90	8	14.42	0.17	1.21	15	14.54	0.16	1.07	8
Fe_2O_3	1.62	0.12	7.14	14	1.63	0.02	1.49	8	3.79	0.07	1.88	15	3.90	0.05	1.26	8
MnO	0.04	0.00	8.77	14	0.04	0.01	13.36	8	0.09	0.00	4.73	15	0.08	0.00	4.35	8
MgO	2.83	0.04	1.42	14	2.75	0.04	1.36	8	1.10	0.02	2.04	15	1.00	0.01	0.75	8
CaO	10.42	0.13	1.20	14	10.23	0.05	0.47	8	3.59	0.08	2.09	15	3.48	0.03	0.76	8
Na_2O	5.77	0.08	1.41	14	5.96	0.13	2.13	8	4.03	0.09	2.25	15	3.86	0.17	4.37	8
K_2O	0.83	0.06	6.88	14	0.81	0.01	0.91	8	2.05	0.07	3.31	15	2.09	0.02	0.84	8
P_2O_5	0.30	0.00	1.22	14	0.30	0.01	1.81	8	0.09	0.00	2.71	15	0.08	0.00	0.00	8
SUM	99.53	0.58	0.58	14	97.27	1.23	1.26	8	99.84	0.56	0.56	15	100.90	0.49	0.48	8
LOI	2.99	0.21	6.90	14	3.36	0.03	0.95	8	0.47	0.09	18.56	15	0.41	0.00	0.86	8
Cr	30.18	12.75	42.24	14	34.14	7.97	23.33	7	133.77	9.65	7.22	15	200.50	7.91	3.95	8
Ni	na				51.86	19.80	38.19	7	na			15	7.00	1.93	27.53	8
Co	12.14	1.17	9.61	14	9.57	4.12	43.02	7	8.73	0.96	11.01	15	5.25	2.12	40.41	8
V	183.23	12.22	6.67	14	177.57	4.43	2.49	7	58.27	5.01	8.59	15	63.88	3.48	5.45	8
Cu	1293.6	29.77	2.30	14	1402.00	86.69	6.18	7	2.35	2.40	101.85	15	23.63	12.39	52.43	8
Pb	1.29	0.83	64.20	14	1.15	1.80	156.88	6	5.41	2.27	41.86	15	7.87	1.73	22.04	6
Zn	26.79	14.36	53.61	14	21.86	10.73	49.09	7	71.33	56.93	79.81	15	43.63	14.96	34.28	8
Ba	292.86	47.46	16.21	14	269.29	13.35	4.96	7	853.33	83.38	9.77	15	795.50	22.26	2.80	8
Rb	27.31	9.72	35.58	14	15.47	2.56	16.53	6	53.87	8.43	15.66	15	44.90	2.63	5.86	6
Sr	990.38	38.04	3.84	14	762.55	15.93	2.09	6	250.00	0.00	0.00	15	216.72	2.99	1.38	6
Ga	na			14	18.07	0.35	1.94	6	na			15	14.87	0.45	3.00	6
Nb	10.77	6.80	63.11	14	0.77	1.08	141.13	6	11.07	5.64	50.94	15	5.32	1.33	25.08	6
Zr	60.00	12.33	20.55	14	78.98	6.12	7.75	6	137.47	11.66	8.48	15	114.62	5.89	5.14	6
Y	18.08	8.25	45.64	14	21.07	2.72	12.92	6	21.53	7.41	34.39	15	21.68	2.75	12.70	6
Th	1.16	0.18	15.66	14	0.00	0.00		6	3.99	0.34	8.42	15	0.00	0.00		6
U	1.04	0.22	21.51	14	0.00	0.00		6	1.53	0.20	12.98	15	1.70	1.74	102.43	6

Appendix C.1 (continued). Analyses of in-house standards.

	QGRM-100 Accepted				QGRM-100 Measured			
Element	Mean	1 St. Dev	% Error	n	Mean	1 St. Dev	% Error	n
SiO_2	48.63	0.26	0.53	11	49.11	0.15	0.31	7
TiO_2	1.98	0.03	1.33	11	2.02	0.02	0.80	7
Al_2O_3	15.51	0.23	1.47	11	16.10	0.06	0.39	7
Fe_2O_3	15.04	0.22	1.46	11	15.04	0.10	0.69	7
MnO	0.19	0.00	2.35	11	0.19	0.00	0.00	7
MgO	5.60	0.14	2.58	11	5.73	0.05	0.88	7
CaO	8.51	0.10	1.14	11	8.60	0.04	0.52	7
Na_2O	2.83	0.07	2.58	11	3.15	0.20	6.33	7
K_2O	1.07	0.05	4.42	11	1.07	0.01	0.76	7
P_2O_5	0.20	0.00	2.29	11	0.19	0.00	0.00	7
SUM	99.72	0.53	0.53	11	101.34	0.37	0.37	7
LOI	0.11	0.06	58.36	11	0.05	0.00	0.00	7
Cr	82.80	14.09	17.01	11	102.14	19.74	19.32	7
Ni	43.33	2.50	5.77	11	49.43	3.78	7.65	7
Co	56.91	2.84	5.00	11	42.43	5.35	12.61	7
V	235.55	25.90	11.00	11	258.29	11.97	4.63	7
Cu	91.50	8.03	8.77	11	139.71	7.99	5.72	7
Pb	2.33	2.10	90.15	11	6.50	0.42	6.41	4
Zn	107.67	5.82	5.41	11	116.00	3.06	2.63	7
Ba	225.27	41.66	18.49	11	245.57	53.67	21.86	7
Rb	35.55	10.57	29.73	11	27.03	1.37	5.08	4
Sr	232.18	8.86	3.82	11	273.70	9.80	3.58	4
Ga	na			11	22.48	1.27	5.64	4
Nb	17.36	8.83	50.88	11	4.93	2.12	43.02	4
Zr	153.18	10.45	6.82	11	139.95	5.89	4.21	4
Y	25.91	8.46	32.63	11	36.88	2.02	5.48	4
Th	1.94	0.20	10.14	11	2.65	3.07	115.84	4
U	0.86	0.29	33.67	11	7.80	6.07	77.80	4

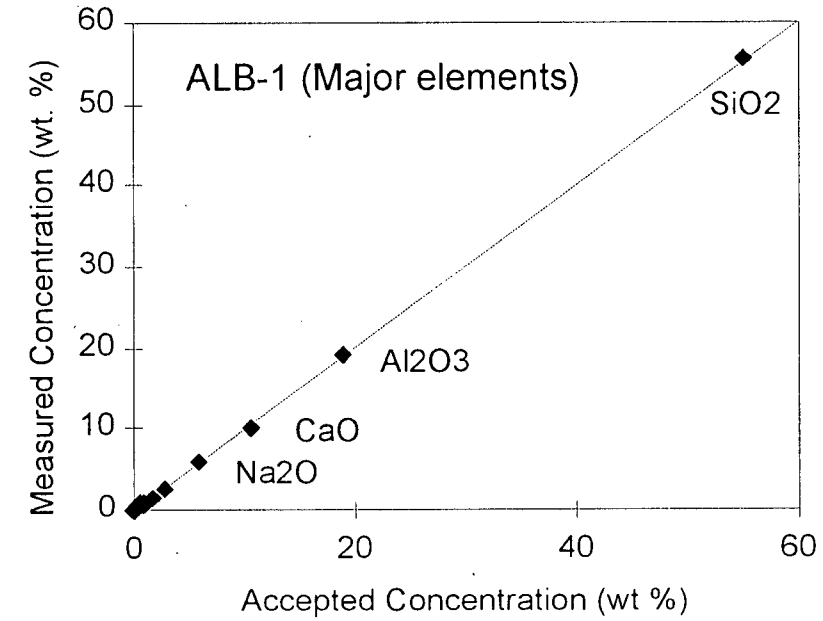

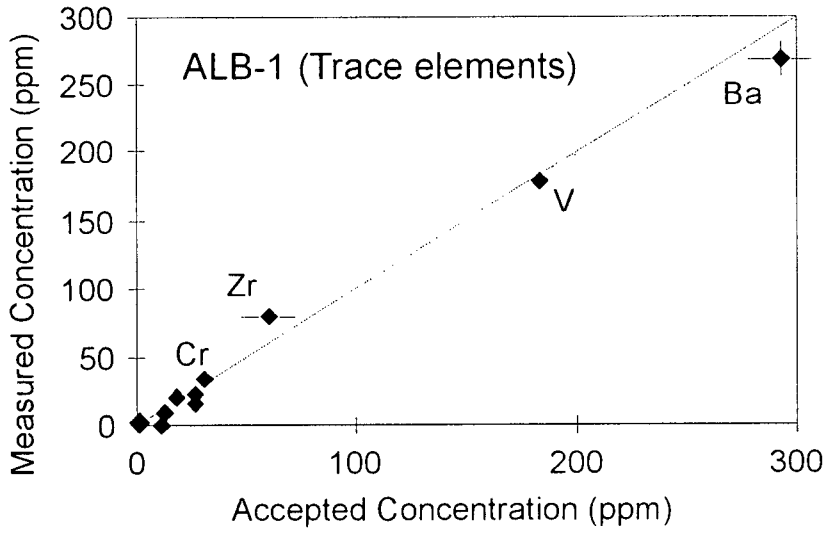

Figure C.1. Comparison of analyses of major and trace element concentrations of in-house standard ALB-1 measured at McGill University versus accepted values (compiled by MDRU) measured at X-Ray Assay Labs. Error bars are +/- 1 standard deviation (App. C.1).

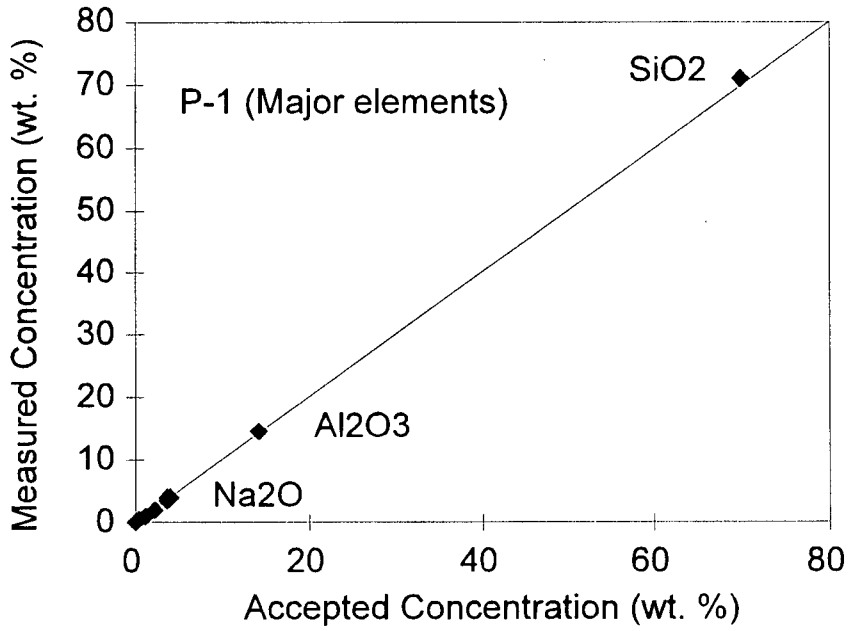

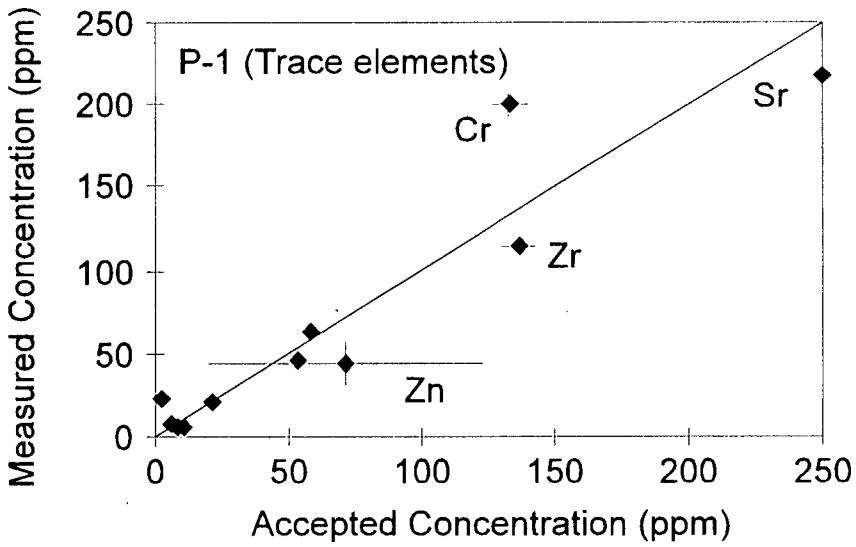

Figure C.2. Comparison of analyses of major and trace element concentrations for in-house standard P-1 measured at McGill University versus accepted values (compiled by MDRU) measured at X-Ray Labs. Error bars are +/- 1 standard deviation (App. C.1).

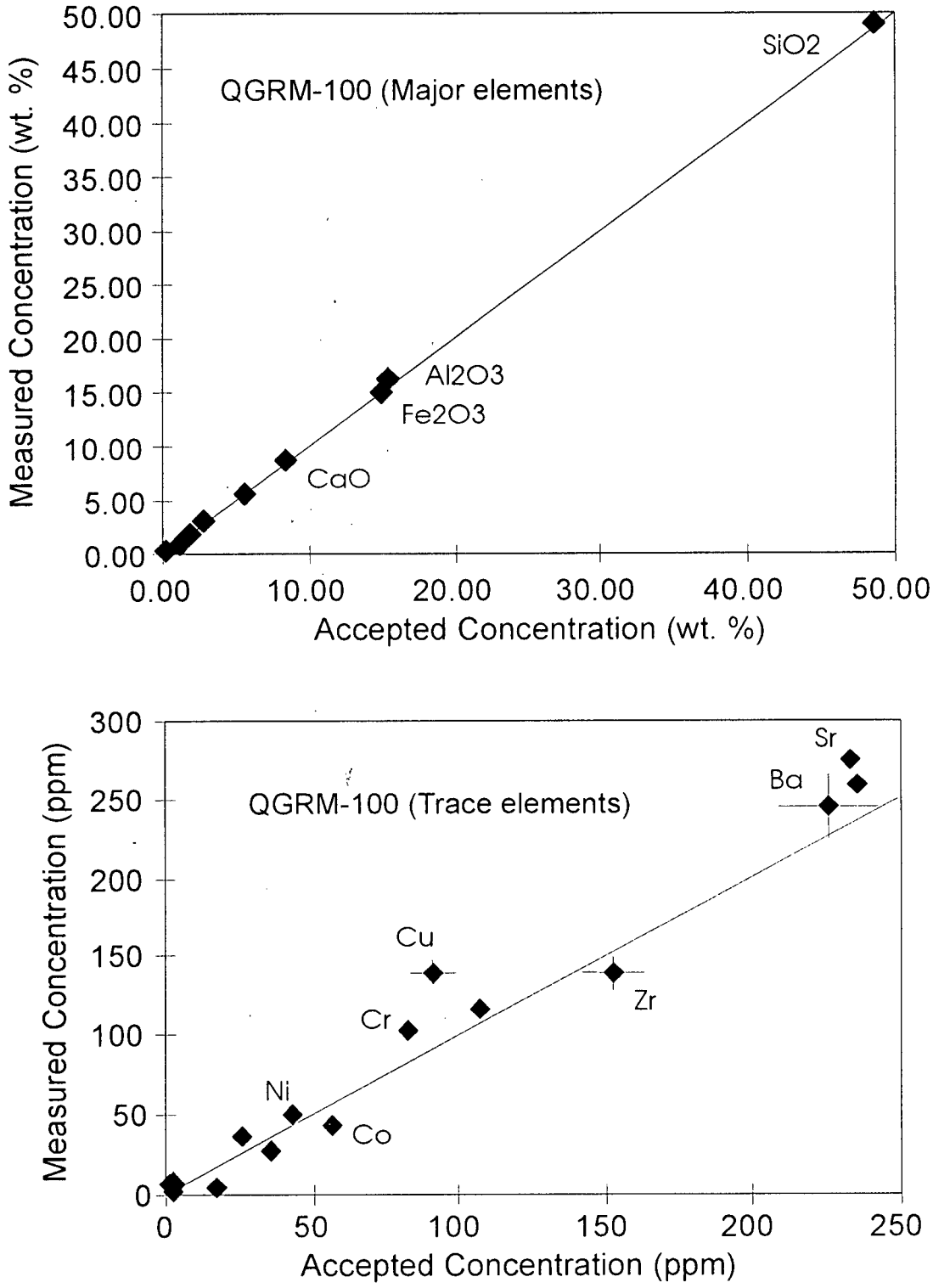

Figure C.3. Comparison of analyses of major and trace element concentrations of in-house standard QGRM-100 measured at McGill University versus accepted values (compiled by MDRU) measured at X-Ray Assay Labs. Error bars are +/- 1 standard deviation (App. C.1).

Appendix C.2. Duplicate analyses of five samples.

Sample	85-03-70	85-03-70	91-02-85	91-02-85	91-16-307	91-16-307	91-16-233	91-16-233	85-03-92	85-03-92	
Hole	85-03		91-02		91-16		91-16		85-03		
Depth (m)	70.5		85.2		307.5		232.9		91.8		Det.
Depth (ft)	231.2		279.4		1008.9		764.0		301.2		Limits
Rock Type	FP	Duplicate	QFP	Duplicate	FP	Duplicate	MAFIC	Duplicate	VCLT	Duplicate	(ppm)
(Wt. %)											
SiO_2	69.26	69.17	73.93	73.79	67.91	67.97	43.75	43.91	73.62	73.84	60
TiO_2	0.41	0.41	0.28	0.27	0.52	0.51	0.66	0.67	0.26	0.26	35
Al_2O_3	14.94	14.97	13.61	13.70	14.48	14.50	16.10	16.03	13.25	13.33	120
Fe_2O_3	3.89	3.87	2.34	2.44	4.39	4.42	9.52	9.56	2.52	2.50	30
MnO	0.08	0.08	0.06	0.06	0.20	0.20	0.33	0.32	0.04	0.05	30
MgO	2.27	2.33	1.22	1.31	3.95	4.01	9.04	9.13	1.82	1.88	95
CaO	0.43	0.47	0.34	0.46	0.89	0.92	8.19	8.26	0.75	0.76	15
Na_2O	5.97	6.29	4.94	5.01	2.05	2.58	3.08	3.13	3.29	3.68	75
K_2O	0.49	0.50	1.94	1.90	2.09	2.04	0.20	0.20	1.82	1.82	25
P_2O_5	0.14	0.15	0.05	0.06	0.13	0.14	0.11	0.11	0.04	0.06	35
LOI	2.05	1.91	1.63	1.35	3.54	3.37	9.34	9.37	3.04	2.63	100
Total	99.93	100.20	100.34	100.44	100.15	100.74	100.32	100.79	100.45	100.84	100
(ppm)											
Cr	48	57	153	34	68	77	132	118	32	37	2
Ni	7	3	6	16	4	19	23	22	7	4	3
Co	7	5	6	0	10	4	36	28	6	0	10
V	52	52	28	43	72	68	229	271	40	28	10
Cu	7	94	11	33	25	43	93	100	10	39	15
Pb	4	0	4	0	4	0	10	3	10	6	2
Zn	57	135	42	82	125	174	273	313	58	108	2
Ba	17	55	529	495	374	380	88	160	88	112	50
Rb	8	7	17	18	28	27	12	1	30	31	1
Sr	64	66	73	77	63	65	177	187	82	86	1
Ga	14	15	11	13	13	14	13	14	12	14	1
Nb	5	5	5	6	7	7	1	2	5	7	1
Zr	109	99	119	112	131	123	44	37	117	111	1
Y	22	24	17	18	28	31	14	17	20	22	1

Analytical method: X-ray fluorescence, induced neutron activation analysis
The major elements plus Cu-Zn-Ni-Cr-V-Sc were analysed using glass beads.
The elements Zr-Y-Nb-Rb-Sr-Ga-Pb were analysed using pressed pellets.
(bd = below detection limit; na = not analysed)

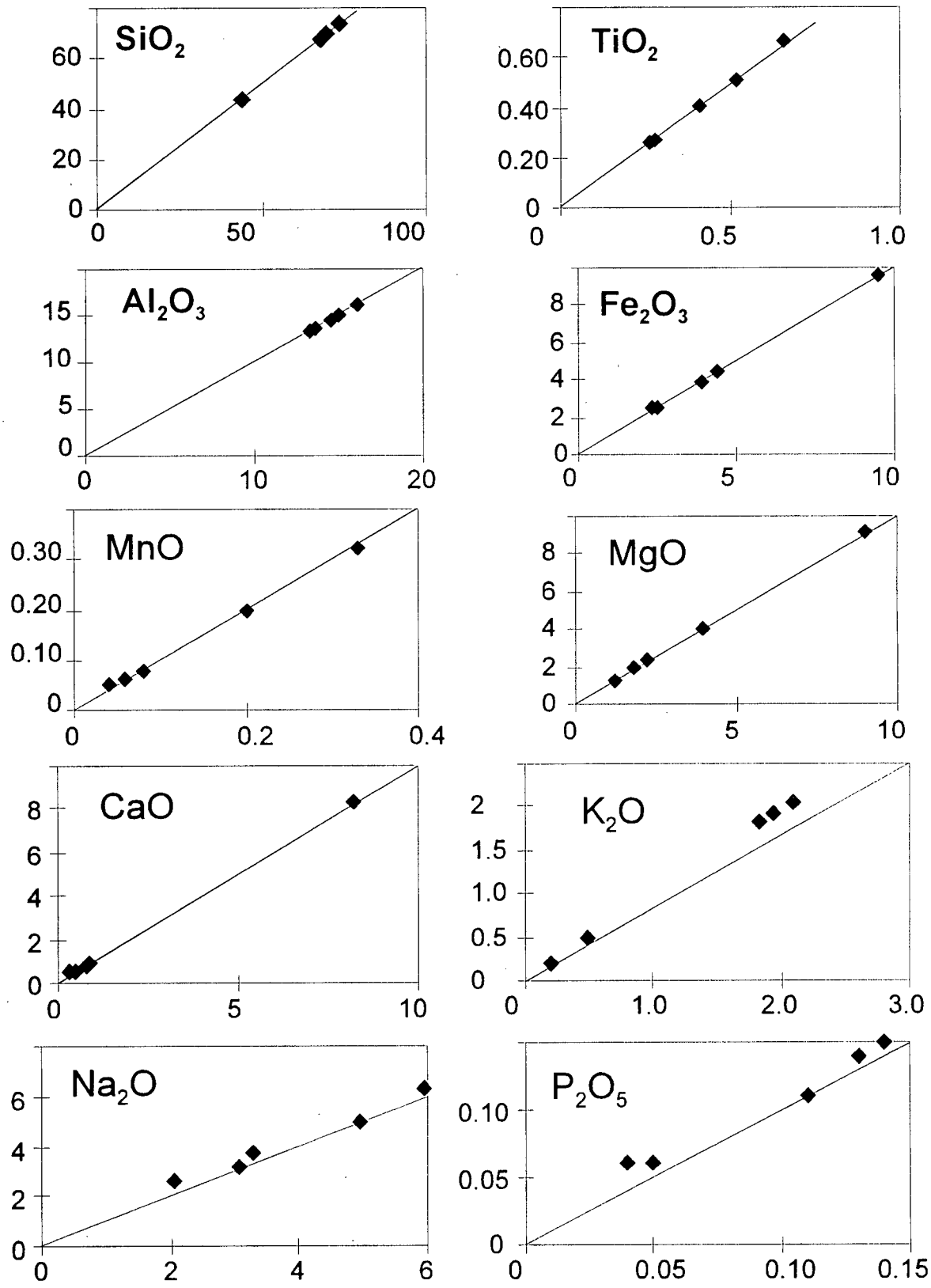

Figure C.4. Plots of major elements for five duplicate samples. Data is included in Appendix C.2. All concentrations are in weight percent.

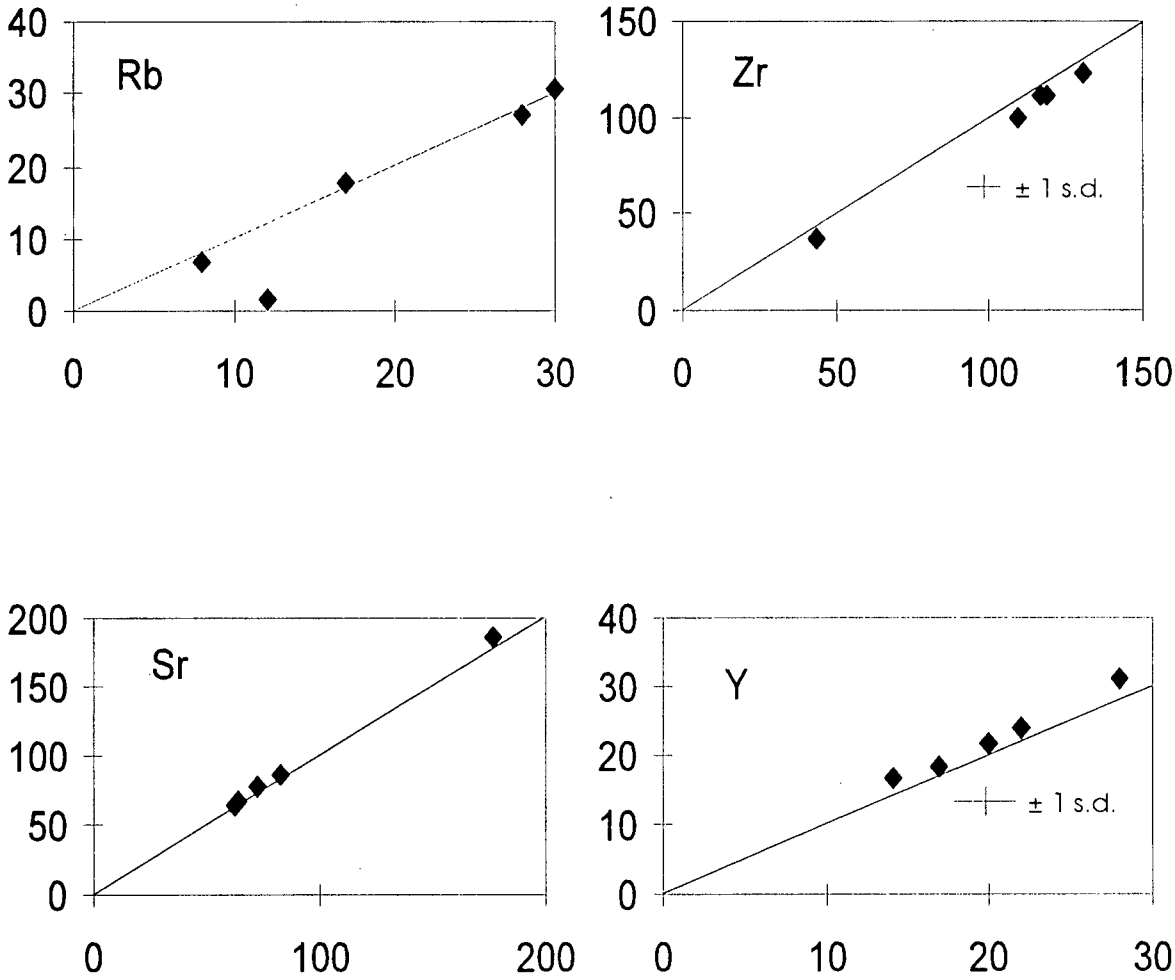

Figure C.5. Plots of selected trace elements for five duplicate samples. Data is included in Appendix C.2. Error bars are approximated by standard deviations calculated in Appendix C.1. All concentrations are in ppm.